1990

Homo- And Heteronuclear Clusters Of Platinum And Gold

Ravindranath Ramachandran

NOTICE

The quality of this microform is heavily dependent upon the quality of the original thesis submitted for microfilming. Every effort has been made to ensure the highest quality of reproduction possible.

If pages are missing, contact the university which granted the degree.

Some pages may have indistinct print especially if the original pages were typed with a poor typewriter ribbon or if the university sent us an inferior photocopy.

Reproduction in full or in part of this microform is governed by the Canadian Copyright Act, R.S.C. 1970, c. C-30, and subsequent amendments.

AVIS

La qualité de cette microforme dépend grandement de la qualité de la thèse soumise au microfilmage. Nous avons tout fait pour assurer une qualité supérieure de reproduction.

S'il manque des pages, veuillez communiquer avec l'université qui a conféré le grade.

La qualité d'impression de certaines pages peut laisser à désirer, surtout si les pages originales ont été dactylographiées à l'aide d'un ruban usé ou si l'université nous a fait parvenir une photocopie de qualité inférieure.

La reproduction, même partielle, de cette microforme est soumise à la Loi canadienne sur le droit d'auteur, SRC 1970, c. C-30, et ses amendements subséquents.

Canada

HOMO- AND HETERO-NUCLEAR CLUSTERS OF PLATINUM AND GOLD

by

Ravindranath Ramachandran

Department of Chemistry

Submitted in partial fulfilment
of the requirements for the degree of
Doctor of Philosophy

Faculty of Graduate Studies
The University of Western Ontario
London, Ontario
February 1990

ISBN 0-315-55284-0

ABSTRACT

The work presented in this thesis can be broadly classified into three sections. Firstly, chapters 2, 3 and 4 deal with the chemistry of homonuclear gold complexes derived from the reaction of [AuC≡C*t*-Bu], "AuC_2", with various diphosphine ligands. Secondly, in chapter 5 the synthesis, characterization and reactivity of some heteronuclear platinum-gold cluster complexes are discussed. Finally, chapters 6, 7 and 8 deals with the chemistry of homonuclear platinum cluster complexes derived from the reaction of the coordinatively unsaturated triplatinum cluster, $[Pt_3(\mu_3\text{-}H)(\mu\text{-}dppm)_3](PF_6)$, "$Pt_3H$", with various reagents.

The reaction of "AuC_2" with the diphosphine ligands, $CH_2(PR_2)_2$ (R = Me, dmpm; R = Ph, dppm), yielded the complexes [*t*-BuC≡C-Au-$R_2PCH_2PR_2$], which were fluxional in solution. The dmpm complex dimerizes in chlorinated solvents to form $[Au_2(\mu\text{-}dmpm)_2]Cl_2.2H_2O$. The crystal and molecular structures of the chloride and the iodide salts have been determined by X-ray diffraction methods.

The reaction of "AuC_2" with $(MeO)_2PCH_2P(OMe)_2$, dmopm, forms $[CH_2\{P(OMe)_2AuC{\equiv}Ct\text{-}Bu\}_2]$, which oligomerizes upon crystallization from CH_2Cl_2/pentane to give $[Au_2(C{\equiv}Ct\text{-}Bu)\{\mu_3\text{-}(MeO)_2PCHP(OMe)_2\}]_3$, "$Au_6$". A further

slow crystallization of "Au_6" from $CHC\ell_3$/pentane gave $[Au_8C\ell_2(\mu_3\text{-}(MeO)_2PCHP(OMe)_2)_2(\mu_4\text{-}(MeO)_2PCP(OMe)_2)_2]$, "$Au_8$", as the $CHC\ell_3$ solvate, whose structure was determined by X-ray diffraction. "Au_8" is a new type of cage containing the first structurally characterized example of a $[\mu_4\text{-}R_2PCPR_2]^{2-}$ ligand.

The diphosphine ligand, dppm, reacts with "AuC_2" to yield $[Au_2(C{\equiv}Ct\text{-}Bu)_2(\mu\text{-}dppm)]$, whose structure was determined by x-ray crystallography. Pyrolysis of this digold complex yielded a tetranuclear gold complex, $[Au_4(\mu_3\text{-}Ph_2PCHPPh_2)(\mu\text{-}Ph_2PCH_2PPh_2)(C{\equiv}Ct\text{-}Bu)_3]$. The combination of the results of the reaction of "AuC_2" with the dppm ligand and those with the dmopm ligand suggest a possible reaction pathway for the formation of the novel octagold cage complex, "Au_8".

Auration of the triplatinum complex "Pt_3H" with LAu^+, L=PPh_3, gave $[Pt_3(\mu_3\text{-}H)(\mu_3\text{-}AuPPh_3)(\mu\text{-}dppm)_3](PF_6)_2$, which can be deprotonated to $[Pt_3(\mu_3\text{-}AuPPh_3)(\mu\text{-}dppm)_3](PF_6)$ and then further aurated to $[Pt_3(\mu_3\text{-}AuPPh_3)_2(\mu\text{-}dppm)_3](PF_6)_2$ thus providing a route to novel platinum cluster hydrides. The reactions of these hetero bimetallic complexes with various main group reagents were also studied.

The reaction of tertiary phosphines and phosphites with the triplatinum complex "Pt_3H" yielded the clusters $[Pt_3(\mu_3\text{-}H)(L)(\mu\text{-}dppm)_3](PF_6)$, L = Phosphine or phosphite. The cluster complex $[Pt_3(\mu_3\text{-}H)(P(OMe)_3)(\mu\text{-}dppm)_3](PF_6)$ was

characterized by X-ray crystallography. These clusters contain an asymmetrically capping hydride ligand for which the spectroscopic parameters were obtained. The phosphine and phosphite ligands displayed a unique fluxionality which was deduced using multinuclear NMR data.

The triplatinum complex "Pt_3H" can be protonated rapidly and reversibly by aq. HPF_6, to give $[Pt_3(\mu_3\text{-}H)_2(\mu\text{-}dppm)_3]^{2+}$, and $[Pt_3(\mu_3\text{-}H)_3(\mu\text{-}dppm)_3]^{3+}$. When the protonation was carried out using CF_3COOH, an asymmetric complex, $[Pt_3(\mu_3\text{-}H)(H)(\mu\text{-}dppm)_3(\mu\text{-}CF_3COO)]^{+}$, was obtained. These dihydrido complexes react with CO to quantitatively eliminate hydrogen and form the parent carbonyl complex, $[Pt_3(\mu_3\text{-}CO)(\mu\text{-}dppm)_3]^{2+}$, "$Pt_3CO$". They also react with various phosphine and phosphite ligands, L, to yield $[Pt_3(\mu\text{-}H)(H)(L)(\mu\text{-}dppm)_3]^{2+}$. However, phenyl phosphine, $PPhH_2$, reacted with "Pt_3H" to yield $[Pt_3(\mu_3\text{-}PPh)(H)(\mu\text{-}dppm)_3]^{+}$.

Finally, the chemistry of some tetraplatinum clusters was examined. The reaction of "Pt_3H" and "Pt_3CO" with the Pt(0) reagent, $[Pt(CO)_2L_2]$, L = PPh_3, yielded $[Pt_4(\mu\text{-}H)(\mu\text{-}CO)_2(PPh_3)(\mu\text{-}dppm)_3]^{+}$, and $[Pt_4(\mu\text{-}CO)_2(PPh_3)(\mu\text{-}dppm)_3]^{2+}$, respectively. The fluxionality of these clusters was deduced on the basis of variable temperature multinuclear NMR data and by comparison with the previously characterized cluster $[Pt_4(\mu\text{-}H)(\mu\text{-}CO)_2(\mu\text{-}dppm)_3(\eta^1\text{-}dppm)]^{+}$.

ACKNOWLEDGEMENTS

I wish to express my appreciation to Dr. R.J. Puddephatt and Dr. N.C. Payne for their advice and support during the course of this work. I would therefore like to express my deepest gratitude for their patience, guidance and encouragement which they have continuously provided during the course of this work.

I wish to thank Valerie Richardson and Susan England who have provided excellent NMR service. I would also like to thank members of the electronic shop for their technical assistance in the preparation of this thesis. I sincerely appreciate the secretarial assistance of Barb Smieja, Elizabeth Dejaegher and Eleanor Egan at various stages of the thesis preparation.

Dr. Lucio Gelmini rendered exceptionally valuable assistance to draw the molecular structures and to him I offer my special thanks.

I would also like to thank my fellow coworkers, both past and present, who have made the duration of my stay here most enjoyable.

Most of all, I would like to thank my beloved wife, Bagavathi, for her patience, support and understanding throughout the course of this work. I am also grateful to her for her contributions to the typing of this thesis. Finally, my special thanks to my daughter, Nisha, whose love and laughter have seen me through these years.

To my dearest Parents

Work, Work, Work and stop not till the goal is reached.

Swamy Vivekananda

TABLE OF CONTENTS

LIST OF TABLES

LIST OF FIGURES

LIST OF APPENDICES

KEY ABBREVIATIONS

Anal. Calcd. = analysis calculated
atm = atmosphere
t-Bu = tertiary butyl
br = broad
dppm = bis(diphenylphosphino)methane
dmpm = bis(dimethylphosphino)methane
vdpp = bis 1,1-(diphenylphosphino)vinylidene
edpp = bis 1,1-(diphenylphosphino), 2-ethoxy ethane
cdpp = bis 1,1-(diphenylphosphino) cyclopropane
δ = chemical shift
s = singlet
d = doublet
t = triplet
q = quartet
quint = quintet
sept = septet
Hz = Hertz
FAB = Fast atom bombardment
J = coupling constant
IR = infrared
λ = wavelength
L = phosphine, phosphite
MO = molecular orbital
HOMO = highest occupied molecular orbital
LUMO = lowest unoccupied molecular orbital
M = metal center
MHz = megahertz
Mp = melting point
MS = mass spectrum
ν = frequency
NMR = nuclear magnetic resonance

Ph = phenyl

psi = pounds per square inch

R = alkyl or aryl

THF = tetrahydrofuran

UV = ultraviolet

X = halogen

m = mirror

Me = methyl

MLCT = metal to ligand charge transfer

Å = Angstrom

F_O = Observed structure factor

F_C = calculated structure factor

σ = standard deviation

e = electron

nm = nanometer

Z = number of molecules per unit cell

pm = picometer

dmopm-H = $[(MeO)_2PCHP(OMe)_2]^-$

dmopm-H_2 = $[(MeO)_2PCP(OMe)_2]^{2-}$

dmpm-P = Monodentate diphosphine coordinated through one phosphorus atom.

SUMMARY OF NUMBERS USED TO REPRESENT VARIOUS COMPLEXES

Chapter 2

1a $[Au_2(\mu\text{-dppm})_2Cl_2]$

1b $[Au_2(\mu\text{-dppm})_2Br_2]$

1c $[Au_2(\mu\text{-vdpp})_2Cl_2]$

2 $[Au_2(\mu\text{-cdpp})_2Cl]Cl$

3 $[Au_2(\mu\text{-edpp})_2Cl]Cl$

4 $[Au_2(\mu\text{-dppm})_2I]I$

5a $[Au_2(\mu\text{-dmpm})_2]Cl_2.2H_2O$

5b $[Au_2(\mu\text{-dppm})_2]I_2.2H_2O$

6a $[Au(C{\equiv}Ct\text{-Bu})(dmpm\text{-}P)]$

6b $[Au(C{\equiv}Ct\text{-Bu})(dppm\text{-}P)]$

7a $[Au_2(\mu\text{-dmpm})_3]Cl_2$

7b $[Au_2(\mu\text{-dmpm})_3]I_2$

Chapter 3

1a $[Au_2(C{\equiv}Ct\text{-Bu})_2(\mu\text{-dmopm})]$

3 $[Au_2(C{\equiv}Ct\text{-Bu})(\mu_3\text{-dmopm-H})]_3$

4 $[Au_8Cl_2(\mu_3\text{-dmopm-H})_2(\mu_4\text{-dmopm-H}_2)_2].CHCl_3$

Chapter 4

1a $[Au_2(C{\equiv}Ct\text{-Bu})_2(\mu\text{-dmopm})]$

1b $[Au_2(C{\equiv}Ct\text{-Bu})_2(\mu\text{-dppm})]$

2b $[Au_4(C{\equiv}Ct\text{-Bu})_3(\mu_3\text{-dppm-H})(\mu\text{-dppm})]$

3 $[Au_2(C{\equiv}Ct\text{-Bu})(\mu_3\text{-dmopm-H})]_3$

4 $[Au_8Cl_2(\mu_3\text{-dmopm-H})_2(\mu_4\text{-dmopm-H}_2)_2].CHCl_3$

Chapter 5

1 $[Pt_3(\mu_3\text{-CO})(\mu\text{-dppm})_3](PF_6)_2$

2 $[Pt_3(\mu_3\text{-H})(\mu\text{-dppm})_3](PF_6)$

3a $[Pt_3(\mu_3\text{-H})(\mu_3\text{-AuPPh}_3)(\mu\text{-dppm})_3](PF_6)_2$

3b $[Pt_3(\mu_3\text{-H})(\mu_3\text{-AgPPh}_3)(\mu\text{-dppm})_3](PF_6)_2$

4 $[Pt_3(\mu_3\text{-AuPPh}_3)(\mu\text{-dppm})_3](PF_6)$

5 $[Pt_3(\mu_3\text{-}AuPPh_3)_2(\mu\text{-}dppm)_3](PF_6)_2$

6 $[Pt_3(\mu_3\text{-}S)(H)(\mu\text{-}dppm)_3](PF_6)$

7 $[Pt_3(\mu_3\text{-}AuPPh_3)(CO)(\mu\text{-}dppm)_3](PF_6)$

7* $[Pt_3(\mu_3\text{-}AuPPh_3)(^{13}CO)(\mu\text{-}dppm)_3](PF_6)$

Chapter 6

1 $[Pt_3(\mu_3\text{-}CO)(\mu\text{-}dppm)_3](PF_6)_2$

2 $[Pt_3(\mu_3\text{-}H)(\mu\text{-}dppm)_3](PF_6)$

3a $[Pt_3(\mu_3\text{-}H)\{P(OMe)_3\}(\mu\text{-}dppm)_3](PF_6)\cdot\frac{1}{2}CH_2C\ell_2$

3b $[Pt_3(\mu_3\text{-}H)\{P(OEt)_3\}(\mu\text{-}dppm)_3](PF_6)$

3c $[Pt_3(\mu_3\text{-}H)\{P(OPh)_3\}(\mu\text{-}dppm)_3](PF_6)$

3d $[Pt_3(\mu_3\text{-}H)(PPh_2Me)(\mu\text{-}dppm)_3](PF_6)$

3e $[Pt_3(\mu_3\text{-}H)(PPhH_2)(\mu\text{-}dppm)_3](PF_6)$

4 $[Pt_3(\mu_3\text{-}CO)(\mu\text{-}dppm)_3L](PF_6)_2$

5 $[Pt_3(\mu_2\text{-}CO)(\mu\text{-}dmpm)_4](PF_6)_2$

6 $[Pt_3(\mu_3\text{-}PPh)(\mu\text{-}dppm)_3H](PF_6)$

7 $[Pt_3(\mu_3\text{-}PPh)(\mu\text{-}dppm)_3(OH)](PF_6)$

8 $[Pt_3(\mu_3\text{-}AuPPh_3)(PPh_3)_5(\mu\text{-}CO)_3](NO_3)$

Chapter 7

1 $[Pt_3(\mu_3\text{-}CO)(\mu\text{-}dppm)_3](PF_6)_2$

2 $[Pt_3(\mu_3\text{-}H)(\mu\text{-}dppm)_3](PF_6)$

3a $[Pt_3(\mu_3\text{-}H)_2(\mu\text{-}dppm)_3](PF_6)_2$

3b $[Pt_3(\mu_3\text{-}H)H(\mu\text{-}dppm)_3(CF_3COO)](CF_3COO)$

3b* $[Pt_3(H)(D)(\mu\text{-}dppm)_3(CF_3COO)](CF_3COO)$

3b** $[Pt_3(\mu_3\text{-}D)D(\mu\text{-}dppm)_3(CF_3COO)](CF_3COO)$

3c $[Pt_3(\mu_3\text{-}H)H(\mu\text{-}dppm)_3(CF_3COO)](PF_6)$

4 $[Pt_3(\mu\text{-}H)_3(\mu\text{-}dppm)_3](CF_3COO)_3$

5a $[Pt_3(\mu\text{-}H)H\{P(OMe)_3\}(\mu\text{-}dppm)_3](PF_6)(CF_3COO)$

5b $[Pt_3(\mu\text{-}H)H\{P(OEt)_3\}(\mu\text{-}dppm)_3](PF_6)(CF_3COO)$

5c $[Pt_3(\mu\text{-}H)H\{P(OPh)_3\}(\mu\text{-}dppm)_3](PF_6)(CF_3COO)$

5c' $[Pt_3(\mu\text{-}H)H\{P(OPh)_3\}(\mu\text{-}dppm)_3](PF_6)_2$

5d $[Pt_3(\mu\text{-}H)H(PPh_3)(\mu\text{-}dppm)_3](PF_6)(CF_3COO)$

6 $[Pt_2(\mu\text{-}H)(H)_2(\mu\text{-}dppm)_2](PF_6)$

7 $[Pt_3(\mu_3\text{-}CO)(CO)(\mu\text{-}dppm)_3](PF_6)_2$

8 $[Pt_2(\mu\text{-}dppm)_2(H)(CO)](PF_6)$

8d $[Pt_2(\mu\text{-dppm})_2(H)(PPh_3)](PF_6)$

9 $[Pt_3(\mu\text{-H})_3(P^tBu_3)_3]$

Chapter 8

1 $[Pt_3(\mu_3\text{-CO})(\mu\text{-dppm})_3](PF_6)_2$

2 $[Pt_3(\mu_3\text{-H})(\mu\text{-dppm})_3](PF_6)$

3 $[Pt_4(\mu\text{-H})(\mu\text{-CO})(PPh_3)(\mu\text{-dppm})_3](PF_6)$

4 $[Pt_4(\mu\text{-CO})_2(PPh_3)(\mu\text{-dppm})_3](PF_6)_2$

5 $[Pt_4(\mu\text{-H})(\mu\text{-CO})_2(\eta^1\text{-dppm-P})(\mu\text{-dppm})_3](PF_6)$

6 $[Pt_4(\mu\text{-CO})_2\{\eta^1\text{-}Ph_2PCH_2P(:O)Ph_2\}(\mu\text{-dppm})_3](PF_6)$

7 $[Pt_4(\mu\text{-CO})_5L_5]$

8 $[Pt_3(\mu\text{-CO})_3(PPh_3)_3]$

Chapter 9

1 $[Pt_3(\mu_3\text{-H})(\mu\text{-dppm})_3](PF_6)$

2 $[Pt_3(\mu_3\text{-CO})(\mu\text{-dppm})_3](PF_6)_2$

CHAPTER 1

INTRODUCTION

As this thesis deals with the chemistry of gold and platinum cluster complexes, we shall review the chemistry of these two elements individually. This will be followed by a section on the chemistry of mixed metal clusters containing platinum and gold. Finally, this chapter concludes with a section on the scope of this thesis.

1.1 GOLD:

1.1.1 Physical properties:

The concentration of gold in earth's crust is on average about 0.004 ppm, thus making it one of the rare elements on this planet. Gold usually occurs in nature in the metallic form. It is a soft, yellow metal with the highest ductility and malleability of any element. Gold also has high thermal and electrical conductivity; hence its use in electronics. The pure metal melts at 1063°C and boils at 2966°C. The beauty and rarity of gold has led to its use in jewellery and as a standard for monetary systems throughout the world. Like other group IB metals, gold crystallizes in the face-centred cubic lattice and the closest inter-nuclear distance is 2.884 Å.[1]

1.1.2 Chemical reactivity of gold:

Gold is the most noble of the metals, being the only one which is not attacked by either oxygen or sulfur at any temperature. Gold will dissolve in aqueous solutions containing a good ligand for gold and an oxidizing agent, but neither condition alone is sufficient. Thus gold will not dissolve appreciably in aqueous $HC\ell$ or HNO_3, but dissolves readily in aqua regia to give tetrachloroauric (III) acid, $H[AuC\ell_4]$.

In complexes containing a single gold atom, the oxidation states 0, +1, +2, +3 and +5 are well established and gold also forms many complexes with metal-metal bonds in which it is difficult to assign a formal oxidation state to the metal atom. Gold has the electronic configuration $[Xe]4f^{14}5d^{10}6s^1$. Complexes of gold(I) with two-coordinate, linear geometry at the metal centre are the most common[3], although three-coordinate trigonal and four-coordinate, tetrahedral species have also been prepared.[2,3] Gold(I_I) complexes have the four co-ordinate square-planar stereochemistry. Five-coordinate and six-coordinate gold(III) complexes are rare, but when formed they have square pyramidal and octahedral geometries, respectively (see Table 1.1). The oxidation states 0, +2 and +5 are considered unusual for gold, but crystallographically characterized complexes do exist for them.[2]

In each of the oxidation states gold forms a host of complexes with a variety of ligands. In general, gold(I) and

Table 1.1: Geometries and Oxidation States of Gold

Oxidation State	Coordination Number	Geometry	Complex	Ref.
0	2	trans-bent geometry	$[(Ph_3P)Au]_2$	4
1	2	linear	$[(Ph_3P)AuC_6F_5]$	5
	3	trigonal	$[(Ph_3P)_2AuCl]$	6
	4	tetrahedral	$[(Ph_2MeP)_4Au]^+$	3
2	4	distorted. Square planar	$[Au_2(\mu\text{-}CH_2PEt_2CH_2)_2Cl_2]$	7
3	4	square planar	*cis*-$[(Ph_3P)Au(C_6F_5)_2Cl]$	8
	5	square pyramidal	$[AuCl_3(dmphen)]$	9
	6	octahedral	$[Au(diars)_2I_2]$	10
5	6	octahedral	$[AuF_6]^-$	11

dmphen = 2,9-dimethyl-1,10-phenanthroline

gold(III) form stable complexes with isocyanides, phosphines, halogens, sulfides and acetylenes, whereas gold(V) complexes are limited to only the fluoride ligand.

Gold in its +1 and +3 formal oxidation states also forms many organometallic compounds with η^1-alkyls, aryls, η^2-olefins and acetylenes, and η^5-cyclopentadienyl rings.

Some of the organogold compounds of the type [AuR(CNR')], where R and R' are alkyl and aryl groups, have low thermal stability. As a result of their volatility, the more stable members of the series have been used as precursors for chemical vapour deposition of gold.[12] Gold complexes have also been used as drugs in the treatment of certain type of arthritis. For example, various gold(I) thiol compounds are used in the treatment

of rheumatoid arthritis.

1.1.3 Gold Cluster Compounds

This class of compounds contain two or more gold atoms in which the average oxidation state of gold is less than one. A number of reviews are available on this topic.[3,13,18,19]

The simplest complex is the binuclear $[Au_2(PPh_3)_2]$, prepared by reaction of $[AuI(PPh_3)]$ with sodium naphthalide, $NaC_{10}H_8$. It has the *trans* bent structure with r(AuAu) = 2.76 Å and angle AuAuP = 129°, rather than the expected linear structure.[4]

In general gold cluster compounds have been synthesized by the reduction of mononuclear gold phosphine complexes[13,14], $AuX(PR_3)$ (X = halide, NO_3^- etc.), Equations 1.1 to 1.3.

$$AuI(PPh_3) + NaBH_4 \longrightarrow Au_{11}I_3(PPh_3)_7$$

Equation 1.1

$$AuCl(PPh_3) + Ti(\eta\text{-}C_6H_5CH_3)_2 \longrightarrow [Au_9(PPh_3)_8]^{+3}$$

Equation 1.2

$$AuCl(PCyPh_2) + NaBH_4 \longrightarrow [Au_6(PCyPh_2)_6]^{+2}$$

Equation 1.3

An attractive but not widely used synthetic route

is derived from metal vapour synthesis technology and involves the evaporation of gold metal atoms into cooled (-100°C) ethanolic film containing $AuX(PAr_3)$ and PAr_3. Good yields (60 - 80%) have been reported for $[Au_{11}(SCN)_3(PAr_3)_7]$ and $[Au_9(PAr_3)_8](NO_3)_3$.[15]

Cluster aggregation may also be achieved either by the addition of labile monomeric gold(I) complexes or by the addition of $C\ell^-$ or Br^-. Examples of such processes are shown in equations 1.4 and 1.5.

$$[Au_{11}(PMe_2Ph)_{10}]^{+3} + \begin{matrix} 2\ C\ell^- \\ \text{or} \\ 2\ AuC\ell(PMe_2Ph) \end{matrix} \xrightarrow{EtOH} [Au_{13}C\ell_2(PMe_2Ph)_{10}]^{+3}$$

Equation 1.4

$$[Au_8(PPh_3)_8]^{+2} + Au(NO_3)(PPh_3) \longrightarrow [Au_9(PPh_3)_8]^{+3}$$

Equation 1.5

It appears that in the gold phosphine cluster cations the extent of cluster growth is primarily limited by the steric demands of the peripheral ligands. When small ions such as $C\ell^-$ or Br^- replace one of the bulkier phosphine ligands then cluster growth proceeds until it is limited once more by the steric demands of the new set of ligands.

For low nuclearity clusters the competing demands of adopting a compact arrangement of metal atoms and a minimization of the non-bonded repulsions between the

ligand atoms can be resolved in an alternative fashion, that is, changing the cluster geometry. This possibility is particularly important in the case of gold cluster compounds, because the energy differences separating the alternate skeletal geometries are rather small. Examples can be drawn from the known hexanuclear gold cluster

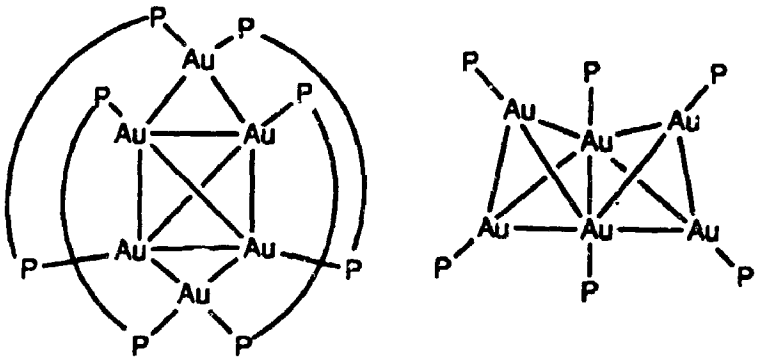

Scheme 1.1

geometries. An edge sharing bi-tetrahedral geometry has been reported for $[Au_6(PPh_3)_6]^{2+}$ and bi-edge bridged tetrahedral geometry for $[Au_6(dppp)_4]^{+2}$, scheme 1.1.

1.1.4 Structure and bonding in gold clusters

The bonding in gold cluster compounds originates primarily from the overlap of 6s orbitals and is of a multicentre nature. This type of interaction is maximized when the number of nearest gold atoms is the largest and is achieved for deltahedral clusters, that is those which have

triangular faces exclusively.[16] For low nuclearity clusters the observed geometries either conform to this generalization, for example, $Au_4I_2(PPh_3)_4$ - tetrahedral; $[Au_6(C)\{P(p\text{-}C_6H_4CH_3)_3\}_6]^{2+}$ - octahedral; $[Au_7(PPh_3)_7]^+$ - pentagonal bipyramidal or form condensed polyhedra derived from these fundamental polyhedra, for example $[Au_6(PPh_3)_6]^{2+}$ - edge-sharing bi-tetrahedral.

The high nuclearity clusters are characterized by the presence of an additional central gold atom and the presence of this atom makes a fundamental contribution to the bonding because the radial metal-metal bonding to the central metal atom is stronger than the peripheral metal-metal bonding on the surface of the cluster.[16] In particular, the radial Au-Au bonds in such clusters are 10 to 20 pm shorter than the peripheral Au-Au bonds.[2]

Structurally these higher nuclearity clusters fall into two categories which relate to the topology of the gold atoms on the surface of the polyhedron. Scheme 1.2 illustrates the difference in topology in these complexes. Thus the compounds illustrated in scheme 1.2(c) and 1.2(d) can be described as spherical because the metal atoms lie on or close to a sphere, whereas those illustrated in scheme 1.2(a) and 1.2(b) have a more open structure wherein the peripheral atoms lie approximately on a torus or resemble more closely a 'doughnut' arrangement. This topological distinction has an electronic significance since the spherical polyhedra of formula $[Au(AuPR_3)_n]^{X+}$ are

(A)

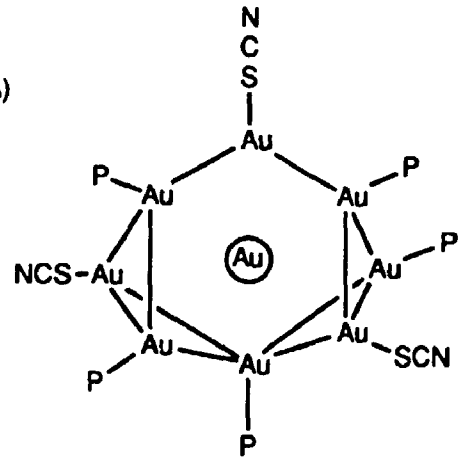

$Au_9(SCN)_3(PCy_3)_5$

(C)

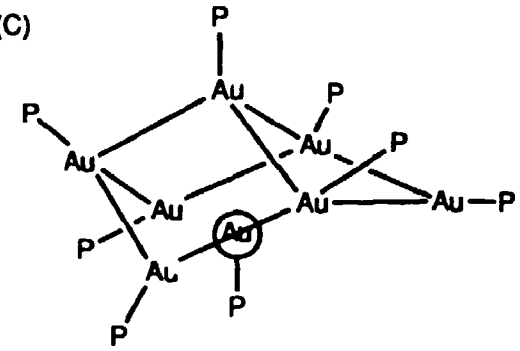

$[Au_8(PPh_3)_8]^{2+}$

(B)

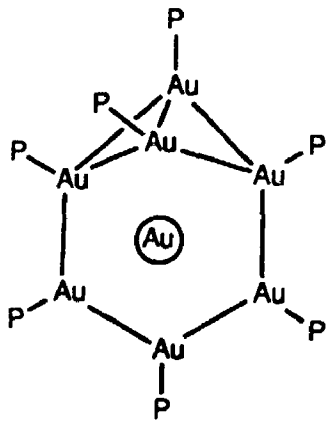

$[Au_8(PPh_3)_7]^{2+}$

(D)

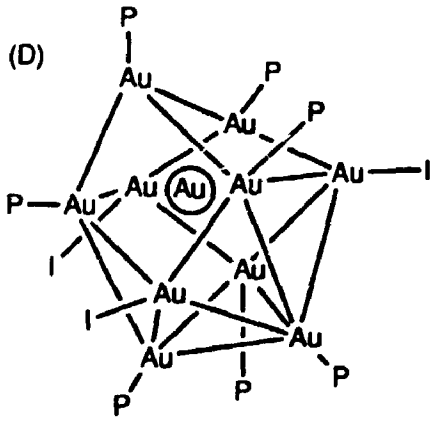

$Au_{11}I_3(PPh_3)_7$

Scheme 1.2 : Examples of Gold Cluster cations, $[Au(AuPR_3)_n]^{x+}$, with toroidal and spherical topologies.

characterized by a total of 12n + 18 electrons and the toroidal polyhedra by a total of 12n + 16 electrons.[17] The use of general topological descriptions for this class of cluster compounds is particularly necessary because of the stereochemical non-rigidity of these compounds. For example, $[Au_9\{p\text{-}C_6H_4OMe)_3\}_8](NO_3)_3$ cluster cation co-crystallizes in two modifications, one-orthorhombic and

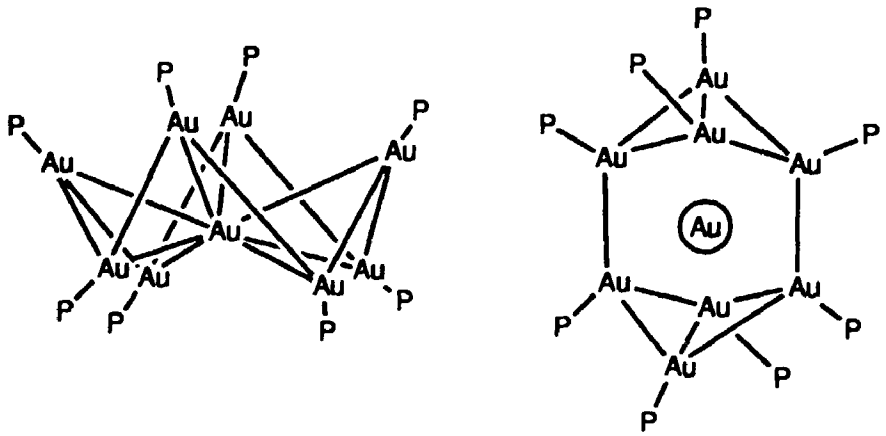

Scheme 1.3

the other tetragonal with quite different skeletal geometries shown in scheme 1.3.

$^{31}P\{^1H\}$ NMR studies have established that the majority of centred gold phosphine clusters are stereochemically non-rigid on the NMR time-scale.[18] Thus the studies described above demonstrates that the molecular clusters of gold are so flexible that minor electronic and steric effects can result in dramatic skeletal rearrangements.[19]

1.2 PLATINUM

1.2.1 Physical properties:

Platinum is a grey-white, lustrous metal which is sufficiently ductile and malleable, and for these reasons, its major use was in jewellery until the middle of this century. The corrosion resistance properties and high melting point (1772°C) of platinum led to its use in the lining of orifices and crucibles in the manufacture of high grade optical glass.[20,21] The chemist exploited the metal's inherent unreactivity and developed platinum labware although some chemists did experiment with platinum compounds as early as the 1820's.

1.2.2 Chemical reactivity of platinum:

The first organometallic derivative, $K[Pt(C_2H_4)C\ell_3].H_2O$, was prepared by William Christopher Zeise in 1827.[22] The organometallic chemistry of platinum was dormant for the next seventy years. It awoke slowly with the formation of "Me_3PtI" and other methyl platinum compounds early in this century.[23] Despite its slow advance, the organic chemitry of platinum was growing faster than that of most other transition metals.

From 1951 and into the 1970's, the preparation of ferrocene, and the availability of X-ray crystallography, IR and NMR spectroscopy for molecular structure elucidation

led to renaissance of organometallic chemistry. Many different classes of complexes and reaction types were discovered.

Platinum has a partially filled d-orbital (electronic configuration being $[Xe]4f^{14}5d^{9}4s^{1}$) and hence forms stable compounds in various oxidation states.[20] The oxidation states 0, +2 and +4 are the most common although more recently +1, +3, +5 and +6 species have been prepared.[24] Oxidation and reduction may take place in two electron steps between the three main oxidation states and is usually accompanied by the addition or loss of two ligands. The stereochemistry of Pt(II) is varied, depending on the coordination number, while Pt(II) complexes are usually square planar and Pt(IV) complexes are octahedral (see Table 1.2).

Table 1.2 : Geometries and Oxidation States of Platinum

Oxidation State	Coordination Number	Geometry	Complex	Ref.
0	2	linear	$[Pt(PPh^{t}Bu_2)_2]$	25
	3	trigonal	$[Pt(PPh_3)_3]$	26
	4	tetrahedral	$[Pt(PF_3)_4]$	27
1	4	Square planar	$[PtCl(\mu\text{-dppm})]_2$	28
2	4	Square planar	$[PtCl_2(PMe_3)_2]$	29
	5	trigonal bipyramidal	$[Pt(SnCl_3)_5]^{-3}$	30
4	6	octahedral	$[(CH_3)_3PtI]_4$	31

Platinum forms a host of complexes with a variety of ligands in each of oxidation states. In general, Pt(0) forms stable complexes with carbonyl, isocyanides, phosphines, olefins and acetylenes whereas Pt(II) and Pt(IV) show preference for nitrogen in aliphatic amines, halogens, cyanide and ligands with heavy donors such as phosphorus, arsenic, sulfur and selenium.[20,21] Platinum in its +2 and +4 formal oxidation states also forms a number of organometallic complexes with ligands such as η^1-alkyls, aryls and vinyls, η^2-olefins and acetylenes, η^3-allylic groups, and η^5-cyclopentadienyl rings.

The NMR active Pt nucleus (33.7% ^{195}Pt, $I = \frac{1}{2}$) gives an ideal probe for determining connectivities in platinum complexes. The coupling constants between platinum and other nuclei, and in some cases the ^{195}Pt chemical shifts give invaluable aid in determining the structure.

1.2.3 Comparison of clusters and metal surfaces

The correlations that exist between metal surfaces and clusters has been discussed in detail elsewhere.[32] Metal core structures of clusters can be viewed as fragments of hexagonal close-packed, or body-centred cubic metal bulk structures. The average bond energies for ligand-metal and metal-metal bonds are comparable for specific metals in both the cluster and the transition metal surface, and the geometry of ligands bound to

clusters and to metal surfaces are similar in many instances. In addition, ligand mobility has been observed for both ligands bound to transition metal clusters and molecules bound to surfaces.

However, there are some important differences between surfaces and clusters. There is a greater degree of metal-metal interactions for surfaces, while the degree of metal-ligand interactions are larger for clusters. There is also a difference in the degree of coordinative unsaturation between the cluster state and the surface state. The metal atoms of surfaces are less coordinatively saturated, even for states in which molecules or molecular fragments are chemisorbed at the surface, than the metal atoms at the periphery of a molecular metal cluster. Metal surfaces are more reactive than metal clusters. This is due, in part, to the high degree of coordinative unsaturation of the surface which results in surfaces exhibiting a wide range and high level of catalytic activity.

1.2.4 Trinuclear clusters of Platinum

One object of the research into complexes containing triplatinum centres was to mimic the chemistry occuring on a surface. A trinuclear cluster is, perhaps, the simplest model of a surface. It allows all possible bridging species to be formed and brought close enough to react.

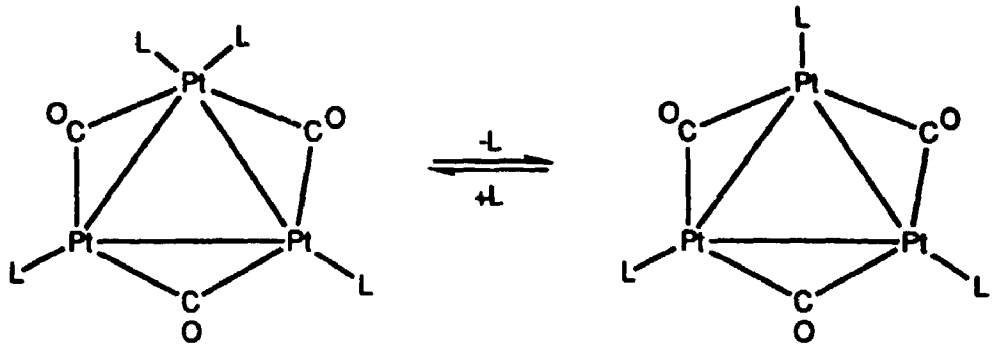

I II

Scheme 1.4 : L = Phosphine

The earliest reported triplatinum clusters of Chatt showed novel equilibrium based on the bulkiness of the phosphine (scheme 1.4).[33] The reaction of species I

$$[Pt_3(\mu\text{-}CO)_3L_4] \longrightarrow 3[Pt(CO)L_3]$$

Equation 1.6

$$[Pt_3(\mu\text{-}CO)_3L_4] \xrightarrow{2L,\ 3CO} 3[Pt(CO)_2L_2]$$

Equation 1.7

with excess phosphine or carbonyl ligands, however, leads to cluster degradation and formation of monomeric products, equations 1.6 and 1.7.

Farrar and coworkers have shown[34] that reaction of species II with various reagents also results in degradation products, scheme 1.5.

The problem of cluster degradation is overcome by using appropriate bridging ligands to bind the trinuclear

cluster together. The most widely used bridging ligand in transition metal chemistry is the diphosphine ligand,

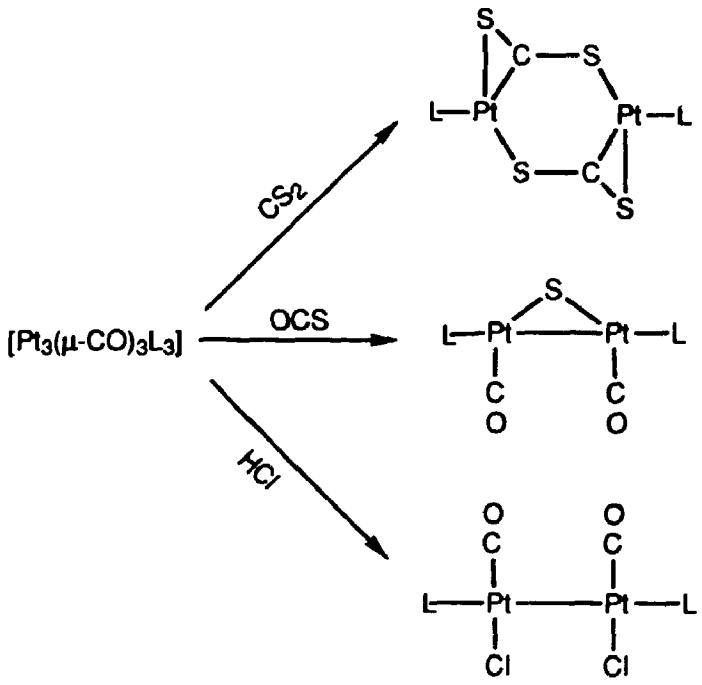

Scheme 1.5

bis(diphenyl phosphino)methane, (dppm), and its chemistry has been reviewed.[35] Recently, a triplatinum cluster with three bridging dppm ligands has been prepared in this laboratory; $[Pt_3(\mu_3\text{-}H)(\mu\text{-}dppm)_3](PF_6)$, 1. This cation is a 42 electron, coordinatively unsaturated cluster and, as has been argued,[32] should be able to mimic the reactions occurring at a metal surface. It is indeed the case that 1 sucessfully mimics the Pt(111) surface.[36] Triplatinum clusters with 42, 44 and 46 electron counts have all been prepared, although 42 and 46 electron species are the most

common. The molecular orbital theory which predicts the geometry and the number of valence electrons for stabilized triplatinum clusters is discussed in the following section.

1.2.5 Molecular orbital theory of a trinuclear cluster

It has been proposed that D_{3h} trinuclear metal clusters are the inorganic equivalent of cyclopropane.[37] The isolobal connection between a d^8-ML_4 fragment and a CH_2 fragment has been discussed in Hoffmann's Nobel lecture paper in 1982.[37] He has extended the isolobal analogy to show a relationship between d^n-ML_4 and d^{n+2}-ML_2 (scheme 1.6).

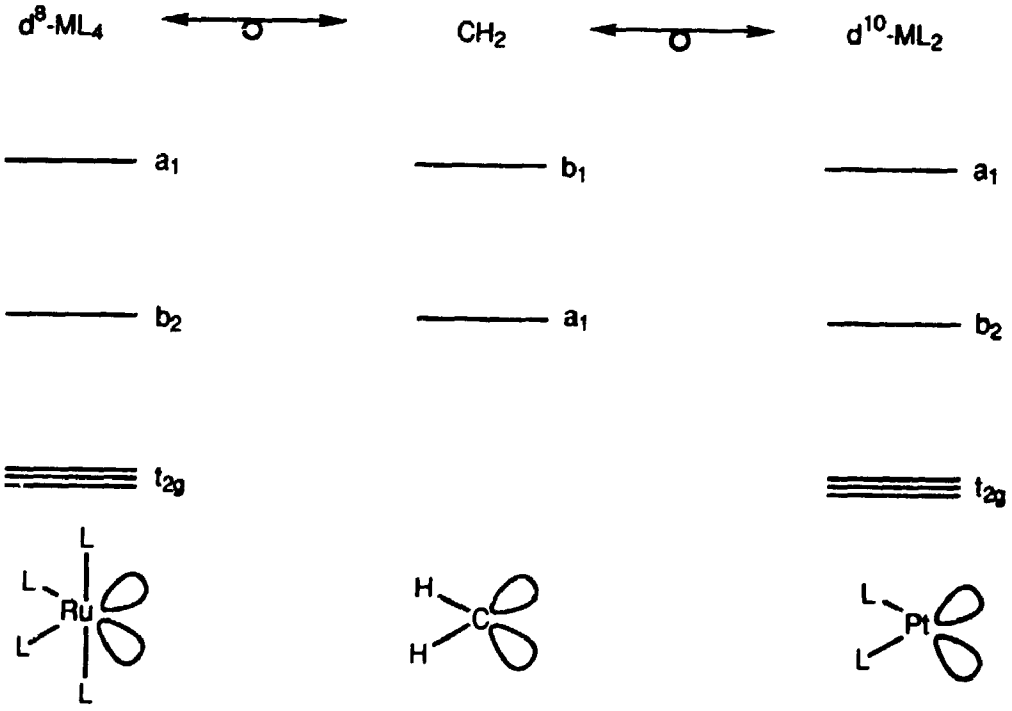

Scheme 1.6 : Isolobal analogy

The CH_2 is derived from tetrahedral geometry while the PtL_2 fragment is derived from square planar geometry. This leads to a difference in relative energies of the b_2 and a_1 orbitals. The isolobal analogy predicts the assembly of three ML_2 fragments to form, using Mingos's terminology[38], a latitudinal trimer, $[Pt_3L_6]$. This means that the ligands are in the plane of platinum triangle. This predicted geometry is observed in the 42 electron cluster, 1. There are no known $[Pt_3L_6]$ species with just terminal ligands. Usually one gets three bridging and three terminal ligands which effectively stabilizes the a_1 orbital, and increases HOMO-LUMO gap.[39]

Mealli has examined the MO interactions of the $[Pt_3L_6]$ species with μ_3-CO^{2+} (CO^{2+} is isolobal to H^+).[39] The ligands, L, he has chosen for his calculation are carbonyls, so the MO's obtained will be similar in that they will have the correct ordering but the actual energies may differ slightly. Thus, with a valence electron count of 42, the μ_3-CO ligand stabilizes the cluster. The MO interaction of the $[Pt_3L_6]$ is discussed in detail in chapter 5.

If two or more electrons are added to the valence shells of these clusters the electrons can enter the non-bonding platinum orbital (p_z) on any of the platinum atoms, or the anti-bonding orbitals. The addition of 4 electrons to the molecular orbitals of $[Pt_3L_6]$ gives a valence count of 46 and fills two anti-bonding orbitals.

Many stable 46 electron species are found experimentally and indeed contain only a single metal-metal bond.[40]

1.3 HETERONUCLEAR CLUSTERS CONTAINING PLATINUM AND GOLD

The introduction of a hetero metal unit into a cluster would probably increase the reactivity because of the inherent polarity in mixed metal bonds. The class of heteronuclear complexes which has received much recent interest are those with Pt-Au bonds and their chemistry has been reviewed[41]. Most of such compounds are clusters containing $PtAu_2$, Pt_2Au, Pt_2Au_2, Pt_3Au, Pt_3Au_2, $PtAu_6$, $PtAu_7$ and $PtAu_8$ units, all having been prepared since 1984.[41]

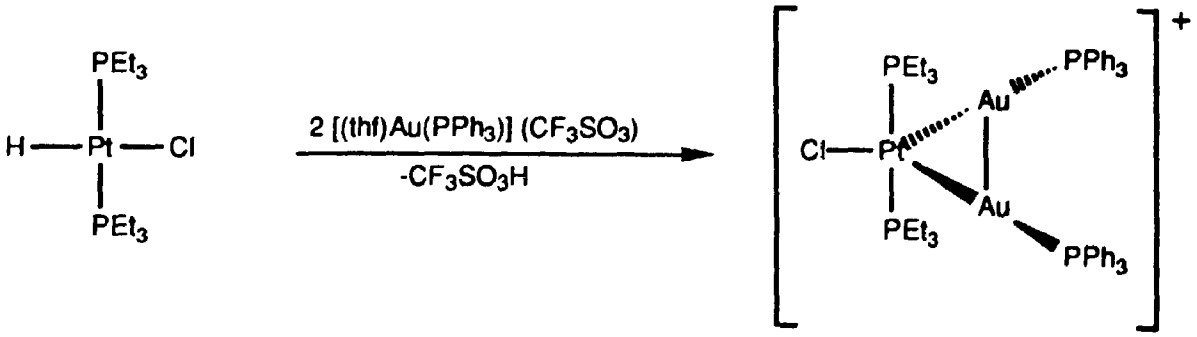

Equation 1.8

Most of these compounds have been prepared by reactions of Ph_3PAu^+ with a platinum hydride or an electron-rich cluster of platinum and are based on the

isolobal relationship for H^+ and Ph_3PAu^+.[42] Some complexes are shown in equations 1.8 and 1.9.

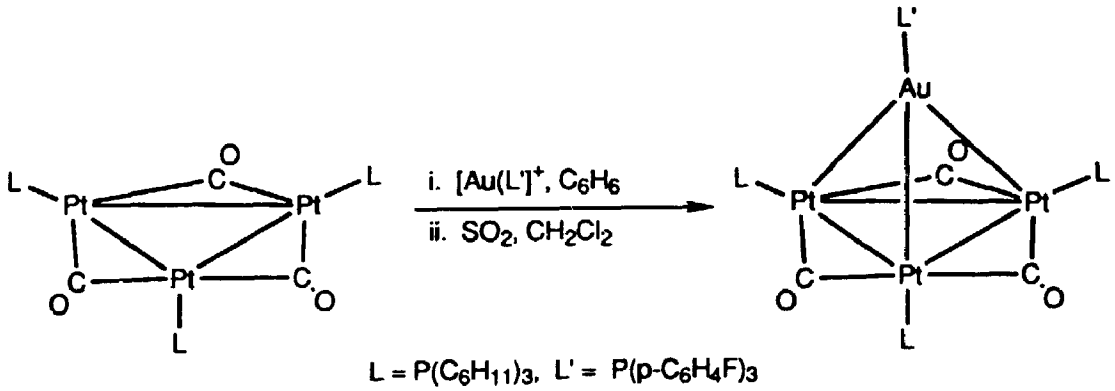

L = $P(C_6H_{11})_3$, L' = $P(p\text{-}C_6H_4F)_3$

Equation 1.9

In most of these clusters the L→Au groups are μ_2–bridging an edge or μ_3-capping a face but μ_4 and μ_5 situations are also encountered in higher nuclearity clusters.

In clusters containing one L→Au fragment, the gold unit generally occupies the edge-bridging or face-capping position of H in the corresponding hydrido cluster.[43] In cases where the location of the H atom of an hydrido cluster could not be directly found by diffraction methods, the postition of Ph_3P-Au fragment may serve to predict the H bonding site.

According to electron counting rules[44] relating to bonding, the 12 electron $[L\text{-}Au]^+$ fragment contributes no electron to cluster bonding. As a result, its incorporation into such a system is not expected to alter

its structure. When two or more L→Au fragments are present in a cluster, the isolobal analogy cannot be applied for predicting the structures since Au-Au bonding interactions between adjacent groups become significant.

The principle that seems to govern the build-up of the L→Au unit containing clusters is that the first L→Au unit occupies the position of H in the corresponding hydrido complex, taking into account the steric factors. The successive gold atoms add to the least hindered triangular faces next to existing gold atoms. This leads to a compact arrangement consisting of face-sharing tetrahedra with as many adjacent gold atoms as possible.[45] Exceptions have been noted[46] to this general trend.

Mingos and coworkers have discussed the bonding in several gold-platinum cluster compounds on the basis of semi-empirical molecular orbital calculations.[47] The extent of Pt-Au bonding has been quantified in terms of reduced overlap populations.

Platinum-gold cluster complexes also exhibit interesting reactivity. For example, CO reacts with $[PtAu_8(PPh_3)_8]^{2+}$ to give $[PtAu_8(PPh_3)_8(CO)]^{2+}$. During this reaction an interesting change occurs in the cluster geometry[48], as shown in equation 1.10.

The starting material contains a centred crown structure with the Pt atom in the middle surrounded by eight gold atoms. On reacting with the carbonyl ligand, the Pt atom is lifted out of the hole to the surface of the

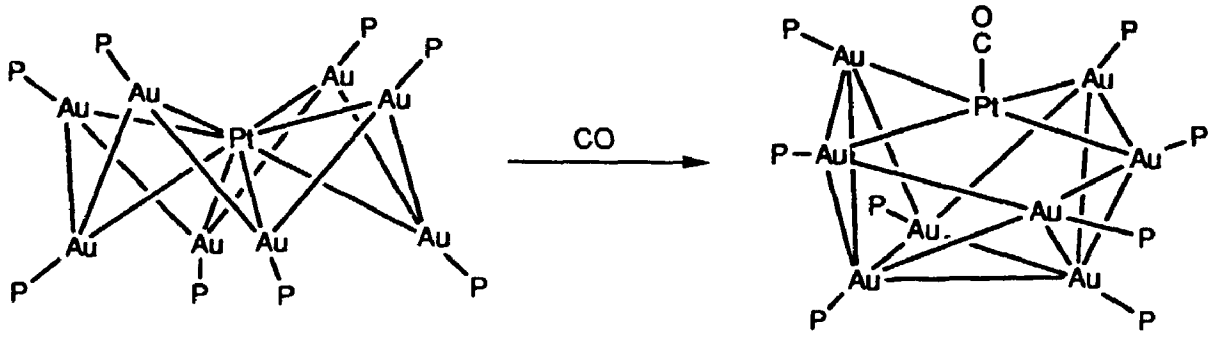

Equation 1.10

crown. The resulting structure is similar to those observed in Pt-Au alloys. The central platinum is surrounded by eight Au atoms in a structure similar to two (100) planes of an f.c.c.packing.[48]

There have been relatively few investigations on the use of transition metal-gold complexes as homogeneous catalysts. Some studies indicate that the addition of $AuPPh_3^+$ unit to a transition metal complex may lead to an increase in both reactivity and selectivity. For example, $[AuRu_4(H)_3(CO)_{12}(PPh_3)]$ is more active and selective than the parent complex, $[Ru_4(H)_4(CO)_{12}]$, for the catalytic isomerization of 1-pentene at 35°C.[49] More work is needed in this area to understand why the gold enhances the reactivity in such systems.

1.4 SCOPE OF THE THESIS:

This thesis deals with the study of homo- and heteronuclear clusters of platinum and gold.

Initially, the synthesis and characterization of some homo-nuclear gold complexes with various diphosphines will be considered. The diphosphine ligands, $CH_2(PR_2)_2$, used in this study are dppm (R = Ph), dmpm (R = Me) and dmopm (R = OMe). The mechanism of formation of the complexes and their structures will also be discussed. This work is important in that the rational synthesis of metal clusters is rarely presented due to the general lack of mechanistic details in the synthesis itself.[50]

This thesis is also concerned with the reactions between the 42 electron, cationic cluster, $[Pt_3(\mu_3\text{-}H)(\mu\text{-}dppm)_3](PF_6)$, 1, and various main group reagents. The impetus for this study was the similarity of 1 to the Pt(111) surface. Various reagents were reacted with the cluster and, whenever possible, the reactions were compared to the analogous surface reaction with the hope of gaining some insight on the kind of species formed on a platinum surface. These clusters also exhibit a novel chemistry in their own right.

The reagents used were acids such as CF_3COOH and aq. HPF_6, phosphines and phosphites, gold and silver cations. The products were fully characterized using spectroscopic techniques and in some cases X-ray crystallographic studies were carried out. In addition the

characterization and a study of the reactivity of some novel tetraplatinum clusters were also carried out.

1.5 REFERENCES

1. R.J. Puddephatt, " The chemistry of gold", Elsevier scientific publishing Co., Oxford, (1978). Ch. 1.

2. P.G. Jones, *Gold Bull.*, 14 (1981) 102; 14 (1981) 159; 16 (1983) 114; 19 (1986) 46.

3. R.C. Elder, E.H.K. Zeiher, M. Onady, R.R. Whittle, *J. Chem. Soc. Chem. Commun.*, (1981) 900

4. D.M.P. Mingos, *Pure and Appl. Chem.*, 52 (1980) 705.

5. R.W. Baker, P. Pauling, *J. Chem. Soc. Dalton Trans.*, (1972) 2264.

6. N.C. Baenziger, K.M. Dittemore, J.R. Doyle, *Inorg. Chem.*, 13 (1974) 805

7. H. Schmidbaur, J.R. Mandl, A. Frank, G. Huttner, *Chem. Ber.*, 109 (1976) 466

8. R.W. Baker, P. Pauling, *J. Chem. Soc. Chem. Comm.*, (1969) 745.

9. W.T. Robinson, E. Sinn, *J. Chem. Soc. Dalton Trans.*, (1975) 726

10. V.F. Duckworth, N.C. Stephenson, *Inorg. Chem.*, 8 (1969) 166

11. K.Leary, A. Zalkin, N. Bartlett, *Inorg. Chem.*, 14 (1974) 775

12. R. J. Puddephatt, I. Treurnicht, *J. Organomet. Chem.*, 319 (1987) 129

13. L. Malatesta, *Gold Bull.*, 8(2) (1975) 48

14. C.E. Briant, B.R.C. Theobold, J.W. White, L.K. Bell, D.M.P. Mingos, *J. Chem. Soc. Chem. Commun.*, (1981) 201

15. F.A. Vollenbroek, D.C.P. Bouten, J.M. Trooster, J.P. Van der Berg, J.J. Bour, *Inorg. Chem.*, 19 (1980) 2685

16. D.M.P. Mingos, *J. Chem. Soc. Dalton Trans.*, (1976) 1163; D.G. Evans, D.M.P. Mingos, *J. Organometal. Chem.*, 232 (1982) 171.

17. K.P. Hall, B.R.C. Theobold, D.I. Gilmour, A.J. Welch, D.M.P. Mingos, *J. Chem. Soc. Chem. Commun.*, (1982) 528

18. K.P. Hall, D.M.P. Mingos, *Prog. Inorg. Chem.*, 32 (1984) 237; J.J. Steggerda, J.J. Bour, J.W.A. Van der Welden,

Recl.Trav. Chim. Pays-Bas.,101 (1982) 164;
R.J. Puddephatt, In "Comprehensive coordination chemistry, Vol. 5", Ed. by G.Wilkinson, J.A. McCleverty R.D. Gillard, Pergamon press, (1987), P.861

19. D.M.P. Mingos, *Gold Bull.*, 17(1) (1984) 5.

20. F.R. Hartley, "The Chemistry of Platinum and Palladium", Applied Science, London, (1973), Ch. 1.

21. F.R. Hartley, In "Comprehensive organometallic chemistry", E.W. Abel, F.G.A. Stone, G. Wilkinson, Eds Pergamon Press (1984)

22 W.C. Zeise, *Mag. Parm.*, 35, (1830) 105; *Pogg. Ann.*, 21 (1831) 497

23 W.J. Pope, S.J. Peachy, *Proc. Chem. Soc.*, 95 (1909) 571

24 B.R. Steele, K. Vrieze, *Trans. Met. Chem.*, 2 (1977) 169 J. Kuyper, K. Vrieze, *ibid*, 1 (1976) 208; J.D. Schagen, A.R. Overbeek, H. Schenk, *Inorg. Chem.*, 17 (1978) 1938; N. Bartlett, F. Einstein, D.F. Stewart, J. Trotter, *J. Chem. Soc. Chem. Commun.*, (1966) 550; N. Bartlett, *Proc. Chem. Soc.*, (1962) 218; E. Weinstock, H.H Claasen, J.G. Malm, *J. Am. Chem. Soc.*, 79 (1957) 5832; B. Weinstock, J.G. Malm, E.E. Weaver, *J. Am. Chem. Soc.*, 83 (1961) 431

25 S. Otsuka, T. Yoshida, M. Matsumoto, K. Nakatsu, *J. Am. Chem. Soc.*, 98 (1976) 5850

26 V.G. Albano, P.L. Bellon, V. Scatturin, *J. Chem. Soc. Chem. Commun.*, (1966) 507

27 J.C. Mariott, J.A. Salthouse, M.J. Ware, J.M. Freeman, *J. Chem. Soc. Chem. Commun.*, (1970) 595

28 M.P. Brown, R.J. Puddephatt, M. Rashidi, Lj. Manojlovic -Muir, K.W. Muir, T. Solomun, K.R. Seddon, *Inorg. Chim. Acta*, 23 (1977) L33

29 G.G. Messmer, E.L. Amma, J.A. Ibers, *Inorg. Chem.*, 6 (1967) 725

30 R.D. Cramer, R.V. Lindsey, C.T. Prewitt, U.G. Stolberg *J. Am. Chem. Soc.*, 87 (1965) 658

31 G. Donney, L.B. Coleman, N.G. Krieghoff, D.O. Cowan *Acta. Cryst.*, B24, (1968) 157

32 E.L. Muetterties, J.N. Rhodin, E. Band, C.F. Brucker, W.R. Pretzer, *Chem. Rev.*, 79 (1971) and references therein

33 J. Chatt, P. Chini, *J. Chem. Soc. (A)*, (1970) 1538; A. Moor, P.S. Pregosin, C.M. Venanzi, *Inorg. Chim. Acta*, 48 (1981) 153; 61 (1982) 135

34 C.S. Browning, D.H. Farrar, R.R. Gukathasan, S.A. Morris *Organometallics*, 4 (1985) 1750; D.H. Farrar, R.R. Gukathasan, S.A. Morris, *Inorg. Chem.*, 23, (1984) 3258; C. Coutre, D.H. Farrar, D.S. Fisher, R.R. Gukathasan, *Organometallics*, 4 (1987) 532

35 R.J. Puddephatt, *Chem. Soc. Rev.*, 12 (1983) 99; B. Chaudret, B. Delavaux, R. poilblanc, *Coord. Chem. Rev.*, 86 (1988) 191

36 M. Rashidi, R.J. Puddephatt, *J. Am. Chem. soc.*, 108 (1986) 7111; *Organometallics*, 7 (1988) 1636

37 R. Hoffman, *Angew. Chem. Int. Ed. Engl.*, 21 (1982) 71

38 D.G. Evans, D.M.P. Mingos, *J. Organomet. Chem.*, 240 (1982) 321

39 C. Mealli, *J. Am. Chem. Soc.*, 107 (1985) 2245

40 N. Hadj-Bagheri, R.J. Puddephatt, *J. Chem. Soc. Chem. Commun.*, (1987) 1269; M.C. Jennings, N.C. Payne, R.J. Puddephatt, *Inorg. Chem.*, 26 (1987) 3776

41 K.P. Hall, D.M.P. Mingos, *Prog. Inorg. Chem.*, 32 (1984) 237; P. Braunstein, J. Rose, *Gold Bull.*, 18 (1985) 17; A.M. Mueting, W. Bos, B.D. Alexander, P.D. Boyle, J.A. Casalnuovo, S. Balaban, L.N. Ito, S.M. Johnson, L.H. Pignolet, *New J. Chem.*, 12 (1988) 505 and references therein

42 D.G. Evans, D.M.P. Mingos, *J. Organomet. Chem.*, 232 (1982) 171; J.W. Lauher, K.Wald, *J. Am. Chem. Soc.*, 103 (1981) 7648

43 R. Ramachandran, N.C. Payne, R.J. Puddephatt, *J. Chem. Soc. Chem. Commun.*, (1988) 128

44 K. Wade, *Adv. Inorg. Chem. Radiochem.*, 18 (1976) 67; D.M.P. Mingos, 'Comprehensive organometallic chemistry, Vol. III', F.G.A. Stone, J. Wilkinson, Eds., Pergamon, Oxford, P.1

45 M.I. Bruce, B.K. Nicholson, *Organometallics*, 3 (1984) 101

46 B.F.G. Johnson, J. Lewis, W.J.H. Nelson, P.R. Raithby, M.D. Vargas, *J. Chem. Soc. Chem. Commun.*, (9183) 608

47 D.I. Gilmour, D.M.P. Mingos, *J. Organomet. Chem.*, 302 (1986) 127

48 R.P.F. Kanters, P.P.J. Schlebos, J.J. Bour, W.P. Bosman H.J. Behm, J.J. Steggerda, *Inorg. Chem.*, 27 (1988) 4034

49 J.Evans, G. Jingxing, *J. Chem. Soc. Chem. Commun.*, (1985) 39

50 W. Gladfelter, G.L. Geoffroy, *Adv. Organomet. Chem.*, 18 (1980) 209

CHAPTER 2

GOLD(I) DIMERS. THE SYNTHESIS AND REACTIONS OF [t-BuC≡C-Au(dmpm-P)]$_2$ AND THE CRYSTAL AND MOLECULAR STRUCTURES OF [Au$_2$(μ-dmpm)$_2$]X$_2$.2H$_2$O, X = Cℓ, I

2.1 INTRODUCTION

Diphosphine ligands such as $CH_2(PR_2)_2$ [R = Ph, dppm, R = Me, dmpm]; $CH_2{=}C(PPh_2)_2$ (vdpp), $EtOCH_2CH(PPh_2)_2$ (edpp) and $\overline{CH_2CH_2C}(PPh_2)_2$ (cdpp) are commonly used to bind two metal centres in close proximity[12-16]. A number of gold complexes have been

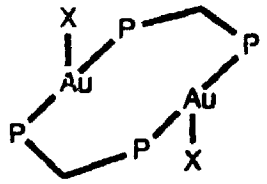

1a, PP = dppm, X = Cl
1b, PP = dppm, X = Br
1c, PP = vdpp, X = Cl

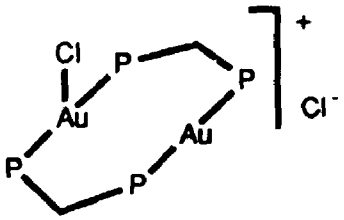

2, PP = cdpp

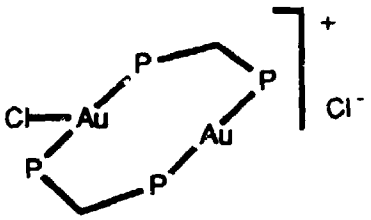

3, PP = edpp

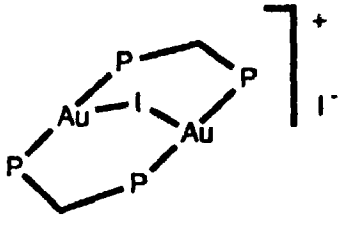

4, PP = dppm

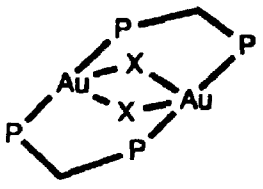

5, PP = dmpm, X = Cl

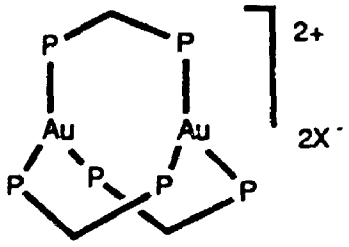

7, PP = dmpm

Scheme 2.1

synthesized using these ligands. Unlike the usual two-coordinate, linear geometry in Au(I) complexes[12], the complexes prepared using these ligands tend to be three coordinate. Some complexes containing dppm and related ligands whose structures have been determined by X-ray crystallography are shown in scheme 2.1, 1-4 [13-16].

In complexes 1 and 4 both gold(I) centres are 3-coordinate, but the former has only terminal halides and is neutral while the latter has a bridging halide and is cationic. Complexes 2 and 3 each have one 3-coordinate and one 2-coordinate gold(I) centre, but in 2 the chloride ligand is approximately perpendicular to the 8-membered $Au_2P_4C_2$ ring whereas in 3 the chloride is approximately coplanar with this ring. These changes in the coordination environment have a major effect in the ^{197}Au Mossbauer spectra[14]. These structures, 1-4, provide good examples of surprisingly large structural effects originating from relatively small changes in the ligand geometry (e.g. 1a, 1b, 4)[12-16]. The reasons for the structures being different are not known, but the energy differences are small and the unsymmetrical complexes 2 and 3 are fluxional in solution[14,15].

In these complexes, the gold-halogen bonds are long and presumably weak but are still strong enough to give a considerable distortion of the PAuP angle away from the normal 180° found for 2-coordinate gold(I). Gold(I) coordination geometry seems to be particularly sensitive to

these second order interactions, since ligands present in excess of coordination number 2 are structurally effective, although only weakly bonded.

We were interested in studying how the coordinating ability of the ligand X (*t*-BuC≡C, Cℓ, I) and the steric bulk of the diphosphine ligand affected the structures of complexes of the formula $(AuX(R_2PCH_2PR_2))_n$ and chose to investigate the molecules containing the ligand $Me_2PCH_2PMe_2$, dmpm, which is less bulky than the phenyl substituted ligands dppm, vdpp and cdpp. Despite this lesser steric effect, the X-ray analyses revealed that the molecular structures of the gold(I) chloride and iodide derivatives possess the ionic structure $[Au_2(\mu\text{-dmpm})_2]X_2.2H_2O$, where X = Cℓ, I (5a and 5b respectively)[18-20]. To date, we have been unable to obtain suitable crystals of the acetylide species for crystallographic analysis. The acetylide complex [*t*-BuC≡C-Au(dmpm-P)], 6a, undergoes a fluxional process involving a three coordinate Au(I) centre. Complex 6a dimerizes by a first-order process in chlorinated solvents, with substitution of the acetylide ligand by chloride ion, to form $[Au_2(\mu\text{-dmpm})_2]Cℓ_2.2H_2O$, 5a.

2.2 EXPERIMENTAL

All experiments were carried out under a dry, oxygen free dinitrogen atmosphere.

2.2.1 [AuCℓ(SMe$_2$)]

Solid gold (10 g) was dissolved in aqua regia (200 mL) and diluted by the addition of water. On dropwise addition of SMe$_2$ (40 mL) to this solution, a yellow precipitate of [AuCℓ(SMe$_2$)] separated out. Recrystallization in $CH_2C\ell_2$ yielded a white crystalline solid. Yield: 85%

2.2.2 [AuC≡Ct-Bu]

The acetylide complex [AuC≡C*t*-Bu] has been synthesized by the reaction of *t*-BuCCH with an aqueous solution of Au(I)[22]. We found a different synthetic route which gave [AuC≡C*t*-Bu] in good yields. To a stirred solution of [AuCℓ(SMe$_2$)] (6.0 g, 20.4 mmol) in diethyl ether at -80°C, an ethereal solution of *t*-BuCCLi (45 mmol) was added slowly. On warming the solution to room temperature over a period of 1.5 h, and hydrolysing the excess lithium reagent by adding saturated $NH_4C\ell$ solution, the ether layer turned yellow. The ether layer was separated and dried over $MgSO_4$. On removal of solvent, a pale yellow solid was obtained. Yield: 80%. Anal. calcd. for C_6H_9Au: C, 25.9; H,3.3%. Found: C,25.7; H,3.3%. ^{1}H NMR (in acetone-d_6) δ 1.25 [s, t-Bu]. IR (Nujol): 2000, 1972 cm^{-1} [ν(C≡C)].

2.2.3 [Au(C≡C*t*-Bu)(dmpm-P)], 6a

To a yellow suspension of [AuC≡C*t*-Bu] (0.350 g,

1.259 mmol) in acetone (10 mL) was added dmpm (0.171 g, 1.257 mmol). An instant colour change from a yellow suspension to a white powder was observed. The solution was stirred for 2 h. The white solid was filtered, dried under vacuum, and identified as [Au(C≡C*t*-Bu)(dmpm-P)]. Yield: 72%. Mp: 165°C (dec); IR (nujol): 2100 cm^{-1} [ν(C≡C)]; ^1H NMR in $CDC\ell_3$ at 20°C: δ1.19 (s, 9H, *t*-Bu); 1.77 (br.s, 12H, MeP); 2.93 (s, 2H, PCH_2P); $^{31}P\{^1H\}$ NMR: δ3.8 (br.s, P). ^1H NMR in $CD_2C\ell_2$ at -80°C: δ1.08 (s, 9H, *t*-Bu); 1.70 and 1.88 (br.s, each 6H, MeP); 3.1 (m, PCH_2P). Anal. Calcd. for $C_{11}H_{23}AuP_2$: C, 31.9; H, 5.60. Found: C, 29.8; H, 5.47. MS: Calcd for $C_{11}H_{23}AuP_2$: m/e = 414; Found m/e = 414; 333 (P - C≡C*t*-Bu).

2.2.4 [Au(C≡C*t*-Bu)(dppm-P)], 6b

[AuC≡C*t*-Bu] (0.256 g, 0.922 mmol) was suspended in $CH_2C\ell_2$ (3 mL). To this was added dppm (0.354 g, 0.922 mmol) in $CH_2C\ell_2$ (5 mL). After 3 h. stirring, the product was precipitated by slow addition of pentane. The product was washed with diethyl ether and dried under vacuum. Yield: 68%. Mp: 99°C (dec); ^1H NMR in $CD_2C\ell_2$ at 20°C: δ1.25 (s, 9H, *t*-Bu); 3.25 (br.s, 2H, PCH_2P); 7.31 to 7.51 (m, 20H, PC_6H_5); $^{31}P\{^1H\}$ NMR at 20°C: -Au-P^a P^b; δ23.35 (br.s; P^a); -27.20 (br.s, P^b). MS calcd for $C_{30}H_{29}AuP_2$: m/e = 662; Found: m/e = 662; 384 (P - AuC≡C*t*-Bu); 278 (P - dppm).

2.2.5 $[Au_2(\mu\text{-dmpm})_2]Cl_2 \cdot 2H_2O$, 5a

This complex was obtained by two different procedures.

(a) To a yellow suspension of [AuC≡Ct-Bu] (0.345 g, 1.241 mmol) in CH_2Cl_2 (10 mL) was added dmpm (0.169 g, 1.241 mmol). Immediately the solution turned milky. The solution was stirred for 3 h. On slow evaporation of solvent, colourless crystals were obtained which were characterized as $[Au_2(\mu\text{-dmpm})_2]Cl_2 \cdot 2H_2O$. Yield: 75%. Mp: 228°C (dec); ^1H NMR in CD_2Cl_2 at 20°C: δ1.84 (m, $^2J(PH) + {}^4J(PH) = 7$, 24H, MeP); 2.98 (quintuplet, $^2J(PH) + {}^4J(PH) = 10$, 4H, PCH_2P); $^{31}P(^1H)$ NMR at 20°C: δ5.6 (s, P). Anal. Calcd for $C_{10}H_{32}Au_2Cl_2O_2P_4$: C, 15.53; H, 4.17. Found: C, 15.94; H, 3.85.

(b) To a solution of $[AuCl(SMe_2)]$ (0.305 g, 1.037 mmol) in CH_2Cl_2 (6 mL) was added dmpm (0.141 g, 1.037 mmol) and the mixture was stirred for 3 h. On removal of solvents, a white solid was isolated. Yield: 70%. Anal. Calcd. for $C_{10}H_{32}Au_2Cl_2O_2P_4$: C, 15.53; H, 4.17. Found: C, 15.30; H, 3.96.

2.2.6 $[Au_2(\mu\text{-dmpm})_2]I_2 \cdot 2H_2O$, 5b

A solution of NaI (0.051 g, 0.340 mmol) in acetone (5 mL) was added to a suspension of $[AuCl(SMe_2)]$ (0.103 g, 0.349 mmol) dissolved in acetone (5 mL). The contents were stirred at -78°C for 0.5 h. $[AuI(SMe_2)]$ was then filtered into a Schlenck tube containing dmpm (0.049 g, 0.360 mmol)

and the contents were stirred at -78°C for 3 h. A pale yellow solid turning white on exposure to air was isolated. The product was washed with cyclohexane and dried under vacuum. Recrystallization in water gave colourless crystals. Yield: 60%. Mp: 233°C (dec); ^{1}H NMR in $CD_2C\ell_2$ at 20°C: δ1.71 (s, 24H, MeP); 2.44 (br.m, $^2J(PH) + {}^4J(PH) = 8$, 4H, PCH_2P); $^{31}P\{^1H\}$ NMR at 20°C: δ-7.8 (s, P). Anal. Calcd. for $C_{10}H_{32}Au_2I_2O_2P_4$: C, 12.56; H, 3.37. Found: C, 12.61; H, 3.08. MS: m/e = 793 [P - (I, $-2H_2O$)], 657 [P - (dmpm, I)].

2.2.7 $[Au_2(\mu\text{-dmpm})_3]Cl_2$, 7a

To a solution of $[AuC\ell(SMe_2)]$ (0.511 g, 1.736 mmol) in $CH_2C\ell_2$ (10 mL) was added dmpm (0.354 g, 2.604 mmol). The contents were stirred for 3 h. A yellow solid was obtained which was filtered and dried under vacuum. Yield: 69%. ^{1}H NMR in $CD_2C\ell_2$ at 20°C: δ1.76 (m, $^2J(PH) + {}^4J(PH) = 8$, 36H, MeP); 2.97 (br.m, $^2J(PH) + {}^4J(PH) = 12$, 6H, PCH_2P). $^{31}P\{^1H\}$ NMR at 20°C: δ3.24 (s, AuP). Anal. Calcd. for $C_{15}H_{42}Au_2C\ell_2P_6$: C, 20.63; H, 4.85. Found: C, 20.30; H, 4.86.

2.2.8 $[Au_2(\mu\text{-dmpm})_3]I_2$, 7b

The work-up procedure was similar to that of $[Au_2(\mu\text{-dmpm})_2]I_2$. The stoichiometries of the reagents used were as follows: NaI (0.070 g, 0.457 mmol). $[AuC\ell(SMe_2)]$ (0.103 g, 0.349 mmol) and dmpm (0.070 g, 0.515 mmol).

Yield: 73%. Mp: 290°C (dec). ^{1}H NMR in $CD_2C\ell_2$ at 20°C: δ1.71 (s, 36H, MeP); 2.40 (br.s, 6H, PCH_2P): $^{31}P\{^1H\}$ NMR at 20°C: δ -8.5 (s, AuP). Anal. Calcd. for $C_{15}H_{42}Au_2I_2P_6$: C, 17.06; H, 4.01. Found: C, 16.79; H, 4.00.

2.2.9 Kinetic Studies

The reaction kinetics of the conversion of the acetylide product 6a to chloride product 5a was followed by monitoring the decay of the MLCT band of 6a. [AuC≡Ct-Bu)(dmpm-P)] (0.0083 g, $2x10^{-5}$ M) was dissolved in $CHC\ell_3$ (10 mL) and was transferred to a 1 cm cuvette and placed in a cell compartment, maintained at 25°C. The absorbance (at λ = 282 nm) was recorded at 20 min intervals for 5 h. Computer treatment of the data showed good first-order kinetics, with the rate constant, $k = 7.9x10^{-5}$ s^{-1}.

2.3 X-RAY DIFFRACTION STUDIES OF $[Au_2(\mu\text{-dmpm})_2]C\ell_2.2H_2O$, 5a

2.3.1 Photographic examination

The first phase of a single crystal X-ray diffraction study is the determination of the symmetry of the crystal lattice, the unit cell constants and the number of formula units per cell. A photographic examination employing Weissenberg and precession techniques was undertaken to provide this information. The theoretical basis behind these methods are covered in many texts[1] and

will only be dealt with in a brief fashion.

Colorless crystals of 5a were provided by Dr. Ilse Treurnicht of this department. They were obtained by slow diffusion of pentane into a chloroform solution of 6a at room temperature. The crystals were observed under binocular and polarising microscopes to find a suitable crystal for photographic study. At this stage, several possible defects, such as macroscopic twinning or poor mosaicity can be identified. A crystal was chosen such that it was transparent, with well formed faces and displaying sharp extinctions when rotated under plane polarized light. It was mounted such that the long dimension of the crystal was roughly coincident with the rotation axis of the goniometer head. It was along this dimension that the crystal extinguished plane polarized light. The goniometer head was then transferred to a Weissenberg camera and the crystal was accurately aligned by taking a series of setting photographs. Zero, first and second-level Weissenberg photographs were recorded. These photographs revealed, as expected from Friedel's law, a centre of symmetry, but no additional symmetry, suggesting that the crystal belonged to the triclinic system. The crystal was then transferred onto a precession camera. The precession technique involves rotation of the crystal about a reciprocal axis. Thus, a reorientation of the crystal was needed such that the real axis was replaced by the reciprocal axis as the rotation axis. The crystal had a

face nearly perpendicular to the direct axis. On the assumption that this was the face associated with the real axis, the crystal was reoriented on an optical goniometer such that this face was perpendicular to the camera rotation axis. Again, a series of setting photographs was taken to align the crystal more accurately about the reciprocal axis. Precession photographs of the zero, first and second level nets were recorded. From the photographs the following approximate unit cell constants were deduced.

$a = 12.9$ Å $\quad \alpha = 82.8°$

$b = 10.0$ Å $\quad \beta = 89.4°$

$c = 9.17$ Å $\quad \gamma = 65.7°$

Volume = 1072 Å^3

The presence of systematic extinctions h+k+l = 2n in these photographs indicated that the photographic cell was I-centered. Using the program TRACER[4], this I-centered cell was reduced to a primitive cell. The reduced primitive cell had the following cell parameters;

$a = 8.14$ Å $\quad \alpha = 103.7°$

$b = 10.0$ Å $\quad \beta = 108.3°$

$c = 7.49$ Å $\quad \gamma = 69.0°$

Volume = 536.1 Å^3

There were no other systematic absences other than the one stated above, and this suggests that the crystal belongs to triclinic system, with possible space groups P1, No.1, and $P\bar{1}$, No.2 [2]. A search for additional symmetry at 10° intervals of precession camera dial settings was

unsuccessful.

The density of the crystal was determined by flotation in a mixture of bromoform and methylene chloride, and was found to be 2.283(1) g cm^{-3}. This datum indicates one formula unit of $[Au_2(\mu\text{-dmpm})_2]C\ell_2$ per cell, for which the calculated density is 2.264 g cm^{-3}. In which case the complex has a crystallographically imposed centre of symmetry (in space group $P\bar{1}$), or is a discrete salt without any symmetry constraints in space group P1. The crystal data obtained in the preliminary investigation are summarized in Table 2.1. The origin of cell constants presented in the table is explained in the following section 2.3.2.

2.3.2 Collection and reduction of intensity data

2.3.2.1 Data collection

Having determined the cell dimensions and space group, the next stage in a structural analysis is the collection of intensity data. A crystal of approximate dimensions 0.25 x 0.12 x 0.42mm^3 was selected, glued (using epoxy resin) to a glass fibre and transferred onto an Enraf-Nonius CAD4F diffractometer. Monochromatic (graphite, 002, $2\Theta = 12.2^\circ$) MoK_α radiation ($\lambda = 0.71073$ Å) was used at 22°C. The crystal, mounted in a random orientation, was positioned optically in the centre of the X-ray beam. The Enraf-Nonius routines[3] were then used to determine an orientation matrix and accurate cell

dimensions as follows. A Φ rotation photograph of the crystal was taken, at $\kappa = 0°$ and the (X,Y) coordinates of twenty one reflections were measured. Setting angles were determined using SCAN routine[3]. Of these, one was used to optimize the crystal centering using the ALIGN routine[3]. The reflections were centred using the routine SETANG[3].

An orientation matrix was generated and these reflections were indexed using the routine INDEX[3]. The mosaicity of the crystal[5] was examined by recording ω-scans of three low-angle, intense reflections, using a wide-open counter[3]. These scans, varying in widths at half-height from 0.10 to 0.115°, indicated that the crystal was single and suitable for data collection. Program TRACER[4] and the routine TRANS[3], were used to obtain the reduced cell and the standard setting[2]. Several cycles of recentering the reflections and refining the cell constants and orientation matrix were then performed. Reflections were then centred at both + and -2θ. In order to obtain a more accurate orientation matrix and cell constants, high angle reflections were examined over the range $30° < 2\theta < 40°$. From this set, twenty intense reflections were chosen and used to obtain cell parameters and the orientation matrix for data collection.

Several checks of operating conditions and crystal quality were undertaken before data collection. Four intense, low angle reflections well distributed in reciprocal space were chosen as 'standard' reflections,

(100, 010, 001 and $\bar{1}02$). ω-scans of these reflections were recorded; the average width at half-height was 0.10°. The experimental conditions associated with data collection are given in Table 2.1.

Variable scan rates within a maximum time per datum of 90s were used in order to optimize counting statistics. For extremely strong reflections, a Zr foil attenuator with an accurately known transmission factor was inserted in front of the counter to prevent counter overflow (ie, coincidence losses). Background measurements were recorded at 25% extensions of the scan range. Four standard reflections were recorded every 10,800s of X-ray exposure time, as a check on machine and crystal stability. There was no significant change in the intensity of standards throughout the data collection. Hence no decay correction was neccessary. An orientation check, using three reflections, was also performed at 200 reflection intervals throughout the data collection to test for any crystal movement and instrumental instability. A total of 4311 reflections was measured. The range of Miller indices for data collection was $\bar{h}$ to h, $\bar{k}$ to k and 0 to ℓ for which $0 < 2\theta < 66°$. A ω-2θ scan technique was used to collect the data. ω-scans of the four standards were remeasured at the conclusion of data collection; scan widths at half-height remained the same as they were at the start.

The crystal was measured on a microscope fitted

with a filar eye-piece to permit an absorption correction. Eight faces were identified by optical goniometry as (001), (100) and the forms $\{1\bar{1}0\}$, {010}, and $\{10\bar{1}\}$. Faces (100) and {010} were the most prominent. A perspective view of the crystal produced by programs CRYSTL[4] and ORTEP is presented in appendix 5.

2.3.2.2 Data reduction:

Conversion of the raw intensity data into the commonly used form (structure amplitudes) is known as data reduction. Data reduction, structure solution and refinement were performed using the Enraf-Nonius structure determination package[4] running on a DEC PDP 11/23+ computer. Data reduction was performed by the program BEGIN[4]. Corrections for background, monochromator polarization, and Lorentz and polarization effects were applied to the data. Each peak was corrected for the background effects which arises from the presence of white radiation in the X-ray beam, the corrections made by assuming that the two background counts recorded at the limits of the scan (ie, high and low angle portions of the scan) are related linearly to each other. Lorentz and polarization effects are functions of 2θ. The Lorentz correction originates because the time that each reflection is in the diffraction position is not constant[1], being dependent on machine geometry and the diffracting angle[1]. Polarization effects arise because the efficiency of

Table 2.1. Summary of X-ray Structure Determinations

	5a	5b
Crystal Data		
compound, formula weight	$Au_2C\ell_2O_2P_4C_{10}H_{32}$, 773.10	$Au_2I_2O_2P_4C_{10}H_{32}$, 956.00
crystal system, space group	Triclinic , $P\bar{1}$ (No.2)	
temperature, °C	23	
cell dimens ;		
a (Å)	7.962(1)	8.243(1)
b (Å)	9.987(1)	9.057(1)
c (Å)	7.895(1)	8.167(1)
α (deg)	90.11(1)	90.23(1)
β (deg)	109 13(1)	110.33(1)
γ (deg)	112.84(1)	89.92(1)
cell volume (Å^3), Z	540.6(3), 1	571.6(3), 1
density, g cm^{-3}, obsd; calc	2.283(2), 2.375	2.718(2) 2.777
Experimental Details		
diffractometer, monochromator	Enraf-Nonius CAD4F, graphite	
radiation, wavelength (Å)	Mo, λ(Kα mean) 0.71073	
cryst-detec (mm), t.o.a. (°)	205, 2.5	
aperture (mm), vert; horiz	4.0; 6.0 + 0.35tanθ	
centering reflec; θ range	20; 30.0 < 2θ < 40.0	20; 30.0 < 2θ < 40.0
Data Collection		
approx. crystal dimens (mm)	0.25 × 0.12 × 0.42	0.32 × 0.09 × 0.14

Table 2.1 continued,

cryst vol (mm^3); no of faces	5.53×10^{-3}; 8	3.08×10^{-3}; 9
face indices	100, $\{1\bar{1}0\}$, $\{010\}$ $\{10\bar{1}\}$ and 001	$\bar{1}20$, $\{100\}$, $\{010\}$, $\{001\}$ and $\{10\bar{1}\}$
ω-scan widths, before, after	0.11 0.11	
scan mode, width (°)	ω-2θ, 0.7 + 0.35tanθ	
index and θ ranges	$-12 \leq h \leq 12$ $-15 \leq k \leq 15$ $0 \leq \ell \leq 12$ $0 \leq \theta \leq 33°$	$-12 \leq h \leq 12$ $-13 \leq k \leq 13$ $0 \leq \ell \leq 12$ $0 \leq \theta \leq 32.5°$
scan speed (deg min^{-1})	3.3 to 0.9	3.3 to 1.0
max time per datum, total time	90s,92.9h	90s, 98.1h
standard reflections	$\bar{1}02$, 100, 010, 001	$\bar{1}01$, 100, 010, 001
monitor frequency, % var	180m, 1.6	180m, 2.3
no of data, standards collected	4311, 132	4383, 148
Data Processing		
corrections	Lorentz, polarization and monochromator polarization	
decay, absorption corrections	None; Gaussian	None; Gaussian
abs coeff (cm^{-1}); grid size	140.74, 12 × 8 × 20	157.47, 22 × 6 × 10
transmission, max., min.	0.283, 0.112	0.857, 0.109
R (F) for averag, before, aft.	0.009, 0.014	0.011, 0.011
no of unique data, signif.	$3225 > 3\sigma$	$2971 > 3\sigma$
Structure Refinement		
no. of observ., variables	3225, 92	2971, 92
final model; R_1 and R_2	0.035, 0.047	0.030, 0.054
top resid., (e $Å^{-3}$), coord.	3.45 (0.791 0.889 0.082)	1.80 (0.791 0.305 0.291)

reflection is greater for radiation polarized parallel to the reflecting plane. Reflection of components parallel to the surface depend on electron density only while those perpendicular suffer from destructive interference as well[1].

A standard deviation $\sigma(I)$ was assigned to each intensity I, where

$$\sigma(I) = \frac{20.1166 \times A \times (C - BR^2)}{N \times L}$$

and $I = F^2_{obs}$ = magnitude of reflection intensity

A = attenuator factor (1.0 if not used)

C = total count

B = total background count

R = ratio of scan time to background time = 2.0

N = ratio of fastest scan rate to actual scan rate

L = Lorentz-polarization factor.

A factor p,[10] of value 0.04 was used to down-weight intense reflections and to account for variations in counting statistics[4]. This value was later modified to improve the weighting scheme. The data were corrected for absorption by applying a Gaussian absorption correction[11] (routine ABSCOR[4]). Absorption of the X-ray beam is dependent on the chemical composition of the crystal and the pathlength through the crystal[1]. A grid of dimensions 12 x 8 x 20 was used for the calculation. Transmission factors for the crystal ranged from 0.112 to

0.283, for an absorption coefficient of 140.74 cm^{-1}. Program PAINT[4] was then used to average the pairs of symmetry equivalent reflections hk0 and $\bar{h}\bar{k}0$. R factors for averaging (on F) were 0.009 and 0.014, respectively before and after the absorption correction. Of the 4311 reflections processed, 3225 unique reflections with $I > 3\sigma(I)$ were used in the solution and refinement of the structure.

2.3.3 Solution and Refinement of the structure:

If the positions of the atoms in the unit cell are known, it is possible to calculate structure factors to correspond to each measured intensity. The structure factor for a given 'plane' in the crystal represents the combined scattering power of the atoms in the crystal in the direction of the reflected beam. A structure factor consists of an amplitude and a phase angle, and its modulus can be expressed as

$$|F_{hkl}| = (A^2_{hkl} + B^2_{hkl})^{\frac{1}{2}}$$ (see Appendix 4)

where the phase angle of the structure factor, α_{hkl}, is $\alpha = \tan^{-1} [B_{hkl}/A_{hkl}]$. Unfortunately, the signs of A_{hkl} and B_{hkl} are not known and the phase angle, α_{hkl}, cannot be measured experimentally. Hence atomic positions cannot be calculated directly from the experimental data. One early solution to this 'Phase problem' was developed by Patterson[7], which depends on the phaseless quantity $|F_{hkl}|^2$, which can be readily obtained from the intensity

data. The peaks in three-dimensional Patterson space represent interatomic vectors in real space, with the intensity of the peaks being roughly proportional to the product of the atomic numbers. A Patterson synthesis will therefore be dominated by heavy atom:heavy atom vectors, allowing the heavy atoms (eg. Au) to be located. Usually the heavy atoms make the largest contribution to the structure factors, and once located, they can be used to "phase" a diffference Fourier synthesis using the calculated phase of the heavy atom contribution.

Since the molecule crystallized in the triclinic system, it could belong to either the acentric space group P1, or the centrosymmetric space group $P\bar{1}$. A statistical analysis of the data using the N(Z) test[1] suggested that the space group was P1, so a solution was attempted in this space group.

Positional parameters for the Au and P atoms were obtained from a three dimensional Patterson synthesis calculated with the program FOURIER[4]. A series of least square refinements (program LSBD[4]) and difference Fourier synthesis (program FOURIER[4]) were used to locate the remaining 12 non-hydrogen atoms. At this stage it became apparent that the cation possessed a centre of symmetry, so the space group was changed to $P\bar{1}$, and the analysis was continued with the cation placed on the centre at (0,0,0).

Since Z = 1 and the salt sits on a

crystallographic centre of symmetry, it was only necessary to locate one-half of the atoms. Once the positional coordinates, (x,y,z) of the atoms in one-half of the molecule were obtained, then (-x,-y,-z) translation of these atoms gives those of the second-half of the molecule. Thus, only the coordinates of one Au, one Cℓ, two P's, five C's and fourteen H's need to be determined.

The atomic parameters were refined by full matrix least-squares techniques on F, minimizing the function $\Sigma w(|F_o|-|F_c|)^2$, where F_o and F_c are the observed and calculated structure factor amplitudes and w, the weighting factor, is given by $w = 4F_o/\sigma^2(F_o^2)$ (Program LSBD[4]). Scattering factors for neutral, non-H atoms were those of Cromer and Waber[8], and the real components of anomalous dispersion were those of cromer[6] and were included for all atoms. Until all non-hydrogen atoms were found, atoms were refined as isotropic spheres. In subsequent cycles, beginning with the heavy atoms and progressing to lighter atoms, isotropic spheres were changed to anisotropic thermal ellipsoids in order to improve the descriptions of the thermal vibration of atoms. This model, with only non-hydrogen atoms was refined to convergence with agreement factors $R_1 = \Sigma(||F_o| - |F_c||) / \Sigma|F_o| = 0.094$ and $R_2 = [\Sigma w(|F_o| - |F_c|)^2 / \Sigma w(F_o)^2]^{\frac{1}{2}} = 0.129$.

The 14 H atoms were located in a difference Fourier synthesis with peaks ranging from 1.4(2) to 0.7(2)eÅ^{-3}, and included in ideal positions (C-H = 0.95 Å

sp^3 hybridization) in calculations of F_c, but were not refined (program HYDRO[4]). Positions for the methyl hydrogen atoms were optimized by a least-squares routine (program HYDRA[4]). The scattering factor values were taken from Stewart *et al*[9]. Refinement continued until no shifts were observed upon H atom recalculation.

A difference Fourier synthesis run at this stage revealed the presence of the oxygen atom of a water molecule. The hydrogen atoms on the water molecule were clearly visible in a difference Fourier, see Figure 2.2. This solvent molecule was included in the model. For the final cycles, positional and anisotropic thermal parameters were refined for all non-H atoms, and H atom positions were recalculated after each cycle. The model converged (3225 unique reflections for which $I > 3\sigma(I)$, 92 variables) with agreement factors $R_1 = 0.035$ and $R_2 = 0.047$.

In the final cycle no parameter shift exceeded 0.01 of its estimated standard deviation, and, with a p value of 0.06, the error in an observation of unit weight was 1.28e. A total difference Fourier synthesis showed that the highest peak, with an electron density of $3.4(1)e\text{Å}^{-3}$ is situated 0.88 Å from the Au atom.

A statistical analysis of R_1 and R_2 in terms of $|F_o|$, $\lambda^{-1}\sin\theta$, and classes of indices showed no unusual trends. There was no secondary extinction. Final positional and U equivalent thermal parameters for the non-H atoms are presented in Table 2.2. H atom parameters,

anisotropic thermal parameters, selected torsion angles, weighted least square planes are given in Tables 2.3, 2.4, 2.5 and 2.6. Structure amplitudes are listed in appendix 1.

2.4 X-RAY DIFFRACTION STUDIES OF $[Au_2(\mu\text{-dmpm})_2]I_2.2H_2O$, 5b

Clear, colourless, bladed crystals of 5b were obtained by recrystallization from water solutions. Preliminary photography showed the crystals to belong to triclinic system, and cell constants were obtained. The calculated cell volume was 572(1)$Å^{-3}$. The crystal density was determined by neutral buoyancy in mixtures of $CHBr_3$ and 1,2-$C_2H_4Br_2$. The value was found to be 2.718(1) g cm^{-3}, suggesting a Z value of 1.

The crystal selected for data collection was of approximate dimensions 0.32 x 0.09 x 0.14 mm^3, with nine faces as revealed by optical goniometry to be {010}, {$\bar{1}$01}, {001}, {100} and {$\bar{1}$20}. A perspective view of the crystal is presented in appendix 5. Accurate unit cell parameters were obtained from 20 reflections with $30^\circ < 2\theta < 40^\circ$. ω-scans of several intense, low angle reflections had an average width at half height of 0.11°. A summary of crystal data and the experimental conditions used for data collection is given in Table 2.1.

No significant decomposition was observed during data collection. Background, monochromator polarization, Lorentz, and polarization corrections were applied to the data, and standard deviations were calculated based on

counting statistics[4]. A Gaussian absorption correction[11] using a grid of size 22 x 6 x 10 was applied. The data were processed, and a starting value of 0.04 was chosen for p. Of the 4383 data collected, 2971 unique data with $I > 3\sigma(I)$ were used in the solution and preliminary refinement of the structure.

The structure solution was begun on the assumption that the space group was $P\bar{1}$. The positional parameters of the Au atom were obtained from a three dimensional Patterson synthesis, and the remaining 9 non-H atoms were located from a series of least-squares refinements and difference Fourier syntheses. Refinement proceeded smoothly yielding residuals of $R_1 = 0.053$ and $R_2 = 0.074$ for the model where only Au, P, I were refined with anisotropic thermal parameters.

The 14 H atoms were located in a difference Fourier synthesis with electron densities varying from 1.1(3) to 0.5(3)eÅ^{-3}, and their idealized contributions included in the calculation of F_C; those on the water molecule could not be found. The refinement of 92 variables with 2971 unique observations ($I > 3\sigma(I)$) converged at $R_1 = 0.030$ and $R_2 = 0.054$. In the final cycle all parameter shifts were less than 0.01σ, and, with a p value of 0.06, the error in an observation of unit weight was 1.38e. The highest peak in a difference Fourier synthesis is of electron density 1.8(1)eÅ^{-3} is at a distance of 0.72 Å from the I atom. A statistical analysis

of the structure factors showed no unusual trends. Final positional parameters of non-H atoms are given in Table 2.2. Hydrogen atom parameters, anisotropic thermal parameters, selected torsion angles and weighted least-squares planes, are given in Table 2.3, 2.4, 2.5, and 2.6 respectively. Structure factor amplitudes are listed in appendix 1.

2.5 RESULTS AND DISCUSSION

2.5.1 Synthesis and characterization of [t-BuC≡CAuPR$_2$CH$_2$PR$_2$], R=Me, 6a; R=Ph, 6b

The above complexes 6a, R = Me and 6b, R = Ph were prepared by reaction of AuC≡Ct-Bu with an equimolar amount of the corresponding diphosphine ligand as shown in equation 2.1. They were readily characterized by

$$[AuC{\equiv}Ct\text{-}Bu] + R_2PCH_2PR_2 \longrightarrow [t\text{-}BuC{\equiv}C\text{-}Au\text{-}PR_2CH_2PR_2]$$

R = Me (6a)

Ph (6b)

Equation 2.1

elemental analysis and mass spectroscopy, and the structures were defined by the ^1H and ^{31}P NMR spectra. Both 6a and 6b gave a parent ion peak in the mass spectrum.

2.5.2 Spectroscopic characterization of 6a and 6b

The i.r spectum of 6a in nujol mull showed a C≡C stretch at 2100 cm^{-1}. The ^{31}P NMR spectrum of 6a at room temperature revealed a broad singlet at δ 3.8, contrary to the expected pattern. The NMR labelling scheme of 6a and 6b is shown in scheme 2.2. We would expect 6a to generate

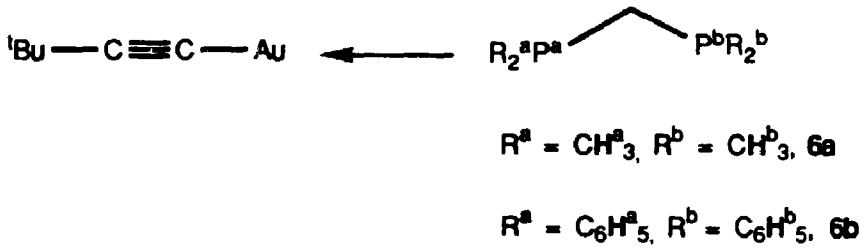

Scheme 2.2 NMR labelling scheme of 6a and 6b

two signals; one due to the coordinated phosphine and the other due to the free phosphorus atom. The fact that only a broad singlet was observed suggests that a rapid fluxional process is involved. In contrast, the $^{31}P\{^1H\}$ NMR spectrum (Figure 2.1) of the dppm analogue, 6b, synthesized and characterized by Dr. Ilse Treurnicht of this laboratory, revealed two singlets at δ 29.4 and −27.2, characteristic of coordinated and free phosphorus atoms, respectively. The ^1H NMR spectrum of 6a at room temperature showed a singlet due to MeP resonances at δ 1.77. However, this resonance was split into two singlets at − 80°C, $\delta[P^a(CH^a_3)_2]$ 1.70 and $\delta[P^b(CH^b_3)_2]$ 1.88, of equal intensity. The above results clearly indicate that 6a and 6b undergo a fluxional

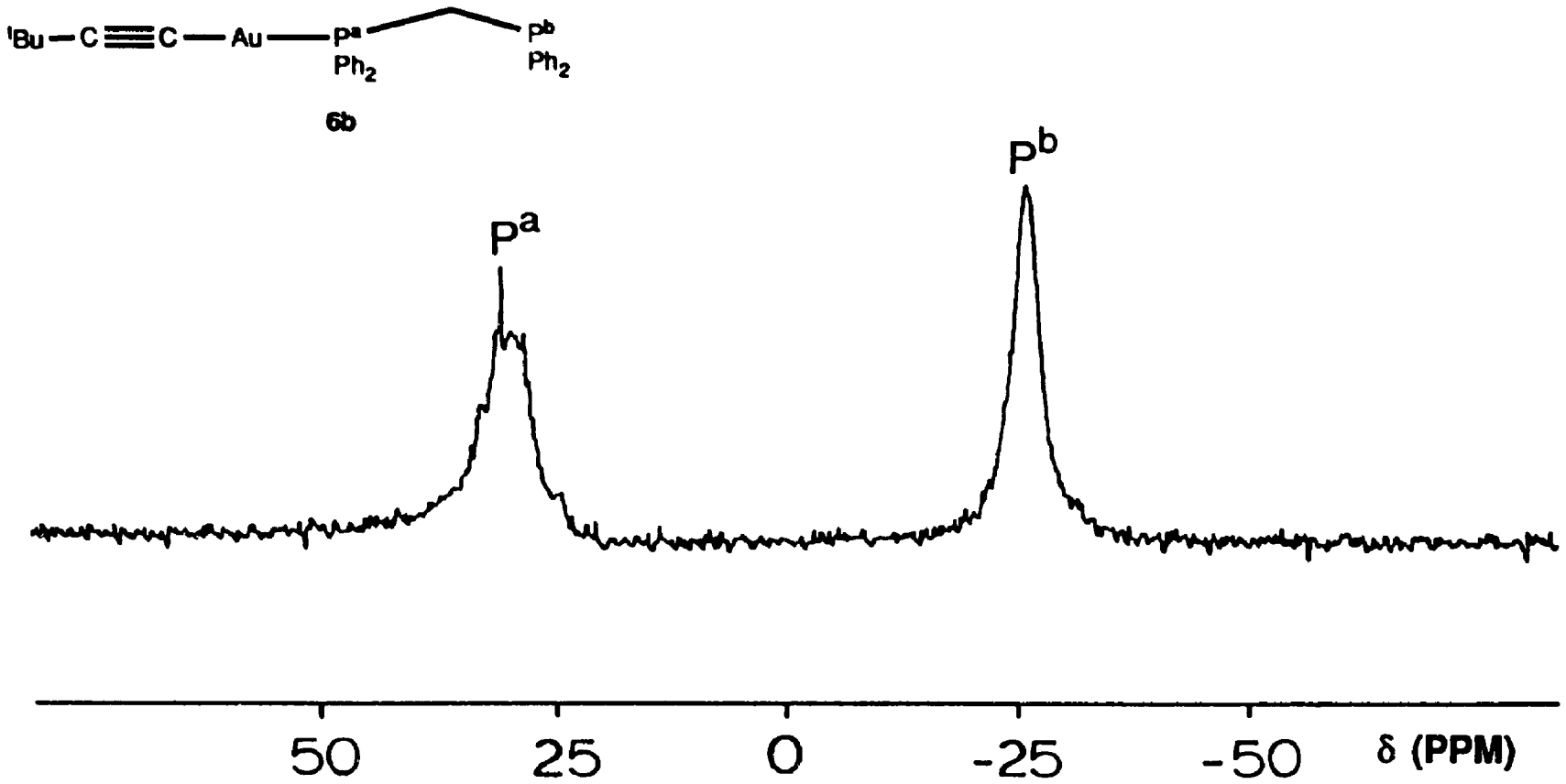

Figure 2.1: $^{31}P\{^{1}H\}$ NMR spectrum of 6b at room temperature

process.

2.5.3 Mechanism of the fluxional process in 6a and 6b

The complexes 6a and 6b contain monodentate diphosphine ligands as shown by the variable temperature NMR spectra. In the former case, the two MeP resonances observed in the ^1H NMR at – 80°C coalesce to a single resonance at room temperature indicating fluxionality according to Scheme 2.3, but the coalescence of ^{31}P resonances did not occur for 6b indicating slower

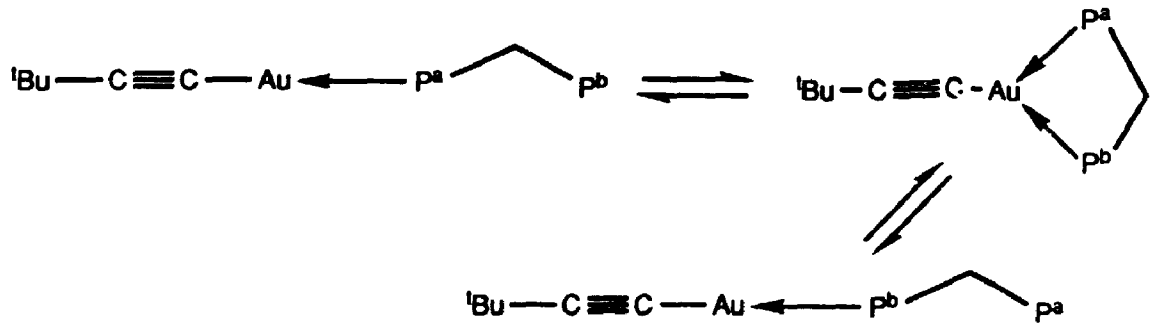

Scheme 2.3

fluxionality. Hence, in complexes 6, it is clear that gold(I) is 2-coordinate and that 3-coordination occurs only in the transition state for exchange as shown in scheme 2.3. A similar fluxionality of dppm ligands has been observed previously[23,24], and monodentate phosphines also undergo exchange in gold(I) complexes, for example the exchange of free and coordinated PMe_3 in [$MeAuPMe_3$] with PMe_3 [25].

2.5.4 Synthesis and characterization of $[Au_2(\mu\text{-dmpm})_2]X_2.2H_2O$, X=Cℓ, 5a; X=I, 5b.

The complex 5a was formed when complex 6a was recrystallized slowly from the chlorinated solvents $CHC\ell_3$ or $CH_2C\ell_2$. Thus, although the gold-acetylide bond is usually considered strong[26], it can be cleaved in these complexes. 5a was prepared more rationally by reaction of $[AuC\ell(SMe_2)]$ with one equivalent of dmpm and when recrystallized from $CHC\ell_3$/n-pentane, it formed the hydrate $[Au_2(\mu\text{-dmpm})_2]C\ell_2.2H_2O$, 5a. The iodide complex 5b was prepared from $[AuI(SMe_2)]$, prepared *in situ*, with dmpm and again it formed a hydrate $[Au_2(\mu\text{-dmpm})_2]I_2\cdot 2H_2O$, 5b, when recrystallized from water. The ^{31}P NMR spectrum of 5a revealed a singlet at δ 5.6 suggesting that all the phosphorus atoms are equivalent. In the ^1H NMR spectrum, the resonances due to the CH_2P_2 protons appeared as a quintuplet, δ 2.98, $^2J(PH) + {}^4J(PH) = 10$ Hz, suggesting a dimeric structure 5a. The NMR spectral data of 5b were similar to those observed for 5a. The structure of 5a and 5b were determined by X-ray diffraction methods and are discussed in detail in section 2.5.8.

2.5.5 Kinetic studies of the conversion of 6a to 5a

The reaction kinetics of the conversion of the acetylide product 6a to chloride product 5a in chloroform solvent were followed by the decay of the metal-ligand charge transfer band of 6a (λ = 282nm). Analysis of the

data showed good first-order kinetics with a rate constant $k = 7.9 \times 10^{-5}\ s^{-1}$. A detailed kinetic study involving variation of concentration of solvent, temperature etc. was not carried out. This reaction is likely to follow a pseudo-first order kinetics. No attempt was made to study other side products of this reaction.

2.5.6 Synthesis and characterization of $[Au_2(\mu\text{-dmpm})_3]X_2$, X = Cℓ, 7a; X = I, 7b.

Reaction of $[AuI(SMe_2)]$, prepared *in situ*, with either 1.5 or 2 equivalents of dmpm gave the white complex $[Au_2(\mu\text{-dmpm})_3]I_2$, 7b. The chloride analogue of this complex, $[Au_2(\mu\text{-dmpm})_3]Cℓ_2$, 7a, was prepared by Dr. Ilse Treurnicht of this laboratory by a similar method. Both species were obtained in analytically pure form and gave single resonances in the NMR spectra due to $C\underline{H}_3P$, $C\underline{H}_2P_2$ and ^{31}P groups, indicating a symmetrical structure. Slow crystallization of these complexes led to partial loss of dmpm and formation of the bis(diphosphine) complexes 5a and 5b respectively. Hence an X-ray structure of 7 could not be obtained. However, the X-ray structure of the corresponding tetrafluoroborate salt, $[Au_2(\mu\text{-dmpm})_3](BF_4)_2$ has recently been reported[27] which shows the symmetrical structure 7, scheme 2.1, as suggested for 7a and 7b.

2.5.7 Reaction of 7b with excess dmpm

Coordination number four is known for gold(I)

complexes[28]. Attempts to prepare $[Au_2(\mu\text{-dmpm})_3(dmpm\text{-}P)]I_2$, 8, by reacting 7b with excess dmpm were not successful. This, together with the observation that dissociation of dmpm from 7a and 7b occurs rapidly, suggests that the binuclear Au(I) system has little tendency to exceed coordination number three. In contrast, the isoelectronic $[Pt_2(\mu\text{-dmpm})_3]$ readily adds one or two triphenylphosphine ligands to give 4-coordinate platinum(0) centres[29].

2.5.8 Description of crystal and molecular structures of 5a and 5b

The crystal structures of compounds 5a and 5b consist of discrete $[Au_2(\mu\text{-dmpm})_2]^{+2}$ cations, halide anions and water molecules. The anions are located above and below the 8-membered ring formed by two gold atoms and the atoms of the bidentate diphosphine ligands of the cation. A stereo view of the salt 5a is presented in figure 2.4. A perspective view of the complex cation 5a showing the atom numbering scheme is presented in figure 2.3. The structures are almost identical.

In the solid state the cationic dimers 5a and 5b have an exact C_i symmetry, the mid-point of the Au—→Au' vector coinciding with a crystallographic center of inversion. The $Au_2P_4C_2$ ring adopts a chair conformation. In both structures, the metal atoms are spanned by two bridging dmpm ligands in a mutually trans arrangement. The Au...Au separation, 3.014(3) Å in 5a, is

Table 2.2 Atomic Positional ($\times 10^4$) and Thermal ($\times 10^3$) Parameters

Atom	x	y	z	$U_{eq}^*(\AA^2)$
Compound 5a				
Au	1392.2(2)	161.0(2)	-976.8(2)	30.10(4)
Cℓ	3461(3)	2454(2)	3132(3)	64.3(6)
P(1)	864(2)	2089(1)	-2283(2)	27.0(3)
P(2)	-2102(2)	1682(1)	-401(2)	27.5(3)
O	2589(8)	5302(7)	3607(9)	80(2)
C(1)	-790(10)	1624(9)	-4624(9)	58(2)
C(2)	3048(8)	3613(6)	-2300(9)	49(2)
C(3)	-120(6)	2934(5)	-1039(6)	28(1)
C(4)	-2520(7)	2921(6)	937(8)	41(1)
C(5)	-4271(7)	938(7)	-2450(8)	41(1)
Compound 5b				
Au	5919.6(3)	-192.7(3)	-1294.7(3)	36.55(5)
I	2275.5(7)	-2615.8(7)	-2120.7(8)	58.0(2)
P(1)	2433(2)	2095(2)	-312(2)	34.5(4)
P(2)	4299(2)	1668(2)	-3008(2)	33.3(4)
O	1196(22)	-4976(15)	-5766(22)	189(8)
C(1)	2216(11)	3671(10)	955(11)	57(2)
C(2)	268(11)	1655(13)	-1646(13)	62(3)
C(3)	3446(8)	2941(7)	-1758(8)	37(1)
C(4)	5412(10)	2964(10)	-3965(11)	59(2)
C(5)	2451(10)	1048(10)	-4808(9)	50(2)

$$U_{eq}^* = \frac{1}{3} \sum_i \sum_j U_{ij}\, a_i^*\, a_j^*\, \mathbf{a}_i \cdot \mathbf{a}_j$$

TABLE 2.3. Hydrogen atom positional ($\times 10^4$) and thermal ($\times 10^3$) parameters for 5a and 5b.

	Atom	x	y	z	U(Å^2)
5a	H1C1	-858	2491	-5066	71
	H2C1	-313	1191	-5329	71
	H3C1	-2044	948	-4688	71
	H1C2	3981	3929	-1102	61
	H2C2	3570	3301	-3067	61
	H3C2	2722	4398	-2738	61
	H1C3	-585	3558	-1774	30
	H2C3	913	3505	39	30
	H1C4	-1525	3226	2104	54
	H2C4	-2493	3754	347	54
	H3C4	-3756	2425	1050	54
	H1C5	-4420	1720	-3074	53
	H2C5	-4131	278	-3205	53
	H3C5	-5382	432	-2129	53
	H1O	3050	4600	3499	51
	H2O	3600	6100	4490	51
5b	H1C1	3318	4112	1499	70
	H2C1	1450	4365	204	70
	H3C1	1765	3357	1820	70
	H1C2	-307	2530	7816	75
	H2C2	286	965	7481	75
	H3C2	-317	1238	9058	75
	H1C3	4377	3538	8941	41
	H2C3	2602	3545	7432	41
	H1C4	6420	3325	6921	71
	H2C4	5729	2470	5161	71
	H3C4	4660	3763	5526	71
	H1C5	1745	1872	4682	63
	H2C5	2833	581	4347	63
	H3C5	1808	366	5605	63

H1C1, H2C1 and H3C1 are bonded to C(1), etc.

Table 2.4. Anisotropic Thermal Parameters ($\times 10^3$)

Atom	U_{11}	U_{22}	U_{33}	U_{12}	U_{13}	U_{23}
Compound 5a						
Au	38.06(5)	29.96(6)	38.23(6)	22.41(4)	22.87(4)	15.06(5)
Cℓ	69.6(8)	57.3(8)	56.7(9)	28.9(6)	7.9(7)	-5.8(7)
P(1)	30.5(4)	27.5(4)	27.7(4)	15.3(3)	12.1( )	8.2(3)
P(2)	29.3(3)	25.9(4)	33.9(4)	15.6(3)	14.1(3)	8.2(4)
O	49(2)	63(3)	101(4)	28(2)	-10(3)	14(3)
C(1)	57(3)	85(4)	30(2)	35(2)	4(2)	4(3)
C(2)	39(2)	34(2)	79(3)	11(2)	32(2)	6(2)
C(3)	29(1)	24(1)	33(2)	14(1)	12(1)	7(1)
C(4)	51(2)	39(2)	50(2)	28(1)	27(1)	10(2)
C(5)	21(1)	44(2)	49(3)	12(1)	3(2)	3(2)
Compound 5b						
Au	44.22(9)	36.1(1)	35.14(8)	16.25(8)	21.00(6)	12.59(8)
I	49.6(3)	50.5(3)	65.2(3)	-6.1(2)	8.7(2)	5.8(2)
P(1)	35.7(6)	34.0(7)	35.0(6)	9.5(6)	13.7(5)	6.7(6)
P(2)	37.1(6)	33.2(7)	30.8(5)	5.1(6)	13.4(5)	7.9(5)
O	267(17)	98(8)	184(12)	-41(10)	53(11)	-7(9)
C(1)	79(4)	47(4)	59(3)	20(3)	40(2)	3(3)
C(2)	32(3)	82(6)	60(4)	2(4)	-0(3)	3(4)
C(3)	46(3)	35(3)	35(2)	4(2)	20(2)	9(2)
C(4)	62(3)	59(4)	58(3)	1(3)	38(2)	23(3)
C(5)	49(4)	62(5)	30(3)	-1(4)	2(3)	-7(3)

The general temperature factor expression is

$$U_{ij} = \left[-2\pi^2\left[U_{11}h^2a^{*2} + U_{22}k^2b^{*2} + U_{33}\ell^2c^{*2} + 2U_{12}hka^*b^* + 2U_{13}h\ell a^*c^* + 2U_{23}k\ell b^*c^* \right]\right]$$

Table 2.5. Selected Torsion Angles in Degrees

Atom 1	Atom 2	Atom 3	Atom 4	Angle 5a	5b
P(2)'	Au	P(1)	C(3)	-101.7(8)	137(1)
Au	P(1)	C(3)	P(2)	-45.9(3)	45.6(4)
P(1)'	Au'	P(2)	C(3)	-147.8(10)	-178(1)
Au'	P(2)	C(3)	P(1)	49.3(3)	-46.8(4)

Table 2.6. Selected Least-Squares Plane

i. in 5a Crystallographic Equation of Plane

-2.3602 X - 3.7097 Y - 4.5204 Z - 0.0532 = 0

Atom	X	Y	Z	Distance
Au	1.2988	0.2561	-0.7205	0.00
P(1)	0.4693	2.1749	-1.6841	0.00
P(2)	-2.2225	1.5927	-0.2954	0.00
	----- Other Atoms -----			
Cℓ	0.9943	1.9126	2.3103	-3.196(2)
O	-0.9275	4.4814	2.6609	-4.262(7)
C(1)	-0.0596	2.0061	-3.4105	1.620(7)
C(2)	1.6209	3.5799	-1.6965	-1.073(7)
C(3)	-0.9645	2.8157	-0.7667	-0.643(5)
C(4)	3.3811	-2.5854	-0.6908	0.859(5)
C(5)	3.1308	-1.1345	1.8072	-1.821(6)

ii. in 5b Crystallographic Equation of Plane

-2.0810 X - 2.0782 Y - 6.4754 Z - 0.0000 = 0

Atom	X	Y	Z	Distance
Au	5.2470	-0.1705	-0.9915	0.00
P(1)	2.0969	1.8977	-0.2386	0.00
P(2)	4.3997	1.5193	-2.3033	0.00
	----- Other Atoms -----			
I	2.4746	-2.3622	-1.6240	3.443(1)
O	2.6169	-4.4881	-4.4159	4.519(17)
C(1)	1.5601	3.3210	0.7310	-1.842(8)
C(2)	0.6903	1.5040	-1.2602	1.190(6)
C(3)	3.3429	2.6690	-1.3463	-0.666(9)
C(4)	5.5909	2.6962	-3.0367	0.826(8)
C(5)	3.3868	0.9639	-3.6817	1.385(7)

TABLE 2.7. Selected Bond Distances in 5a and 5b (Å).

Compound			5a, X = Cℓ	5b, X = I
Bond			Distance	
	Au	Au'	3.0143(3)	3.0190(4)
	P(1)	P(2)	3.084(2)	3.116(3)
	Au	X	3.467(2)	3.5903(7)
	Au	X'	3.534(2)	3.6780(6)
	Au	P(1)	2.302(1)	2.303(2)
	Au	P(2)	2.303(1)	2.301(2)
	P(1)	C(1)	1.813(6)	1.804(9)
	P(1)	C(2)	1.817(6)	1.783(8)
	P(1)	C(3)	1.819(6)	1.837(8)
	P(2)	C(3)	1.817(5)	1.831(7)
	P(2)	C(4)	1.817(7)	1.83(1)
	P(2)	C(5)	1.822(5)	1.798(7)
	X	O	3.227(8)	3.512(16)
	X	O'	3.277(5)	3.532(15)
Angle			Degrees	
P(1)	Au	P(2)	176.80(3)	177.42(7)
Au	P(1)	C(1)	115 2(3)	116.7(4)
Au	P(1)	C(2)	114.8(2)	114.9(3)
Au	P(1)	C(3)	111.6(2)	111.8(2)
Au	P(2)	C(3)	112.2(2)	112.1(2)
Au	P(2)	C(4)	117.1(2)	117.5(3)
Au	P(2)	C(5)	111.4(2)	114.7(3)
X	Au	X'	129.01(6)	130.93(2)
X	Au	P(1)	86.33(5)	86.44(4)
X	Au	P(2)	91.91(5)	93.64(4)
X'	Au	P(1)	95.13(4)	94.66(4)
X'	Au	P(2)	88.05(4)	87.24(4)
P(1)	C(3)	P(2)	116.1(2)	116.3(4)
Au	X	Au'	50.99(2)	49.07(1)
O	X	O'	76.5(2)	44.7(5)
X	O	X'	103.5(2)	135.3(6)

X' is related to X by the centre at (0,0,0).

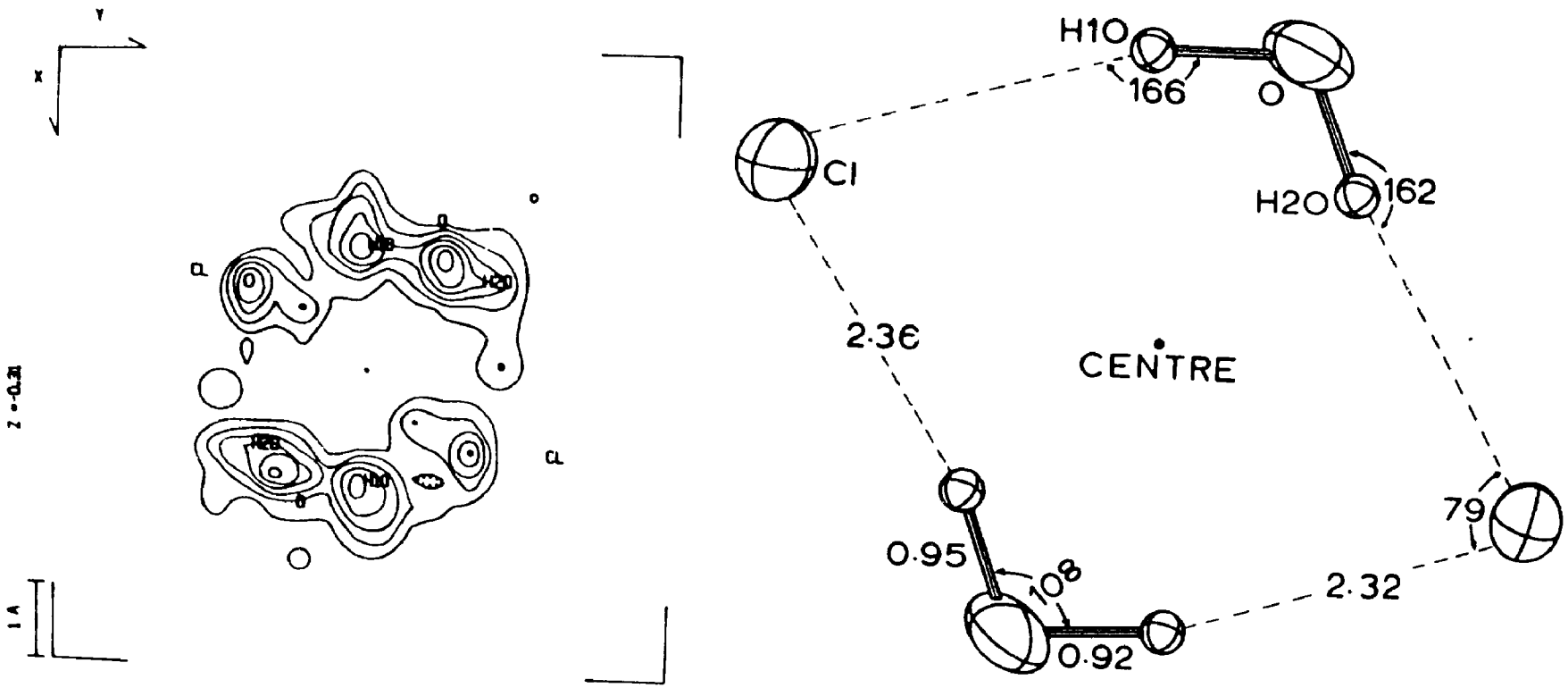

Figure 2.2: A difference Fourier contour map of 5a showing the presence of hydrogen atoms on water molecule (left), and the hydrogen bonding scheme (right).

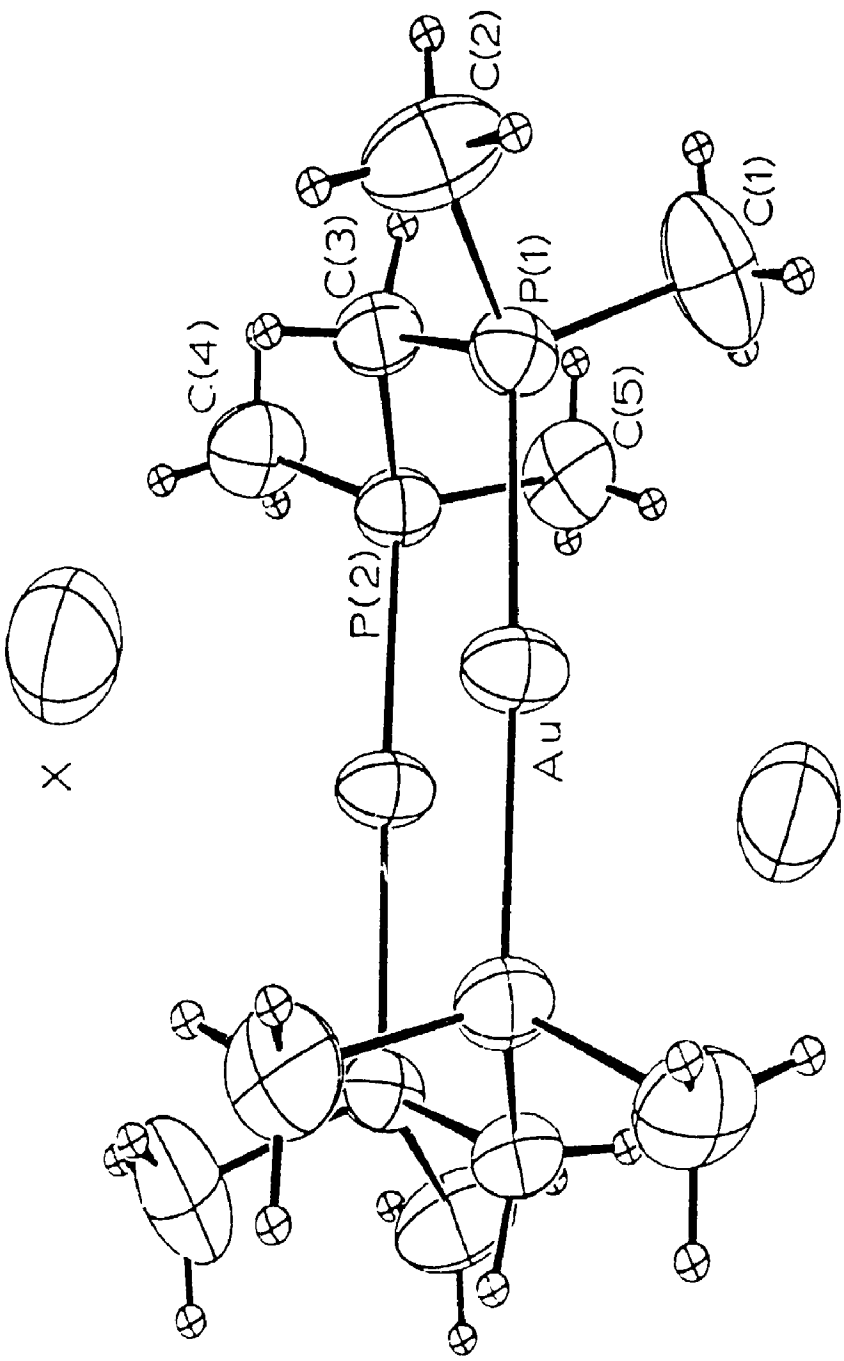

Figure 2.3: A perspective view of 5a, giving the atom numbering scheme.

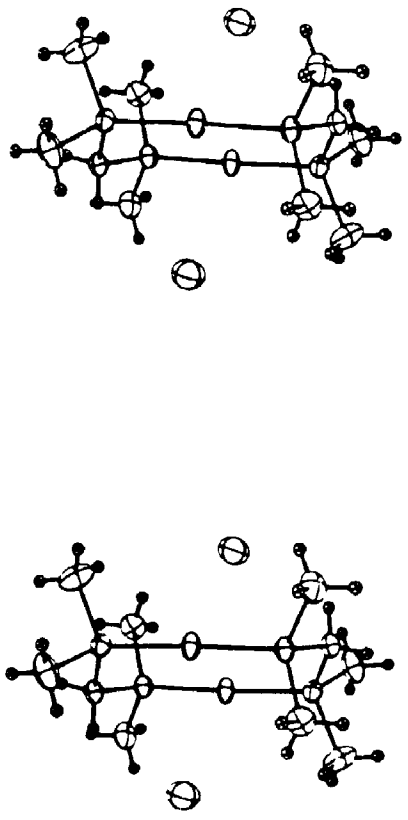

Figure 2.4: A stereoview of the salt in 5a

shorter than that of 3.0190(4) Å in 5b (λ = 9.4, appendix 3), and both fall well outside the range considered typical for Au-Au single bonds[30] (Ca. 2.757 - 2.780 Å) and there is no formal Au-Au bond present. The P...P bite distance of 3.084(2) Å in 5a is shorter than that of 3.116(3) Å in 5b (λ = 8.9). Thus, we see that the P....P distances are slightly larger than the Au...Au distance, suggesting a weak metal-metal interaction. The Au-P bond lengths in 5a and 5b are indistinguishable, with a mean of 2.302(2) Å. The halide anions are located approximately normal to the Au_2P_4 plane, as indicated by the P-Au-X angles (see Table 2.10). The closest distances of approach between the gold atoms and the halide anions are 3.467(2) and 3.534(2) Å in 5a and 3.590(1) and 3.678(1) Å in 5b. These distances clearly indicate that the interaction is essentially ionic, with little covalent character. In the analogous chloride, bromide and iodide dppm complexes, there is at least one covalently bonded halide atom with
Au-Cℓ = 2.771(4) - 2.963(4) Å in compounds 1-3 and
Au-I = 3.127(3) - 3.196(2) Å in 4 [12-16].

Each formula unit of the gold dimer in the crystal lattice is associated with two molecules of water of crystallization. A difference Fourier map of 5a showing the presence of H-atoms on the water molecule and the hydrogen bonding scheme is presented in figure 2.2. Each of the two water molecules forms two hydrogen bonds to chloride ions of two neighbouring unit cells. The bond

distances and bond angles between the atoms involved in Hydrogen bonding are given in Table 2.7. Thus, the crystal structure contains polymeric chains made of discrete molecules linked together by hydrogen bonds formed between water molecules and the halide anions.

2.6 SUMMARY AND CONCLUSIONS

The acetylide complexes 6a and 6b undergo a fluxional process involving a three-coordinate Au(I) centre. Complex 6a dimerizes by a first order process in chlorinated solvents, with the substitution of acetylide ligand by chloride ion, to form $[Au_2(\mu\text{-dmpm})_2]Cl_2.2H_2O$, 5a. The iodide complex, 5b, was found to have a similar structure to that of the chloride salt, 5a.

It is interesting to note that widely different structures 1-5 are adopted by complexes containing similar ligands. It has been suggested that the Au_2dppm_2 ring, and the other rings with phenyl substituents on phosphorus, must twist (giving non-linear PAuP groups) in order to reduce steric hindrance between phenyl substituents, and that this favours halide coordination above the $Au_2P_2C_2$ ring. Thus, steric effects would be responsible for the greater tendency of the halide to coordinate in the dppm complexes compared to the dmpm complexes[19]. However, this argument is contrary to the more general trend that increased steric hindrance usually leads to lower

coordination numbers. In addition, there are now more structures which do not conform to the expected pattern; for example, in 3 the halide is coordinated in the plane of the $Au_2P_4C_2$ ring rather than above the ring[15]. Therefore, it is more probable that the lower tendency of halide to coordinate in the dmpm complexes is primarily an electronic effect, and the greater basicity of the dmpm ligand, compared to that of the dppm ligand, overrides the steric effect of the ligand in gold(I) dimers.

2.7 REFERENCES

1. G.H. Stout, L.H. Jensen, X-ray structure determination (A practical guide), Collier-Macmillan Limited, London, 1968.

2. "International Tables for X-ray crystallography"; D. Reidel publishing company, Boston, USA. Volume A, 1983.

3. "Enraf-Nonius CAD4F users manual", Enraf-Nonius Delft, Delft, The Netherlands, 1982.

4. "Enraf-Nonius Structure determination package, SDP-PLUS", Version 1.0, 1982.

5. U.W. Arndt and B.T.M. Willis, "Single crystal diffractometry", p.243, Cambridge University press, London, England, 1966.

6. D.T. Cromer, D. Liberman, *J. Chem. phys.*, 53 (1970) 1891

7. A.L. Patterson, *Z. Krist.*, A90 (1935) 517

8. D.T. Cromer, J.T. Waber, *Acta cryst.*, 18 (1965) 104

9. R.F. Stewart, E.R. Davidson. W.T. Simpson, *J. Chem. phys.*, 42 (1965) 3175

10. W.R. Busing, H.A. Levy, *J. Chem. Phys.*, 26 (1957) 563

11. P. Coppens, L. Leiserowitz, D. Rabinovich, *Acta Crystallogr.*, 18 (1965) 1035

12. R.J. Puddephatt, *Chem. Soc. Rev.*, 99 (1983)

13. H. Schmidbaur, A. Wohlleben, U. Schubert, A. Frank, G. Huttner, *Chem. Ber.*, 110 (1977) 2951

14. H. Schmidbaur, Th. Pollock, R. Herr, F.E. Wagner, R. Bau J. Riede and G. Muller, *Organometallics*, 5 (1986) 566

15. H. Schmidbaur, R. Herr, G. Muller, J. Riede, *Organometallics*, 4 (1985) 1208

16. J. Shain, J.P. Fackler Jr., *Inorg. Chim. Acta*, 131 (1987) 157

17. R.J. Puddephatt, "The chemistry of gold", Elsevier, New York, 1978, pp. 53-58

18. W. Ludwig, W. Meyer, *Helv. Chim. Acta.*, 65 (1982) 934

19. J. Kozelka, H.R. Oswald, E. Dubler, *Acta. Crystallogr.*, C42 (1986) 1007

20. N.C. Payne, R.J. Puddephatt, R. Ravindranath, I. Treurnicht, *Can. J. Chem.*, 66 (1988) 3176

21. P.G. Jones, *Gold Bull.*, 14 (1981) 102; P.G. Jones, ibid., 14 (1981) 159

22. In Gmelin Handbuch der Anorganischen chemie, Edited by H. Schmidbaur, Springer-Verlag, Heidelberg, 1985, p.296

23. M.P. Brown, J.R. Fischer, R.H. Hill, R.J. Puddephatt, K.R. Seddon, *Inorg. Chem.*, 20 (1983) 3516

24. P.A.W. Dean, J.J. Vittal, R.S. Srivastava, *Can. J. Chem.*, 65 (1987) 2628

25. A. Shiotani, H.-F. Klein, H. Schmidbaur, *J. Amer. Chem. Soc.*, 93 (1971) 1555; H. Schmidbaur, A. Shiotani, H.-F. Klein, *Chem. Ber.*, 104 (1971) 2831

26. R.J. Puddephatt, In Comprehensive Organometallic Chemistry. Edited by G. Wilkinson, F.G.A. Stone, E.W. Abel. Pergamon, Oxford, 1982, Chap. 15

27. W. Bensch, M. Prelati, W. Ludwig, *J. Chem. Soc., Chem. Commun.*, (1986) 1762

28. R.J. Puddephatt, In Comprehensive Coordination Chemistry Edited by G. Wilkinson, R.D. Gillard, J.A. McCleverty. Pergamon, Oxford. 1987, Chap. 55

29. S.S.M. Ling, I.R. Jobe, Lj. Manojlovic Muir, K.W. Muir R.J. Puddephatt, *J. Chem. Soc., Chem. Commun.*, (1985) 566

30. D.M.P. Mingos, *Gold Bull.*, 17 (1984) 5

CHAPTER 3

SYNTHESIS AND CHARACTERIZATION OF A REMARKABLE CAGE COMPLEX: THE CRYSTAL AND MOLECULAR STRUCTURE OF $[Au_8Cl_2\{\mu_3\text{-}(MeO)_2PCHP(OMe)_2\}_2\{\mu_4\text{-}(MeO)_2PCP(OMe)_2\}_2].CHCl_3$

3.1 INTRODUCTION

3.1.1 Gold cluster complexes

The first example of a gold cluster compound, $Au_{11}I_3(PPh_3)_7$, was synthesized in 1968[3], and subsequent developments in this rapidly expanding field have originated mainly from research laboratories at the Universities of Nijmegen and Oxford[1]. The interest in this area of gold chemistry is apparent from the number of reviews published recently[1,3-6]. Despite appreciable practical difficulties both with synthesis and purification, and with crystal structure determinations (gold cluster compounds often display disorder and/or pseudosymmetry[2]), a number of new structures have appeared in the past 15 years.

All the known gold cluster entities are stabilized by tertiary phosphines and halide ligands. Gold clusters are broadly classified into two types. Firstly, 'low nuclearity' clusters, a term used to describe species which contain six or less gold atoms; While 'high nuclearity' clusters refers to complexes containing more than six gold atoms. The low nuclearity clusters have the

stoichiometries $[Au_x(PR_3)_{x+y}]^{n+}$ (y = 0,2) and the higher nuclearity derivatives $[Au_{x+1}(PR_3)_{x+y}X_y]^{n+}$, where

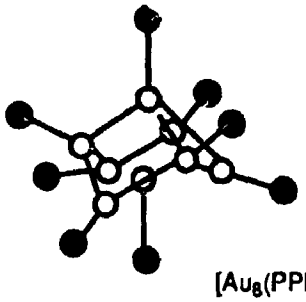

$[Au_8(PPh_3)_8]^{2+}$

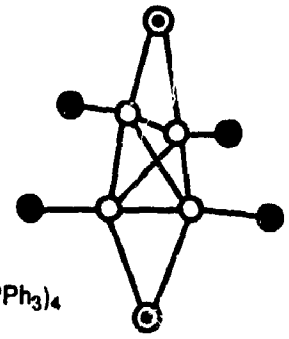

$Au_4I_2(PPh_3)_4$

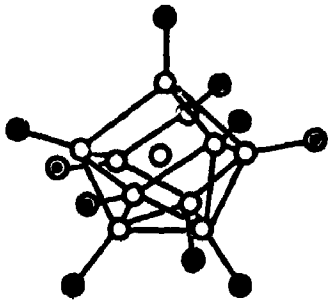

$Au_{11}I_3(PPh_3)_7$

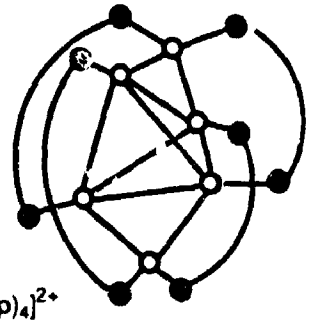

$[Au_6(dppp)_4]^{2+}$

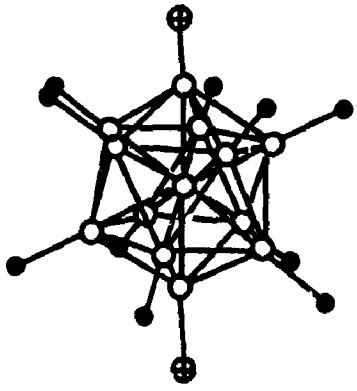

$[Au_{13}Cl_2(PMe_2Ph)_{10}]^{3+}$

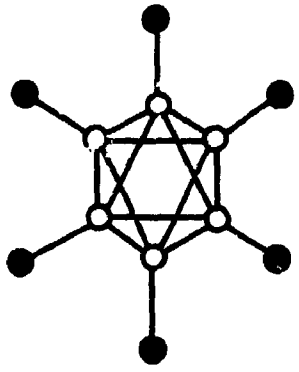

$[Au_6(Ptol_3)_6]^{2+}$

Legend: ○ Au, ● P, ◎ I, ⊕ Cl

Scheme 3.1

PR_3 = phosphine and X = halide. This difference arises because the higher nuclearity clusters contain an additional metal atom at the centre of the polyhedron. Scheme 3.1 illustrates the difference in stoichiometry. To the best of our knowledge, there are only two polynuclear gold complexes (nuclearity > 2) which contain deprotonated diphosphines, namely, $[Au_5(dppm)_3(\mu_3\text{-dppm-H})](NO_3)_2$ [7] and $[Au_4(C_6F_5)_2(\mu_3\text{-dppm-H})_2]$ [8], shown in scheme 3.2.

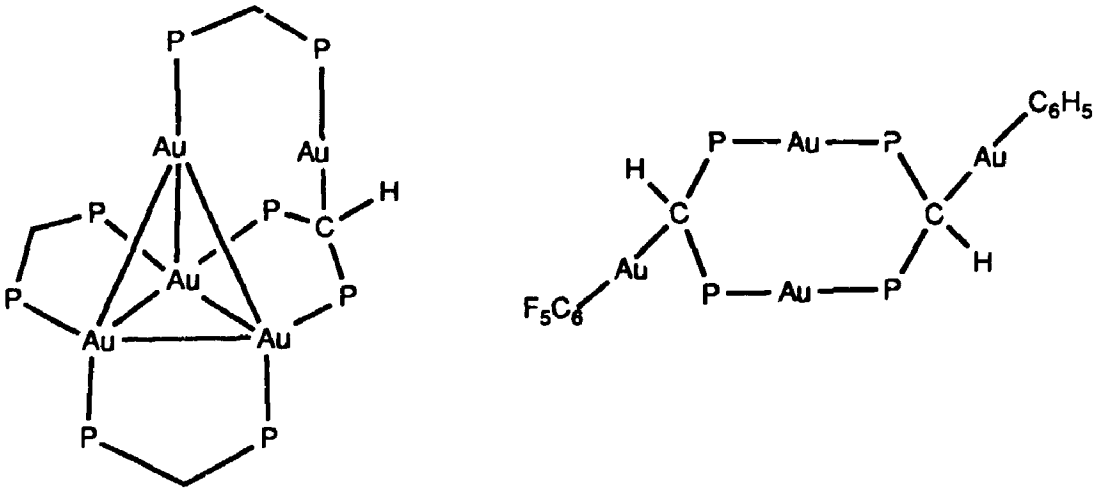

Scheme 3.2

As a continuation of our work on reactions of [AuCC*t*-Bu] with various diphosphines (as seen in chapter 2), we studied reactions with the diphosphine $CH_2[P(OMe)_2]_2$ (dmopm). The synthesis and isolation of dmopm ligand related complexes were carried out by Dr. Ilse Treurnicht of this laboratory. The products were unstable in solution and attempted crystallization resulted in loss of alkynyl ligands and oligomerization of the initial product was observed. During attempts to grow single crystals for X-ray analysis, recrystallization in $CHCl_3$/pentane resulted

in further loss of alkynyl ligands and yielded suitable crystals. A three-dimensional X-ray analysis on these crystals revealed a novel cage complex containing eight Au atoms and hitherto structurally uncharacterized $[\mu_4\text{-}(MeO)_2PCP(OMe)_2]^{2-}$ ligands, and the results are described in this chapter.

3.2 EXPERIMENTAL

3.2.1 Synthesis of $[Au_2(C{\equiv}Ct\text{-}Bu)_2(\mu\text{-dmopm})]$, 1a

[AuCCt-Bu] (0.400g, 1.44 mmol) was suspended in $CH_2C\ell_2$ (16mL). To this was added dmopm (MW 200.11, d 1.113 g cm^{-3}, 0.719 mmol). The mixture was stirred under nitrogen for 20 h. during which the solution developed a slight yellow colour. Solvent was then removed under reduced pressure yielding an orange oil which was quite unstable in air. Attempts at recrystallization were unsuccessful. ^1H n.m.r in $CD_2C\ell_2$, 20°C; [s, 18H, t-Bu], 2.67 [t, 2H, $^2J(PH)$ = 11, $P_2C\underline{H}_2$], 3.88 [m, 12H, $^3J(PH)$ = 15, MeO]. $^{31}P[^1H]$ NMR in $CD_2C\ell_2$, 20°C; δ +166.6 [s, P]

3.2.2 Synthesis of $[Au_2(\mu_3\text{-dmopm-H})(C{\equiv}Ct\text{-}Bu)]_3$, 3

Attempted crystallization of 1a by slow diffusion of pentane into a $CH_2C\ell_2$ solution yielded microcrystalline solid of complex 3. This conversion was shown by ^1H and ^{31}P NMR spectroscopy to take place in quantitative yield over several days. The crystals were needle-shaped and

macroscopically twinned; hence were not suitable for X-ray diffraction studies. Mp: 208°C. Anal. calcd. for $C_{11}H_{22}Au_2O_4P_2$: C, 19.6; H, 3.5. Found: C, 19.6; H, 3.4. ^1H NMR data in $CD_2C\ell_2$, 20°C: δ 1.13 [s, 9H, t-Bu]; 3.66 [d, 12H, $^3J(PH)$ = 13.2, OCH_3^a]; 3.85 [d, 6H, $^3J(PH)$ = 13.8, OCH_3^c]; 3.88 [d, 12H, $^3J(PH)$ = 13.6, OCH_3^b]; 4.01 [d, 6H, $^3J(PH)$ = 12.5, OCH_3^d]; 4.34 [dt, 3H, $^2J(PH)$ = 15.5, $^3J(PH)$ = 10, P_2CHAu]. $^{31}P\{^1H\}$ NMR data in $CD_2C\ell_2$, 20°C: δ 161.6 [m, P^a], 152.0 [m, P^x]; J(AA') = +20, J(AX) = J(A'X') = +130, J(AX') = J(A'X) = −4.8, J(XX') = 0. The ^{31}P NMR spectrum was simulated as an AA'XX' spin system, figure 3.1, but is consistent with $[AX]_n$ where $n > 2$ and probably $n = 3$.

3.2.3 Synthesis of $[Au_8C\ell_2\{\mu_3\text{-dmopm-H}\}_2\{\mu_4\text{-dmopm-H}_2\}_2].CHC\ell_3$, 4

Crystals of 3 were dissolved in $CHC\ell_3$ and layered with n-pentane. Slow diffusion of pentane into the $CHC\ell_3$ solution over several days yielded colourless, bladed X-ray diffraction quality crystals of 4 as the $CHC\ell_3$ solvate. Anal. calcd. for $C_{21}H_{51}Au_8C\ell_5O_{16}P_8$: C, 9.85; H, 2.0. Found: C, 9.80, H, 2.1. ^1H NMR data in $CD_2C\ell_2$, 20°C: 3.03 [dt, 1H, $^2J(PH)$ = 17, $^3J(PH)$ = 8, CHP_2], 3.12 [dt, 1H, $^2J(PH)$ = 17, $^3J(PH)$ = 8, CHP_2], 3.70 - 4.03 [m, 48H, OCH_3]. $^{31}P\{^1H\}$ NMR data in $CD_2C\ell_2$, 20°C: δ 157.7 [dd, $^3J(P^2P^3)$ = 64, $^3J(P^2P^7)$ = 18, 1P, P^2], 155.5 [dq, $^3J(P^4P^6)$ = 69, $^3J(P^3P^6)$ = $^3J(P^5P^6)$ = $^3J(P^8P^6)$ = 18, 1P,

P^6], 150.4 [dd, $^3J(P^4P^6)$ = 69, $^3J(P^4P^5)$ = 18, 1P, P^4], 149.9 [dd, $^3J(P^2P^3)$ = 64, $^3J(P^3P^6)$ = 18, 1P, P^3], 148.4 [d, $^3J(P^1P^5)$ = 25, 1P, P^1], 145.6 [dt, $^3J(P^1P^5)$ = 25, $^3J(P^4P^5)$ = $^3J(P^6P^5)$ =18, 1P, P^5], 126.4 [d, $^3J(P^2P^7)$ = $^3J(P^6P^8)$ = 18, 2P, P^7 and P^8].

3.2.4 X-ray data collection, data reduction and structure solution of 4

Transparent, colourless, bladed crystals of 4 were grown by slow diffusion of pentane into a chloroform solution. A preliminary photographic analysis showed no symmetry other than triclinic. The crystal density was determined by neutral buoyancy in mixtures of CH_2I_2 and pentane, and found to be 3.158(2) g cm^{-3}. The calculated volume was 2684 $Å^3$. With an empirical formula of $Au_8C\ell_5(dmopm)_4$, which was known at the beginning of crystal structure analysis, Z was calculated to be equal to 2 for which the calculated density is 3.168 g cm^{-3}. Thus the molecules have no crystallographically imposed symmetry.

The crystal chosen for collection of intensity data was of approximate dimensions 0.22 × 0.24 × 0.48 mm^3 with eight faces revealed by optical goniometry to be of the forms (100), (010), $(\bar{1}11)$ and $(01\bar{1})$. The (100) and $(\bar{1}11)$ forms were well developed, and a perspective view of the crystal is presented in appendix 5. Cell constants and an orientation matrix were obtained from the setting angles of 19 reflections with $25 < 2\theta < 40^\circ$. ω-scans of several

Table 3.1. Summary of X-ray Structure Determination of complex 4

Crystal Data	
compound, formula weight	$C_{21}H_{51}Au_8Cl_5O_{16}P_8$ 2560.4
crystal system, space group	triclinic, $P\bar{1}$ (no. 2)
cell dimens (Å, deg.)	a = 14.152(2) α = 91.17(1)
	b = 18.373(2) β = 114.77(1)
	c = 12.151(2) γ = 108.16(1)
cell volume (Å^3), Z	2684(2), 2
temperature, °C	23
density, g cm^{-3}, obsd; calc	3.158(2), 3.158
Experimental Details	
diffractometer, monochromator	Enraf-Nonius CAD4F, graphite
radiation, wavelength (Å)	Mo, λ(Kα mean) 0.71073
cryst-detec (mm), t.o.a. (°)	205, 2.5
aperture (mm), vert; horiz	4.0; 6.0 + 0.35tanθ
centering reflec; θ range	19; 25 < 2θ < 40
Data Collection	
approx. crystal dimens (mm)	0.22 × 0.24 × 0.48
cryst vol (mm^3); no of faces	12.9 × 10^{-3}; 8
face indices	{100}, {0$\bar{1}$1}, {010} and {$\bar{1}$11}
scan mode, width (°)	ω-2θ, 0.90 + 0.35tanθ
index, θ ranges	-16 ≤ h ≤ 16, -21 ≤ k ≤ 21,
	0 ≤ l ≤ 14; 0 ≤ θ ≤ 25°
scan speed (deg min^{-1})	1.0 to 2.5
max time per datum, total time	90s, 220h
standard reflections	00$\bar{4}$, 020, 060 and 430
monitor frequency, % var	180m. 12.2
no of data, standards collected	10219, 308

Table 3.1, continued.

Data Processing	
corrections	Lorentz, polarization and monochromator polarization
decay, absorption corrections	Isotropic; Gaussian
abs coeff (cm^{-1}); grid size	222.8, 8 × 10 × 20
transmission, max., min.	0.094, 0.024
no of unique data, signif.	9418, I > 0
Structure Refinement	
no. of observ., variables	5677, 436
final model; R_1 and R_2	0.036, 0.037
top resid., (e $Å^{-3}$ coord.)	1.76 (0.230 0.341 0.453)
largest shift, parameter	0.23, Y-coordinate of O42(A)
Computer software	SHELX-86 and SHELX-76

intense, low-angle reflections had an average width of 0.125 and 0.142° before and after the data collection, respectively. 10219 reflections were collected over 9 days using a ω-2θ scan, out to a maximum 2θ of 50°. Scan widths of 0.90° and variable scan rates within a maximum time per datum of 90s were used. Standard reflections $00\bar{4}$, 020, 060 and $\bar{4}30$ were recorded every 10800s of X-ray exposure time and showed an average decay of -12.2%. As this was thought to be significant, an isotropic decay correction was applied[14]. The data were corrected for background, monochromator polarization, Lorentz and polariztion. A Gaussian absorption correction was applied[14] and 663 symmetry equivalent reflections were averaged to give 9418 unique reflections with $I > 0$ for the analysis. Crystal data and parameters associated with data collection are given in Table 3.1.

Several attempts to solve the structure using Patterson and Fourier techniques were unsuccessful due to the complexity of the structure. The presence of a large number of heavy atoms gave rise to several unresolved, intense, overlapping peaks. Using Sheldrick's SHELXS-86 program[9], the position of the eight Au atoms, eight P atoms and those of five chlorines were found. After several cycles of least-squares refinement and a difference Fourier synthesis, the positions of all the remaining non-H atoms in the complex were revealed. Refinement proceeded smoothly yielding residuals of $R_1 = 0.0375$ and $R_2 = 0.0471$

for the model where Au, P and Cℓ atoms were assigned anisotropic, and O and C atoms isotropic thermal parameters. Several of the methoxy groups showed excessive thermal motion, so the final refinement was carried out using SHELX-76[10]. A disorder model was necessary for one of the methoxy groups, namely -O(42)C(42), while assignment of anisotropic thermal parameters was sufficient for C(12), C(81) and C(82). The geometries of the disordered -OMe groups and those of O(12)-C(12), O(81)-C(81), O(82)-C(82) were constrained with DFIX (O-C = 1.43(1)Å and P-C = 2.625(1)Å).

48 Hydrogen atoms (all but those of the disordered methoxy group O(42)/C(42)) could be located in a difference Fourier map with peak heights between 0.33(6) and 0.79(6) eÅ^{-3} and were included in idealized positions (sp^3, C-H = 0.95Å, staggered conformation) in calculations of F_C, but not refined. The structure was refined by full-matrix least-squares on F, minimizing $\Sigma w(|F_O| - |F_C|)^2$, weight = $0.854/[(\sigma(F))^2 + 0.000938F^2]$. Neutral atom scattering factors were taken from ref.15 and H atom scattering factors were those of Stewart *et al*[16]. Refinement progressed until no shifts in atomic positional parameters greater than 0.1 were observed. A statistical analysis of structure factors showed evidence for the presence of secondary extinction (i.e, $F_C > F_O$ for intense low angle reflections). Hence an extinction correction was included[17], refined coefficient = $8.8(13) \times 10^{-5}$. In the

final cycle 436 variables were refined using 5677 unique reflections with $I > 2.5\sigma(I)$. The final residuals were $R_1 = 0.0355$ and $R_2 = 0.0371$. A total difference Fourier synthesis showed the highest peak, with an electron density of 1.76 $eÅ^{-3}$, located 1.12 Å from Au(1). A statistical analysis of R_1 and R_2 in terms of data collection order, $|F_o|$, $\lambda^{-1}\sin\theta$ and classes of indices showed no unusual trends, thus indicating a satisfactory weighting scheme. Final positional and U(equivalent) thermal parameters for non-H atoms are given in Table 3.2. Anisotropic thermal parameters, H-atom parameters, selected torsion angles and weighted least-squares plane calculations are given in Tables 3.3, 3.4, 3.5 and 3.6 respectively. Structure amplitudes are listed in appendix 1.

3.3 RESULTS AND DISCUSSION

3.3.1 Characterization of the products of reaction of [AuC≡Ct-Bu] with dmopm

The reaction of [AuC≡Ct-Bu] with the ligand dmopm, is complex. The first product formed, **1a**, was obtained as an orange oil which was short-lived in solution and attempts to isolate it as a solid gave a mixture of complexes. The ^1H NMR spectrum of **1a** reveals a triplet centred at δ 2.67 due to CH_2P_2 protons, with $^2J(PH) = 11$ Hz. The $^{31}P\{^1H\}$ NMR spectrum of **1a** gave a singlet at δ 166.6 indicating that the phosphorus nuclei are chemically equivalent. These data suggest a symmetric dimeric

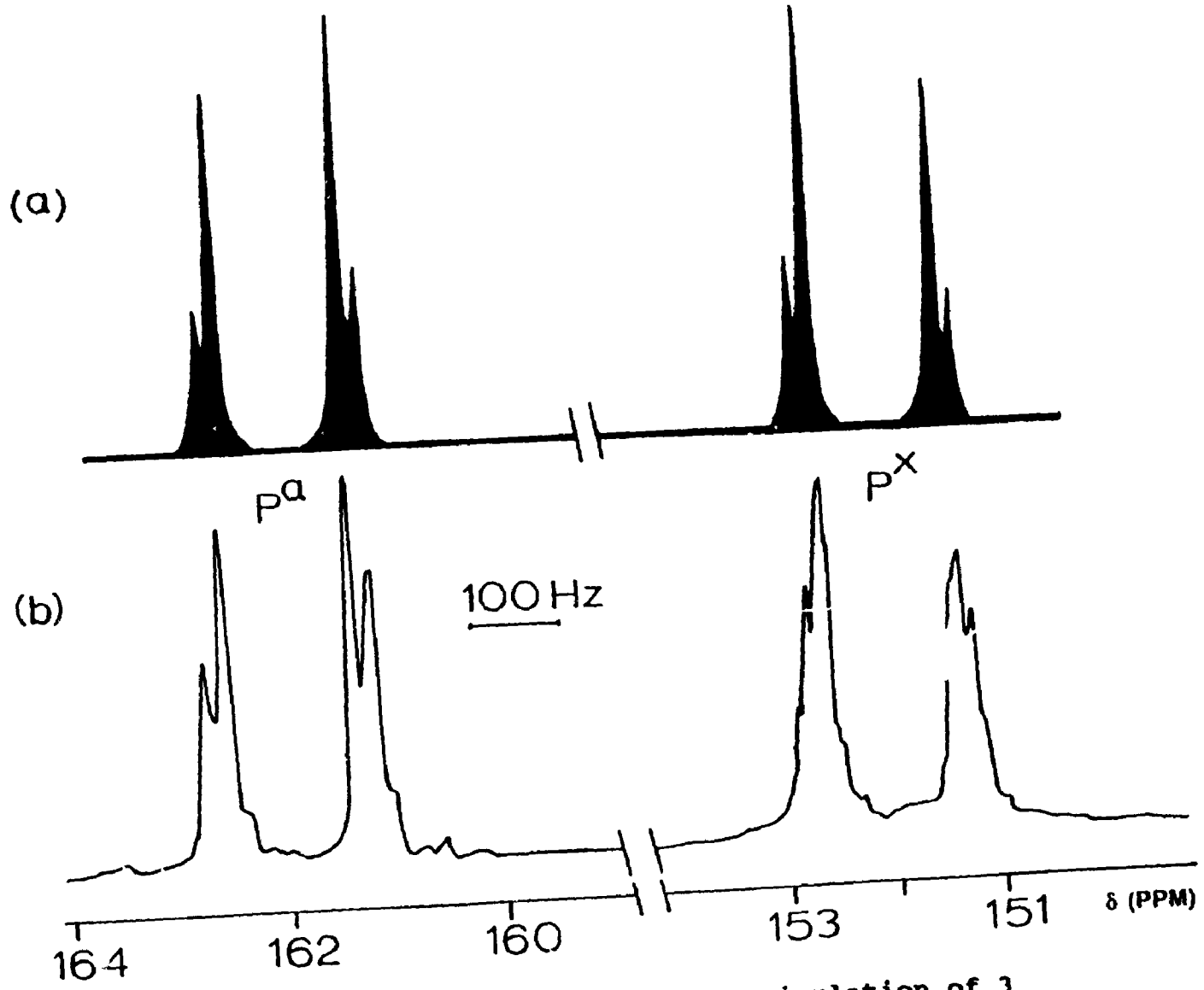

Figure 3.1: (a) $^{31}P\{^1H\}$ NMR spectrum simulation of **1**
(b) Observed $^{31}P\{^1H\}$ NMR spectrum (121.4 MHz) of **1**

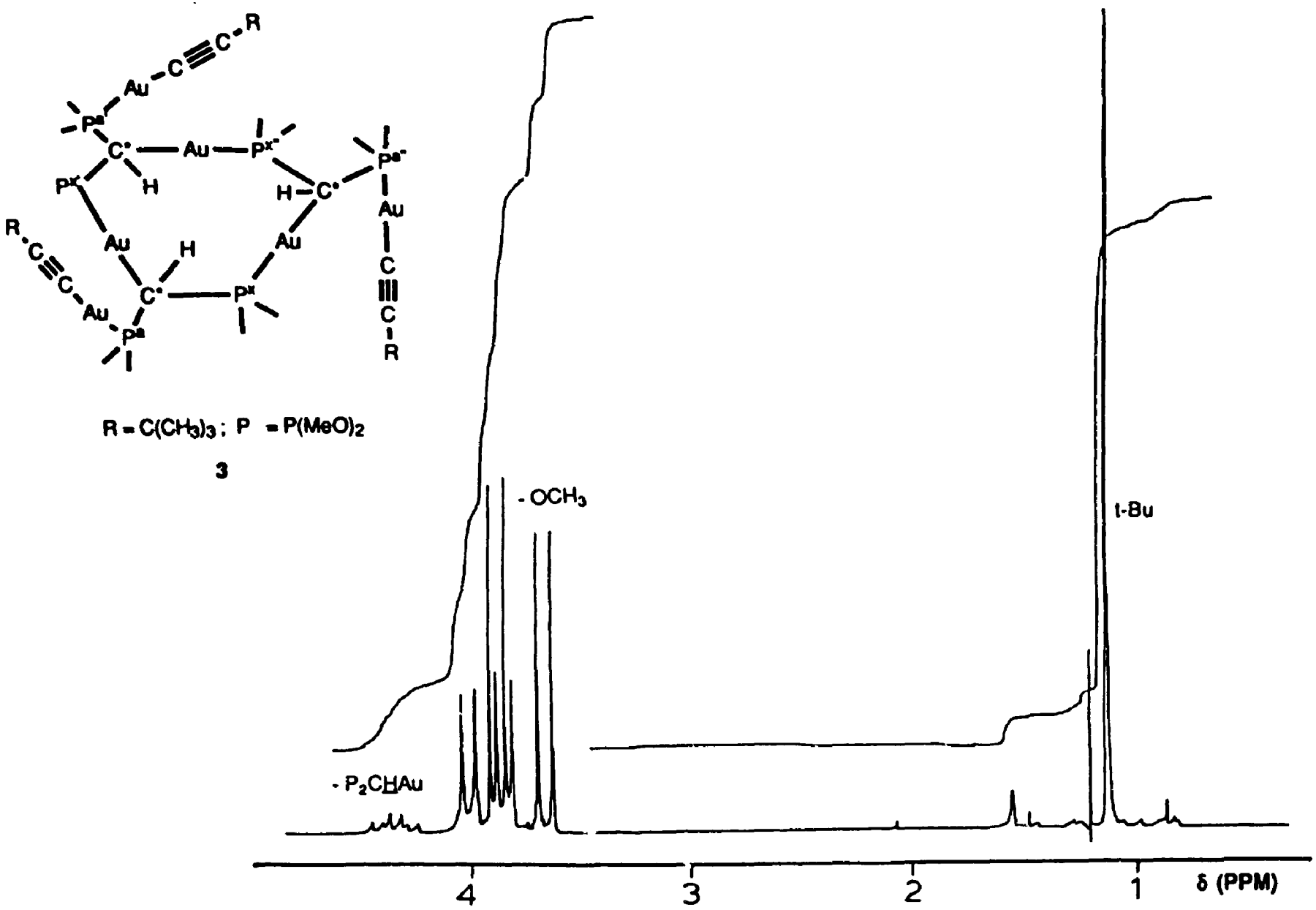

Figure 3.2: ^{1}H NMR spectrum (200 MHz) of 3

structure for 1a, as shown in scheme 3.3.

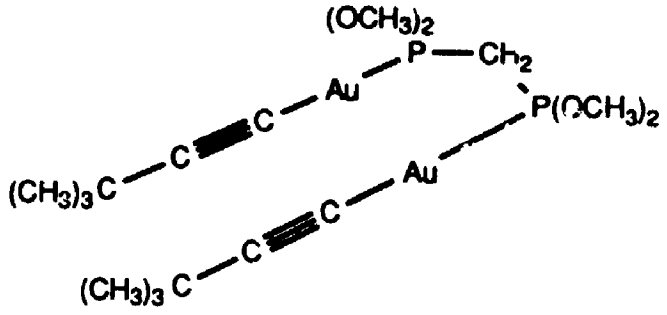

Scheme 3.3

3.3.2 Characterization of $[Au_2(\mu_3\text{-dmopm-H})(C{\equiv}Ct\text{-Bu})]_n$, 3

Slow crystallization of 1a from $CH_2C\ell_2$/pentane gave a single colourless product whose elemental analysis suggested a formulation as $[Au_2(\mu_3\text{-dmopm-H})(C{\equiv}Ct\text{-Bu})]_n$, 3. The $^{31}P\{^1H\}$ NMR spectrum (figure 3.1) of this complex appeared as an apparent AA'XX' multiplet. The ^1H NMR spectrum (figure 3.2) showed four sets of doublets in the methoxy region in the ratio 2:1:2:1, while the methylene protons of the diphosphine gave a single resonance appearing as a doublet of triplets. We were unable to deduce the structure of 3 from these data. Unfortunately the crystals were twinned and unsuitable for single-crystal studies , so a further crystallization was attempted.

3.3.3 Syntheis and characterization of $[Au_8C\ell_2(\mu_3\text{-dmopm-H})_2(\mu_4\text{-dmopm-H}_2)_2].CHC\ell_3$, 4

A different solvent system was then tried in an

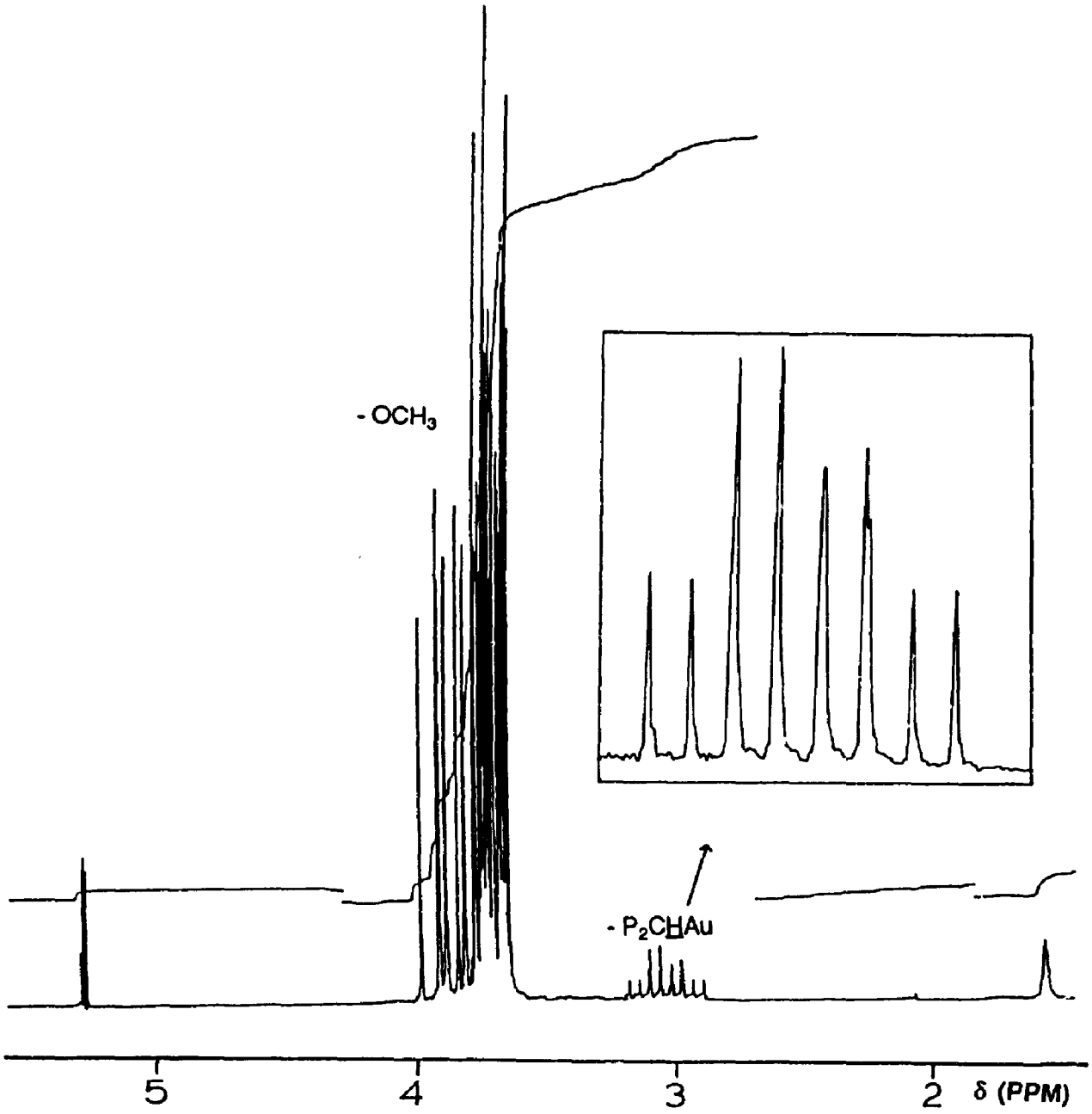

Figure 3.3: ^1H NMR spectrum (200 MHz) of 4

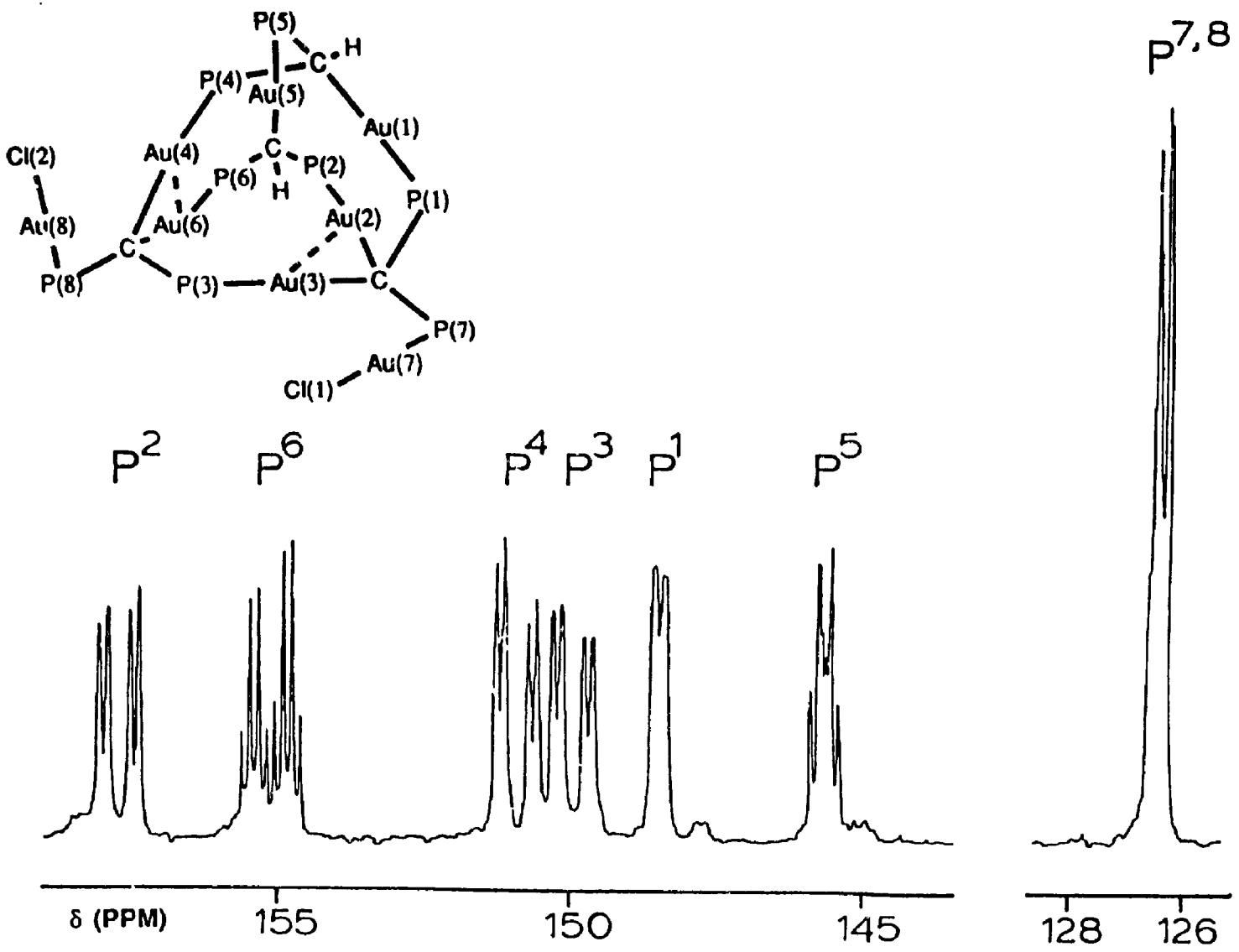

Figure 3.4: $^{31}P\{^{1}H\}$ NMR spectrum (121.4 MHz) of 4

attempt to grow suitable single crystals of 3 for structural studies. Recrystallization of 3 from $CHC\ell_3$/pentane was carried out over several days, and yielded beautiful, colourless, single crystals suitable for X-ray analysis. The ^1H and $^{31}P\{^1H\}$ NMR spectra (figure 3.3 and 3.4) were very complex and different from that observed for 3, and elemental analysis also suggested formation of another new complex. The only information that was derived from the $^{31}P\{^1H\}$ NMR spectrum was that there were eight phosphorus atoms in the new complex; six of which were chemically inequivalent. This suggested that there were four dmopm ligands coordinated to eight gold atoms. A combination of elemental analysis, NMR spectral data and the preliminary X-ray data indicated that complex 4 had an empirical formula, $Au_8C\ell_5(dmopm)_4$, and a full, three-dimensional X-ray analysis was undertaken.

3.3.4 Description of the crystal and molecular structure of 4

The crystal structure consists of discrete molecules of the octagold complex, 4, and chloroform. The closest distance of approach being 2.19Å between the symmetry related atoms of H723 at (x,y,z) and (1-x, 1-y, 1-z). The molecular structure of 4 shown in figure 3.5 is characterized by the bond lengths and angles listed in Tables 3.7 and 3.8 respectively. Some weighted least-squares planes are given in Table 3.6. A stereo view

Table 3.2. Atomic Positional ($\times 10^4$) and Thermal ($\times 10^3$) Parameters of 4

Atom	x	y	z	$U_{eq}(\AA^2)$
Au(1)	1085.7(6)	1525.6(4)	1352.6(6)	40.4(3)
Au(2)	2358.2(5)	3338.1(4)	3646.9(6)	38.5(3)
Au(3)	661.8(5)	3516.6(4)	1336.9(6)	35.2(3)
Au(4)	-1521.4(5)	1785.4(4)	953.0(6)	36.3(3)
Au(5)	721.2(6)	1561.4(4)	4275.5(6)	40.3(3)
Au(6)	-783.4(5)	2868.0(4)	3220.7(6)	36.5(3)
Au(7)	2795.9(6)	5171.0(4)	3130.1(7)	45.3(3)
Au(8)	-3616.5(6)	1561.0(4)	1904.1(7)	52.0(3)
Cℓ(1)	2332(5)	5860(3)	4317(5)	67(2)
Cℓ(2)	-4042(7)	502(4)	2829(7)	98(4)
Cℓ(3)	5841(7)	2339(5)	4817(9)	125(5)
Cℓ(4)	5256(12)	1011(8)	5886(12)	192(9)
Cℓ(5)	3572(8)	1357(8)	3887(13)	212(8)
P(1)	2246(4)	2623(3)	1157(4)	39(2)
P(2)	2525(4)	3189(3)	5536(4)	40(2)
P(3)	-1023(3)	3594(2)	860(4)	32(2)
P(4)	-1344(4)	659(2)	463(4)	42(2)
P(5)	162(4)	463(3)	2954(4)	44(2)
P(6)	189(4)	2862(3)	5232(4)	38(2)
P(7)	3107(4)	4403(3)	1970(4)	39(2)
P(8)	-3156(4)	2561(3)	998(4)	40(2)
O(11)	1990(11)	2666(8)	-246(11)	54(6)
O(12)	3511(10)	2674(7)	1685(12)	57(6)
O(21)	2982(11)	4028(7)	6386(11)	58(6)
O(22)	3402(11)	2780(8)	6276(12)	59(6)
O(31)	-1011(9)	4372(6)	1494(10)	39(5)
O(32)	-1746(9)	3628(7)	-547(10)	45(5)
O(41)	-1328(11)	557(8)	-838(11)	59(6)
O(42)B	-2346(23)	-106(23)	569(28)	49(7)
O(42)A	-2384(15)	-108(14)	141(18)	49(4)
O(51)	-851(12)	-153(7)	3055(13)	63(7)
O(52)	1070(11)	63(7)	3325(12)	58(6)

Table 3.2, continued.

Atom	x	y	z	U_{eq}(Å^2)
O(61)	-487(9)	2244(7)	5772(11)	47(5)
O(62)	564(10)	3645(7)	6153(11)	53(6)
O(71)	2813(10)	4548(7)	590(10)	49(5)
O(72)	4384(9)	4504(7)	2401(11)	51(5)
O(81)	-3840(10)	2411(9)	-452(12)	74(7)
O(82)	-3454(11)	3301(8)	1277(10)	64(7)
C(1)	4923(27)	1349(20)	4497(30)	124(11)
C(11)	919(25)	2651(17)	-1126(26)	98(8)
C(12)	3771(12)	2055(13)	1291(26)	114(17)
C(17)	2252(14)	3455(10)	1864(15)	40(4)
C(21)	3267(18)	4090(13)	7667(19)	65(6)
C(22)	4469(22)	3101(16)	6329(24)	87(7)
C(26)	1336(15)	2547(10)	5640(17)	47(4)
C(31)	-394(16)	5109(11)	1347(17)	54(5)
C(32)	-1901(16)	3076(11)	-1508(18)	55(5)
C(38)	-1757(13)	2829(9)	1326(14)	36(4)
C(41)	-2088(24)	743(17)	-1860(26)	97(8)
C(42)A	-3240(14)	-116(13)	480(30)	54(4)
C(42)B	-3451(10)	-138(22)	-209(44)	54(4)
C(45)	-79(13)	503(10)	1422(14)	39(4)
C(51)	-1278(22)	-942(15)	2462(23)	84(7)
C(52)	1610(20)	-59(14)	4597(21)	73(6)
C(61)	-1560(18)	2226(13)	5605(19)	64(5)
C(62)	559(21)	4356(15)	5698(23)	82(7)
C(71)	3365(16)	5294(11)	389(17)	54(5)
C(72)	5042(18)	4374(12)	3637(19)	62(5)
C(81)	-4991(16)	1932(27)	-1057(13)	218(26)
C(82)	-3139(20)	3604(10)	2522(14)	82(13)

$$U_{eq} = \frac{1}{3} \sum_i \sum_j U_{ij}\, a_i\, a_j\, a_i \cdot a_j .$$

Table 3.3. Anisotropic thermal parameters (x 10^3)

Atom	U_{11}	U_{22}	U_{33}	U_{12}	U_{13}	U_{23}
Au(1)	38.8(4)	34.0(4)	49.4(4)	12.7(3)	20.5(3)	8.6(3)
Au(2)	36.2(4)	39.4(4)	40.3(4)	13.3(3)	17.2(3)	10.7(3)
Au(3)	28.7(3)	36.5(4)	42.4(4)	13.4(3)	16.4(3)	11.2(3)
Au(4)	35.1(4)	30.4(3)	42.3(4)	12.7(3)	15.4(3)	5.1(3)
Au(5)	45.2(4)	30.4(4)	45.1(4)	13.4(3)	20.0(3)	5.1(3)
Au(6)	38.6(4)	36.5(4)	34.9(4)	16.8(3)	14.2(3)	10.3(3)
Au(7)	43.9(4)	40.1(4)	48.3(4)	17.3(3)	15.6(3)	4.9(3)
Au(8)	48.2(5)	45.6(4)	61.2(5)	11.0(3)	27.2(4)	18.8(4)
Cℓ(1)	77(4)	65(3)	63(3)	45(3)	23(3)	4(3)
Cℓ(2)	129(6)	62(4)	102(5)	13(4)	63(5)	42(4)
Cℓ(3)	80(5)	105(6)	174(9)	14(4)	56(5)	0(6)
Cℓ(4)	237(15)	184(12)	177(11)	92(11)	97(11)	91(10)
Cℓ(5)	75(6)	209(13)	263(15)	-4(7)	31(8)	87(11)
P(1)	31(2)	42(3)	44(3)	14(2)	16(2)	8(2)
P(2)	37(2)	41(3)	40(2)	13(2)	15(2)	7(2)
P(3)	32(2)	33(2)	36(2)	13(2)	18(2)	12(2)
P(4)	50(3)	27(2)	48(3)	12(2)	21(2)	4(2)
P(5)	54(3)	30(2)	52(3)	16(2)	26(2)	10(2)
P(6)	39(2)	39(2)	34(2)	15(2)	14(2)	8(2)
P(7)	30(2)	37(2)	47(3)	10(2)	15(2)	12(2)
P(8)	34(2)	44(3)	48(3)	17(2)	21(2)	17(2)

Table 3.3, continued.

Atom	U_{11}	U_{22}	U_{33}	U_{12}	U_{13}	U_{23}
O(11)	61(8)	67(9)	47(7)	28(7)	32(7)	6(6)
O(12)	37(7)	50(8)	81(9)	18(6)	24(7)	0(7)
O(21)	72(9)	43(7)	50(8)	-0(6)	33(7)	-10(6)
O(22)	50(8)	70(10)	65(9)	33(7)	30(7)	21(7)
O(31)	39(6)	24(6)	53(7)	12(5)	18(6)	11(5)
O(32)	39(7)	55(8)	42(7)	25(6)	13(6)	20(6)
O(41)	61(9)	66(9)	49(8)	34(7)	15(7)	7(7)
O(51)	73(10)	37(7)	83(10)	9(7)	47(8)	17(7)
O(52)	76(10)	53(8)	61(8)	45(7)	29(7)	17(7)
O(61)	37(7)	59(8)	49(7)	19(6)	20(6)	13(6)
O(62)	59(8)	42(7)	55(8)	21(6)	19(7)	3(6)
O(71)	40(7)	54(8)	43(7)	14(6)	13(6)	16(6)
O(72)	31(7)	67(9)	52(8)	14(6)	17(6)	22(6)
O(81)	40(8)	103(12)	55(9)	15(8)	7(7)	27(8)
O(82)	73(10)	66(9)	99(11)	48(8)	61(9)	47(8)
C(12)	104(23)	100(22)	140(27)	64(19)	38(20)	-11(19)
C(81)	196(44)	206(44)	64(21)	-76(34)	-18(24)	24(24)
C(82)	106(20)	51(13)	116(21)	31(13)	70(18)	11(13)

$$U = \exp\left[-2\pi^2\left[U_{11}h^2a^{*2} + U_{22}k^2b^{*2} + U_{33}\ell^2c^{*2} + 2U_{12}hka^*b^* + 2U_{13}h\ell a^*c^* + 2U_{23}k\ell b^*c^* \right]\right]$$

Table 3.4. Hydrogen atom Positional ($\times 10^4$) and thermal ($\times 10^3$) Parameters for 4

Atom	x	y	z	$U(\text{Å}^2)$
H1	4986	1025	3932	136
H26	1581	2484	6477	51
H45	-68	19	1150	43
H111	907	2681	-1912	70
H112	771	3080	-878	70
H113	363	2179	-1177	70
H121	4554	2176	1685	70
H122	3517	1994	421	70
H123	3416	1587	1492	70
H211	3518	4621	8022	70
H212	3842	3885	8062	70
H213	2632	3803	7770	70
H221	4919	2820	6783	70
H222	4797	3630	6719	70
H223	4401	3069	5516	70
H311	-466	5512	1773	70
H312	-671	5142	497	70
H313	368	5164	1673	70
H321	-2347	3177	-2285	70
H322	-2259	2566	-1421	70
H323	-1198	3119	-1464	70
H411	-1967	650	-2554	70
H412	-1990	1276	-1700	70
H413	-2822	429	-2023	70
H511	-1881	-1231	2615	70
H512	-707	-1158	2773	70
H513	-1527	-961	1600	70
H521	2130	-302	4670	70
H522	1065	-378	4812	70
H523	1989	431	5137	70
H611	-1850	1825	5982	70
H612	-2049	2128	4751	70

Table 3.4, continued.

Atom	x	y	z	U(Å²)
H613	-1492	2713	5973	70
H621	804	4760	6365	70
H622	-173	4296	5112	70
H623	1046	4487	5326	70
H711	3109	5295	-469	70
H712	4145	5403	767	70
H713	3209	5683	740	70
H721	5777	4456	3756	70
H722	4708	3854	3717	70
H723	5064	4725	4240	70
H811	-5262	1908	-1922	70
H812	-5400	2147	-781	70
H813	-5077	1422	-871	70
H821	-3368	4036	2539	70
H822	-2353	3767	2983	70
H823	-3483	3212	2869	70

Table 3.5. Selected Torsion Angles (°) in 4

Atom 1	Atom 2	Atom 3	Atom 4	Angle
Au(2)	P(2)	C(26)	Au(5)	44.0 (10)
Au(2)	P(2)	C(26)	P(6)	-69.8 (12)
Au(4)	P(4)	C(45)	Au(1)	-54.0(9)
Au(4)	P(4)	C(45)	P(5)	62.8(11)
Au(5)	P(5)	C(45)	Au(1)	36.2(12)
Au(5)	P(5)	C(45)	P(4)	-74.8(11)
Au(6)	P(6)	C(26)	Au(5)	-43.1(10)
Au(6)	P(6)	C(26)	P(2)	71.4(11)
Au(1)	P(1)	C(17)	Au(3)	-52.2(9)
Au(1)	P(1)	C(17)	P(7)	176.3(9)
Au(7)	P(7)	C(17)	Au(2)	-42.5(10)
Au(7)	P(7)	C(17)	Au(3)	50.0(10)
Au(7)	P(7)	C(17)	P(1)	-175.0(10)
Au(3)	P(3)	C(38)	Au(4)	-40.5(9)
Au(3)	P(3)	C(38)	Au(6)	55.1(9)
Au(3)	P(3)	C(38)	P(8)	-171.5(9)
Au(8)	P(8)	C(38)	Au(4)	49.0(7)
Au(8)	P(8)	C(38)	Au(6)	-45.1(9)
Au(8)	P(8)	C(38)	P(3)	-177.8(9)

Table 3.6. Selected Least-Squares Planes

Plane	Atoms	Crystallographic Equation of Plane
1	P(4) C(45) P(5)	-1.8738 X - 16.0132 Y - 0.1247 Z + 0.8090 = 0
2	Au(1) Au(4) Au(5)	-1.6122 X - 16.2382 Y - 0.0069 Z + 2.6540 = 0
3	P(2) C(26) P(6)	2.1787 X - 5.7422 Y - 10.5441 Z + 7.1182 = 0
4	Au(1) Au(2) Au(3)	12.0020 X + 2.4867 Y - 8.6192 Z - 0.5167 = 0
5	Au(2) Au(3) Au(7)	12.4339 X - 5.6699 Y - 9.5683 Z + 2.4502 = 0
6	P(1) C(17) P(7)	-6.2633 X + 6.5081 Y - 7.6095 Z + 0.5798 = 0
7	Au(3) Au(4) Au(6)	-9.7519 X + 12.9597 Y - 3.0152 Z - 3.5092 = 0
8	Au(4) Au(6) Au(8)	-4.3235 X + 15.3303 Y - 5.9135 Z - 2.8305 = 0
9	P(3) C(38) P(8)	4.1477 X - 9.8459 Y - 9.6457 Z + 4.7927 = 0
10	Au(2) Au(5) Au(6)	0.1631 X - 0.2819 Y - 0.9455 Z - 5.2604 = 0

Plane No.	Plane No.	Dihedral Angle (deg)
1	2	1.5
3	10	0.6
4	5	28.0
4	6	90.1
5	6	89.1
7	8	27.0
7	9	91.1
8	9	89.7

Table 3.7. Selected bond distances in 4 (Å)

Atom 1	Atom 2	Distance	Atom 1	Atom 2	Distance
Au(1)	Au(2)	3.712(1)	Au(6)	C(38)	2.116(23)
Au(1)	Au(3)	3.887(1)	Au(7)	Cl(1)	2.313(7)
Au(1)	Au(4)	3.699(1)	Au(7)	P(7)	2.236(7)
Au(1)	Au(5)	3.798(1)	Au(8)	Cl(2)	2.310(8)
Au(8)	P(8)	2.225(7)	Cl(3)	C(1)	1.80(5)
Au(2)	Au(3)	2.938(1)	Cl(5)	C(1)	1.74(5)
Au(2)	Au(5)	3.671(1)	Cl(4)	C(1)	1.74(5)
Au(2)	Au(6)	4.054(1)	P(2)	C(26)	1.79(3)
Au(2)	Au(7)	3.351(1)	Au(3)	Au(4)	3.534(1)
P(6)	C(26)	1.77(3)	Au(3)	Au(6)	3.655(1)
P(7)	C(17)	1.75(3)	Au(3)	Au(7)	3.406(1)
Au(4)	Au(5)	4.085(1)	Au(4)	Au(6)	2.951(1)
Au(4)	Au(8)	3.525(2)	Au(5)	Au(6)	3.601(1)
P(1)	C(17)	1.74(2)	Au(6)	Au(8)	3.587(2)
Au(1)	P(1)	2.258(7)	O(42)B	C(42)B	1.44
Au(1)	C(45)	2.108(25)	O(42)A	C(42)A	1.43
Au(2)	P(2)	2.238(7)	O(82)	C(82)	1.43(2)
Au(2)	C(17)	2.129(24)	O(51)	C(51)	1.43(4)
Au(3)	P(3)	2.258(6)	O(52)	C(52)	1.47(4)
Au(3)	C(17)	2.107(24)	O(61)	C(61)	1.43(3)
Au(4)	P(4)	2.258(6)	O(62)	C(62)	1.44(4)
Au(4)	C(38)	2.117(23)	O(71)	C(71)	1.43(3)
Au(5)	P(5)	2.255(7)	O(72)	C(72)	1.47(3)
Au(5)	C(26)	2.115(26)	O(81)	C(81)	1.43
Au(6)	P(6)	2.249(6)	P(3)	C(38)	1.73(2)
P(4)	O(42)B	1.71(5)	P(4)	C(45)	1.80(3)
P(5)	C(45)	1.75(2)	P(8)	C(38)	1.75(2)
P(1)	O(11)	1.60(2)	P(1)	O(12)	1.60(2)
P(2)	O(21)	1.62(2)	P(2)	O(22)	1.61(2)
P(3)	O(31)	1.60(2)	P(3)	O(32)	1.60(2)
P(4)	O(41)	1.60(2)	P(4)	O(42)A	1.58(3)
P(5)	O(51)	1.58(2)	P(5)	O(52)	1.58(2)

Table 3.7, continued.

Atom 1	Atom 2	Distance	Atom 1	Atom 2	Distance
P(6)	O(61)	1.59(2)	P(6)	O(62)	1.60(2)
P(7)	O(71)	1.61(2)	P(7)	O(72)	1.60(2)
P(8)	O(81)	1.58(2)	P(8)	O(82)	1.61(2)
O(11)	C(11)	1.43(4)	O(12)	C(12)	1.43(2)
O(21)	C(21)	1.43(3)	O(22)	C(22)	1.41(4)
O(31)	C(31)	1.43(3)	O(32)	C(32)	1.43(3)
O(41)	C(41)	1.39(4)			

Table 3.8. Selected Bond Angles (°) in 4

Atom 1	Atom 2	Atom 3	Angle	Atom 1	Atom 2	Atom 3	Angle
P(1)	Au(1)	C(45)	176.2(7)	P(2)	Au(2)	C(17)	177.5(7)
P(3)	Au(3)	C(17)	177.5(7)	P(4)	Au(4)	C(38)	177.2(7)
P(5)	Au(5)	C(26)	174.8(8)	P(6)	Au(6)	C(38)	177.4(7)
Cℓ(1)	Au(7)	P(7)	174.4(3)	Cℓ(2)	Au(8)	P(8)	177.5(3)
Au(3)	Au(2)	P(2)	136.5(2)	Au(2)	Au(3)	P(3)	131.2(2)
Au(6)	Au(4)	P(4)	136.9(2)	Au(4)	Au(6)	P(6)	133.2(2)
Au(1)	P(1)	O(11)	112.3(8)	Au(1)	P(1)	O(12)	114.8(8)
Au(1)	P(1)	C(17)	112.3(9)	O(11)	P(1)	O(12)	98.8(10)
O(11)	P(1)	C(17)	110.8(11)	O(12)	P(1)	C(17)	107.0(11)
Au(2)	P(2)	O(21)	110.3(8)	Au(2)	P(2)	O(22)	114.3(8)
Au(2)	P(2)	C(26)	117.1(9)	O(21)	P(2)	O(22)	104.8(11)
O(21)	P(2)	C(26)	110.6(11)	O(22)	P(2)	C(26)	98.7(12)
Au(3)	P(3)	O(31)	115.7(7)	Au(3)	P(3)	O(32)	116.0(7)
Au(3)	P(3)	C(38)	108.6(8)	O(31)	P(3)	O(32)	99.0(9)
O(31)	P(3)	C(38)	106.5(10)	O(32)	P(3)	C(38)	110.6(11)
Au(4)	P(4)	O(41)	114.0(8)	Au(4)	P(4)	O(42)B	109.6(17)
Au(4)	P(4)	O(42)A	116.3(10)	Au(4)	P(4)	C(45)	117.8(8)
O(41)	P(4)	O(42)B	112.2(19)	O(41)	P(4)	O(42)A	95.6(13)
O(41)	P(4)	C(45)	99.5(10)	O(42)B	P(4)	C(45)	103.2(16)
O(42)	P(4)	C(45)	110.4(14)	Au(5)	P(5)	O(51)	107.7(8)
Au(5)	P(5)	O(52)	112.7(8)	Au(5)	P(5)	C(45)	120.3(9)

Table 3.8, continued.

Atom 1	Atom 2	Atom 3	Angle	Atom 1	Atom 2	Atom 3	Angle
O(51)	P(5)	O(52)	104.2(11)	O(51)	P(5)	C(45)	112.4(12)
O(52)	P(5)	C(45)	98.4(11)	Au(6)	P(6)	O(61)	113.9(7)
Au(6)	P(6)	O(62)	115.9(7)	Au(6)	P(6)	C(26)	116.7(9)
O(61)	P(6)	O(62)	100.9(10)	O(61)	P(6)	C(26)	98.2(11)
O(62)	P(6)	C(26)	108.9(11)	Au(7)	P(7)	O(71)	116.7(9)
Au(7)	P(7)	O(72)	115.7(8)	Au(7)	P(7)	C(17)	105.8(8)
O(71)	P(7)	O(72)	97.7(10)	O(71)	P(7)	C(17)	106.7(11)
O(72)	P(7)	C(17)	114.2(11)	Au(8)	P(8)	O(81)	115.3(8)
Au(8)	P(8)	O(82)	115.5(7)	Au(8)	P(8)	C(38)	109.9(8)
O(81)	P(8)	O(82)	97.0(11)	O(81)	P(8)	C(38)	106.8(11)
O(82)	P(8)	C(38)	111.5(11)	P(1)	O(11)	C(11)	120.4(20)
P(1)	O(12)	C(12)	120.0(12)	P(2)	O(21)	C(21)	120.7(19)
P(2)	O(22)	C(22)	116.1(21)	P(3)	O(31)	C(31)	119.3(16)
P(3)	O(32)	C(32)	120.2(16)	P(4)	O(41)	C(41)	120.1(21)
P(4)	O(42)A	C(42)A	121.1(22)	P(4)	O(42)B	C(42)B	113.2(30)
P(5)	O(51)	C(51)	120.5(20)	P(5)	O(52)	C(52)	119.9(18)
P(6)	O(61)	C(61)	120.1(18)	P(6)	O(62)	C(62)	120.4(20)
P(7)	O(71)	C(71)	119.0(16)	P(7)	O(72)	C(72)	119.5(17)
P(8)	O(81)	C(81)	121.3(14)	P(8)	O(82)	C(82)	119.2(12)
Cl(3)	C(1)	Cl(4)	107.4(28)	Cl(3)	C(1)	Cl(5)	107.2(28)
Cl(4)	C(1)	Cl(5)	110.3(29)	Au(2)	C(17)	Au(3)	87.8(9)
Au(2)	C(17)	P(1)	111.2(12)	Au(2)	C(17)	P(7)	107.2(12)
Au(3)	C(17)	P(1)	114.3(13)	Au(3)	C(17)	P(7)	105.2(12)
P(1)	C(17)	P(7)	124.8(14)	Au(5)	C(26)	P(2)	104.8(12)
Au(5)	C(26)	P(6)	103.5(13)	P(2)	C(26)	P(6)	116.6(15)
Au(4)	C(38)	Au(6)	88.4(9)	Au(4)	C(38)	P(3)	111.7(11)
Au(4)	C(38)	P(8)	105.8(11)	Au(6)	C(38)	P(3)	108.1(12)
Au(6)	C(38)	P(8)	110.0(11)	P(3)	C(38)	P(8)	126.3(14)
Au(1)	C(45)	P(4)	99.6(11)	Au(1)	C(45)	P(5)	109.6(12)
P(4)	C(45)	P(5)	114.8(13)				

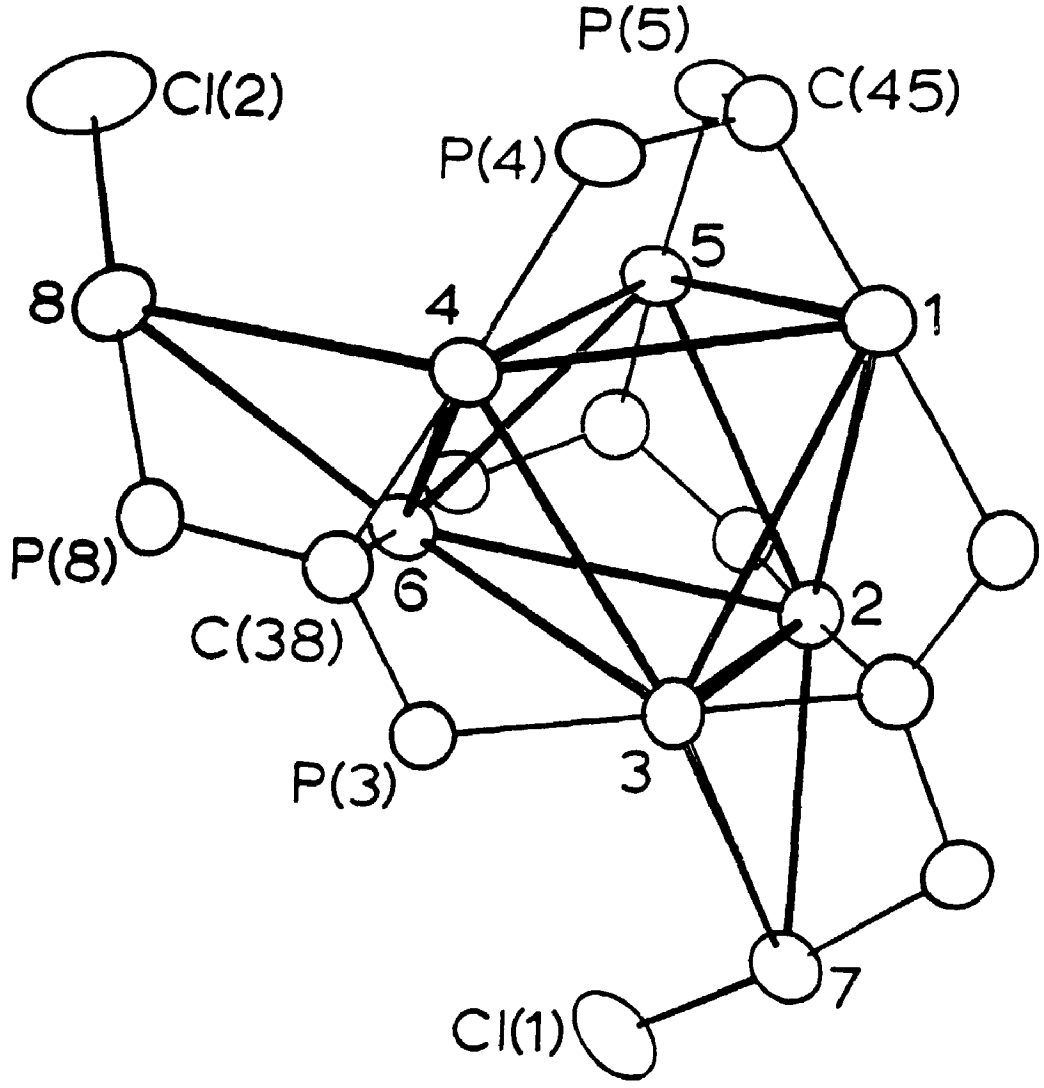

Figure 3.5: A perspective view of 4, giving the atom numbering scheme. Atoms of the methoxy groups and the hydrogen atoms on the methylenic carbons are removed for clarity.

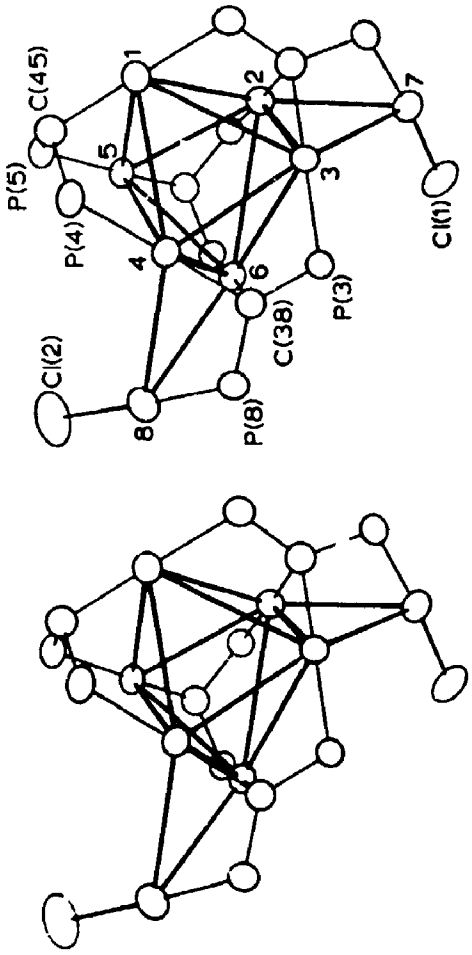

Figure 3.6: A stereoview of 4

of the molecule is shown in figure 3.6.

The cage complex, 4, contains eight gold atoms; Au(1) to Au(6) are arranged as a distorted octahedron. While Au(7) bridges an equatorial edge of the octahedron [defined by Au(2)-Au(3)], Au(8) bridges an axial edge [defined by Au(4)-Au(6)]. Thus, we have a bi-edge bridged distorted octahedral arrangement of gold atoms. The Au-Au distances range from 2.938(1) to 4.085(1)Å and hence there are no formal Au-Au bonds in this cage complex. The equatorial edge Au(2)-Au(3) with a distance of 2.938(1) Å and the axial edge Au(4)-Au(6) at 2.951(1)Å are the shortest Au....Au distances and suggest a weak M-M interaction between these atoms. Each of the eight Au centers is two coordinate, either to a carbon or chlorine atom trans to a bridging phosphine. In Au(1) to Au(6), the P atoms coordinated to Au are trans to a carbon, whereas in Au(7) and Au(8) they are trans to chlorine atoms Cℓ(1) and Cℓ(2), respectively. The P-Au-C and P-Au-Cℓ angles range from 174.4(2) to 177.5(6)°, characteristic of gold in the +1 oxidation state[4-6]. The Au-C distances range from 2.107(20) to 2.128(19)Å, typical for Au-sp^3 C bonds[4] (for example, Au-C = 2.019(12) Å in $[Au_4(C_6F_5)_2(\mu_3\text{-dppm-H})_2]$[8] and 2.124(28)Å in $[Ph_3PAu(CH_3)]$[11]).

There are four bidentate dmopm ligands with each of their eight phosphorus atoms forming a Au-P single bond. Two of the diphosphine ligands, namely P(4)-C(45)-P(5) and P(2)-C(26)-P(6), are singly

deprotonated at the methylenic carbon atom to form a 6-electron donor ligand, $[(MeO)_2PCHP(OMe)_2]^-$; while the other two dmopm ligands, namely P(1)-C(17)-P(7) and P(3)-C(38)-P(8) are doubly deprotonated at the methylenic carbon to give a 8-electron donor ligand, $[(MeO)_2PCP(OMe)_2]^{2-}$. The Au-P distances range from 2.226(5) to 2.258(5)Å, which are typical for gold-phosphine polynuclear complexes[1,4-6]. The triangular faces defined by Au(1), Au(4), Au(5) and Au(2), Au(6), Au(5) are capped by the $(PCHP)^-$ ligands. The ligand is coordinated through the deprotonated methylenic carbon atom and the two phosphorus atoms in a μ_3-bonding mode, and thus forms two fused four-membered Au_2PC dimetallacycles. A view of the Au(2)-Au(6)-Au(5) triangle is presented in figure 3.7(a). The metallation at the methylenic carbon of the dmopm ligand causes significant angular distortions at the sp^3 hybridized methylenic carbon (angles at C(26) are 104.8(2), 103.5(7) and 116.6(11)° and those at C(45) are 99.6(8), 109.6(9) and 114.8(12)°). Similar distortions were observed in $[M_3(\mu_3\text{-}Me_2PCHPMe_2)(CO)_9(\mu\text{-}H)]$ (M = Ru, Os)[12-13]. The dihedral angle between the plane of triangular Au atoms and the plane defined by the methylenic carbon and phosphorus atoms of the $(\mu_3\text{-}PCHP)^-$ ligand is close to zero, showing that the two planes are parallel to each other (the angle between the planes P(4)-C(45)-P(5) and Au(1)-Au(4)-Au(5) is 1.54°; between the planes P(2)-C(26)-P(6) and Au(2)-Au(6)-Au(5) is 0.58°, Table 3.6).

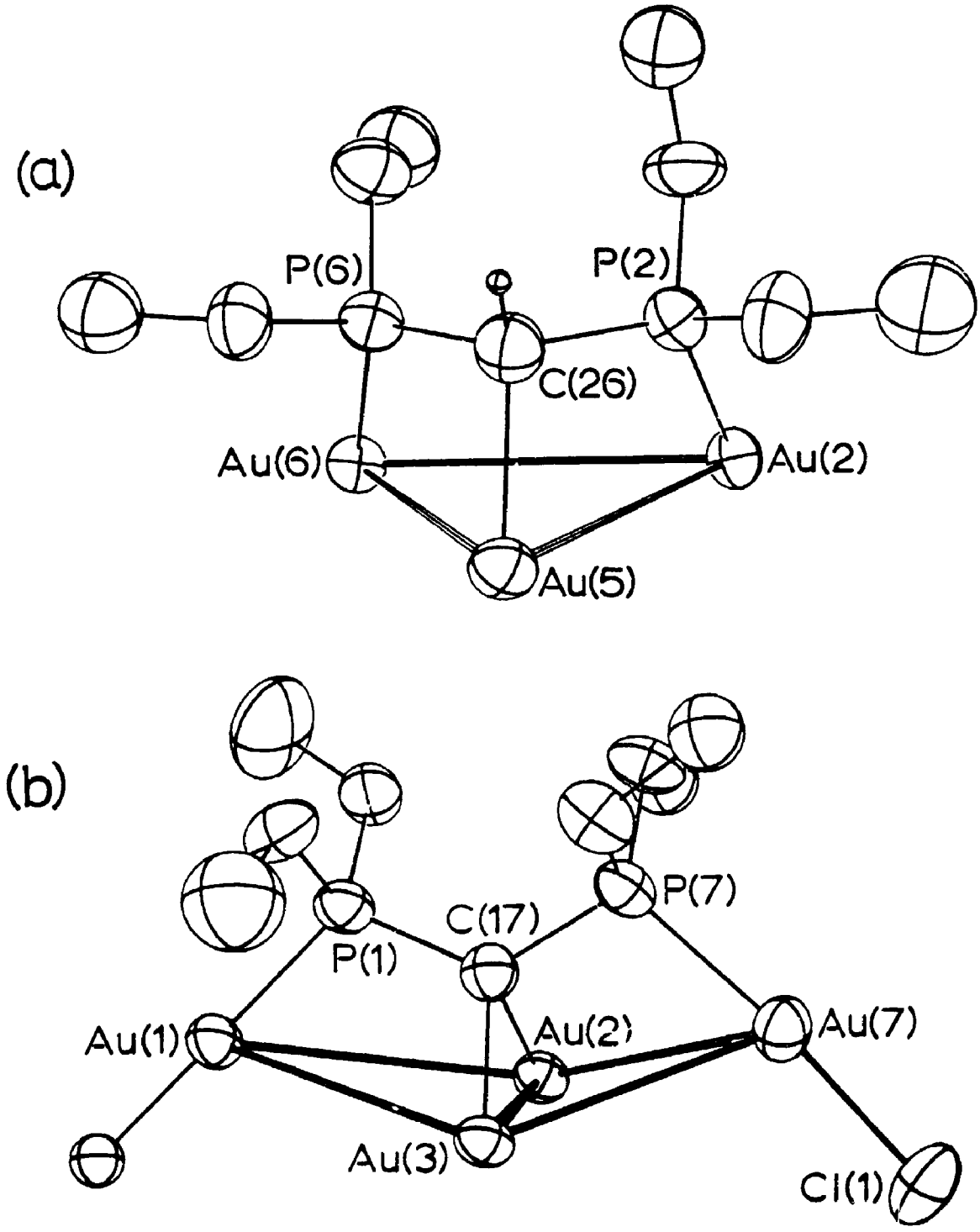

Figure 3.7: (a) A view of the singly deprotonated $\{\mu_4\text{-}(MeO)_2PCHP(OMe)_2\}$ ligand.
(b) A view of the doubly deprotonated $\{\mu_3\text{-}(MeO)_2PCP(OMe)_2\}$ ligand.

Au(7) and the atoms of the triangular face of the octahedron, namely Au(1), Au(2) and Au(3), are arranged in a butterfly configuration. Au(8) along with Au(3), Au(4) and Au(6) are also arranged in this way. Each of these tetranuclear butterfly arrangement is bridged by a doubly deprotonated $[\mu_4\text{-}(RO)_2PCP(OR)_2]^{2-}$ ligand. This novel coordination mode of the diphosphine is shown in the figure 3.7(b). Doubly deprotonated methylenic carbons, C(17) and C(38), bridge the hinge of the butterfly (i.e C(17) bridges Au(2)-Au(3) bond and C(38) bridges Au(4)-Au(6) bond) while P(1), P(7) and P(3), P(8) coordinate to the Au atoms at the "wing-tip" of the butterfly, namely, Au(1), Au(7) and Au(3), Au(8) respectively. Thus, the coordination of the ligand to the butterfly forms four fused four-membered Au_2PC dimetallacycles and one Au_2C dimetallacyclopropyl ring (i.e. Au(2)-C(17)-Au(3) and Au(4)-C(38)-Au(6) rings). Steric requirements of the ligands, and especiallly metallation of the deprotonated methylenic carbon atoms of the dmopm ligand, lead to an unusual concave, rather than convex, ligand geometry. Further, there are substantial angular distortions of the molecular geometry and some short intramolecular non-bonding distances. Thus the $(\mu_4\text{-}PCP)^{2-}$ bridging mode causes severe distortion of angles at the carbons C(17) and C(38) [Au(4)-C(38)-Au(6) 88.4(7)°, P(3)-C(38)-P(8) 126.3(11)°; Au(2)-C(17)-Au(3) 87.9°, P(1)-C(17)-P(7) 124.8(13)°], and results in short Au...Au distances [Au(2)...Au(3) 2.938(1)Å; Au(4)...Au(6)

2.951(1)Å]. It is interesting to note that the dihedral angle between the plane formed by the doubly deprotonated carbon and the phosphorus atoms of the $(\mu_4\text{-PCP})^{2-}$ ligand and the atoms of the butterfly arrangement average to 90.0(8)° (see Table 3.6). The four deprotonated methylenic carbons, namely, C(17), C(26), C(38) and C(45) are in a near tetrahedral arrangement with C....C distance ranging from 5.169 to 5.505Å.

Thus, in summary, we observe that the structure of 4 is a new type of cage containing four fused 9-membered rings. Two of these rings contain $\overline{\text{AuPCAuPCAuPC}}$ units, while the other two rings contain $\overline{\text{AuPCPAuCPAuC}}^*$ unit, incorporating the carbon atom C* of the $\mu_4\text{-(MeO)}_2\text{PC}^*\text{P(OMe)}_2^{2-}$ ligands. The phosphorus atom of each of these $(\mu_4\text{-PCP})^{2-}$ ligands which is not involved in the ring formation is bonded to an exocyclic AuCℓ unit. The cage complex is electrically neutral. There are eight gold centres in +1 oxidation state. These are neutralized by the presence of two $C\ell^-$ ligands, two singly negative $(\mu_3\text{-PCHP})^-$ units and two doubly negative $(\mu_4\text{-PCP})^{-2}$ units. The cage has 112 cluster valence electrons and cannot be classified under any of the known cluster skeletal geometries[1]. None of the other known octanuclear gold derivatives adopt di-edge bridged pseudo octahedral structure[1].

3.3.5 Spectroscopic characterization of 4

Having solved the crystal and molecular structure of 4, we can now attempt to interpret the $^{31}P\{^{1}H\}$ and ^{1}H NMR spectra of 4.

The $^{31}P\{^{1}H\}$ NMR spectrum of 4 is shown in figure 3.4. Seven resonances in the intensity ratio 1:1:1:1:1:1:2 are observed. The signal at the high field (δ 126.4), integrating to two phosphorus atoms can readily be assigned to the two phosphorus atoms P^{7} and P^{8} which are in almost identical chemical environments. There are several possible ways of assigning the other six resonances. The NMR labelling scheme of one such structure is shown in scheme 3.4. Each of the two signals due to P^{2} and P^{3}

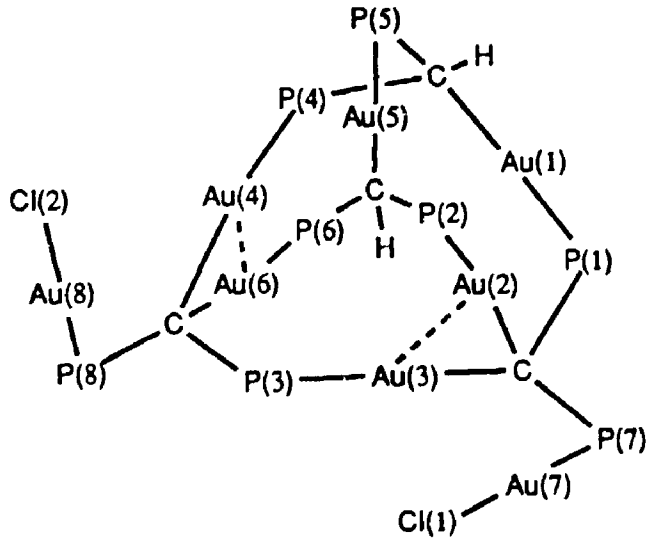

Scheme3.4: NMR labeling scheme for **4**

appear as a doublet of doublets with J_1 = 64 Hz and J_2 = 18 Hz. The larger of the couplings is assigned to $^{3}J(P^{2}P^{3})$

and is mediated through the Au^2-Au^3 bond. A coupling of similar magnitude is found for P^6 and P^4, where $^3J(P^4P^6)$ = 69 Hz, and we believe that this coupling takes place via the Au^4-Au^6 bond. Each of the seven phosphorus resonances shows multiplets with a coupling constant of 18 Hz, and these are assigned to ^3J(P-Au-C-P) type couplings. Such coupling between the phosphorus atoms was seen in $[Au_4(C{\equiv}Ct\text{-}Bu)_3(\mu_3\text{-dppm-H})(\mu\text{-dppm})]$, 2b, (details in chapter 4). The remainder of the ^{31}P NMR parameters can be found in the experimental section of this chapter.

In the ^1H NMR spectrum, the signals due to the -OMe groups of the dmopm ligands appear as a complex, overlapping group of peaks at δ 3.70 to 4.03 (figure 3.3). Apart from the -OMe protons, there are only two other hydrogen atoms in the cage complex. These are from the singly deprotonated $[(MeO)_2PCHP(OMe)_2]^-$ ligands. The signal due to these protons appear as doublet of doublets at δ 3.03 and 3.12, each with $^2J(PH)$ = 17 Hz and $^3J(PH)$ = 8 Hz.

3.3.6 Spectroscopic characterization of complex 3

In a similar fashion, we should now be able to identify the precursor complex, 3, whose ^1H and $^{31}P\{^1H\}$ NMR spectrum are shown in figures 3.2 and 3.1 respectively. The ^1H NMR of 3 reveals four different signals in the $-OCH_3$ region (δ 3.66 - 4.01) with an intensity ratio 2:1:2:1, which suggests that the molecule contains six phosphorus

centres or multiples thereof. However, as complex 3 is the precursor to the cage complex 4, it reasonable to assume that 3 contains only three dmopm ligands (ie. 6 phosphorus atoms). Since the elemental analysis suggested the

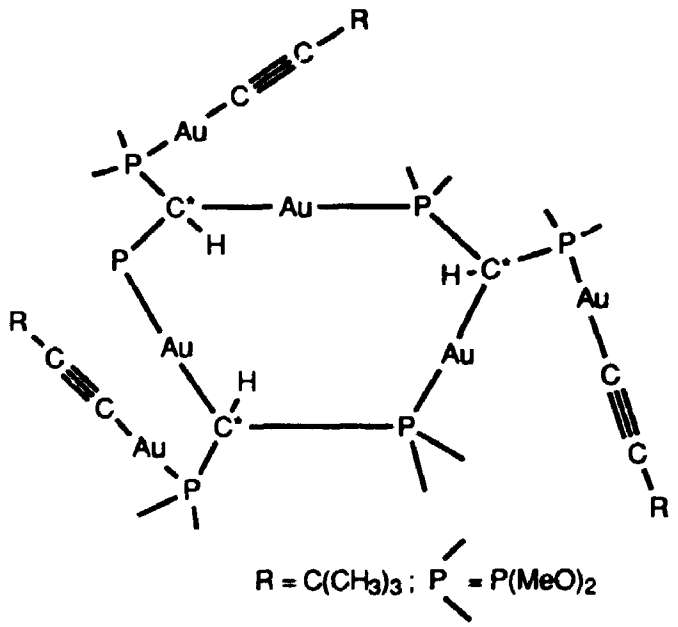

Scheme 3.5

formulation as $[Au_2(dmopm\text{-}H)(C{\equiv}Ct\text{-}Bu)]_n$, it is likely that n = 3. Thus we assign the molecular formula of 3 as $[Au_6(dmopm\text{-}H)_3(C{\equiv}Ct\text{-}Bu)_3]$, for which a likely structure is proposed in scheme 3.5. The proposed structure contains three P_2C^*HAu units, where C^* is a chiral carbon centre. This leads to the possibility of four stereoisomers, namely RRR, RRS, RSS and SSS, where R and S represent the chirality at the carbon centres of the P_2C^*HAu unit. These configurations are represented in scheme 3.6.

In the ^1H NMR spectrum of 3, the methine protons, $P_2C^*\underline{H}Au$, appear as a single resonance centred at δ 4.34

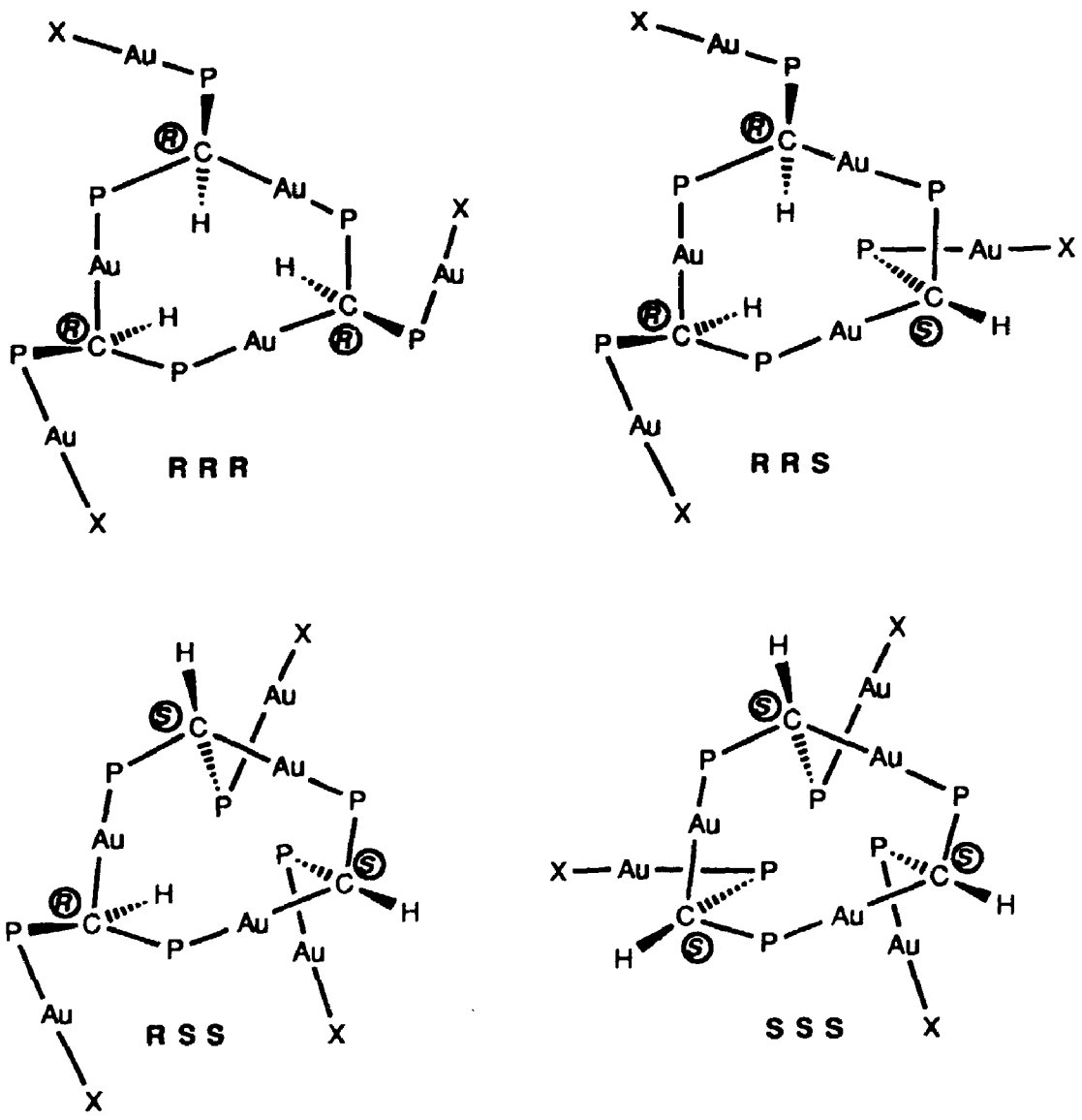

Scheme 3.6

with $^{2}J(PH)$ = 15.5 Hz and $^{3}J(PH)$ = 14 Hz. As stated earlier, the ^{31}P NMR revealed two peaks centred at δ 161.0 and 152.0 and appear as a $[AX]_2$ spin system (figure 3.1) but is consistent with $[AX]_n$ where $n \geq 2$ and probably $n = 3$.

If we consider either the RRS or RSS species, we should observe six different phosphorus resonances in the $^{31}P\{^{1}H\}$ NMR, since there is no symmetry in the molecule.

Hence all six phosphorus nuclei are chemically and magnetically inequivalent. If we assume accidental degeneracy of some of the nucleii, the simplest spin system expected in the ^{31}P NMR is A_2BX_2Y, where A_2 and X_2 are the four phosphorus nuclei in the *R*-$CHAuP_2$ units and B, Y are the phosphorus nuclei in the *S*-$CHAuP_2$ unit.

In the ^{1}H NMR spectrum, the methine protons should appear in a 2:1 intensity ratio to say the least, and all the 12 $-OC\underline{H}_3$ groups may appear as four sets of protons in a 2:1:2:1 ratio.

Let us look at the NMR spectral features that are expected for the RRR or SSS model. Both of these diastereomers have a three-fold symmetry axis perpendicular to the plane containing the 9-membered ring. This makes all three exo-cyclic P^a atoms equivalent, as are the three endo-cyclic P^x atoms. Thus, we would expect an AA'XX' spin system in the ^{31}P NMR spectrum. The three-fold degeneracy makes all three methine protons chemically and magnetically equivalent. The $-OC\underline{H}_3$ protons should appear as four sets of resonances in a 1:1:1:1 ratio.

Considering the two pairs of models, RRS/RSS and RRR/SSS as discussed above, we find that RRR/SSS model agrees well with two of three spectral characteristics observed; while the RRS/RSS does not agree with any. However, when spectral resonance degeneracy is considered, one of the resonances (i.e., $-OC\underline{H}_3$ groups) that is expected from RRS/RSS model agrees with the observed spectrum.

Under these conditions we are inclined to tentatively assign RRR/SSS structure for complex 3, but in the absence of a crystal structure analysis, nothing more can be said.

3.4 SUMMARY AND CONCLUSIONS

Reaction of [AuC≡C*t*-Bu] with $(MeO)_2PCH_2P(OMe)_2$, dmopm, followed by recrystallization from $CH_2C\ell_2$ and then $CHC\ell_3$ gave a novel cage complex, 4, which contains four fused nine-membered rings and the first example of a structurally characterized $[\mu_4\text{-}\ R_2PCPR_2]^{2-}$ ligand. A possible structure has been assigned to one of the intermediates, 3, involved in the sequential metallation of the dmopm ligand.

The deprotonation of the diphosphines in these complexes has been achieved under mild conditions, contrary to the conventional methods which involve rigorous reaction conditions. It is likely that the very easy deprotonation of the dmopm ligand is aided by the electronegative substituents on phosphorus which may increase the acidity of the CH_2P_2 protons compared to the more common $R_2PCH_2PR_2$ ligands with R = alkyl or aryl. The presence of the basic alkynyl ligand also enhances the possibility of a nucleophilic attack on the CH_2P_2 protons. In turn, this promises a rich chemistry of ligands $(RO)_2PCH_2P(OR)_2$ in forming and stabilizing unusual cage and cluster complexes of other elements.

3.5 REFERENCES

1. D.M.P. Mingos, *Gold Bull.*, 17 (1984) 5

2. J.M.M. Smits, P.T.Beurskens, J.J.Steggerda, *J. Cryst. Spectrosc. Res.*, 13 (1983) 381

3. L. Malatesta, *Gold Bull.*, 8 (1975) 48

4. P.G. Jones, *Gold Bull.*, 14 (1981) 102

5. P.G. Jones, *Gold Bull.*, 16 (1983) 114

6. P.G. Jones, *Gold Bull.*, 19 (1986) 46

7. Vander Velden, J.J. Bour, F.A. Vollenbroek, P.T. Beurskens, J.M.M. Smits, *J. Chem. Soc., Chem. Commun.*, (1979) 1162

8. R. Uson, A. Laguna, M. Laguna, M.C. Gimeno, P.G. Jones, C. Fittschen, G.M. Sheldrick, *J. Chem. Soc., Chem. Commun.*, (1986) 509

9. G.M. Sheldrick, "SHELX-86: Structure Solving Program", University of Gottingen, West Germany, (1986)

10. G.M. Sheldrick. "SHELX-76: A Program for crystal structure determination", Cambridge University Press, England, (1976)

11. P.D. Gavens, J.J. Guy, M.J. Mays, G.M. Sheldrick, *Acta. Crystalogr.*, B33 (1977) 137

12. Lj. Manojlovic Muir, D.A. Brandes, R.J. Puddephatt, *J. Organomet. Chem.*, 332 (1987) 201

13. S.R. Hodge, B.F.G. Johnson, J. Lewis, P.R. Raithby, *J. Chem. Soc., Dalton Trans.*, (1987) 931

14. "Enraf-Nonius Structure Determination Package, SDP-PLUS", version 3.0, 1982.

15. *International tables for X-ray crystallography;* Kynoch, Birmingham, England, (1974) vol.4.

16. R.F. Stewart, E.R. Davidson, W.T. Simpson, *J. Chem. Phys.*, 42 (1965) 3175

17. W.H. Zachariasen, *Acta crystallogr., Sect. A: Cryst. Phys., Diffr. Theor. Gen. Crystallogr.*, A24, (1968) 212

CHAPTER 4

A STUDY OF THE CRYSTAL AND MOLECULAR STRUCTURE OF [(t-BuC≡C)$_2$Au$_2$(μ-dppm)] AND ITS REACTIONS

4.1 INTRODUCTION

4.1.1 Chemistry of deprotonated diphosphines

The ligand $R_2PCH_2PR_2$ (R = alkyl, aryl, alkoxy or aryloxy) are often used as ligands to bridge two metal atoms and have been of great significance in the development of organometallic chemistry of bimetallic and cluster complexes[1]. These ligands can be deprotonated to

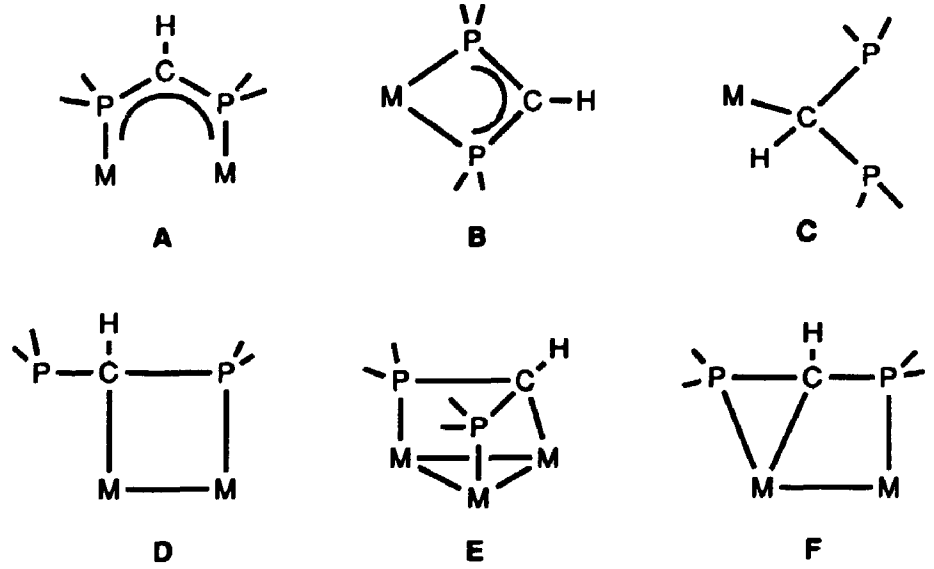

Scheme 4.1

give the 6 electron donor $[R_2PCHPR_2]^-$ ligand, which can then coordinate to metal centres in different bonding modes as shown in scheme 4.1. Thus the $[R_2PCHPR_2]^-$ ligand can

act as a monodentate anion (C-donor)[2], C; a neutral chelate (P,P donors)[3-5], B; a bidentate μ_2-(P,P or P,C donors)[6-8], A, D; or tridentate anion μ_3-(P,C,P donors)[9-11], E; or μ_2-(P,C,P donors)[12], F.

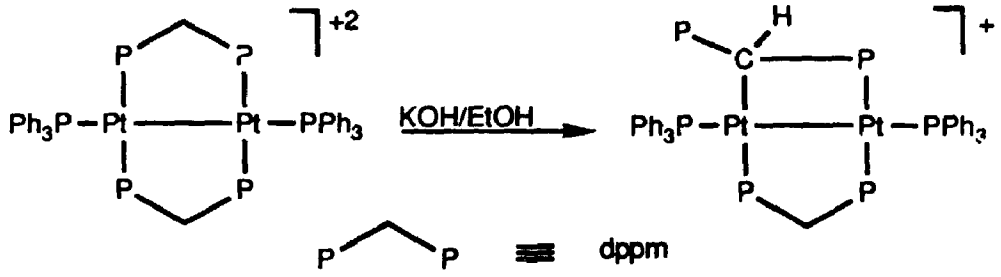

Equation 4.1

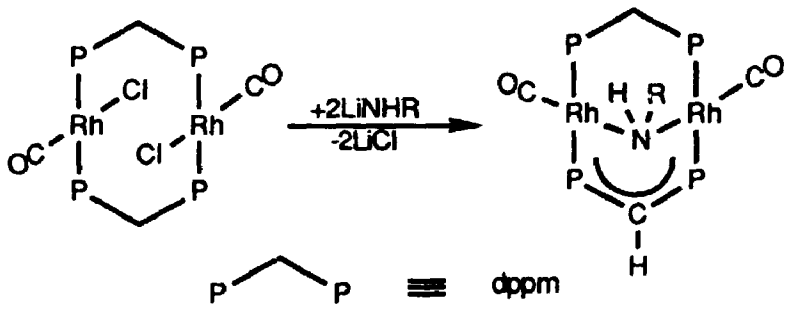

Equation 4.2

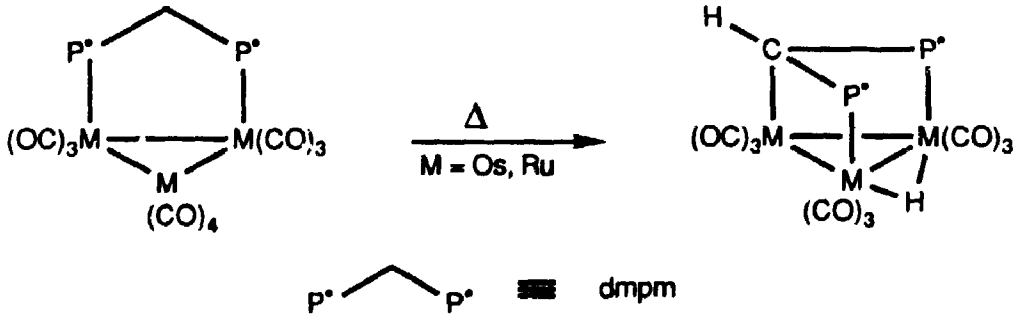

Equation 4.3

The deprotonation of the methylene group of the diphosphine occurs usually in presence of strong bases[7]

(equations 4.1, 4.2) or on pyrolysis of the cluster complex[9,10] (equation 4.3).

In other cases, the groups attached to the metal centre are basic enough to deprotonate the diphosphine[11-14], equations 4.4 to 4.5.

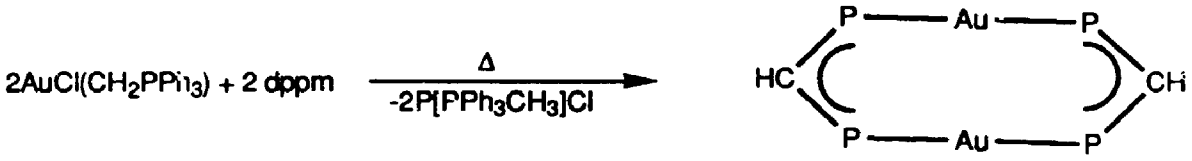

Equation 4.4

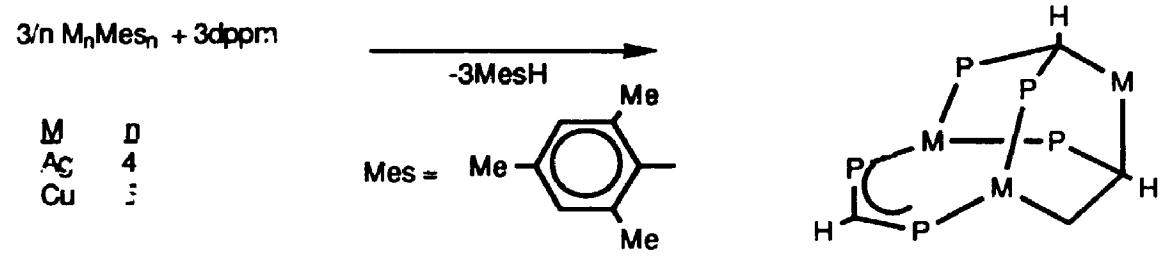

Equation 4.5

Apart from the eight gold cage complex 4, described in chapter 3, there is only one report on the

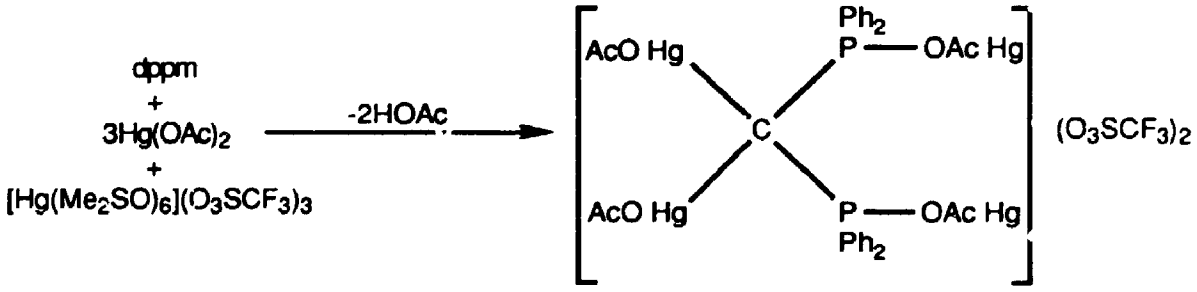

Equation 4.6

doubly deprotonated diphosphine ligand, $[R_2PCPR_2]^{2-}$, in which a species containing four Hg atoms coordinated to a dppm ligand (equation 4.6). This species was observed only in solution by ^{199}Hg NMR spectroscopy[15]. The complex was unstable in solution and could not be isolated.

In the previous chapter we concluded by saying that the easy deprotonation of the dmopm ligand is aided by the electronegative substituents on phosphorus which in turn increases the acidity of the CH_2P_2 protons. These hydrogens were then abstracted by the alkynyl ligand, and resulted in the formation of a Au-C bond. We decided to investigate the course of similar reactions using other diphosphines. One such study was conducted on the $Ph_2PCH_2PPh_2$ (dppm) ligand coordinated gold (I) complex, $[Au_2(\mu\text{-dppm})(C{\equiv}Ct\text{-}Bu)_2]$, 1b. This complex has all the characteristics that are needed for the deprotonation of its diphosphine ligand to occur. It has phenyl groups as the substituents on the phosphorus, which in turn would make the methylenic protons reasonably acidic. The t-butyl acetylide ligands bound to Au atoms could then attack the CH_2P_2 protons and deprotonate them forming new organometallic gold complexes.

This chapter describes the synthesis, characterization and crystal structure of the precursor 1b. Pyrolysis of 1b resulted in $[Au_4(\mu_3\text{-dppm-H})(\mu\text{-dppm})(C{\equiv}Ct\text{-}Bu)_3]$, 2b; a complex containing a singly deprotonated dppm ligand. A

combination of this and the results seen earlier in chapter 3, gave some insight into the possible reaction pathway for the formation of the octagold cage complex $[Au_8C\ell_2\{\mu_4\text{-}(MeO)_2PCP(OMe)_2\}_2\{\mu_3\text{-}(MeO)_2PCHP(OMe)_2\}_2]$, 4.

4.2 EXPERIMENTAL

4.2.1 Synthesis of $[Au_2(\mu\text{-dppm})(C{\equiv}Ct\text{-Bu})_2]$; 1b

To a suspension of [AuC≡Ct-Bu] (0.650 g, 2.33 mmol) in acetone (10 mL) was added a solution of dppm (0.453 g, 1.18 mmol) in acetone (10 mL). The yellow suspension dissolved giving a reddish-yellow solution. After 1 h. stirring, the solution was concentrated and layered with n-pentane. After 3 h. a white crystalline solid precipitated, which was filtered, washed with cold acetone and dried under vacuum. Yield: (77.5%). Anal. calcd. for $C_{37}H_{40}Au_2P_2$: C, 47.23; H, 4.29. Found: C, 47.01; H, 4.60. ^{1}H NMR data (in $CDC\ell_3$) at 20°C: δ 2.09 [s, 18H, t-Bu], 4.35 [t, $^2J(PH)$ = 10, 2H, P_2CH_2], 8.0-8.6 [m, 20H, $P(C_6H_5)$]. $^{31}P\{^1H\}$ NMR data (in $CDC\ell_3$) at 20°C: δ 26.7 (s).

4.2.2 Synthesis of $[Au_4(\mu\text{-dppm-H})(\mu\text{-dppm})(C{\equiv}Ct\text{-Bu})_3]$, 2b

Complex 1b (0.100 g, 0.11 mmol) was dissolved in toluene (10 mL) and refluxed under an atmosphere of N_2 for 24h. The initially colourless solution turned yellow. The solvent was removed under vacuum. The yellow precipitate

was dissolved in acetone and layered with pentane. Pale yellow crystals separated out, and were filtered and dried in vacuum. Yield: 55%. Anal. calcd. for $C_{68}H_{70}Au_4P_4$: C, 45.40; H, 3.92. Found: C, 45.69, H, 4.04. ^{1}H NMR data (in $CDC\ell_3$) at 20°C: δ 1.22, 1.26, 1.41 [s, 27H, t-Bu], 3.30 [t, 2H, $^2J(PH^a)$ = 11, $P_2C\underline{H}^a_2$], 4.48 [dt, 1H, $^2J(P^cH^b)$ = 12.5, $^3J(P^bH^b)$ = 7, $P_2C\underline{H}^bAu$], 6.75-8.60 [m, 40H, $P(C_6\underline{H}_5)$]. ^{31}P NMR data (in $CDC\ell_3$) at 20°C: δ 28.9 [d, $^2J(P^aP^b)$ = 73, 1P, $\underline{P}^a$], 32.9 [dt, $^2J(P^aP^b)$ = 73, $^3J(P^bP^c)$ = 15, 1P, $\underline{P}^b$], 31.2 [d, $^3J(P^bP^c)$ = 15, 2P, $\underline{P}^c$].

4.2.3 X-ray data collection, reduction and structure solution of 1b

Clear, colourless prismatic crystals of 1b were obtained by slow diffusion of pentane into an acetone solution. Photographic analysis showed Laue symmetry 2/m, and the systematic absences observed defined the space group $P2_1/c$.[16] The density of the crystal was determined by neutral buoyancy in a mixture of 1,2-dibromoethane and pentane.

The crystal selected for data collection had six-faces as revealed by optical goniometry to be of the forms {100} and {011}, with the {100} form well developed. A perspective view of the crystal is presented in appendix 5. Unit cell parameters and an orientation matrix were obtained from 21 reflections with $20 < 2\theta < 30°$. ω-scans of several intense, low angle reflections had an average

Table 4.1. Summary of X-ray Structure Determination of complex 1b

Crystal Data	
compound, formula weight	$C_{37}H_{40}Au_2P_2 \cdot \frac{1}{2}C_3H_6O$ 1027.23
crystal system, space group	monoclinic, $P2_1/c$ (no. 14)
systematic absences	h0ℓ, ℓ odd; 0k0, k odd
cell dimens (Å, deg.)	a = 14.047(1) b = 16.124(1)
	c = 17.140(3) β = 103.17(2)
cell volume (Å^3), Z	3780(1), 4
temperature, °C	23
density, g cm^{-3}, obsd; calc	1.724(3), 1.755
Experimental Details	
diffractometer, monochromator	Enraf-Nonius CAD4F, graphite
radiation, wavelength (Å)	Mo, λ(Kα mean) 0.71073
cryst-detec (mm), t.o.a. (°)	205, 2.5
aperture (mm), vert; horiz	4.0; 5.0 + 0.35tanθ
centering reflec: θ range	20; 20 < 2θ < 30
Data Collection	
approx. crystal dimens (mm)	0.16 × 0.40 × 0.42
cryst vol (mm^3); no of faces	12.9 × 10^{-3}; 6
face indices	{100} and {011}
scan mode, width (°)	ω-2θ, 0.75 + 0.35tanθ
index, θ ranges	-13 ≤ h ≤ 13, -15 ≤ k ≤ 15,
	0 ≤ ℓ ≤ 14; 0 ≤ θ ≤ 20°
scan speed (deg min^{-1})	1.0 to 2.5
max time per datum, total time	60s, 98h
standard reflections	$\bar{1}$00, 020, 002
monitor frequency, % var	180m, 0.3
no of data, standards collected	7288, 174

Table 4.1, continued.

Data Processing	
corrections	Lorentz, polarization and monochromator polarization
decay, absorption corrections	none; Gaussian
abs coeff (cm^{-1}); grid size	78.52, 8 × 16 × 16
transmission, max., min.	0.395, 0.162
no of unique data, signif.	4908 > σ(I)
Structure Refinement	
no. of observ., variables	2625, 206
final model; R_1 and R_2	0.0261, 0.0299
top resid., (e $\AA^{-3}$ coord.)	0.054 (0.062 0.104 -0.358)
largest shift, parameter	0.005, B11 of C(6)

width at half-height of 0.12 and 0.13° before and after data collection, respectively. Intensity data were measured at variable scan speeds within maximum time per datum of 60s. 7283 observations were collected over 8 days using ω-2θ scan up to a maximum 2θ of 40°. Standard reflections were monitored regularly, and showed no decay. Standard deviations were assigned based upon counting statistics, and a Gaussian absorption correction applied.[17] 5073 reflections were averaged to give 4908 unique reflections with $I > \sigma(I)$ for the analysis. Crystal data and details of the experimental conditions are presented in Table 4.1.

The structure was solved using Patterson and Fourier methods to locate first the Au atoms and subsequently the remaining non-hydrogen and hydrogen atoms in the complex. The Au and P atoms were refined with anisotropic thermal parameters while C atoms were assigned isotropic values. Refinement proceded smoothly yielding residuals of $R_1 = 0.041$ and $R_2 = 0.065$ for this model prior to the H atom location. All 40 H atoms were located in areas of positive electron density in a difference Fourier synthesis [$(\sin\theta)/\lambda$ maximum 0.35] with 38 of them appearing as distinct peaks with densities ranging from 0.2(1) to 0.7(1) eÅ^{-3}. They were included in idealized positions with thermal parameters set at 110% of that of the atom to which they are bonded. Their positions were updated as the refinement progressed, but not refined. At

this stage of refinement, a difference Fourier synthesis showed the presence of a disordered molecule of acetone included in the crystal as solvent of crystallization, see Figure 4.1. The solvent molecule was located at a centre of symmetry at coordinates (0.5, 0.5, 0.5); a disorder model as shown in figure 4.1 was constructed to account for the electron density, with multiplicities of 0.5 for O and C(14). The methyl carbon, C(15), was assigned a multiplicity of 1. The acetone molecule was refined as a rigid group (C-C = 1.484 Å, C-O = 1.232 Å) in subsequent calculations with one overall temperature factor. The H atoms on the solvent molecule were not located. At this stage the structure was transferred to the SHELX-76 program[18] to complete the refinement. The four phenyl rings were constrained as rigid groups[19] (D_{6h} symmetry, C-C = 1.392 Å) and refined with individual isotropic displacement parameters for the ring carbon atoms. In the final model, the two Au atoms, two P atoms, bridging methylene C atom and the C atoms of the *t*-BuC≡C ligand were refined anisotropically. The structure was refined by full-matrix least-squares techniques on F, minimizing $\Sigma w(|F_o| - |F_c|)^2$, weight = $1.6726/[(\sigma(F))^2 + 0.01484F^2]$. Scattering factors for neutral, non-hydrogen atoms were taken from ref. 16, while H atom scattering factors were taken from Stewart *et al.*[20] The final cycles of refinement included 206 variables, 2625 unique observations with $I > 3\sigma(I)$ converged at agreement factors $R_1 = 0.0261$ and R_2

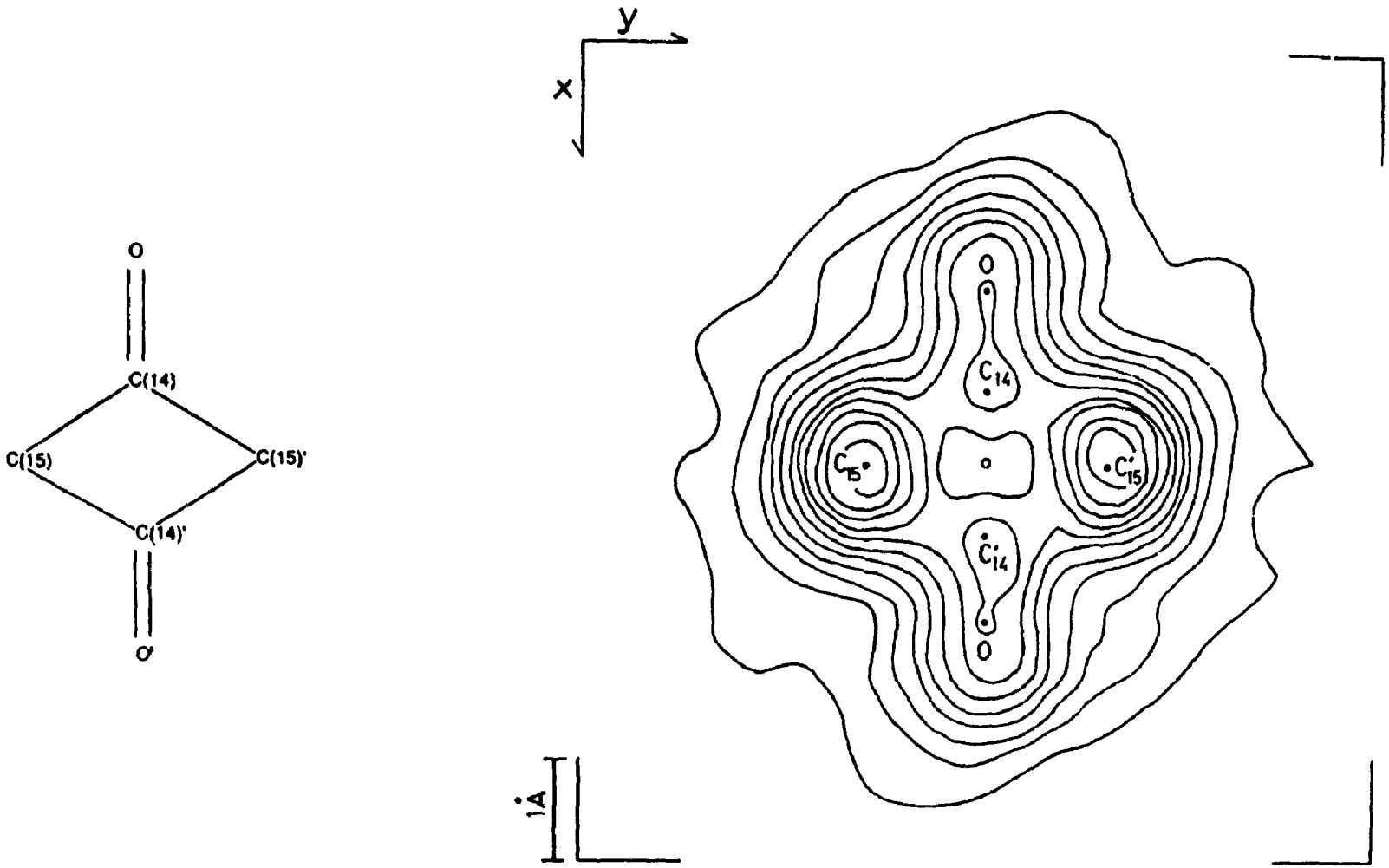

Figure 4.1: A difference Fourier contour map of 1b showing the presence of acetone molecule (right), and the disorder model used to fit the electron density (left).

= 0.0299. The highest residual electron density was 0.54 eÅ^{-3} located midway between C(54) (0.68 Å) and C(55) (0.75 Å) and was of no chemical significance.

A statistical analysis of R_1 and R_2 in terms of data collection order, $|F_o|$, $\lambda^{-1}\sin\theta$ and various combinations of Miller indices showed no unusual trends. This indicates a satisfactory weighting scheme, and the absence of secondary extinction. Final positional and U(equivalent) thermal parameters for the non-H atoms are given in Table 4.2. H-atom parameters, anisotropic thermal parameters, selected torsion angles and least-squares plane calculations are given in Tables 4.3, 4.4, 4.5, and 4.6 respectively. Structure amplitudes are listed in appendix 1.

4.3 RESULTS AND DISCUSSION

4.3.1 Synthesis and characterization of $[Au_2(\mu\text{-dppm})(C{\equiv}Ct\text{-Bu})_2]$, 1b

Complex 1b was synthesized by reaction of [AuC≡Ct-Bu] with the diphosphine in 2:1 ratio (equation 4.7). It was characterized by ^1H, $^{31}P\{^1H\}$ NMR spectra

$$2[AuC{\equiv}Ct\text{-Bu}] + dppm \longrightarrow [Au_2(\mu\text{-dppm})(C{\equiv}Ct\text{-Bu})_2]$$

Equation 4.7

and elemental analysis and the structure of 1b was elucidated by a single crystal X-ray diffraction

technique. The ^1H NMR spectrum of 1b showed a triplet centred at δ 4.35 due to methylene protons, PCH_2P, with $^2J(PH)$ = 10 Hz. $^{31}P\{^1H\}$ NMR revealed a singlet at δ 26.7 indicating that the two phosphorus atoms of the diphosphine ligand are chemically equivalent. These data suggest a

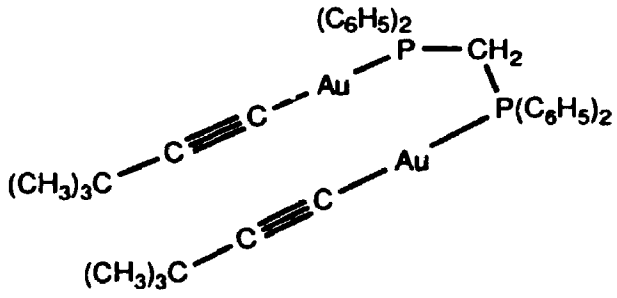

Scheme 4.2

symmetrical structure for 1b as shown in scheme 4.2, which was later confirmed by X-ray crystallography (see section 4.3.2).

4.3.2 Description of Crystal and Molecular structure of 1b

The crystal structure of 1b consists of discrete molecules of $[Au_2(\mu\text{-dppm})(C{\equiv}Ct\text{-Bu})_2]$ and a disordered acetone molecule occluded in the lattice as solvent of crystallization. The closest distance of approach being 2.54(2) Å between HC(12A) and HC(25) in equivalent position ($\bar{X}$, Y + ½ , $\bar{Z}$ + ½). The principal bond distances and bond angles are presented in Table 4.7 and some weighted least-squares planes are given in Table 4.6. Figure 4.2 shows perspective views of complex 1b, in the directions

parallel and perpendicular to $Au_2P_2C_2$ plane. Figure 4.3 is a stereoview of the molecule. The four phenyl rings of the dppm ligand are numbered C(21) to C(26), C(31) to C(36), C(41) to C(46) and C(51) to C(56).

Each molecular unit consists of two gold (I) centres bridged by a dppm ligand. Each Au(I) centre is linearly coordinated to a phosphorus atom of a bridging diphosphine ligand and to a t-butyl acetylide group. The molecule is U-shaped, with the two AuCC*t*-Bu units aligned in close proximity with an intramolecular non-bonding Au....Au distance of 3.330(1) Å. The isoelectronic complexes, $PP(AuC\ell)_2$, (PP = bidentate phosphine ligand) also possess a similar structure in which the Au-Cℓ 'arms' are aligned parallel to each other. For the complex where PP = $(Ph_2P)_2CH_2$ which possesses crystallographic 2-fold symmetry, Au....Au is 3.351 Å and for PP = *cis*-$Ph_2PCHCHPPh_2$ it is 3.05 Å.[21,22] It is expected that the cis-geometry observed for 1b would lead to greater steric repulsion between the *t*-BuC≡C groups attached to Au(I) centres. Indeed this could be seen, in that the angle P(1)-Au(1)-C(1) is 169.1(3)° which is a large deviation from the more usual values close to 180° seen in complexes containing P-Au(I)-X bonds.[23] The linear geometry observed in Au(I) complexes is maintained at Au(2), whose angle P(2)-Au(2)-C(7) is equal to 176.6(4)°. The methylene carbon of the diphosphine ligand is situated above the $Au_2P_2C_2$ plane. The dihedral angle between this plane and

Table 4.2. Atomic Positional ($\times 10^4$) and Thermal ($\times 10^3$) Parameters

Atom	x	y	z	U_{eq}*($Å^2$)
Au(1)	397.1(3)	1384.7(2)	926.6(2)	51.1(2)
Au(2)	824.6(3)	2479.4(2)	-605.6(2)	57.1(2)
P(1)	-1080(2)	1233(1)	64(2)	45.0(8)
P(2)	-433(2)	1821(2)	-1442(2)	48.3(8)
C(1)	1655(8)	1304(6)	1765(6)	56(4)
C(2)	2388(8)	1165(6)	2264(6)	60(4)
C(3)	3280(7)	959(7)	2843(7)	72(4)
C(4)	3117(10)	241(8)	3363(8)	122(6)
C(5)	3600(11)	1684(9)	3396(8)	139(7)
C(6)	4070(10)	822(12)	2457(9)	181(9)
C(7)	1974(8)	3070(6)	78(6)	63(4)
C(8)	2704(8)	3331(6)	488(6)	61(4)
C(9)	3599(8)	3622(7)	1034(7)	69(4)
C(10)	3882(11)	4445(9)	751(8)	151(8)
C(11)	4416(10)	3060(11)	1038(11)	180(10)
C(12)	3457(10)	3739(9)	1867(8)	122(7)
C(13)	-994(6)	985(5)	-962(5)	47(2)
C(14)	5022(24)	4792(11)	4638(9)	141(4)
C(15)	4670(24)	5663(11)	4597(9)	141(4)
C(21)	-1709(5)	355(4)	367(3)	46(2)
C(22)	-2158(5)	-263(4)	-157(3)	57(3)
C(23)	-2603(5)	-932(4)	130(3)	71(3)
C(24)	-2600(5)	-983(4)	941(3)	75(3)
C(25)	-2152(5)	-365(4)	1466(3)	77(3)
C(26)	-1706(5)	304(4)	1179(3)	58(3)
C(31)	-1944(4)	2074(4)	-11(4)	44(2)
C(32)	-1663(4)	2813(4)	396(4)	69(3)
C(33)	-2335(4)	3454(4)	357(4)	83(3)
C(34)	-3290(4)	3356(4)	-88(4)	88(4)
C(35)	-3571(4)	2617(4)	-495(4)	86(4)
C(36)	-2898(4)	1976(4)	-456(4)	71(3)
C(41)	-1428(5)	2513(3)	-1895(4)	56(3)
C(42)	-2166(5)	2251(3)	-2535(4)	72(3)

Table 4.2 continued,

Atom	x	y	z	U_{eq}^{*}(Å²)
C(43)	-2950(5)	2773(3)	-2845(4)	101(4)
C(44)	-2996(5)	3557(3)	-2516(4)	97(4)
C(45)	-2258(5)	3819(3)	-1876(4)	90(4)
C(46)	-1474(5)	3297(3)	-1565(4)	70(3)
C(51)	-119(4)	1323(4)	-2294(4)	52(3)
C(52)	-465(4)	547(4)	-258[illegible](4)	68(3)
C(53)	-202(4)	218(4)	-3255(4)	81(3)
C(54)	408(4)	665(4)	-3637(4)	78(3)
C(55)	754(4)	1441(4)	-3348(4)	75(3)
C(56)	490(4)	1770(4)	-2677(4)	61(3)
O	5104(24)	4432(11)	4023(9)	141(4)

$$U_{eq}^{*} = \frac{1}{3}\sum_i \sum_j U_{ij}\, a_i^{*}\, a_j^{*}\, a_i . a_j .$$

Table 4.3. Hydrogen atom positional (×10⁴) and thermal (×10³) parameters.

Atom	x	y	z	U(Å²)
HC(4C)	3708	115	3739	100
HC(4B)	2629	390	3640	100
HC(4A)	2908	-232	3038	100
HC(5B)	3702	2150	3086	100
HC(5A)	3113	1812	3681	100
HC(5C)	4194	1549	3765	100
HC(6A)	3923	368	2096	100
HC(6B)	4651	707	2849	100
HC(6C)	4159	1308	2170	100
HC(10A)	3370	4833	736	100
HC(10B)	3999	4384	230	100
HC(10C)	4460	4638	1107	100
HC(11C)	4525	3019	512	100

Table 4.3 continued,

Atom	x	y	z	U (Å^2)
HC(11A)	4271	2527	1216	100
HC(11B)	4987	3273	1390	100
HC(12C)	3326	3215	2074	100
HC(12B)	4034	3967	2197	100
HC(12A)	2923	4102	1859	100
HC(13B)	-1635	887	-1274	47
HC(13A)	-612	496	-949	47
HC(22)	-2160	-228	-711	141
HC(23)	-2910	-1353	-228	141
HC(24)	-2905	-1439	1137	141
HC(25)	-2150	-400	2019	141
HC(26)	-1400	725	1536	141
HC(32)	-1011	2880	700	141
HC(33)	-2144	3959	635	141
HC(34)	-3749	3794	-115	141
HC(35)	-4222	2550	-799	141
HC(36)	-3090	1471	-734	141
HC(42)	-2135	1716	-2760	141
HC(43)	-3454	2595	-3282	141
HC(44)	-3531	3914	-2728	141
HC(45)	-2290	4354	-1650	141
HC(46)	-971	3475	-1128	141
HC(52)	-882	242	-2323	141
HC(53)	-438	-312	-3453	141
HC(54)	588	440	-4096	141
HC(55)	1170	1746	-3609	141
HC(56)	727	2300	-2479	141

Table 4.4. Anisotropic Thermal Parameters ($\times 10^3$) in 1b

Atom	U_{11}	U_{22}	U_{33}	U_{12}	U_{13}	U_{23}
Au(1)	45.2(3)	50.5(3)	53.7(3)	4.0(2)	2.8(2)	-0.7(2)
Au(2)	46.8(3)	61.2(3)	63.2(4)	-9.9(2)	12.4(2)	-4.2(2)
P(1)	43(2)	43(2)	48(2)	3(1)	8(1)	4(1)
P(2)	41(2)	47(1)	56(2)	-4(1)	10(1)	2(1)
C(1)	48(7)	58(7)	55(7)	9(5)	-3(6)	1(5)
C(2)	51(7)	67(7)	58(7)	-7(6)	4(6)	-6(5)
C(3)	44(7)	85(8)	75(8)	8(6)	-12(6)	7(7)
C(4)	102(11)	116(11)	126(12)	-7(9)	-17(9)	54(10)
C(5)	134(13)	144(14)	110(12)	-20(11)	[illegible](10)	21(11)
C(6)	98(12)	315(24)	126(14)	111(14)	21(11)	46(15)
C(7)	51(7)	67(7)	73(8)	-12(6)	21(6)	-7(6)
C(8)	41(7)	69(7)	74(8)	-6(6)	14(6)	-7(6)
C(9)	62(8)	71(8)	74(9)	-13(6)	18(6)	-7(6)
C(10)	164(16)	154(16)	115(12)	-83(13)	-8(11)	-8(10)
C(11)	84(12)	182(19)	253(23)	26(13)	-19(13)	-103(18)
C(12)	103(11)	155(14)	104(13)	-29(9)	15(9)	-25(10)

The general temperature factor expression is

$$U_{ij} = \left[-2\pi^2\left[U_{11}h^2a^{*2} + U_{22}k^2b^{*2} + U_{33}\ell^2c^{*2} + 2U_{12}hka^*b^* + 2U_{13}h\ell a^*c^* + 2U_{23}k\ell b^*c^* \right]\right]$$

Table 4.5. Selected Torsional Angles (°) in 1b

Atom 1	Atom 2	Atom 3	Atom 4	Angle	Atom1	Atom2	Atom3	Atom4	Angle
C(1)	Au(1)	P(1)	C(13)	-103.7(21)	C(1)	Au(1)	P(1)	C(21)	12.3(16)
C(1)	Au(1)	P(1)	C(31)	130.8(16)	C(7)	Au(2)	P(2)	C(13)	146.5(51)
C(7)	Au(2)	P(2)	C(41)	-92.3(51)	C(7)	Au(2)	P(2)	C(51)	26.4(51)
Au(1)	P(1)	C(21)	C(22)	-132.1(5)	Au(1)	P(1)	C(21)	C(26)	46.2(5)
Au(1)	P(1)	C(31)	C(32)	5.8(6)	Au(1)	P(1)	C(31)	C(36)	-172.4(4)
Au(2)	P(2)	C(13)	P(1)	38.2(6)	Au(2)	P(2)	C(41)	C(42)	167.4(5)
Au(2)	P(2)	C(41)	C(46)	-16.0(6)	Au(2)	P(2)	C(51)	C(52)	139.1(5)
Au(2)	P(2)	C(51)	C(56)	-42.2(6)	Au(1)	P(1)	C(13)	P(2)	-64.3(5)

Table 4.6. Selected Least-Squares Planes.

Plane No. Crystallographic equation of plane

1 0.5109 X -0.8396 Y -0.1845 Z -2.2597 = 0

Atom	x	y	z	Distance
----------Atoms in Plane----------				
Au(1)	0.1959	2.2327	1.5464	0.200
Au(2)	1.3948	3.9978	-1.0107	-0.198
P(1)	-1.5423	1.9878	0.1066	-0.217(2)
P(2)	-0.0449	2.9368	-2.4068	0.215(2)

Table 4.6 continued,

Atom	x	y	z	Distance
		Other Atoms		
C(13)	-1.0211	1.5874	-1.6049	0.701(9)
C(1)	1.6348	2.1032	2.9450	0.786(9)
C(7)	2.7423	4.9498	0.1302	-0.519(10)
C(2)	2.4696	1.8789	3.7781	1.247(10)
C(8)	3.6072	5.3701	0.8147	-0.556(10)
C(21)	-2.5436	0.5721	0.6130	0.367(6)
C(31)	-2.7259	3.3440	-0.0185	-1.937(6)
C(41)	-1.2664	4.0513	-3.1620	-1.206(6)
C(51)	0.7284	2.1332	-3.8290	1.547(6)

Plane No. 2 — Crystallographic equation of plane: -0.8452 X + 0.4025 Y -0.3515 Z + 2.0662 = 0

Atom	x	y	z	Distance
		Atoms in Plane		
P(1)	-1.5423	1.9878	0.1066	0.000
C(13)	-1.0211	1.5874	-1.6049	0.000
P(2)	-0.0449	2.9368	-2.4068	0.000
		Other Atoms		
C(21)	-2.5436	0.5721	0.6130	0.099(6)
C(31)	-2.7259	3.3440	-0.0185	1.590(6)
C(41)	-1.2664	4.0513	-3.1620	1.746(7)
C(51)	0.7284	2.1332	-3.8290	-0.477(6)

Dihedral Angles Between Planes:

Plane No.	Plane No.	Dihedral Angle
1	2	134.82 +- 0.54

Table 4.7. Selected Bond Distances (Å) and angles (°) in 1b.

Au(1)	P(1)	2.270(3)	Au(1)	C(1)	2.011(11)
Au(2)	P(2)	2.269(2)	Au(2)	C(7)	2.006(11)
Au(1)	Au(2)	3.330(1)	P(1)	P(2)	3.076(4)
P(1)	C(13)	1.833(8)	P(1)	C(21)	1.806(6)
P(1)	C(31)	1.804(7)	P(2)	C(13)	1.849(9)
P(2)	C(41)	1.818(7)	P(2)	C(51)	1.807(7)
C(1)	C(2)	1.201(13)	C(2)	C(3)	1.450(14)
C(3)	C(4)	1.510(15)	C(3)	C(5)	1.508(16)
C(3)	C(6)	1.432(15)	C(7)	C(8)	1.180(13)
C(8)	C(9)	1.464(15)	C(9)	C(10)	1.497(16)
C(9)	C(11)	1.461(16)	C(9)	C(12)	1.497(15)

	Angle		Degrees		Angle		Degrees
P(1)	Au(1)	C(1)	169.1(3)	P(1)	C(21)	C(22)	123.6(2)
P(2)	Au(2)	C(7)	176.6(3)	P(1)	C(21)	C(26)	116.3(2)
Au(1)	P(1)	C(13)	113.4(3)	Au(1)	P(1)	C(21)	109.4(2)
Au(1)	P(1)	C(31)	117.7(2)	C(13)	P(1)	C(21)	104.4(3)
C(13)	P(1)	C(31)	106.6(3)	C(21)	P(1)	C(31)	104.2(3)
Au(2)	P(2)	C(13)	114.2(3)	P(1)	C(31)	C(32)	119.9(2)
Au(2)	P(2)	C(41)	113.3(2)	P(1)	C(31)	C(36)	120.1(2)
Au(2)	P(2)	C(51)	114.9(2)	C(13)	P(2)	C(41)	105.8(4)
C(13)	P(2)	C(51)	104.1(3)	C(41)	P(2)	C(51)	103.5(3)
Au(1)	C(1)	C(2)	172.9(9)	C(1)	C(2)	C(3)	177.0(11)
Au(2)	C(7)	C(8)	172.4(10)	C(7)	C(8)	C(9)	176.7(12)
C(2)	C(3)	C(4)	110.9(10)	P(2)	C(41)	C(42)	120.8(2)
C(2)	C(3)	C(5)	109.9(10)	P(2)	C(41)	C(46)	119.1(2)
C(2)	C(3)	C(6)	111.0(10)	C(4)	C(3)	C(5)	106.7(10)
C(4)	C(3)	C(6)	113.1(12)	C(5)	C(3)	C(6)	105.0(12)
C(8)	C(9)	C(10)	109.3(10)	C(8)	C(9)	C(11)	111.3(10)
C(8)	C(9)	C(12)	111.6(9)	P(2)	C(51)	C(52)	123.9(2)
C(10)	C(9)	C(11)	106.5(12)	P(2)	C(51)	C(56)	116.1(2)
C(10)	C(9)	C(12)	107.5(11)	C(11)	C(9)	C(12)	110.5(12)
P(1)	C(13)	P(2)	113.3(5)				

Numbers in parentheses are estimated standard deviations.

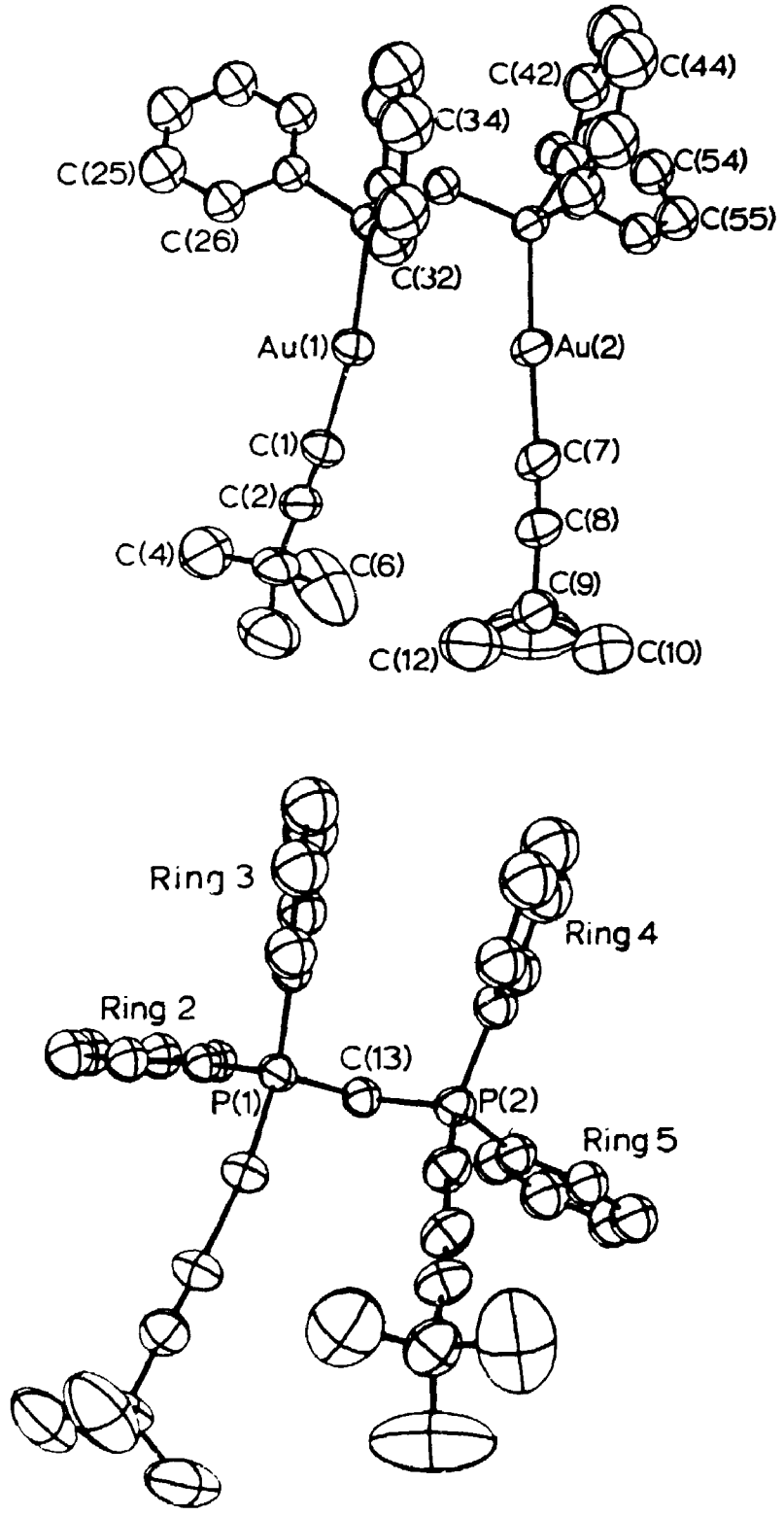

Figure 4.2: Perspective views of 1b, in the directions parallel (below), and perpendicular (above) to $Au_2P_2C_2$ plane.

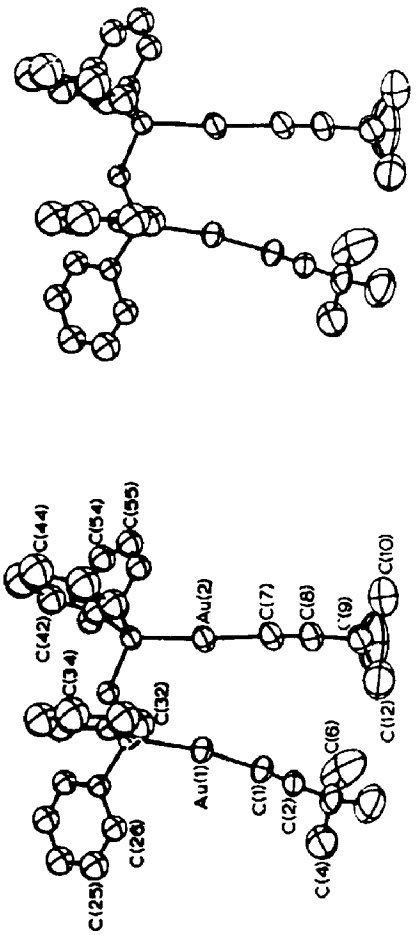

Figure 4.3: A stereoview of 1b

the plane containing P(1), C(13), and P(2) is 134.8(5)°. One of the interesting aspects of this structure is the spatial orientation of the phenyl rings of the diphosphine. The four phenyl rings of the dppm ligand are arranged in such a way that two of them are in the axial plane [rings 3 and 4] while the other two are in the equatorial plane [rings 2 and 5] with respect to the plane containing $P_2Au_2C_2$ atoms [Figure 4.2]. Phenyl ring 3 (ie. atoms C(31) to C(36) inclusive) is situated roughly parallel to, and about 3.5 Å from, phenyl ring 4 (ie. atoms C(41) to C(46) inclusive). The plane of phenyl ring 3 makes an angle of 15.1(6)° to the plane of phenyl ring 4. This interaction is similar to the packing observed in the graphite allotrope of carbon[24] and such packing is also seen in several platinum complexes[25]. The geometry about the acetylenic carbon atoms C(1), C(2), C(7) and C(8) is almost linear (172.9(8) to 177.0(11)°) and is characteristic of *sp* hybridization. The Au-C distances are 2.006(10) and 2.011(9) Å which are slightly longer than those seen in other complexes containing Au-C (acetylenic) bonds[23] (1.935(19) Å in $[C_3H_7NH_2AuC{\equiv}CPh]$[26] and 1.993 Å in $[PPh_3AuC{\equiv}C(C_6F_5)]$[27]). The Au-P distances are indistinguishable with a mean of 2.270(2) Å which is normal for gold-phosphine complexes.[23,28]

4.3.3 Synthesis and characterization of $[Au_4(\mu_3\text{-dppm-H})(\mu\text{-dppm})(C{\equiv}Ct\text{-Bu})_3]$, 2b

On refluxing a solution of 1b in toluene in a inert atmosphere for 24h, a yellow solution is obtained which upon precipitation by addition of n-pentane yields a pale yellow product, 2b (equation 4.8). The product was characterized by elemental analysis ^1H and $^{31}P\{^1H\}$ NMR

$$2[Au_2(\mu\text{-dppm})(C{\equiv}Ct\text{-Bu})_2] \longrightarrow [Au_4(\mu_3\text{-dppm-H})(\mu\text{-dppm})(C{\equiv}Ct\text{-Bu})_3]$$

Equation 4.8

spectra. The proposed structure and the NMR labelling scheme for complex 2b are shown in scheme 4.3.

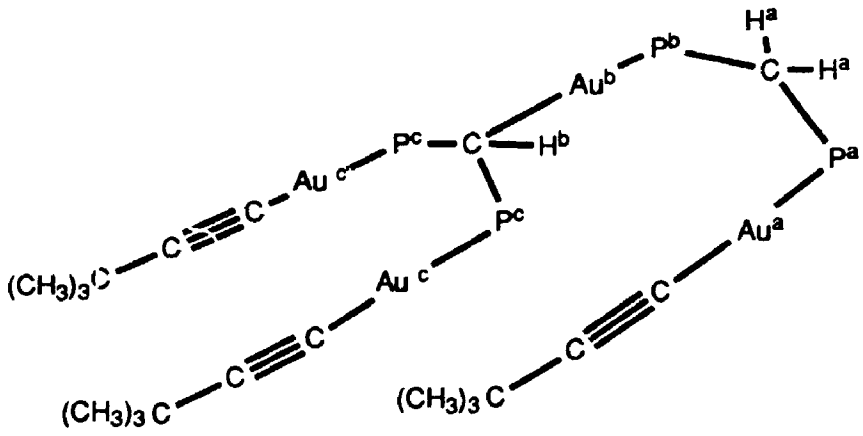

Scheme 4.3: NMR labelling Scheme of **2b**

The $^{31}P(^1H)$ NMR spectrum of 2b revealed three sets of peaks (figure 4.4), indicating three chemically different phosphorus atoms. The signal due to P^a appeared as a doublet centered at δ 28.9 with $^2J(P^aP^b)$ = 73 Hz. P^b appeared at δ 32.9 as a doublet of triplets due to coupling

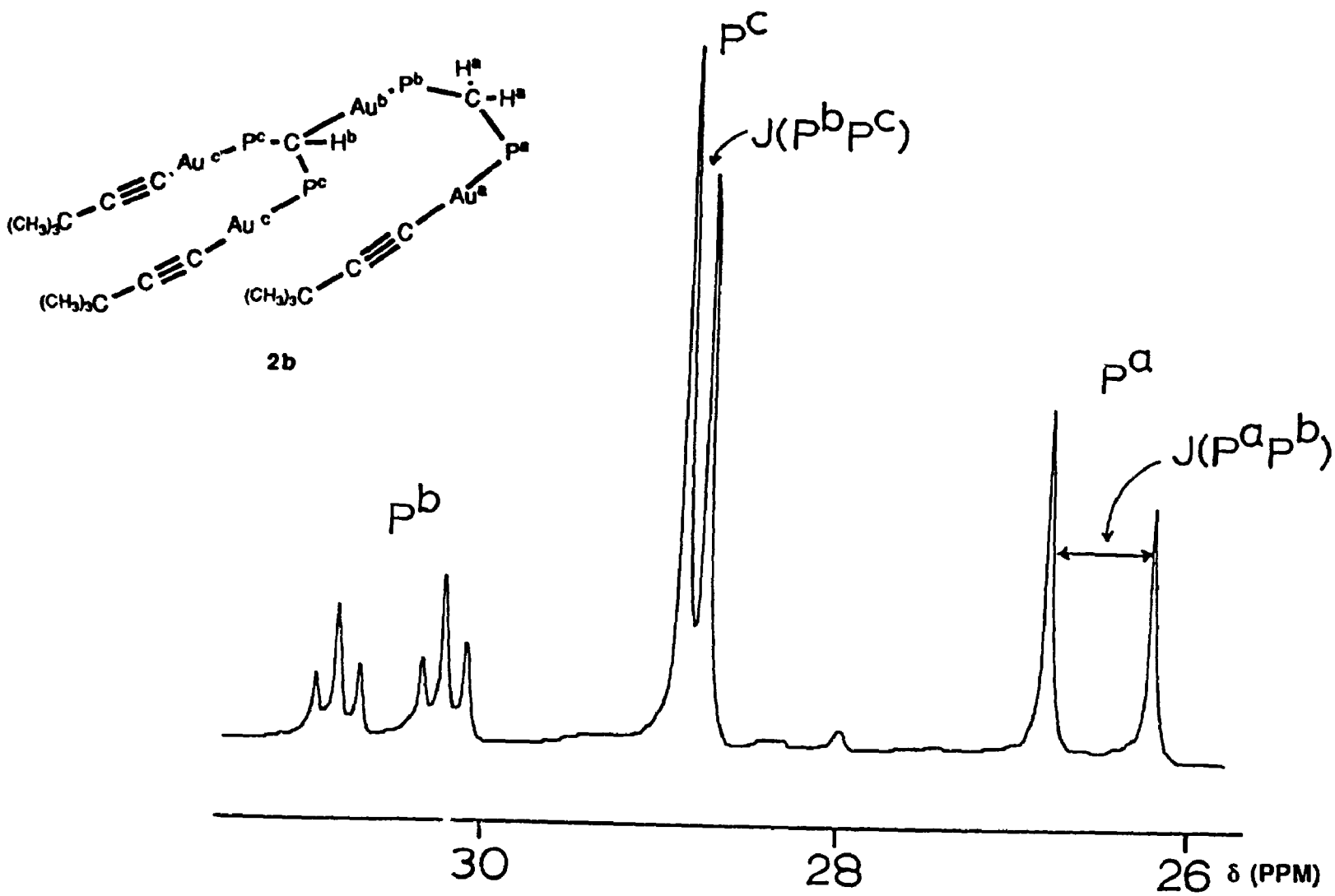

Figure 4.4: $^{31}P\{^{1}H\}$ NMR spectrum (121.4 MHz) of 2b

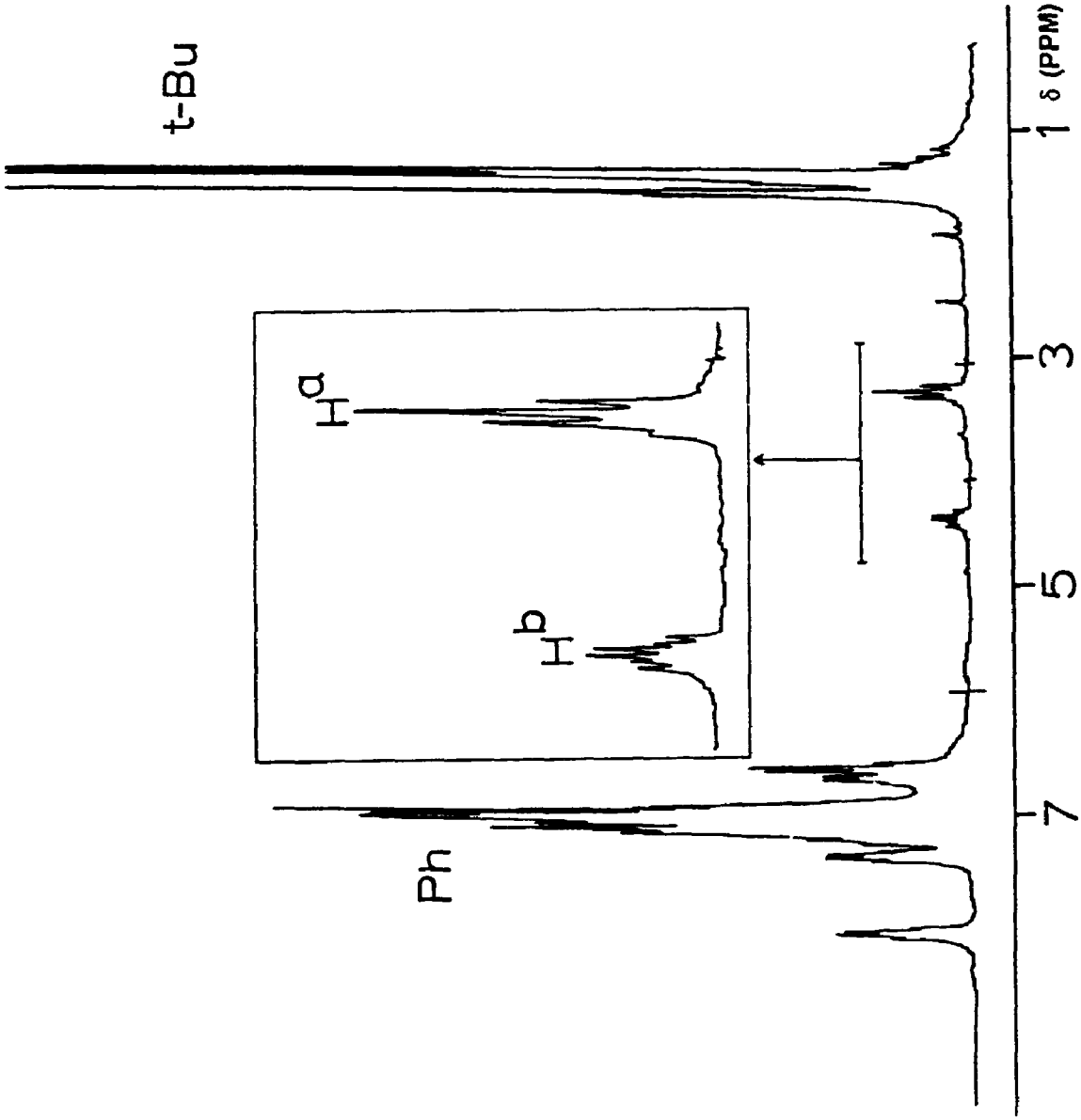

Figure 4.5: ^1H NMR spectrum (200 MHz) of 2b

to P^a [$^2J(P^aP^b)$ = 73 Hz] and two chemically equivalent phosphorus atoms, P^c [$^3J(P^aP^c)$ = 15 Hz]. The signal due to P^c was a doublet centred at δ 32.2 with $^3J(P^aP^c)$ = 15 Hz and this peak was twice as intense as those due to P^a and P^b.

The ^1H NMR spectrum (figure 4.5) of 2b revealed two different signals due to the methylene protons ($P_2C\underline{H}^a_2$) and methine proton ($P_2C\underline{H}^bAu$). The signal due to H^b at δ 4.48 appeared as a doublet of triplets due to coupling to phosphorus nucleii P^b and P^c [$^3J(P^bH^b)$ = 7 Hz and $^2J(P^cH^b)$ = 15 Hz]. The two chemically equivalent protons, H^a, appear as a triplet centred at δ 3.30 with $^2J(PH)$ = 11 Hz, and twice as intense as the signal due to H^b. We could even observe the chemically inequivalent protons of the *t*-BuC≡C groups appearing as singlets at δ 1.22, 1.26 and 1.44. Thus, the ^1H and $^{31}P\{^1H\}$ NMR spectral data strongly support the proposed structure of complex 2b.

Complex 2b consists of four gold atoms and these are linked together by a dppm and a singly deprotonated dppm-H ligand. While the dppm ligand acts as a bidentate ligand, bridging the Au^a and Au^b centres, the deprotonated diphosphine acts as a tridentate μ_3-(P,C,P donor) bridging the Au^b, Au^c, and $Au^{c'}$ centres. To date, we have been unable to grow suitable crystals of 2b for crystallographic studies.

4.3.4 Mechanism of formation of gold cage complex 4

The results obtained in this chapter combined with those from chapter 3 helped us to understand the complex chemistry involved in the formation of the octagold cage complex 4 which was described in chapter 3.

The reaction of [AuC≡C*t*-Bu] with dmopm in a 2:1 ratio is complex. It is probable that the first formed complex is the diphosphine bridged 1a by analogy with the structurally characterized dppm analogue 1b. Complex 1b on pyrolysis gave 2b whose structure is unambiguously determined by multinuclear NMR methods as $[Au_4(\mu\text{-}Ph_2PCH_2PPh_2)(\mu_3\text{-}Ph_2PCHPPh_2)(C{\equiv}Ct\text{-}Bu)_3]$. Slow crystallization of 1a from $CH_2C\ell_2$ resulted in the formation of $[Au_2\{(MeO)_2PCHP(OMe)_2\}(C{\equiv}Ct\text{-}Bu)]_n$, 3, for which a likely structure with n = 3 is proposed (chapter 3). Crystallization of complex 3 in $CHC\ell_3$/pentane resulted in the formation of the novel octagold cage complex $[Au_8C\ell_2\{\mu_4\text{-}(MeO)_2PCP(OMe)_2\}_2\{\mu_3\text{-}(MeO)_2PCHP(OMe)_2\}_2]$, 4, whose structure was characterized by X-ray diffraction methods (details in chapter 3).

Given the structures of 1b, 2b and 4 which are established unambiguously and the proposed structure of 3, it is possible to understand the complex chemistry involved. A possible reaction scheme is shown in scheme 4.4.

In the process of formation of tetranuclear complex 2b, two molecules of 1b react. When the molecules

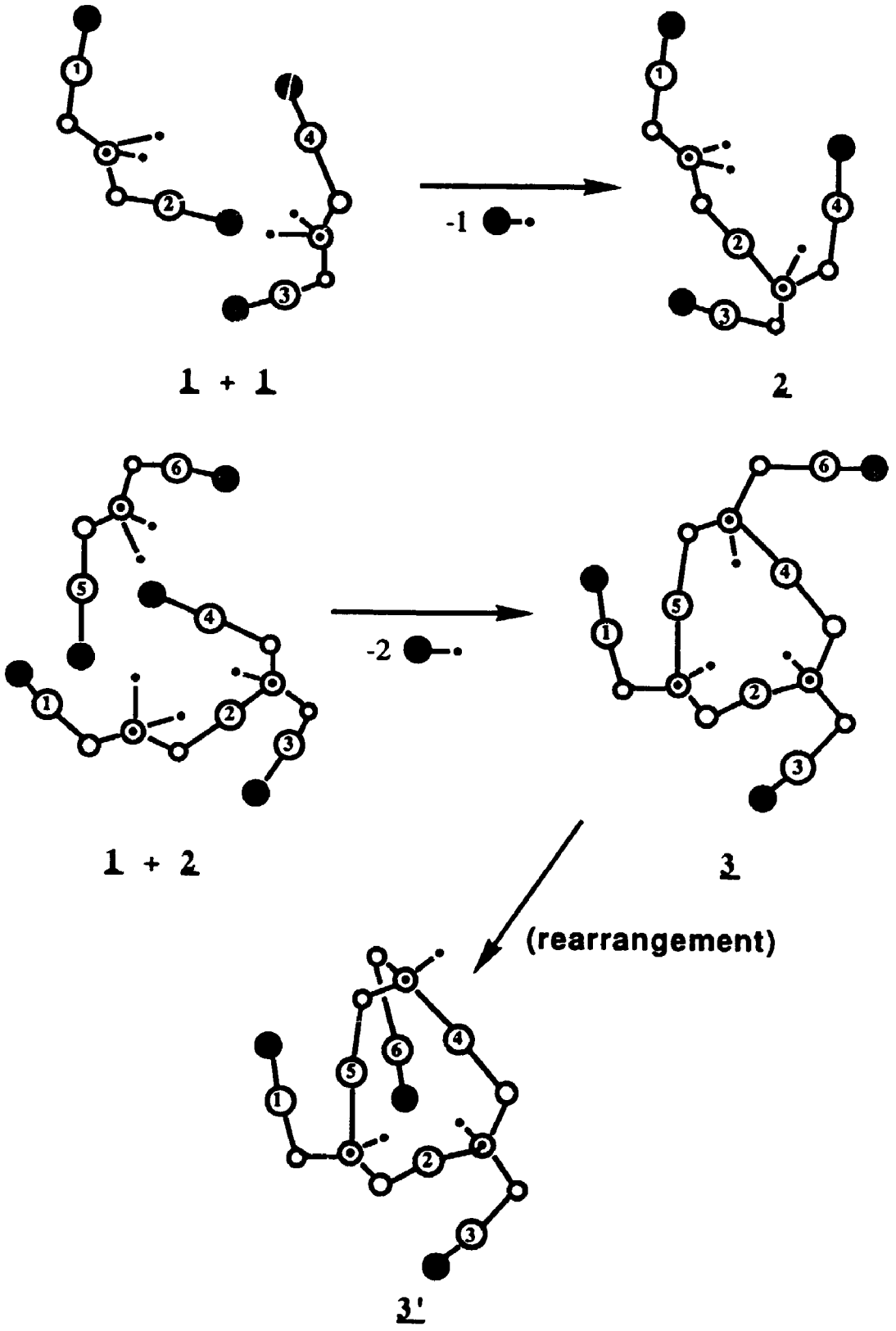
-1
1 + 1
2
-2
1 + 2
3
(rearrangement)
3'

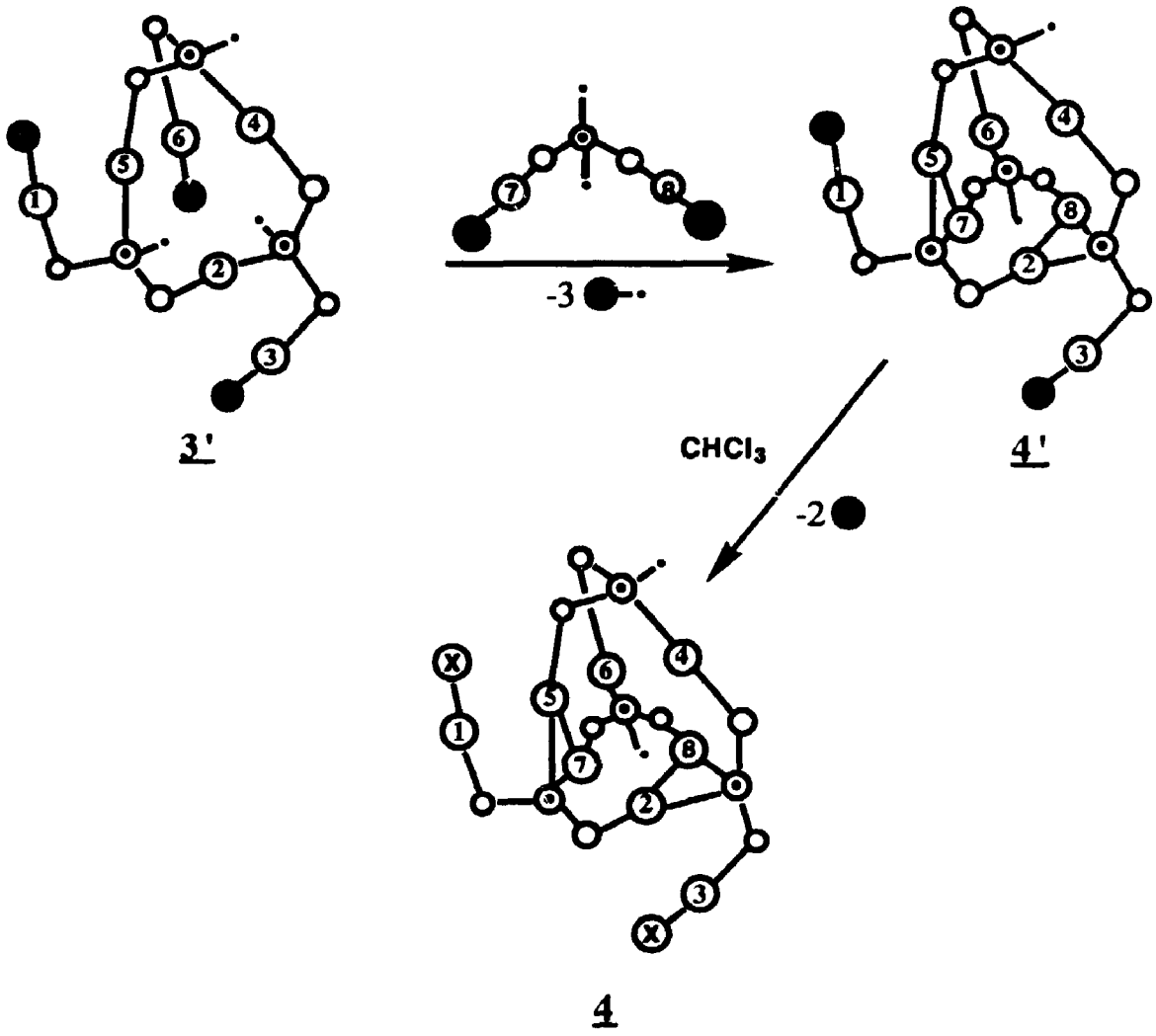

3'

4'

4

Scheme 4.4: Proposed reaction scheme for the formation of cage complex 4

Legend:

● = t-Bu C≡C

①, ② etc., = Au

⊙ = C

○ = P

Ⓧ = Cl

• = H

of dimer 1b come in close contact with each other, the alkynyl end of the first molecule attacks and abstracts one of the methylenic protons of the diphosphine in the second molecule. This results in the elimination of a molecule of *t*-BuCCH, and formation of a new Au-C bond; hence the tetranuclear complex 2b. Deprotonation of the methylene protons of the dppm ligand is well known, but occurs usually in very strong basic medium. For example, the complex cation of $[Pt_2(PPh_3)_2(\mu\text{-dppm})_2](PF_6)_2$ reacts in the presence of KOH/EtOH to yield $[Pt_2(PPh_3)_2(\mu\text{-dppm})(\mu\text{-dppm-H})](PF_6)$, equation 4.1 and reaction of $[PtCl(PEt_3)(dppm)]^+$ with Li^nBu gives $[PtCl(PEt_3)(dppm\text{-H})]$, equation 4.9.[3]

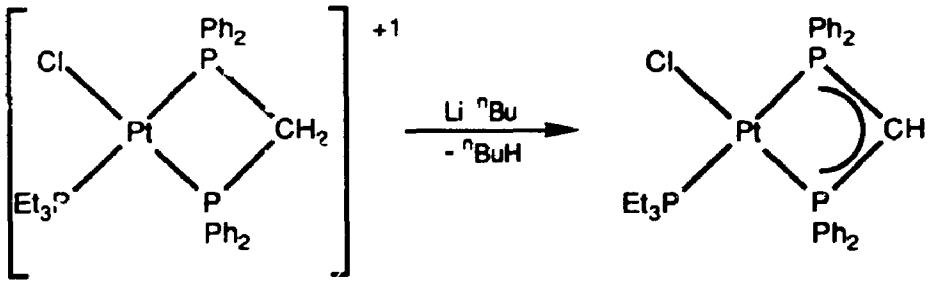

Equation 4.9

However, in the process of formation of 2b from 1b, the alkynyl ligand itself seems to be basic enough to deprotonate the dppm ligand without the necessity of an added base. Extrapolating to the dmopm system, the analogous dmopm product, 2a, is probably formed when two molecules of 1a react, but this product is very unstable

and further reacts with a third molecule of 1a to form the cyclic complex 3. During this process, two more molecules of t-BuCCH are eliminated resulting in two more Au-C bonds and thereby forming a cyclic nine-membered ring containing the AuPCAuPCAuPC unit. There are three $[\mu_3$-PCHP$]^-$ units in complex 3. For the formation of the octagold cage complex 4, complex 3 can then react with one more molecule of dimer 1a. For this reaction to occur, 3 should have either the RRS or RSS conformation (details given in chapter 3). Hence, the proposed RRR/SSS structure of 3 must isomerize to the RSS/RRS diastereomer. This is possible if one of the endocyclic Au-C bond cleaves and rearranges with an exocyclic Au atom. In the RSS/RRS racemic modification, two of the methine protons are directed above the 9-membered cyclic ring, while the third proton is directed below the cyclic ring. The three exocyclic P-Au-C units are free to rotate about the exocyclic P-C bonds. We suggest that one of the exocyclic P-Au-C units rotates along its P-C bond and rearranges, as shown in scheme 4.4, structure 3'.

As there are no dimeric molecules 1a available in the solution of complex 3, it is possible that some molecules of complex 3 in solution reverts to 1a as shown in equation 4.10. Thus, the regenerated molecules of 1a

$$[Au_2(\text{dmopm-H})(C{\equiv}Ct\text{-Bu})]_3 \xrightarrow{3\ t\text{-BuCCH}} 3\ [Au_2(\mu\text{-dmopm})(C{\equiv}Ct\text{-Bu})_2]$$

Equation 4.10

reacts with 3' to yield the cage complex 4. The AuCC*t*-Bu ends of the incoming dimer can thus attack the two methine protons on 3' which are pointing in the same direction, while the P-Au-CC*t*-Bu unit that was swung around towards the ring, can deprotonate one of the methylenic protons of the incoming dimer. This sequence of reactions will result in the elimination of three *t*-BuCCH molecules, and formation of three more Au-C bonds. Construction of cage 4 is completed by a parallel reaction in which the remaining two exocyclic AuCC*t*-Bu units react with chloroform to give two AuCℓ groups. A similar reaction has been observed previously (chapter 2)[28].

4.4 SUMMARY AND CONCLUSIONS

Reaction of [AuC≡C*t*-Bu] with dppm resulted in $[Au_2(\mu\text{-dppm})(C{\equiv}Ct\text{-Bu})_2]$, 1b whose structure was characterized by X-ray diffraction methods. Complex 1b, on pyrolysis yields the tetragold complex, $[Au_4(\mu_3\text{-dppm-H})(\mu\text{-dppm})(C{\equiv}Ct\text{-Bu})_3]$, 2b.

Formation of the novel gold complex 4 described in chapter 3, has been rationalised in terms of a sequential metallation of the diphosphine, resulting in the oligomerization of the initial product, 1a. The driving force for such a reaction to occur has been attributed to the presence of the acidic CH_2P_2 protons and the basic alkynyl ligands in the initial products, 1a and 1b.

4.5 REFERENCES

1. B. Chaudret, B. Delavaux, R. Poilblanc, *Coord. Chem. Rev.*, 86 (1988) 191; R.J. Puddephatt, *Chem. Soc. Rev.*, 99 (1983).

2. A.L. Balch, D.E. Oram, *Inorg. Chem.*, 26 (1987) 1906

3. J. Browning, G.W. Bushnell, K.R. Dixon, *J. Organomet. Chem.*, 198 (1980) C11

4. H. Schmidbaur, J.R. Mandl, *Angew. Chem. Int. Ed. Engl.*, 16 (1977) 640

5. J.M. Basset, J.R. Mandl, H. Schmidbaur, *Chem. Ber.*, 113 (1980) 1145

6. H.H. Karsch, *Chem. Ber.*, 117 (1984) 783

7. M.P. Brown, A. Yavari, Lj. Manojlovic Muir, K.W. Muir, *J. Organomet. Chem.*, 256 (1983) C19

8. C.E. Briant, K.P. Hall, D.M.P Mingos, *J. Organomet. Chem.*, 229 (1982) C5

9. Lj. Manojlovic Muir, D.A. Brandes, R.J. Puddephatt, *J. Organomet. Chem.*, 332 (1987) 201

10. S.R. Hodge, B.F.G. Johnson, J. Lewis, P.R. Raithby, *J. Chem. Soc., Dalton Trans.*, (1987) 931

11. R. Uson, A. Laguna, M. Laguna, M.C. Gimeno, P.G. Jones, C. Fittschen, G.M. Sheldrick, *J. Chem. Soc., Chem. Commun.*, (1986) 509

12. G.M. Dawkins, M. Green, J.C. Jeffry, C. Sambale, F.G.A. Stone, *J. Chem. Soc., Dalton Trans.*, (1983) 499

13. A. Camus, N. Marisch, G. Nardin, L. Randaccio, *J. Organomet. Chem.*, 60 (1973) C39

14. E.M. Meyer, S. Gambarotta, C. Floriani, A.C. Villa, C. Guastini, *Organometallics*, 8 (1989) 1067

15. M. Lusser, P. Peringer, *Organometallics*, 3 (1984) 1916

16. *International Tables for X-ray crystallography*, Kynoch Birmingham, England, Vol.I (1969); Vol.IV (1974).

17. "Enraf-Nonius Structure Determination Package, SDP-PLUS", version 1.0 (1982).

18. G.M. Sheldrick, "SHELX-76: A Program for crystal

structure determination", Cambridge University Press, Cambridge, England (1976).

19. R. Eisenberg, J.A. Ibers, *Inorg. Chem.*, 4 (1965) 3175.

20. R.F. Stewart, E.R. Davidson, W.T. Simpson, *J. Phys. Chem.*, 42 (1965) 3175.

21. H. Schmidbaur, A. Wohlleben, F. Wagner, O. Orama, G. Huttner, *Chem. Ber.*, 110 (1977) 1748.

22. P.G. Jones, *Acta Crystallogr.*, B36 (1980) 2775.

23. P.G. Jones, *Gold Bull.*, 14 (1981) 102; P.G. Jones, *Gold Bull.*, 14 (1981) 159.

24. F.A. Cotton, G. Wilkinson, 'Advanced Inorganic chemistry', Interscience publishers, Toronto, Canada, 1972. p. 288

25. D.H. Farrar, Ph.D. Thesis, University of Western Ontario (1980)

26. P.W.R. Corfield, H.M.M. Shearer, *Acta Crystallogr.*, 23 (1967) 156

27. M.I. Bruce, E. Horn, J.G. Matisons, M.R. Shaw, *Aust. J. Chem.*, 37 (1984) 1163

28. N.C. Payne, R.J. Puddephatt, R. Ravindranath, I. Treurnicht, *Can. J. Chem.*, 66 (1988) 3176; Lj. Manojlovic-Muir, K.W. Muir, I. Treurnicht, R.J. Puddephatt, *Inorg. Chem.*, 26 (1987) 2418

CHAPTER 5

SYNTHESIS, CHARACTERIZATION AND REACTIVITY OF SOME dppm STABILIZED '*triangulo* Pt_3' - Au CLUSTERS

5.1 INTRODUCTION

There has been considerable interest recently in the preparation and characterization of mixed metal cluster compounds that contain Group Ib metal atoms.[1,2,4] Amongst these, compounds containing Pt-Au or Pt-Ag bonds have received much attention. Consideration of bond dissociation energy of the diatomic Au_2 molecule in the gas phase (2.29 eV, 223 $kJmol^{-1}$)[3] suggests a more extensive cluster chemistry for gold than other group Ib metals which have smaller bond dissociation energies (Cu_2 1.95 eV, 190 $kJmol^{-1}$; Ag_2 1.65 eV, 161 $kJmol^{-1}$). Indeed these dissociation energies exactly parallel the relative occurrence of cluster compounds of these metals. Mixed metal gold clusters are important because of their potential use as catalysts in the preparation of materials of definite composition. The reasons for interest in these compounds are three fold. First of all, there are the novel structures and bonding modes available in a mixed metal system. Secondly, these complexes serve as models for hetero bimetallic catalysts. Gold is known to significantly alter the activity and selectivity of platinum catalysts. Finally, an understanding of how the transition metal-gold bond is formed is of fundamental

interest and of importance in the design of syntheses of new clusters.

Heteronuclear Pt-Au compounds of varying nuclearity such as $PtAu$,[5] $PtAu_2$,[6] Pt_2Au,[7] Pt_2Au_2,[8] Pt_3Au,[9,10] Pt_3Au_2,[11] $PtAu_6$,[12] $PtAu_7$,[13] and $PtAu_8$,[13] are known and all these clusters have been characterized only in the past five years. In these complexes, gold has a strong tendency to form Au-Au bonds or bridged AuM_2 or AuM_3 units. A few examples of structurally characterized compounds are shown in scheme 5.1.

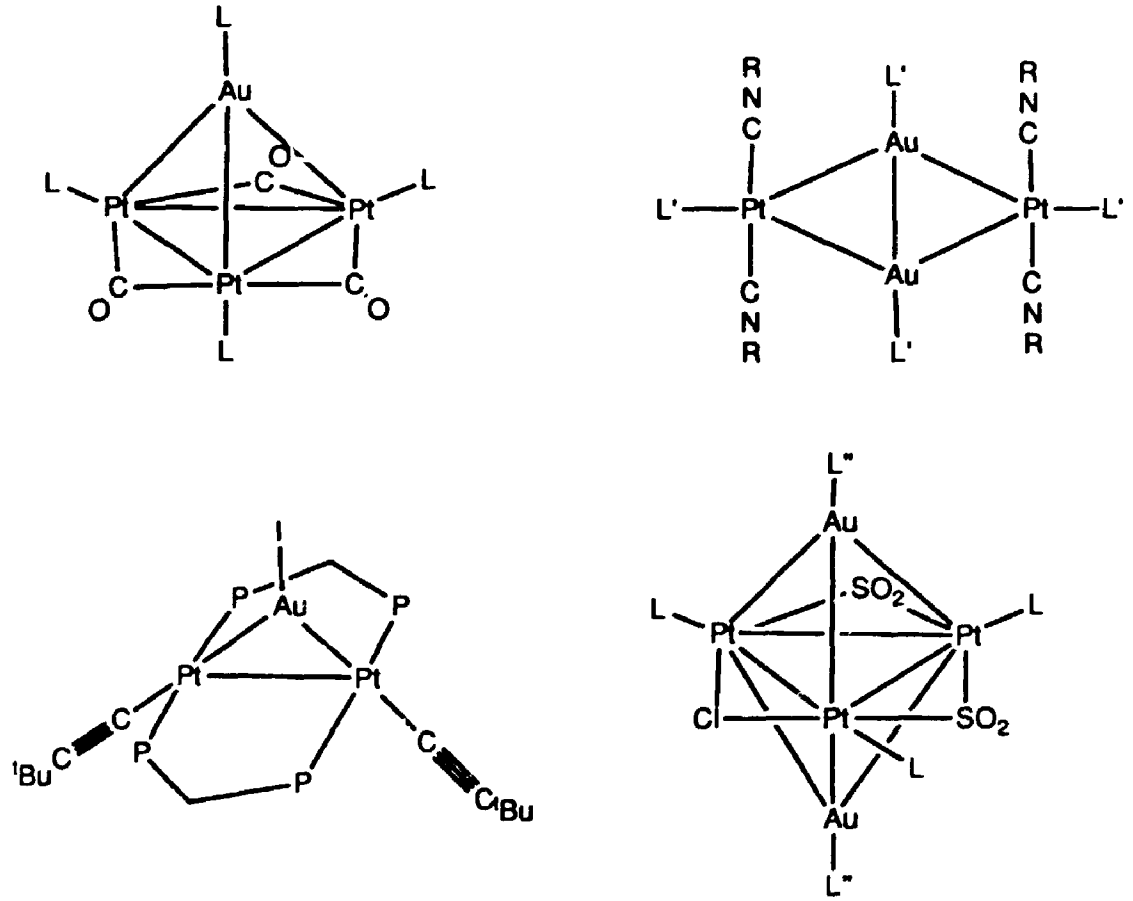

Scheme 5.1 : L = PCy_3 ; L' = PPh_3 ; L" = $P(p\text{-}C_6H_4F)_3$; R = 2,5-$Me_2C_6H_3$

The first Pt-Au cluster, $[PtCl(AuPPh_3)_2(PEt_3)_2]^+$, was synthesized by Braunstein and coworkers in 1984.[6] Equation 5.1 shows the substitution reaction in which the hydride is replaced by an Au_2 fragment. This reaction shows the synthetic route that is widely used in the preparation of transition metal-gold bonds. That is, the isolobal substitution of LAu^+ ($L=PR_3$) for H^+[14,15] and hence, formation of a Au-M bond.

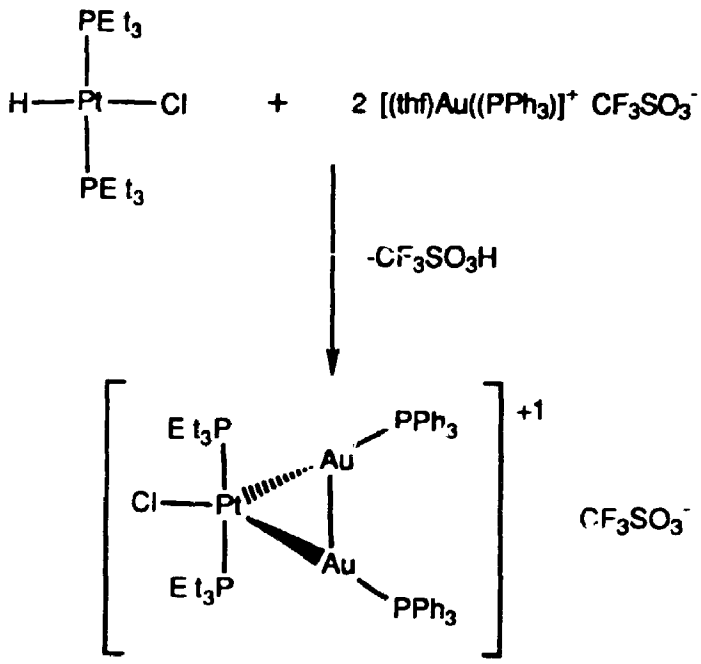

Equation 5.1

It has been shown that electrophilic fragment R_3PAu^+ or $AuCl$ can be added to electron-rich binuclear c trinuclear platinum complexes to yield Pt_2Au or Pt_3Au clusters, respectively[7,9]. The work presented in this chapter shows that similar reaction occurs when Ph_3PAu^+

reacts with the coordinatively unsaturated triplatinum cluster, $[Pt_3(\mu_3\text{-}H)(\mu\text{-}dppm)_3]^+$, 2, to give $[Pt_3(\mu_3\text{-}H)(\mu_3\text{-}AuPPh_3)(\mu\text{-}dppm)_3]^{+2}$, 3a. 3a can be deprotonated to yield $[Pt_3(\mu_3\text{-}AuPPh_3)(\mu\text{-}dppm)_3]^+$, 4, and further aurated to give $[Pt_3(\mu_3\text{-}AuPPh_3)_2(\mu\text{-}dppm)_3]^{+2}$, 5. These reactions provide a route to novel platinum cluster compounds and show clearly how electrophilic ligand substitution can occur by a bimolecular stepwise mechanism. Similarly, reaction of the fragment $AgPPh_3^+$ with 2 gives $[Pt_3(\mu_3\text{-}H)(\mu_3\text{-}AgPPh_3)(\mu\text{-}dppm)_3]^{+2}$, 3b. In addition, the reactivity of some of these clusters with ligands such as PPh_3, CO and H_2S are discussed. The product obtained in the reaction of 4 with CO shows an interesting fluxional process.

5.2 EXPERIMENTAL

All the solvents were degassed with N_2 before use. All preparations were carried out in a dry N_2 atmosphere using Schlenck tube techniques.

5.2.1 $[PPh_3Au(thf)](PF_6)$

In a typical synthesis, a solution of $AgPF_6$ (6 mg, 0.0246 mmol) in THF (10mL) was added to an equimolar solution of $[AuPPh_3C\ell]$ in THF (10 mL). The contents were stirred for 10 minutes and then filtered free from the precipitated $AgC\ell$. The filtrate which contains

$[PPh_3Au(thf)](PF_6)$ was then directly used for the subsequent synthesis of mixed metal complexes.

5.2.2 $[Pt_3(\mu_3\text{-}H)(\mu\text{-}dppm)_3](PF_6)$, 2

In a typical synthesis, an orange suspension of $[Pt_3(\mu_3\text{-}CO)(\mu\text{-}dppm)_3](PF_6)_2$, 1 (50 mg, 0.0246 mmol) in methanol (10 mL) was cooled to 0°C. To this was added a two fold excess of $NaBH_4$ (2 mg, 0.0498 mmol) in methanol (2 mL). The contents dissolved and the solution slowly turned reddish brown in colour. The solution was stirred for 15 minutes, and the solvent was removed at 5°C under reduced pressure. The residue was dissolved in $CH_2C\ell_2$ (15 mL) and filtered free from insoluble sodium salts. On removal of $CH_2C\ell_2$, a red solid was obtained in 80% yield. The product was unstable in air and was characterized in solution by NMR spectroscopic techniques. The NMR data are given in table 5.2.

5.2.3 $[Pt_3(\mu_3\text{-}H)(\mu_3\text{-}AuPPh_3)(\mu\text{-}dppm)_3](PF_6)_2$, 3a

To a solution of 2 (46 mg, 0.0246 mmol) in $CH_2C\ell_2$ (5 mL) was added a solution of $[PPh_3Au(thf)](PF_6)$ (15 mg, 0.0248 mmol) in THF (5 mL). The contents were stirred for 1h. On removal of solvents, a red solid was obtained which was washed with ether (15 mL), giving a red microcrystalline solid in 70% yield. Anal. calcd. for $C_{93}H_{82}AuF_{12}P_9Pt_3$: C, 44.9; H, 3.32. Found : C, 44.4; H, 3.40. mp: 190°C.

5.2.4 $[Pt_3(\mu_3\text{-}H)(\mu_3\text{-}AgPPh_3)(\mu\text{-}dppm)_3](PF_6)_2$, 3b

To a solution of 2 (91 mg, 0.0480 mmol) in THF (10 mL) was added a solution of $[AgPPh_3(thf)](PF_6)$ (19 mg, 0.0484 mmol, prepared by stirring a solution of $AgPF_6$ and PPh_3 in THF for 10 minutes) in THF (15 mL). The contents were stirred at -78°C for 0.5h. On removal of solvent, a red solid was obtained in 70% yield. Due to fairly rapid decomposition of this complex at room temperature, satisfactory analytical data could not be obtained. The species was characterized in solution by multinuclear NMR spectroscopic techniques.

5.2.5 $[Pt_3(\mu_3\text{-}AuPPh_3)(\mu\text{-}dppm)_3](PF_6)$, 4

To a solution of 2 (121 mg, 0.0642 mmol) in $CH_2C\ell_2$ (10 mL) was added a solution of $[PPh_3Au(thf)](PF_6)$ (67 mg, 0.0645 mmol) in THF (15 mL). After the mixture was stirred for 1h., it was washed with dil. NaOH (0.05M, 10 mL), followed by water (25 mL) and dried over $MgSO_4$. Upon filtering and removing the solvent under reduced pressure, a reddish brown solid was obtained which was washed with ether (15 mL) and dried under vacuum. Yield: 73%. Anal. calcd. for $C_{93}H_{81}AuF_6P_8Pt_3$: C, 47.7; H, 3.49. Found: C, 46.9; H, 3.59. mp: 250°C. MS: Calcd. for $[Pt_3(\mu_3\text{-}AuPPh_3)(\mu\text{-}dppm)_3]^+$, m/e 2197; found, m/e 2197.

5.2.6 $[Pt_3(\mu_3\text{-}AuPPh_3)_2(\mu\text{-}dppm)_3](PF_6)_2$, 5

To a solution of 2 (102 mg, 0.0543 mmol) in $CH_2C\ell_2$ (15 mL) was added a solution of $[PPh_3Au(thf)](PF_6)$ (67 mg, 0.1102 mmol) in THF (5 mL). The contents were stirred for 1h. Solvent was then removed on a rotary evaporator. The product was washed with pentane giving a red solid in 78% yield. Anal. calcd. for $C_{111}H_{96}Au_2F_{12}P_{10}Pt_3$: C, 45.2; H, 3.28. Found: C, 45.6; H, 3.39. MS: Calcd. for $[Pt_3(\mu_3\text{-}AuPPh_3)_2(\mu\text{-}dppm)_3]^{+1}$, m/e 2657; found, m/e 2657.

5.2.7 Reaction of 3a with NEt_3

To a stirred solution of 3a (132 mg, 0.0532 mmol) in $CH_2C\ell_2$ (10 mL) was added an excess of NEt_3 (0.542 mmol). After 15 minutes of reaction the solvent was removed under vacuum. The red solid was washed with ether (10 mL). ^{31}P and ^1H NMR characterization of the product indicated complex 4 as the only product.

5.2.8 Reaction of 4 with CF_3COOH

Complex 4 (75 mg, .052 mmol) was dissolved in $CH_2C\ell_2$ (0.7 mL) and placed in an NMR tube (5 mm). To this solution CF_3COOH (2.5 μL, 0.0336 mmol) was added by syringe, the tube sealed, and the contents were mixed thoroughly. The ^{31}P NMR spectral data indicated complete conversion of complex 4 to complex 3a.

5.2.9 Reaction of 4 with one equivalent of $[PPh_3Au(thf)](PF_6)$

To a solution of 3a (62 mg, 0.0250 mmol) in THF (10 mL) was added a solution of $[PPh_3Au(thf)](PF_6)$ (15 mg, 0.0253 mmol) in THF (5 mL) and the contents were left to stir for 1h. The reaction solution was evaporated under reduced pressure and washed with ether. This gave the red solid product 5 in 90% yield.

5.2.10 Reaction of 5 with PPh_3

To a solution of 5 (75 mg, 0.025 mmol) in acetone (10 mL) was added PPh_3 (14 mg, 0.0534 mmol). The contents were stirred for 2h. with no apparent colour change. NMR characterization of the products indicated a mixture of 4 and $[Au(PPh_3)_2](PF_6)$ [$\delta^{31}P$ = 0.1].

5.2.11 Reaction of 4 with H_2S

Complex 4 (60 mg, 0.0253 mmol) was dissolved in acetone (10 mL), and a slow flow of H_2S was passed through the solution. The reaction was accompanied by a color change from red to yellow. Solvent was then removed on the rotary evaporator. The product was washed with ether, giving a yellow crystalline solid Yield: 80%. Anal. calcd. for $C_{75}H_{67}F_6P_7Pt_3S$: C, 47.0; H, 3.52. Found: C, 47.2, H. 3.74. IR (Nujol): ν(PtH) = 2086 cm^{-1}. MS: calcd. for $[Pt_3(\mu\text{-dppm})_3(\mu_3\text{-S})H]^+$, m/e 1771; found, m/e 1770 (P-H). NMR data: $\delta(^{31}P)$ 22.8 [m, ^1J(PtP) = 2992, ^2J(PP) = 27,

P^a]; 2.6 [m, ^1J(PtP) = 3110, ^2J(PtP) = 181, ^3J(PP) = 161, P^b]; -15.1 [m, ^1J(PtP) = 3840, P^c]; 23.1 [s, $S(AuPPh_3)_2$]: $\delta(^1H)$ -9.24 [t, 1H, ^1J(PtH) = 1136, ^2J(PH) = 13.5, PtH]. 4.02 [s, 4H, CH_2P_2], 5.60 [s, 2H, CH_2P_2].

5.2.12 Reaction of 4 with CO to yield 7

Complex 3a (50 mg, 0.0201 mmol) was dissolved in CD_2Cl_2 (0.7 mL) and placed in an NMR tube (5 mm) fitted with a Teflon tap. This tube was attached to a vacuum line along with a vessel containing CO gas. The sample was degassed under vacuum and frozen under liquid N_2. Excess CO was condensed into the tube, which was cooled to liquid nitrogen temperature, and the tap was closed. The ^{31}P NMR spectrum was recorded at -60°C. At -60° C, the spectrum corresponds to that of product 7 in solution. After recording the NMR spectra, the solvent was removed by bubbling CO into the solution. An IR spectrum of the resulting red solid was recorded.

NMR data: $\delta(^{31}P)$ 41.8 [s, $^2J(PtP^a)$ = 620, 1P, P^a]; 14.3 [s, $^1J(PtP^b)$ = 2922, $^2J(PtP^b)$ = 213, $^3J(P^bP^b)$ = 204, 6P, P^b]. IR (Nujol) : ν(C≡O) 1995 cm^{-1}.

5.2.13 Reaction of 4 with ^{13}CO to yield 7*

The procedure was the same as that described above, with the exception that ^{13}CO gas (99.4% abundant) was used instead of ^{12}CO gas. Following the reaction, a series of ^1H, $^{31}P\{^1H\}$, and $^{13}C\{^1H\}$ NMR spectra were run at

-60°C. The NMR and IR data are reported in Table 5.3.

5.3 RESULTS AND DISCUSSION

5.3.1 Synthesis and characterization of complexes 2-5

The new triplatirum cluster complexes 2, 3, 4 and 5 were synthesized as shown in scheme 5.2 and 5.3.

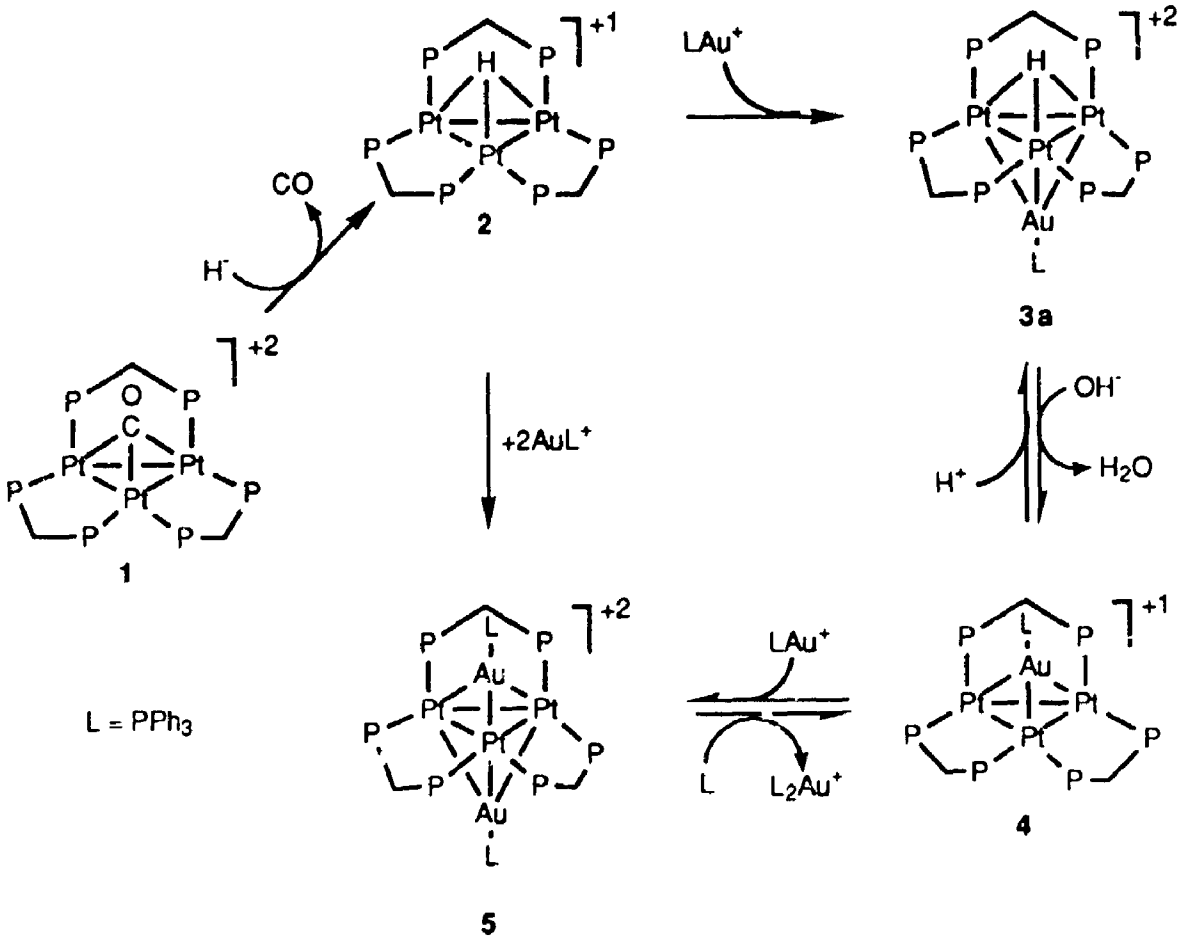

Scheme 5.2

Complex 2 was prepared by a modified literature method[16]. Earlier methods involved a reaction of excess

$NaBH_4$ or Na-amalgam reduction at room temperature with the carbonyl complex 1 for 72h. This results in the formation of a mixture of 2 and the trihydrido A-frame dimer, $[Pt_2(\mu\text{-}H)H_2(\mu\text{-}dppm)_2]^+$.[17] In our method involving reaction of 1 with two equivalents of $NaBH_4$ at 0°C for 15 minutes, complex 2 is obtained in quantitative yield. Furcher

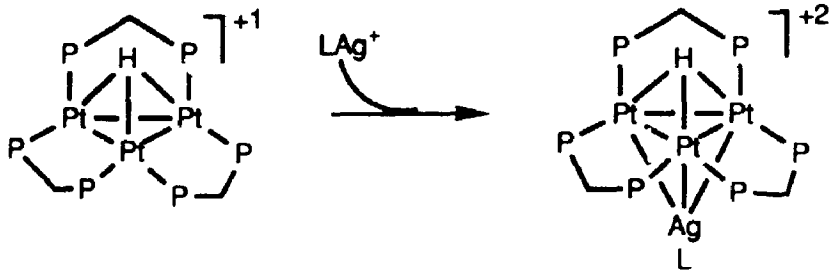

2 L = PPh_3 3b

Scheme 5.3

reaction of 2 with one equivalent of $MPPh_3^+$ (M = Au or Ag) gives the novel complexes $[Pt_3(\mu_3\text{-}H)(\mu_3\text{-}MPPh_3)(\mu\text{-}dppm)_3]^{+2}$ (M = Au, 3a; Ag, 3b).

Reaction of 3a with the bases such as NEt_3 or dil. NaOH results in the formation of the deprotonated product, 4. Further auration of 4 using $AuPPh_3^+$ yields the digold cluster 5. Complexes 3a, 4 and 5 were thermally stable and could be isolated in analytically pure form as the hexafluorophosphate salts which were deep red solids. Complex 3b was thermally unstable and was characterized solely by multinuclear NMR spectroscopy. With the exception of 3b, all the other complexes gave a parent ion peak in the FAB mass spectra (envelopes with the expected

intensities due to the many isotopomers present). All the complexes were characterised unambiguously in solution by multinuclear NMR spectroscopic techniques.

5.3.2 Spectroscopic characterization of complexes 3 - 5

The $^{31}P\{^{1}H\}$ and $^{195}Pt\{^{1}H\}$ NMR spectral data of complexes 3 - 5 are given in Table 5.1 and the NMR labelling scheme for these complexes is shown in scheme 5.4. The main feature of the ^{31}P NMR spectra of 3 - 5

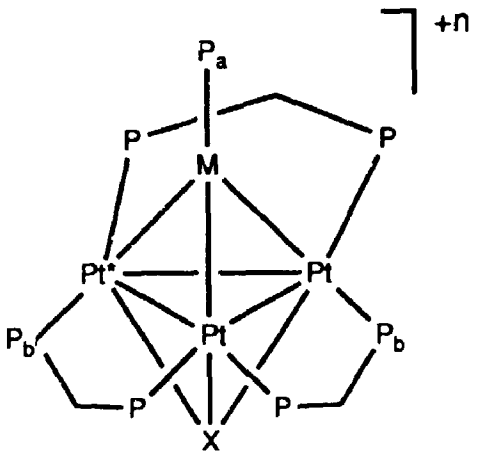

M	X	Complex	n
Au	H	**3a**	2
Ag	H	**3b**	2
Au	—	**4**	1
Au	AuP_a	**5**	2

Scheme 5.4: NMR labelling scheme for **3a - 5**

(figure 5.1, 5.3 and 5.4) is the presence of two distinct phosphorus signals P^a and P^b. The further complexity of the spectra are due to the four isotopomers (see scheme 5.5) which are present as a result of zero, one, two or three spin active ^{195}Pt nuclei; ($I = \frac{1}{2}$, 33.8% natural abundance) in the cluster (see appendix 6).

The major resonances due to isotopomer I, which gives a doublet due to P^b (due to couping with P^a,

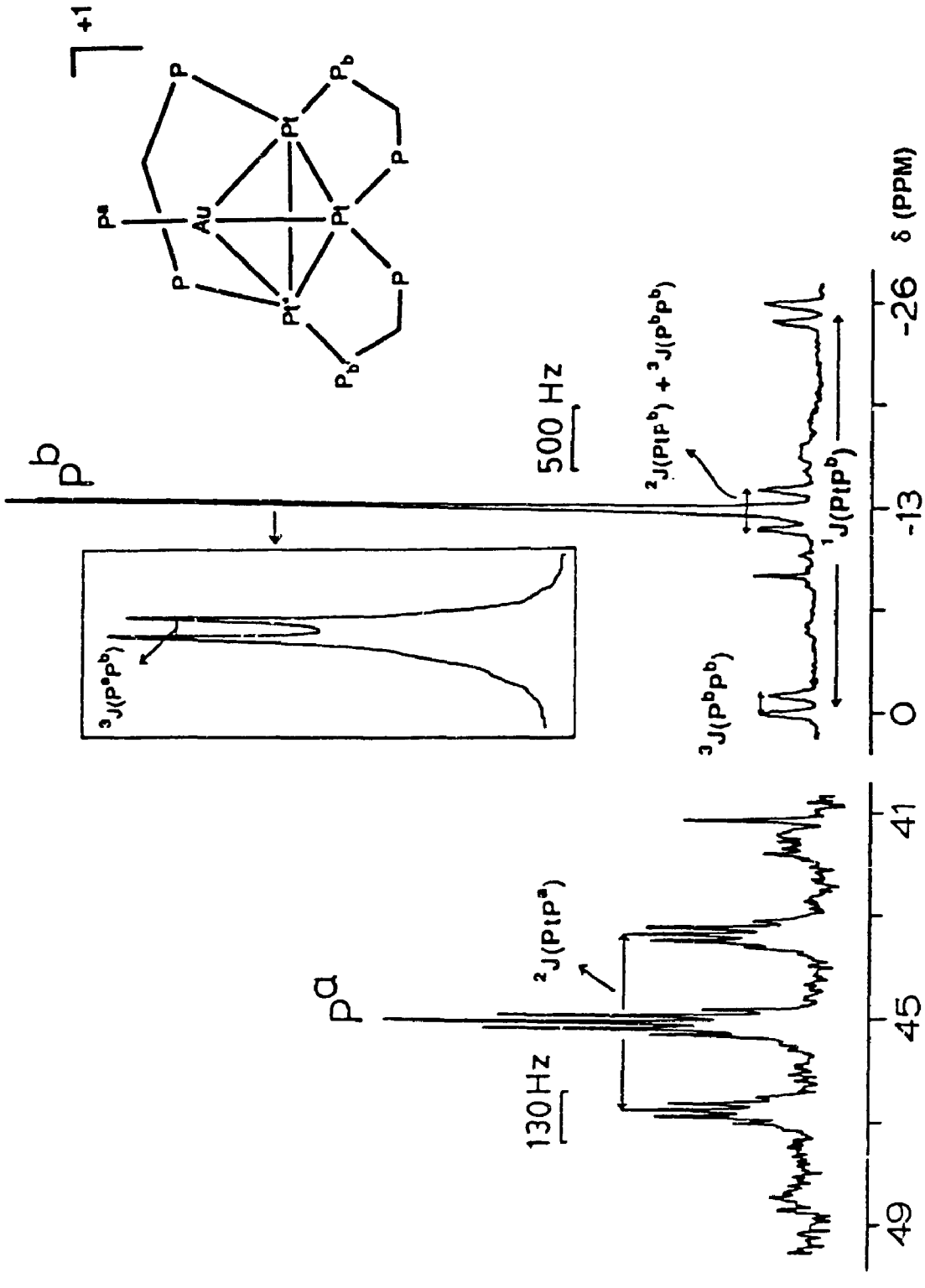

Figure 5.1: $^{31}P\{^1H\}$ NMR spectrum (121.4 MHz) of 3a

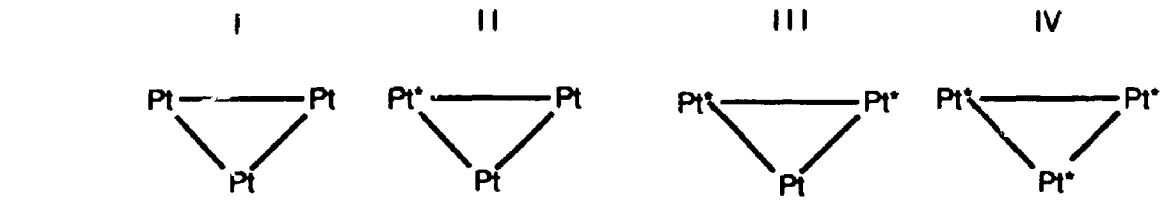

	I	II	III	IV
Natural Abundace	29.0%	44.4%	22.7%	3.9%

Scheme 5.5 : $^{196}Pt = Pt^*$

$^3J(P^aP^b)$ = 19 Hz, 3a; $^3J(P^aP^b)$ = 22.5 Hz, 4) and a septet due to P^a (due to coupling with six equivalent phosphorus nuclei, P^b, in the $Pt_3(\mu\text{-dppm})_3$ unit). In the complex 5, the signal due to P^b appears as a triplet (Figure 5.4) due to coupling with two chemically equivalent P^a nuclei on the μ_3-$AuPPh_3$ units ($^3J(P^aP^b)$ = 21 Hz). For isotopomer II, there is a coupling between P^b and Pt* which manifests itself as a doublet superimposed on the P^b resonance from the isotopomer I. The presence of a single active Pt nucleus made the P^b nuclei magnetically inequivalent, and thus P^b couples to both Pt* and P^b. Both $^1J(PtP^b)$ and $^2J(PtP^b)$ are well resolved and each satellite contains an extra doublet splitting due to $^3J(P^bP^b)$. This observation of long range PtP and PP coupling is characteristic of an almost linear P-Pt-Pt-P unit and has proved to be a useful criterion for the presence of such units. The $^1J(PtP)$ coupling is obtained by measuring from the centre of the upfield satellite to the centre of the downfield satellite. The three bond P^b-P^b coupling is responsible

for the doublet splitting seen in the satellites of the P^b signal. The long range coupling, $^2J(PtP^b)$, is obtained by measuring the separation between the inner satellites. Since only one half of the doublet is observed, one can measure from the downfield outer half of the satellite to its partner on the upfield side and subtract $^3J(P^bP^b)$ as shown in figure 5.1. The spin system is complex in the cases of isotopomers III and IV. Only a spectral simulation would sort out the peaks originating from the contributions made by these two isotopomers.

The septet resonance due to P^a also contains ^{195}Pt satellites and the origin of these satellite spectra are the isotopomers II, III and IV. For isotopomer II, there is a coupling between P^a and Pt* which results in a doublet centred about the P^a resonance from isotopomer I. Similar coupling interactions in isotopomers III and IV resulted in a triplet and a quartet, respectively, and these resonances are also centred about the P^a resonance from isotopomer I. Superposition of the multiplets should give a seven-line spectrum whose intensities are in ratio 1:12:49:84:49:12:1 with lines separated by 0.5 $^2J(PtP^a)$ (see appendix 7) The outer lines were too weak to be observed, but the intensities of the inner five lines were as expected (ie, 1:4:7:4:1). This pattern was observed for the P^a resonance in complexes 3 to 5 and is characteristic of a $Pt_3(\mu_3\text{-}X)$ group in these complexes [X = $AgPPh_3$, 3b or $AuPPh_3$ (3a, 4 and 5)].

Table 5.1 : $^{31}P\{^{1}H\}$ and $^{195}Pt\{^{1}H\}$ NMR Spectral Data for Complexes 3 - 5 §

Complex	3a	3b	4	5
δP^b	-13.4	-14.5	-12.6	-16.0
$^1J(PtP^b)$	3155	3139	3020	3060
$^2J(PtP)$	170	182	190	134
$^3J(P^bP^{b'})$	150	155	200	170
δP^a	44.6	16.5	46.3	44.4
$^2J(PtP^a)$	503	335	892	440
$^3J(P^aP^b)$	19.0	8.5	22.5	21.0
$^1J(^{107}AgP)$	-	536	-	-
$^1J(^{109}AgP)$	-	550	-	-
$^2J(AgP^b)$	-	21.0	-	-
δ Pt	-2463.5	-2504	NA	-2207.3

§ In acetone-d_6

Table 5.2 : ^{1}H NMR Spectral data for Complexes 2 to 5 §

Complex	2	3a	3b	4	5
δ PtH	4.16	-0.90	-1.11	-	-
$^1J(PtH)$	710	317	325	-	-
$^2J(P^bH)$	23	17	16	-	-
$^3J(PAuPtH)$	-	11.5	-	-	-
δCH^aH^b	5.02 5.61	5.0 6.4	5.14 6.20	4.11 6.51	5.20
$^2J(H^aH^b)$	14.0	14.0	11.0	10.0	-
δ Ph	7.30	7.32	7.20	7.35	7.25

§ In acetone-d_6

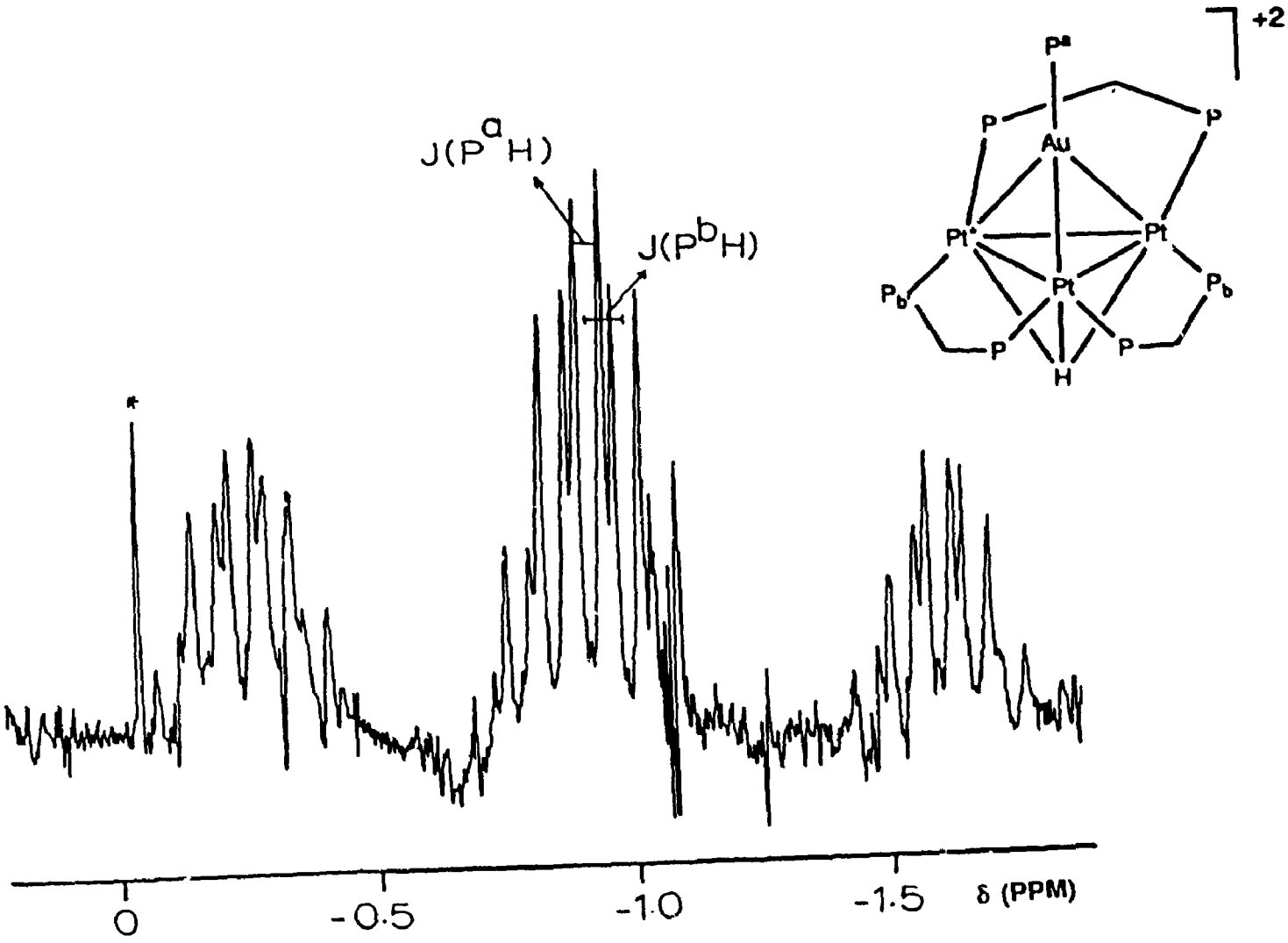

Figure 5.2: ^1H NMR spectrum (200 MHz) of 3a

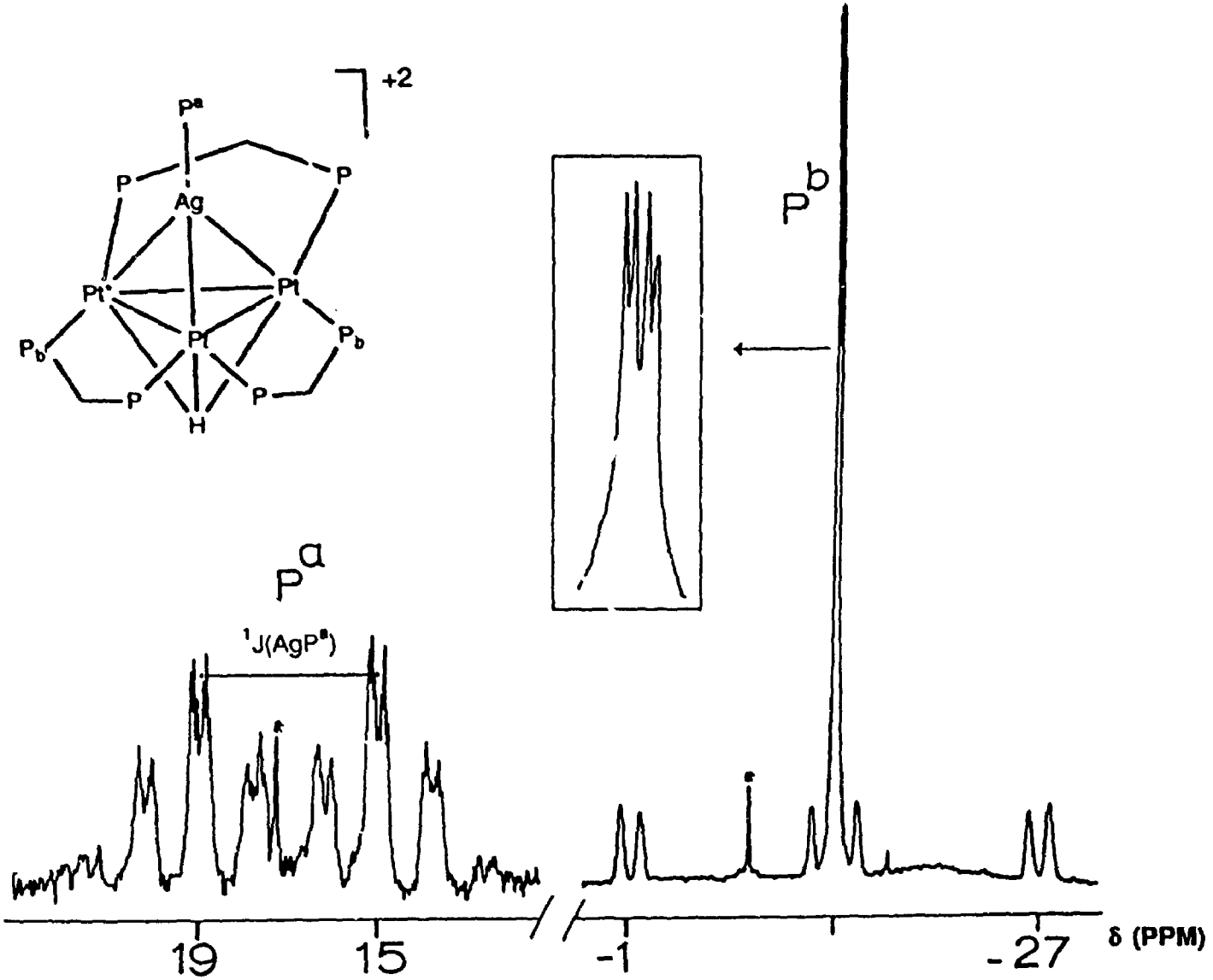

Figure 5.3: $^{31}P\{^{1}H\}$ NMR spectrum (121.4 MHz) of 3b at -40°C

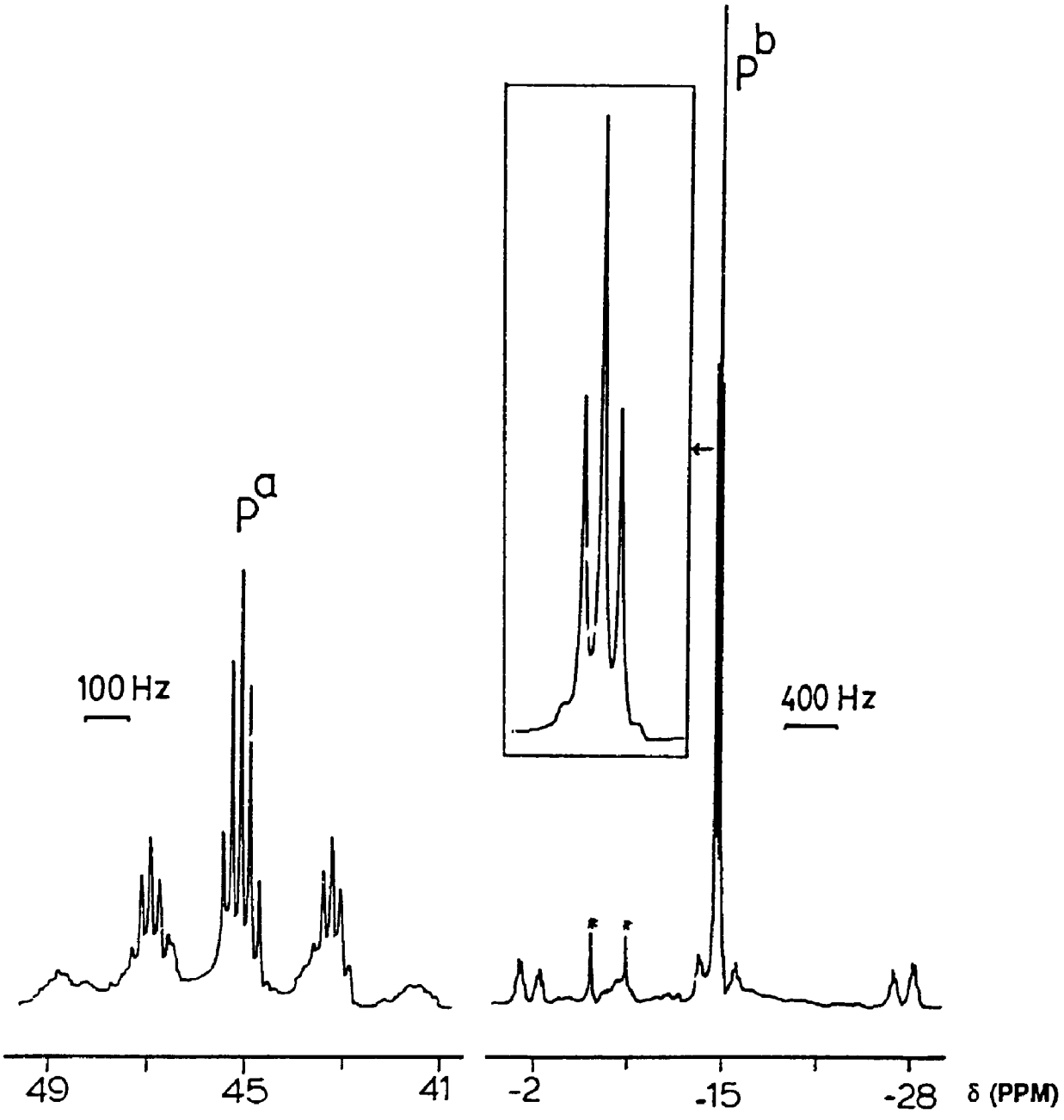

Figure 5.4: $^{31}P(^{1}H)$ NMR spectrum (121.4 MHz) of 5

Characterization of the silver complex, 3b, was aided by the presence of ^{107}Ag and ^{109}Ag, each having spin $I = \frac{1}{2}$. The ^{31}P NMR spectrum of 3b at -40°C (figure 5.3) showed the resonance due to P^a at δ +16.5 appearing as a doublet of septets due to coupling with $^{107}Ag/^{109}Ag$ and the six chemically equivalent phosphorus nucleii of the $Pt_3(\mu\text{-dppm})_3$ unit [$^1J(^{107}AgP^a)$ = 536 Hz; $^1J(^{109}AgP^a)$ = 550 Hz and $^3J(P^aP^b)$ = 8.5 Hz] and is accompanied by the satellites due to ^{195}Pt having the intensities expected for a $Pt_3(\mu_3\text{-}AgPPh_3)$ unit.

The ^1H NMR spectra of 3a and 3b revealed characteristic metal-hydride signals upfield of TMS. The signal in the ^1H NMR spectrum of 3a (figure 5.2) was observed at δ -0.9 and appeared as a septet of doublets due to coupling with six equivalent phosphorus nuclei of the $Pt_3(dppm)_3$ unit ($^2J(P^bH)$ = 17 Hz) and the P^a nucleus of the $(\mu_3\text{-}AuP^aPh_3)$ unit ($^3J(HPtAuP^a)$ = 11.5 Hz), and with satellites due to coupling to ^{195}Pt ($^1J(PtH)$ = 317 Hz) having the intensities expected for a $Pt_3(\mu_3\text{-H})$ group[16]. A similar hydridic resonance was observed for 3b at -40°C, which appeared at δ -1.11 with $^1J(PtH)$ = 325 Hz. We note that the NMR data does not preclude less symmetrical but fluxional structures, such as structure with a $Pt_3(H)(\mu_3\text{-}MPPh_3)$ unit [M = Au, 3a; Ag, 3b], shown in scheme 5.6. However the NMR data are unchanged at -80°C and no terminal Pt-H stretch was observed in the IR spectrum, so such structures are improbable.

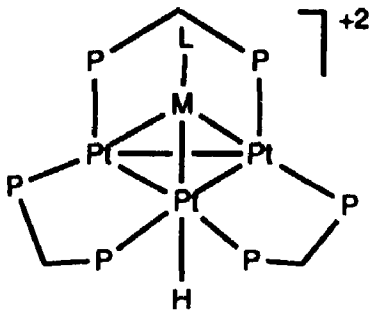

Scheme 5.6 : L = PPh_3 , M = Au, 3a ; Ag, 3b

The resonance due to the CH_2P_2 protons in the ^1H NMR spectra of 3a, 3b and 4 appeared as an "AB" quartet due to non equivalent $CH^aH^bP_2$ protons, thus indicating that these complexes are unsymmetrical, and the groups that are capping above and below the $Pt_3(\mu\text{-dppm})_3$ unit are not the same. In contrast, the resonance due to the CH_2P_2 protons of 5 appeared as a singlet at δ5.20, suggesting a symmetrical structure with μ_3-$AuPPh_3$ groups capping the faces above and below the Pt_3 triangle. Thus, NMR spectral data suggest a tetrahedral Pt_3Au metal skeleton for 4, while 5 adopts a symmetrical trigonal bipyramidal Pt_3Au_2 skeleton. Complexes 3a and 3b have a tetrahedral Pt_3M arrangement of atoms, with the Pt_3 triangular face capped by a triply bridging hydride ligand. Structurally characterized analogous complexes of 4 and 5 are well documented in the literature[9,10,16].

5.3.3 Chemical reactivity of Au-Pt clusters 3 - 5

The chemistry of mixed-metal gold cluster

compounds has not been extensively reported.[1] The reaction of these clusters with the lewis bases is dominated by the abstraction of $AuPR_3^+$ units, and replacement by a phosphine or halide ligand. A number of clusters undergo reactions with either CO or H_2, which suggests the possibility of using these compounds in homogeneous catalysis.

Complex 4 has a vacant face on one side of the $Pt_3(\mu\text{-dppm})_3$ unit and hence various ligands can be added onto this face. The added ligand can bind to one Pt centre in a terminal mode, or it can bridge a Pt-Pt edge in a μ_2-bridging mode, or cap the Pt_3 unit in a μ_3-bridging mode. We have reacted a few selected reagents with the

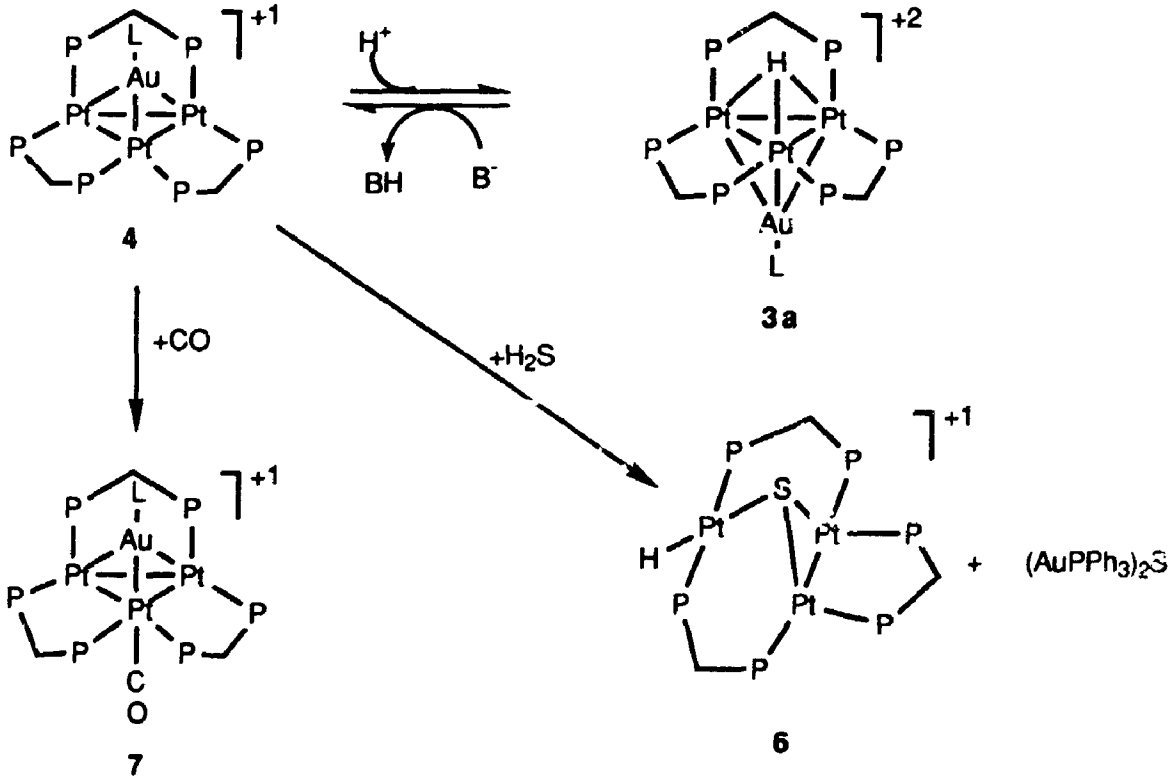

Scheme 5.7

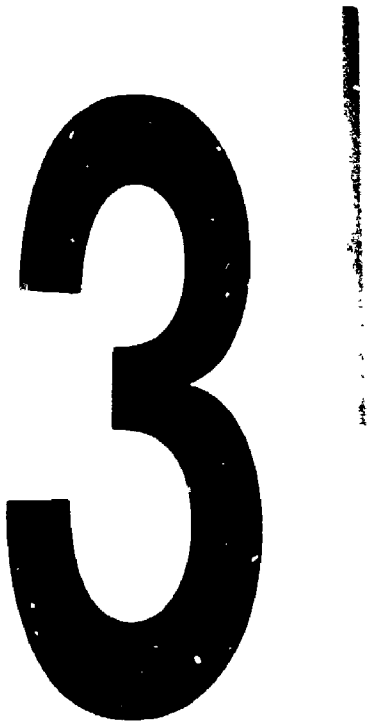

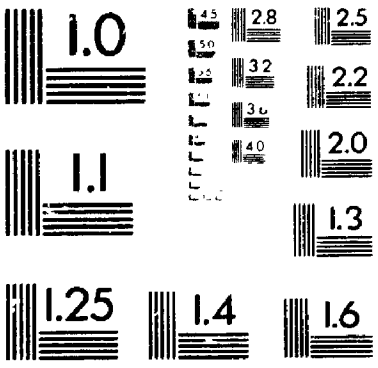
1.0
1.1
1.25
1.4
1.6
2.8
3.2
4.0
2.5
2.2
2.0
1.3


MicroD

species 4 to form a range of compounds. Scheme 5.7 shows the various products formed in these reactions.

5.3.3.1 Reaction of 4 with acids and bases

Complex 4 readily reacts with CF_3COOH and yields the protonated product 3a. The detailed characterization of this product has been described earlier.

3a can be easily deprotonated by reacting with bases like NEt_3 or dil.NaOH to revert to 4. These reactions demonstrate the stability of 3a and 4 towards strong acids and bases. This is a unique feature of these two clusters, since most of the cluster complexes are unstable in acidic or basic medium and result in cluster fragmentation. For example, the reaction of NEt_3 with $Os_4H_3(CO)_{12}AuPPh_3$ induces the disproportionation of the cluster to $Os_4H_3(CO)_{12}$ and $Os_4H_2(CO)_{12}(AuPPh_3)_2$.[19] This was rationalized in terms of nucleophilic attack by NEt_3 at the $AuPPh_3$ centre, followed by heterolytic cleavage of the Au-Os bond and further reaction of the liberated gold cation.

5.3.3.2 Reaction of 4 with H_2S

Reaction of H_2S gas with 4 results in the elimination of the $AuPPh_3$ unit and formation of the known cluster $[Pt_3(\mu_3\text{-}S)(H)(\mu\text{-}dppm)_3]^+$, 6. The spectral data (see experimental) and the elemental analysis of 6 are in full agreement with the reported work.[20] The μ_3-S unit in

6 cannot be displaced by any other ligand. These results demonstrate the poisoning affinity of the sulfide towards platinum, which is often observed in sulfur contaminated heterogeneous catalysts.

5.3.3.3 Reaction of 4 with CO

Complex 4 adds CO readily and reversibly at room temperature to give a 56 electron complex, $[Pt_3(\mu_3\text{-}AuPPh_3)(CO)(\mu\text{-}dppm)_3]^+$, 7. This species was stable only under a positive pressure of CO, and hence was characterized solely by spectroscopic methods. Table 5.3 gives the NMR spectral data of 7 obtained at -60°C. The ^{31}P NMR spectrum of 7 at -60°C is shown in figure 5.5. The NMR labelling scheme for 7 is given in scheme 5.8. The P^a resonance at δ 41.8 appears as a singlet with satellites due to coupling to ^{195}Pt [$^2J(PtP^a)$ = 620 Hz) having the intensities expected for a $Pt_3(\mu_3\text{-}CO)$ group. We should

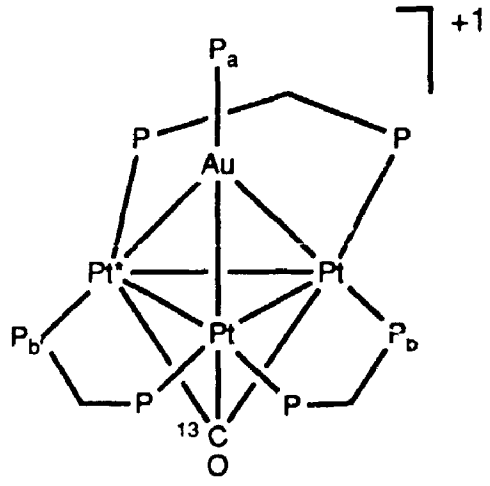

Scheme 5.8: NMR labelling scheme for 7

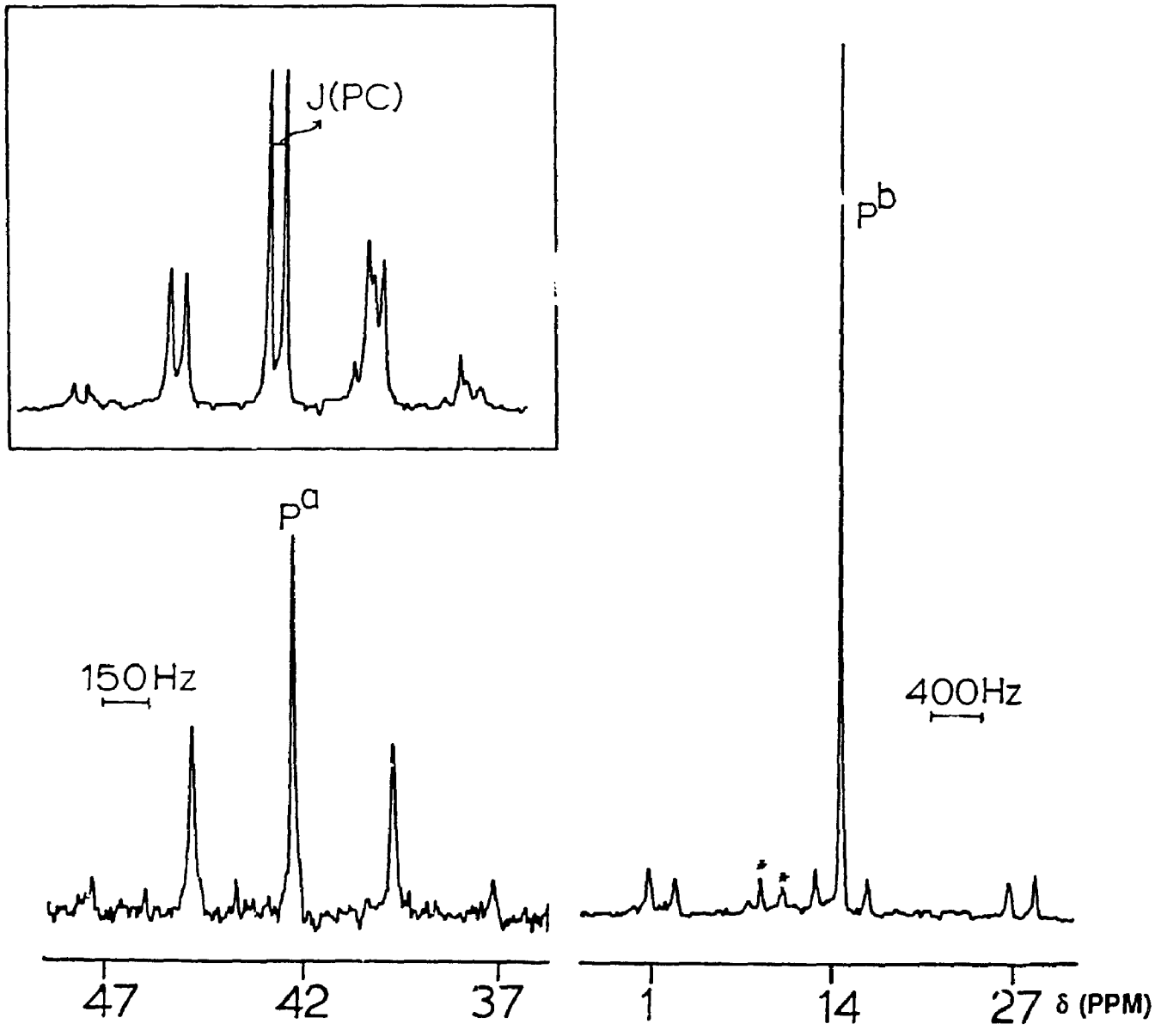

Figure 5.5: $^{31}P(^{1}H)$ NMR spectrum (121.4 MHz) of 7 at -60°C. Inset shows the resonance due to P^a in the ^{13}CO enriched sample, 7*.

note that addition of a CO ligand to 4 leads to a collapse of the $^{3}J(P^{a}P^{b})$ coupling from 22.5 Hz in 4 to zero in 7. Thus, the signal due to P^{a} which appears as septet in4 collapses to a singlet in 7. The dppm resonance appears as a sharp singlet at δ -14.3. The spectrum does not change even at -80°C, though a slight broadening of the dppm resonance is observed.

Table 5.3 : NMR Spectral Data for Complex **7** in CD_2Cl_2

$^{31}P\{^{1}H\}$	
δP^{a}	41.8
$^{2}J(PtP^{a})$	620
$^{3}J(P^{a}AuPt^{13}C)$	48.0
$^{3}J(P^{a}P^{b})$	0.0
δP^{b}	-14.3
$^{1}J(PtP^{b})$	2922
$^{2}J(PtP^{b})$	212
$^{3}J(P^{b}P^{b'})$	204

$^{13}C\{^{1}H\}$	
$\delta^{13}CO$	204.0
$^{1}J(Pt^{13}CO)$	368
$^{3}J(P^{a}AuPt^{13}C)$	48.0

^{1}H	
$\delta CH^{a}H^{b}$	4.71
$\delta CH^{a}H^{b}$	5.83
$^{2}J(H^{a}H^{b})$	14.0
$^{3}J(PtH^{b})$	78.0
δPh	6.6 - 7.6

In the ^{13}CO enriched cluster, 7*, the resonance due to P^{a} appears as a doublet due to coupling with ^{13}CO [$^{3}J(P^{a}C)$ = 48 Hz, see the inset in figure 5.5). This is confirmed by the ^{13}C NMR spectrum of 7* at -60°C (figure 5.6)), where the ^{13}CO resonance appears at δ 204.0 as an apparent 1:4:7:4:1 quintet (due to $^{1}J(PtC)$ = 368 Hz) of doublets ($^{3}J(P^{a}C)$ = 48 Hz). There is no observable change in the ^{13}C NMR spectrum even at -80°C. Thus the ^{31}P and

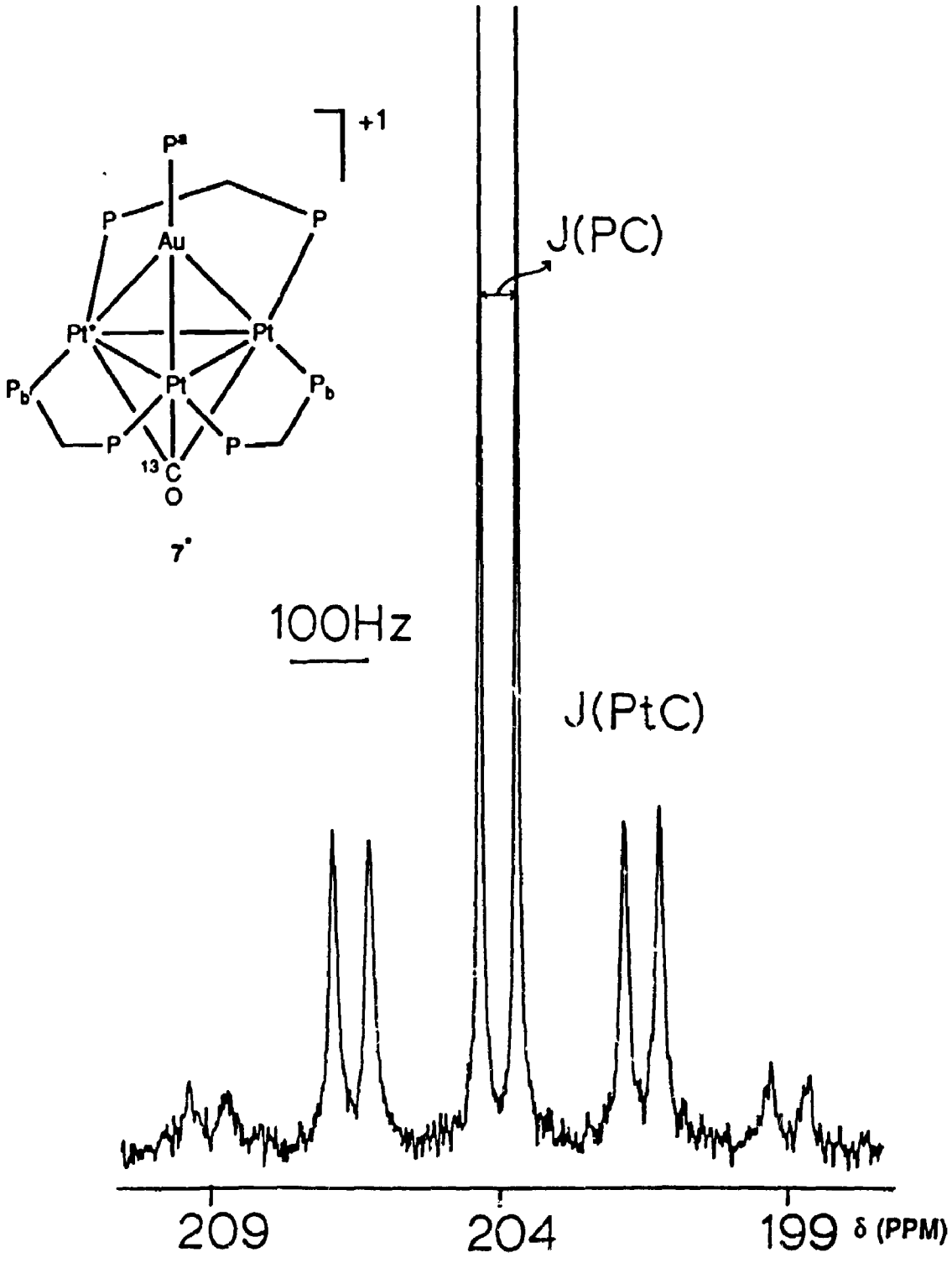

Figure 5.6: $^{13}C(^{1}H)$ NMR spectrum (75.4 MHz) of 7* at -60°C.

^{13}C NMR data suggest that in complex 7 both the $AuPPh_3$ unit and the CO ligand are capping the faces above and below the $Pt_3(\mu\text{-dppm})_3$ unit, in a triply bridging mode, as shown in 9. However, the IR spectrum of 7 shows the $\nu(C\equiv O)$ stretch at 1995 cm^{-1}. The corresponding $\nu(C\equiv O)$ stretch is observed at 1978 cm^{-1} in the ^{13}CO enriched, 7*. These IR data are characteristic of a terminal carbonyl ligand and suggest that in 7 the CO ligand is bound terminally to a single platinum centre.

The IR and NMR spectral data of 7 can be rationalized on the basis of a rapid fluxional process involving migration of the CO ligand around the triangular face of the cluster. The mechanism of fluxionality is likely to occur as shown in equation 5.2. Thus, we see that

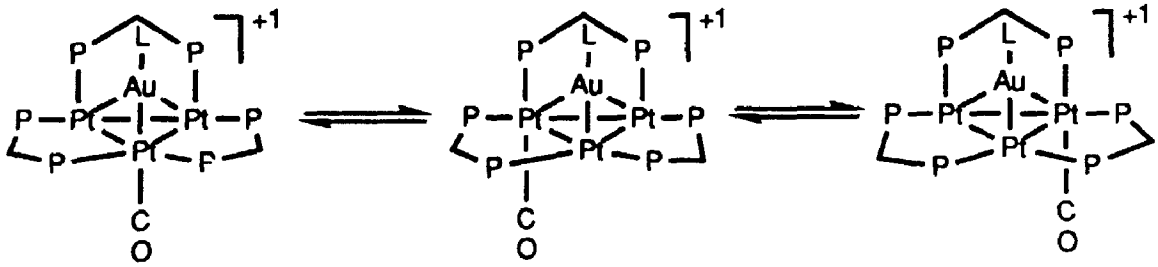

7 7' 7''

Equation 5.2

the fluxional process is fast on the ^{31}P and ^{13}C NMR time scale and is slow on the IR time scale.

We cannot say if the ligand migration involves a $Pt_2(\mu_2\text{-CC})$ or a $Pt_3(\mu_3\text{-CO})$ transition state, 8 or 9 (scheme

5.9), respectively. A similar fluxional process has been observed earlier[22] in the isoelectronic complexes $[Pt_3(\mu_3\text{-}CO)(L)(\mu\text{-}dppm)_3]^{+2}$, where L = PR_3 or $P(OR)_3$, in

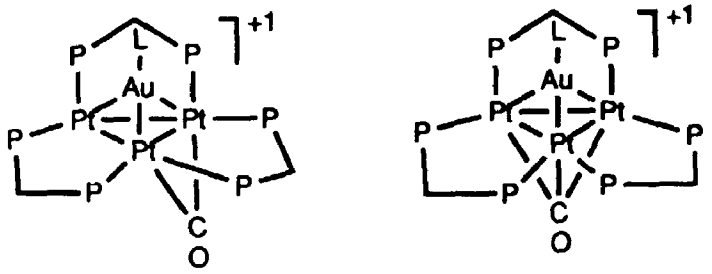

Scheme 5.9

which the ligand L migrates from one platinum to another on the triangular face of the cluster.

5.3.3.4 Reaction of 5 with PPh_3

It is known in gold chemistry that the addition of one or more equivalent of PPh_3 to a gold cluster can lead to the formation of a new cluster. For example, $[Au_2Ir(H)(PPh_3)(NO_3)]^+$ reacts with two equivalents of PPh to form $[AuIr(H)(PPh_3)_4]^+$ and $[Au(PPh_3)_2]^+$.[23] The reaction of the digold cluster 5 with two equivalents of PPh_3 in acetone results in the extrusion of the $AuPPh_3^+$ unit yielding the monogold complex 4 and $[Au(PPh_3)_2]^+$ (see equation 5.3). In this case, more than one equivalent of PPh_3 was necessary to produce a complete reaction because an equilibrium between $[Au(PPh_3)_2]^+$ and PPh_3 ties up free

PPh_3. This equilibrium is rapid on the NMR time scale and results in a signal that appears at δ20.1, which is a

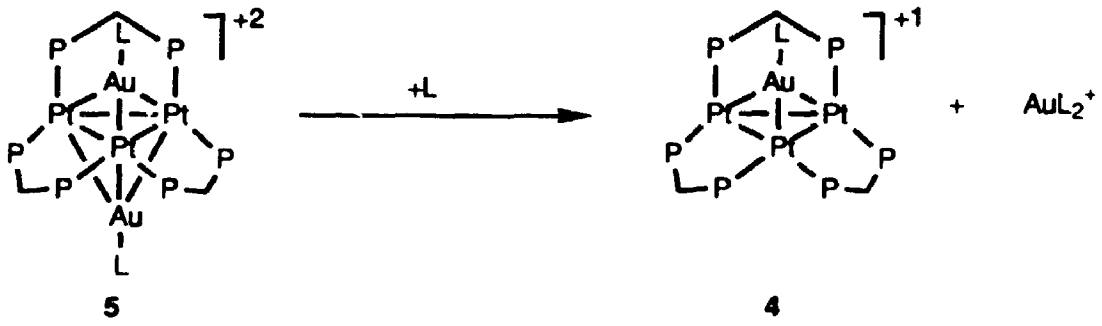

5 4

Equation 5.3

weighted average of the positions of $[Au(PPh_3)_2]^+$ (δ40.1) and free PPh_3(δ-10.2).

5.4 BONDING IN Au-Pt CLUSTERS 3 - 5 AND 7

Clusters 3 - 5 contain a triangle of platinum atoms capped either by a single MPR_3^+ fragment (M = Au in 3a; Ag in 3b) or bicapped by a $AuPR_3^+$ unit on each side of the Pt_3 triangle (as in 5). Complex 4 contains both a (μ_3-H) and a (μ_3-$AuPR_3$) unit, capping opposite sides of the triplatinum centre. Complexes 3 and 4 are isoelectronic and contain 54 valence electrons, while 3a and 3b are analogous to the isoelectronic $[Pt_3(\mu_3\text{-}AuPCy_3)(\mu\text{-}CO)_3(PCy_3)_3]^+$ (see scheme 5.1) cluster, synthesized and structurally characterized by Mingos *et al*; complex 5 is a 66 electron cluster.

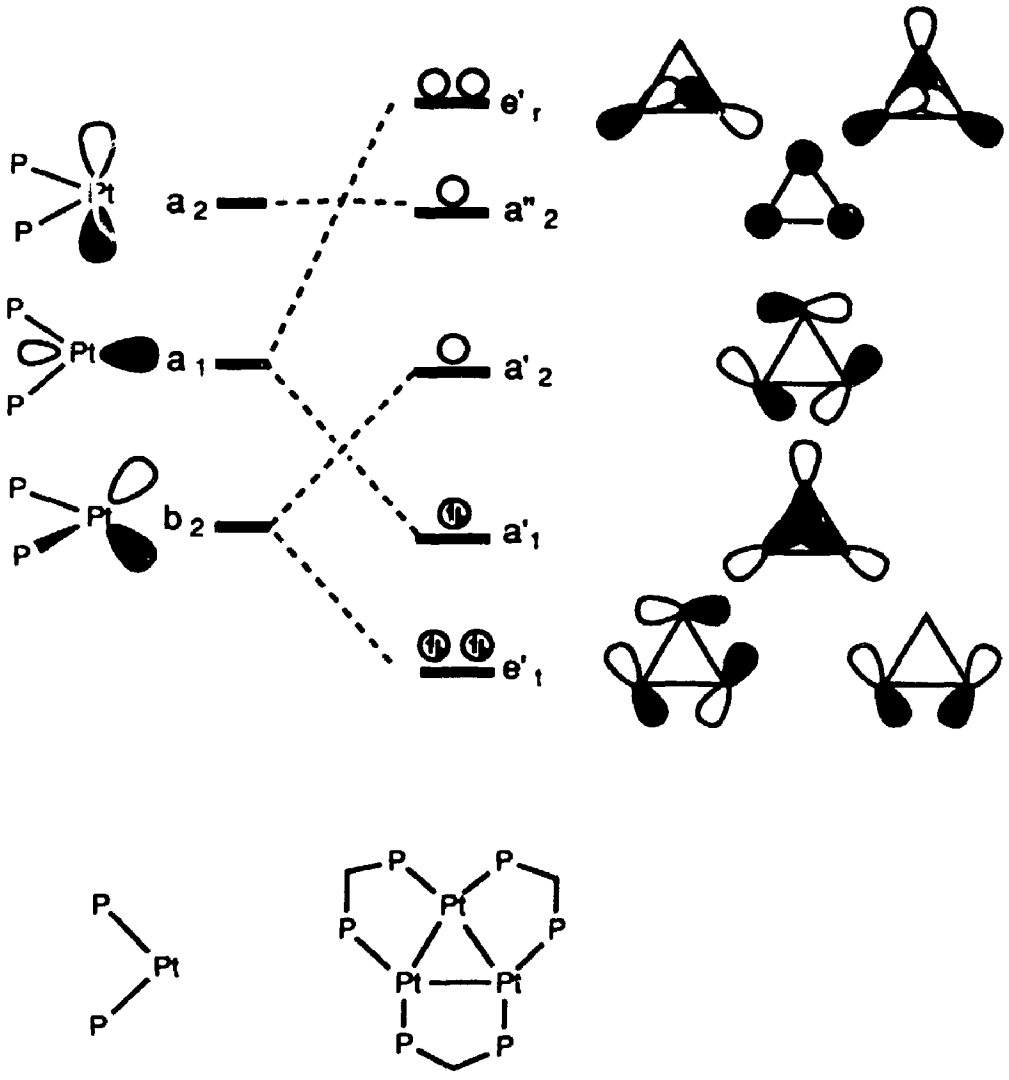

Figure 5.7 : Frontier Molecul: Orbitals of Pt_3 (μ-dppm')$_3$ unit

The bonding in platinum-gold cluster complexes has been discussed in detail elsewhere[24], with reference to semi-empirical molecular orbital calculations. In these complexes the gold is contributing only a single valence orbital (sp hybrid) to the cluster bonding[25].

In complexes 3-5, H^+ and/or $AuPR_3^+$ units cap the 42 electron triangular Pt_3 clusters, based on the $Pt_3(\mu\text{-dppm})_3$ unit. A detailed MO analysis of this triplatinum unit was the subject of recent studies by Evans and others[21,26]. The molecular orbitals and energy levels for the $Pt_3(\mu\text{-dppm})_3$ unit are illustrated in figure 5.7. In this triplatinum system, there are 4 bonding orbitals (namely a_1', a_2'' and the degenerate pair e') derived from the combination of three PtL_2 units. The a_2'' (derived from Pt $6P_y$ orbital) orbital is unavailable for occupation as a result of the high lying nature of the Pt $6P_y$ orbitals. The cluster therefore has three occupied M-M bonding molecular orbitals and a total of 42 electrons. The a_1' bonding orbital contains two electrons and is the HOMO in this system. It is formed by the combination of three PtL_2 units, each having one inward-pointing orbital contributing to the cluster bonding. It has been argued that the addition of a capping ligand to this unit stabilizes the existing molecular orbitals on it.[21] In particular, the capping process strongly stabilizes the a_1 (S^σ) skeletal bonding HOMO.

A qualitative picture of the interaction diagram

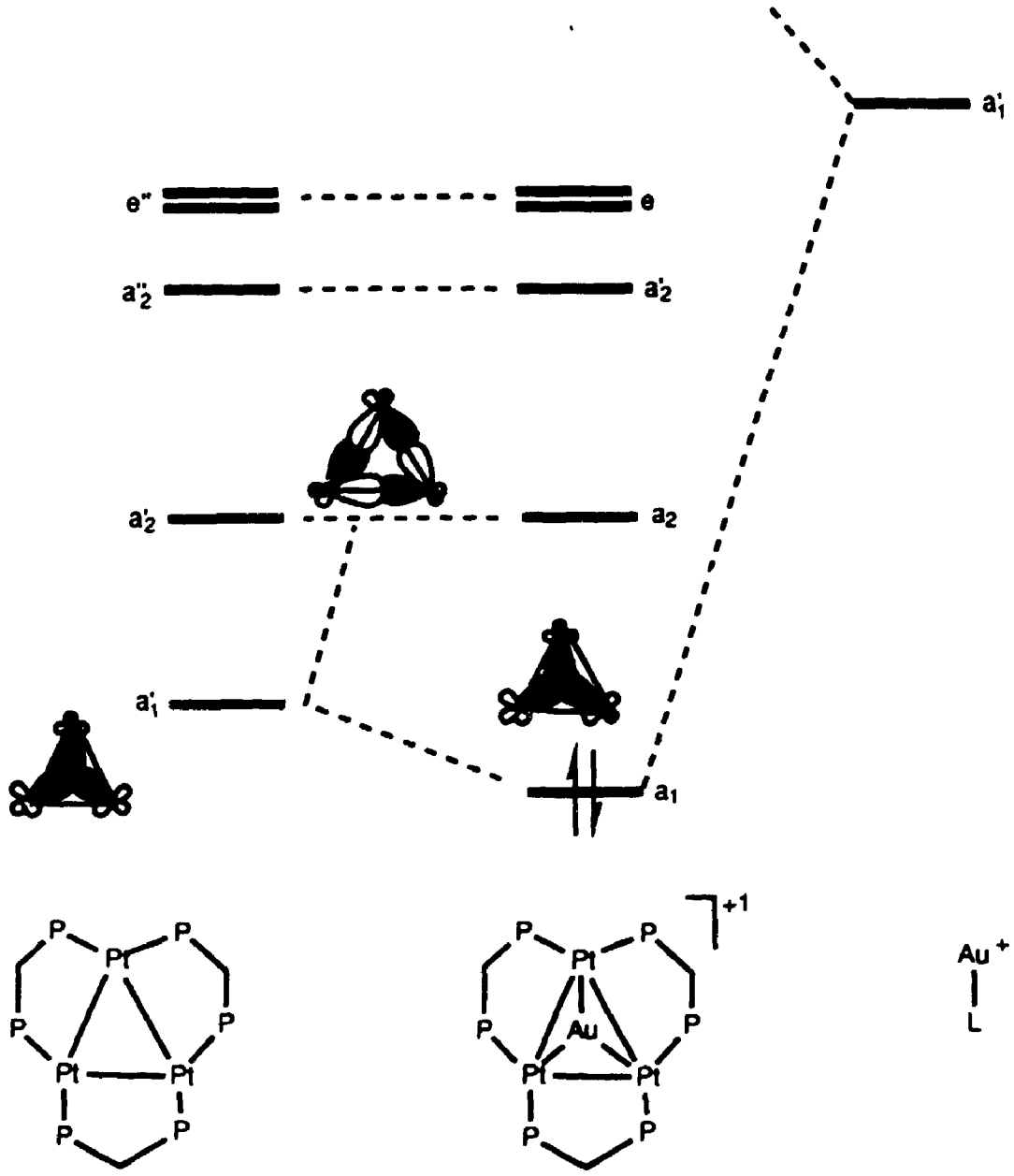

Figure 5.8 : Principal molecular orbitals for the metal skeleton of 4

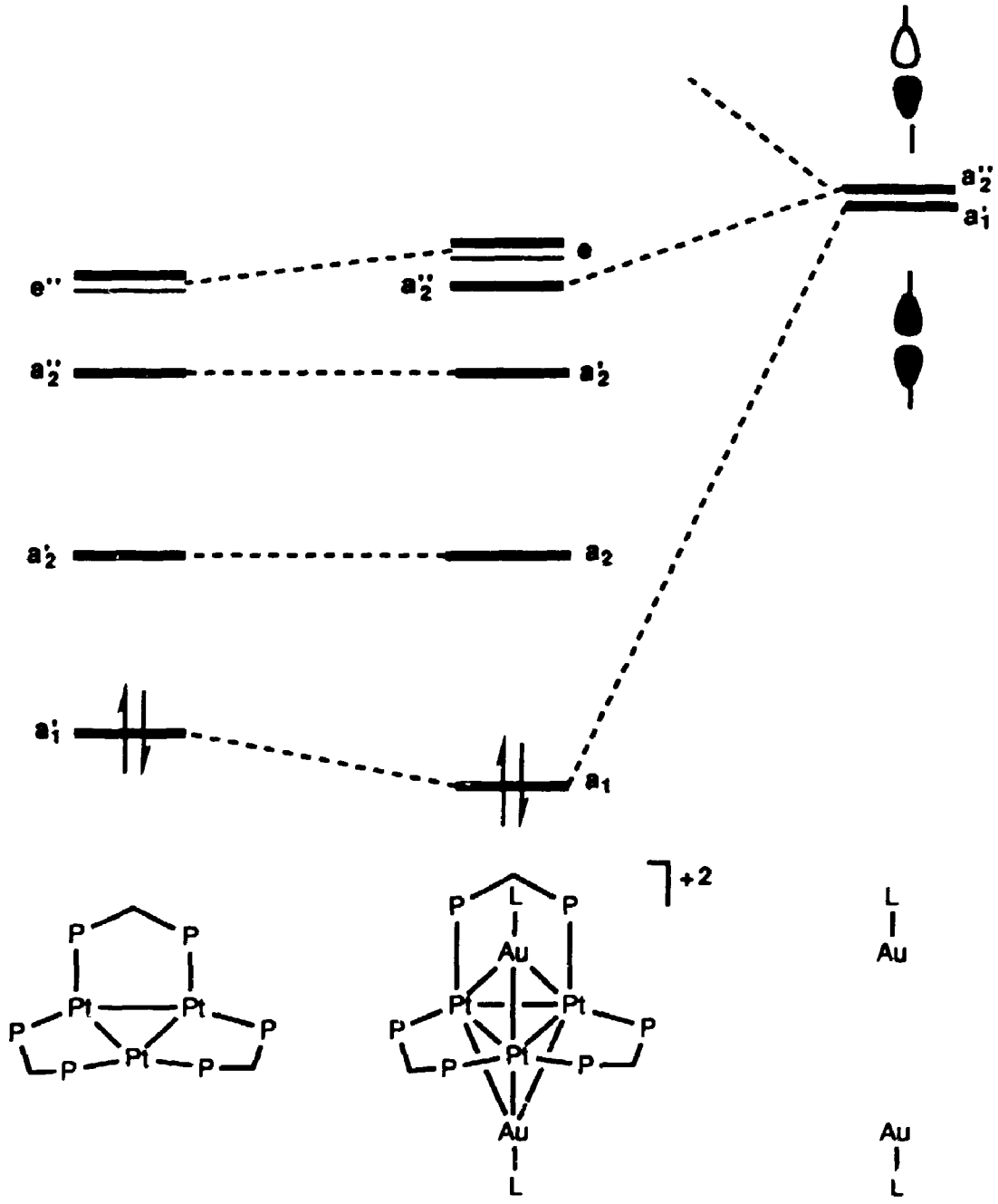

Figure 5.9 : Principal molecular orbitals for the metal skeleton of complex **5**

for $[Pt_3(\mu_3\text{-}AuPPh_3)(\mu\text{-}dppm)_3]^+$, 3a, is presented in figure 5.8. Here, the gold atom is linearly *sp* hybridized. One hybrid accepts a pair of electrons from the phosphine ligand, the other overlaps with the a_1' orbital of the Pt_3 unit, forming a four-centre two-electron bond linking the four metal atoms.

When a second $AuPR_3^+$ unit is added to the cluster complex 5, its *sp* hybrid interacts with the a_1' orbital, which then becomes a five-centre orbital (figure 5.9). The pair of electrons is now even further delocalized, and is expected to consequently increase both the Pt-Pt and Pt-Au bond lengths. Thus, if the capped complexes 3a, 4 and 5 are considered to be formed by consecutive addition to the a_1 HOMO of the $Pt_3(\mu\text{-}dppm)_3$ unit, then the individual Pt-H and Pt-Au bonds are expected to be weaker for the dicapped compounds.

This is reflected by the relative magnitudes of the coupling constants $^1J(PtH)$ and $^2J(PtAuP)$ for the complexes 3-5 and 7. As expected, the magnitudes of the coupling constants $^1J(PtH)$ for the dicapped clusters 3a (317 Hz)) and 3b (325 Hz) are less than those for the monocapped cluster 2 (710 Hz). A similar trend is also observed in $^1J(PtC)$ values for the dicapped complex 7 (368 Hz) relative to the monocapped complex 1 (777 Hz). Similarly, $^2J(PtAuP)$ in 3a (503 Hz) and 5 (440 Hz) are much reduced from the value found in 4 (892 Hz).

The $^1J(PtH)$ value in the symmetric, dicapped,

dihydride complex $[Pt_3(\mu_3\text{-}H)_2(\mu\text{-}dppm)_3]^{+2}$, 12, (the details of this complex are given in chapter 6) is 420 Hz. Consideration of the $^1J(PtH)$ and $^2J(PtAuP)$ coupling constants in complexes 3a, 5, and 12 indicates that the gold atom has a greater share of the a_1 HOMO of the $Pt_3(\mu\text{-}dppm)_3$ unit, than does hydrogen, in the mixed complex 3a [ie, a lower $^1J(PtH)$ and higher $^2J(PtAuP)$ value compared to those in the symmetrical complexes 12 and 5].

5.5 SUMMARY AND CONCLUSIONS

The synthesis and characterization of the platinum group IB mixed metal complexes that were discussed in this chapter resulted largely from the isolobal analogy between AuL^+ and H^+ units[14,15]. The hydrido complex 2 was used as the precursor in all the synthesis, with the aim of substituting the hydridic proton with a LAu^+ fragment. Not only did we succeed, by this strategy in obtaining 4, but we were also able to isolate and characterize the intermediate 3a. A similar rationale explains the selectivity of the substitution reaction defined by the sequence 2 $\longrightarrow$ 3a $\longrightarrow$ 4 (scheme 5.2). This and the sequence 4 $\rightleftharpoons$ 5 (scheme 5.2) involving a symmetric "intermediate", clearly illustrate how electrophilic ligand substitution at the trinuclear site[27] can occur by a bimolecular, stepwise mechanism.

While $AgPPh_3^+$ reacted with 2 to form 3b, its Cu(I)

analogue did not react with 2. Attempts to synthesize silver analogues of 4 and 5 were unsuccessful. Thus, within group Ib metals, it is clear that gold has by far the greatest ability to form heteronuclear Pt-M bonds.

Complexes 3a and 4 were stable towards acids and bases. The ability of 3a to react with either electrophiles such as H^+, LAu^+, LAg^+ etc,) or nucleophiles (such as CO, PPh_3, H^- etc.,) makes it a remarkable complex and suggests that it could be a good candidate for heterometallic homogeneous catalyst. Research in this area is important because the addition of gold to supported transition metal catalysts is known to sometimes favourably affect reactivity and selectivity.[2,29] It may also be possible to use metal-gold cluster compounds to model bimetallic metal-gold surfaces.[13]

The observation of fluxionality of the CO ligand in 7 involving migration about the Pt_3 triangle is almost certainly a result of the coordinative unsaturation of the cluster 3a, and provides a good example of the high reactivity of such clusters. A fluxional process such as this at a triplatinum centre can be considered to mimic CO ligand migration on a Pt(111) surface[28].

Finally, the bonding in complexes 3-7 has been rationalized on the basis of earlier MO calculations. It is observed that in the dicapped complexes the Pt-M and the Pt-L (L = H, CO) bonds are weaker than those observed in the monocapped complexes.

5.6 REFERENCES

1. A.M. Mueting, W. Bos, B.D. Alexander, P.D. Boyle, J.A. Casalnuovo, S. Balaban, L.N. Ito, S.M. Johnson and L.H. Pignolet, *New J. Chem.*, 12 (1988) 505

2. P. Braunstein, J. Rose, *Gold Bull.*, 18 (1985) 17

3. K.S. Pitzer, *Acc. chem. Res.*, P3A,12 (1979) 271

4. K.P. Hall, D.M.P. Mingos, *Prog. Inorg. chem.*, 32 (1984) 237

5. G.J. Arsenault, C.M. Anderson, R.J. Puddephatt, *Organometallics*, 7 (1988) 2094

6. P. Braunstein, H. Lehner, D. Matt, A. Tiripicchio, M. Tiripicchio-Camelini, *Angew. Chem. Int. Ed. Engl.*, 23 (1984) 304

7. Lj. Manojlović-muir, K.W. Muir, I. Treurnicht, R.J. Puddephatt, *Inorg. Chem.*, 26 (1987) 2418

8. C.E. Briant, D.I. Gilmour, D.M.P. Mingos, *J. Chem. Soc., Dalton Trans.*, (1986) 835

9. C.E. Briant, R.W.M. Wardle, D.M.P Mingos, *J. Organomet. Chem.*, 267 (1984) C49; D.M.P. Mingos, R.W.M. Wardle, *J. Chem. Soc., Dalton Trans.*, (1986) 73.

10. J.J. Bour, R.P.F. Kanters, P.P.J. Schlebos, W. Bos, W.P. Bosman, H. Behm, P.T. Beurskens, J.J. Steggerda, *J. Organomet. Chem.*, 329 (1987) 405

11. D.M.P. Mingos, P. Oster, D.J. Sherman, *J. Organomet. Chem.*, 320 (1987) 257

12. D.E. Smith, A.J. Welch, I. Treurnicht, R.J. Puddephatt, *Inorg. Chem.*, 25 (1986) 4616; P.D. Boyle, B.J. Johnson, B.D. Alexander, J.A. Casalnuovo, P.R. Gannon, S.M. Johnson, E.A. Larka, A.M. Mueting, L.H. Pignolet, *Inorg. Chem.*, 26 (1987) 1346

13. J.J. Bour, R.P.F. Kanters, P.P.J. Schlebos, W.P. Bosman, H. Behm, P.T. Beursckens, J.J. Steggerda, *Recl. Trav. Chim. Pays-Bos.*, 107 (1987) 157

14. D.J. Evans, D.M.P. Mingos, *J. Organomet. Chem.*, 232 (1982) 171

15. J.W. Lauher, K. Wald, *J. Am. Chem. Soc.*, 103 (1981) 7648

16. B.R. Lloyd, R.J. Puddephatt, *J. Am. Chem. Soc.*, 107

(1985) 7785

17. M.P. Brown, R.J. Puddephatt, M.Rashidi, K.R. Seldon, *J. Chem. Soc. Dalton Trans.*, (1978) 516

18. S. Bhaduri, K. Sharma, P.G. Jones, C.F. Erdbrugger, *J. Organomet. Chem.*, 326 (1987) C46

19. B.F.G. Johnson, D.A. Kaner, J. Lewis, P.R. Raithby, M.J. Taylor, *Polyhedron.*, 1 (1982) 105

20. M.C. Jennings, N.C. Payne, R.J. Puddephatt, *Inorg. Chem.*, 26 (1987) 3776

21. D.G. Evans, *J. Organomet. Chem.*, 352 (1988) 397

22. A.M. Bradford, M.C Jennings, R.J. Puddephatt, *Organometallics.*, 7 (1988) 792

23. B.D. Alexander, B.J. Johnson, S.M. Johnson, A.L. Casalnuovo, L.H. Pignolet, *J. Am. Chem. Soc.*, 108 (1986) 4409

24. D.I. Gilmour, D.M.P. Mingos, *J. Organomet. Chem.*, 302 (1986) 127

25. R.V. Parish, L.S. Moore, A.J.J. Dens, D.M.P. Mingos, D.J. Sherman, *J. Chem. Soc. Dalton Trans.*, (1989) 539

26. C. Mealli, *J. Am. Chem. Soc.*, 107 (1985) 2245

27. R. Ramachandran, N.C. Payne, R.J. Puddephatt, *J. Chem Soc. Chem. Commun.*, (1989), 128

28. A.B. Anderson, M.K. Awad, *J. Am. Chem. Soc.*, 107 (1985) 7854; N.R. Avery, T.W. Matheson, B.A. Sexton, *Appl. Surf. Sci.*, (1985) 22

29. J. Shwank, *Gold Bull.*, 18 (1985) 2; J. Shwank, *ibid*, 16 (1986) 103

CHAPTER 6

REACTIVITY OF $[Pt_3(\mu_3\text{-}H)(\mu\text{-}dppm)_3](PF_6)$ WITH PHOSPHINES AND PHOSPHITES. CRYSTAL AND MOLECULAR STRUCTURE OF AN ASYMMETRICALLY BRIDGED HYDRIDO COMPLEX, $[Pt_3(\mu_3\text{-}H)(\mu\text{-}dppm)_3\{P(OMe)_3\}](PF_6)$

6.1 INTRODUCTION

The role of tertiary phosphine and phosphite ligands in the chemistry of platinum cluster complexes is well documented in the literature.[1-5] The chemistry is influenced by the steric and electronic factors of these ligands.[2,6] For example, use of bulky tertiary phosphines (i.e, with large cone angles) like P^tBu_3 (182°) or $P(C_6H_{11})_3$ (170°) stabilizes complexes of the type $[Pt_3(\mu\text{-}CO)_3(PR_3)_3]$, whereas the use of phosphines such as PPh_3 (145°) and PMe_2Ph (122°) with intermediate steric and electronic parameters destabilizes these clusters.[6] It has been shown that some phosphine ligands, L, add reversibly to the 42 electron clusters $[Pt_3(\mu\text{-}CO)_3L_3]$ to give $[Pt_3(\mu\text{-}CO)_3L_4]$ and this can lead to either ligand substitution reactions, or with less bulky phosphine ligands L, to cluster fragmentation.[2,7,8]

The triplatinum complex, $[Pt_3(\mu_3\text{-}CO)(\mu\text{-}dppm)_3]^{2+}$, 1, is a coordinatively unsaturated cluster[9] containing 42 valence electrons. Complex 1 reacts with phosphine and phosphite ligands, L, to give $[Pt_3(\mu_3\text{-}CO)(\mu\text{-}dppm)_3L]^{2+}$, 4.[10] In complexes 4, the μ_3-CO ligand is asymmetrically

bridging the triplatinum centre, being strongly bound to the platinum centre with highest coordination number (ie, higher electron density). Similarly, in the 46 electron triplatinum complex[11], $[Pt_3(\mu_2\text{-}CO)(\mu\text{-}dmpm)_4]^{2+}$, 5, the carbonyl ligand is localized on the two platinum atoms which have the extra phosphine ligand, and bridges between

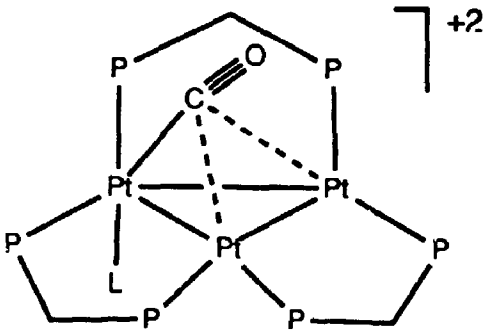

4

L = PR_3 or $P(OR)_3$

P ⌒ P = dppm

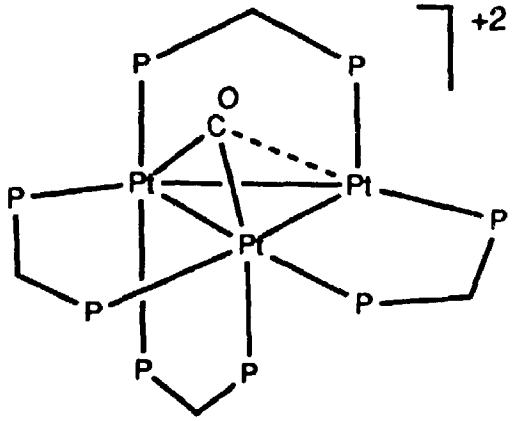

5

P ⌒ P = dmpm

them as a $(\mu_2\text{-}CO)$ ligand. Evans has suggested[12] based on extended Huckel Molecular orbital calculations (EHMO), that, in these complexes, the capping carbonyl acts primarily as a Π-acid ligand and hence binds more strongly to the metal centres with greater electron density.

We were interested to study the reactivity of phosphine and phosphite ligands with the hydrido triplatinum complex[13], $[Pt_3(\mu_3\text{-}H)(\mu\text{-}dppm)_3]^{1+}$, 2, which has a capping hydride ligand that has no Π-acid character. The interest is in whether the ligands add at terminal or

bridging sites[10-15], in how ligand addition affects $Pt_3(\mu_3\text{-}H)$ linkage[12,15], in whether the added ligand and/or hydride ligand is fluxional[10,12,14] and whether there would be major differences from the corresponding chemistry of the carbonyl complex, 1. The results of this study will be discussed in this chapter.

The phosphine ligand, $PPhH_2$, can react with a trinuclear cluster to form an adduct or it could reductively eliminate a molecule of hydrogen to cap the cluster as a bridging phophinidene, $(\mu_3\text{-}PPh)$. There are no complexes containing the $Pt_3(\mu_3\text{-}PPh)$ fragment that have been reported in the literature. Dr. M.C. Jennings of this laboratory has recently synthesized and characterized a few complexes containing this unit[16]. Reaction of complex 2 with $PPhH_2$ resulted in a product containing a $[Pt_3(\mu_3\text{-}PPh)H]^+$ unit. The results of this study will also be discussed in this chapter.

6.2 EXPERIMENTAL

6.2.3 $[Pt_3(\mu_3\text{-}H)(\mu\text{-}dppm)_3(P(OMe)_3)](PF_6)\cdot\frac{1}{2}\ CH_2C\ell_2$, 3a.

The hydrido triplatinum complex, 2, was prepared as described in chapter 5. To a solution of complex 2 (40 mg, 0.0212 mmol) in $CH_2C\ell_2$ (10 mL) was added $P(OMe)_3$ (2.5 μL, 0.0211 mmol) by syringe. The contents were stirred under nitrogen for 20 minutes. The solvent was evaporated under vacuum to give the product 3a, which could be

recrystallized from $CH_2C\ell_2$/pentane as red crystals. The reaction was essentially quantitative as monitored by ^{31}P NMR spectroscopy and isolated yields were ~85%. Anal. calcd. for $C_{79}H_{78}C\ell F_6O_3P_8Pt_3$: C, 46.1; H, 3.8%. Found: C, 46.0; H, 3.8%.

Similarly were prepared,

6.2.2 $[Pt_3(\mu_3\text{-}H)(\mu\text{-}dppm)_3(P(OEt)_3)](PF_6)$, 3b.

Anal.calcd. for $C_{81}H_{82}F_6O_3P_8Pt_3$: C, 47.5; H, 4.0%. Found: C, 47.3; H, 4.1%.

6.2.3 $[Pt_3(\mu_3\text{-}H)(\mu\text{-}dppm)_3(P(OPh)_3)](PF_6)$, 3c.

Anal.calcd. for $C_{93}H_{82}F_6O_3P_8Pt_3$: C, 50.9; H, 3.8%. Found: C, 50.6; H, 4.0%.

6.2.4 $[Pt_3(\mu_3\text{-}H)(\mu\text{-}dppm)_3(PPh_2Me)](PF_6)$, 3d.

Anal. calcd. for $C_{88}H_{80}F_6O_3P_8Pt_3$: C, 50.7; H,3.9%. Found: C, 50.2; H, 3.7%.

6.2.5 $[Pt_3(\mu_3\text{-}PPh)(\mu\text{-}dppm)_3H](PF_6)$, 6.

To a solution of complex 2 (40 mg, 0.0212 mmol) in $CH_2C\ell_2$ (10 mL) was added $PPhH_2$ (2.2 μL, 0.0200 mmol) by syringe. The contents were stirred under nitrogen for thirty minutes. Solvent was removed under vacuum and the resulting solid was washed with diethyl ether (15 mL) followed by pentane (10 mL). The mustard coloured powder was then dried under vacuum. Yield: 65%. The Solid

complex was thermally unstable and hence satisfactory analytical data could not be obtained. Anal. calcd. for $C_{81}H_{72}F_6P_8Pt_3$: C, 48.4; H, 3.6%. Found: C, 47.2; H, 3.4%. IR: ν(PtH) 1962 cm^{-1}.

6.2.6 X-ray crystal structure analysis of $[Pt_3(\mu_3\text{-}H)(\mu\text{-}dppm)_3\{P(OMe)_3\}](PF_6)\cdot\frac{1}{2}\,CH_2Cl_2$, 3a.

6.2.6.1 Data collection and reduction:

Small, bladed, red crystals of complex 3a were grown from CH_2Cl_2/hexane mixtures at room temperature, filtered and dried. A photographic examination showed triclinic symmetry, space group P1, No. 2.[17] The crystal density was determined by neutral buoyancy in mixtures of $CHBr_3$ and hexanes, and preliminary cell constants were obtained.

The cell constants and orientation matrix were refined on an Enraf-Nonius CAD4F diffractometer[23] using the angular settings for 20 high angle reflections. ω-scans of intense, low-angle reflections were recorded. Intensity data were measured with variable scan speeds within a maximum time per datum of 60s. Background estimates were made by extending the scan by 25% on each side. Standard reflections were monitored regularly, and showed decay averaging 3.4%. In all, 11198 data were recorded, of which 448 were standards. The data were processed using Enraf-Nonius Structure Determination Package[24], version 3.0, running on a PDP 11/23+ computer. Standard deviations

Table 6.1. Summary of X-ray Structure Determination of complex 3a

Crystal Data	
compound, formula weight	$C_{79}H_{78}Cl_1F_6O_3P_8Pt_3$ 2058.01
crystal system, space group	triclinic, $P\bar{1}$ (no. 2)
cell dimens (Å, deg.)	a = 14.083(3) α = 91.19(1)
	b = 25.755(3) β = 112.39(2)
	c = 11.609(2) γ = 90.36(1)
cell volume (Å^3), Z	3892(2), 2
temperature, °C	23
density, g cm^{-3}, obsd; calc	1.791(2), 1.756
Experimental Details	
diffractometer, monochromator	Enraf-Nonius CAD4F, graphite
radiation, wavelength (Å)	Mo, λ(Kα mean) 0.71073
cryst-detec (mm), t.o.a. (°)	205, 2.5
aperture (mm), vert; horiz	4.0; 6.0 + 0.35tanθ
centering reflec; θ range	20; 30 < 2θ < 36
Data Collection	
approx. crystal dimens (mm)	0.28 × 0.20 × 0.59
cryst vol (mm^3); no of faces	21.3 × 10^{-3}; 7
face indices	{100}, {11$\bar{1}$}, {010} and 001
scan mode, width (°)	ω-2θ, 0.80 + 0.35tanθ
index, θ ranges	-15 ≤ h ≤ 15, -27 ≤ k ≤ 27,
	-12 ≤ l ≤ 0; 0 ≤ θ ≤ 22.5°
scan speed (deg min^{-1})	1.0 to 2.5
max time per datum, total time	60s, 210h
standard reflections	400, 020, 001 and 2$\bar{1}\bar{2}$
monitor frequency, % var	120m, 3.4
no of data, standards collected	11198, 448

Table 6.1, continued.

Data Processing	
corrections	Lorentz, polarization and monochromator polarization
decay, absorption corrections	Isotropic; Gaussian
abs coeff (cm^{-1})	53.97
absorption, max., min.	0.388, 0.252
no of unique data, signif.	9529, $I > 0$
Structure Refinement	
no. of observ., variables	7581, 326
final model; R_1 and R_2	0.0449, 0.0471
top resid., (e $Å^{-3}$ coord.)	1.28 (0.338 0.500 0.591)
largest shift, parameter	8.1, Z-coordinate of C(6)B
Computer software	SHELX-76

were assigned based on counting statistics[24], and decay and absorption corrections (program AGNOST[18]) applied. 9529 unique data with I > 0 were available for the analysis. Crystal data and experimental conditions are presented in Table 6.1.

6.2.6.2 Solution and refinement of the structure

The structure was solved by Patterson and Fourier techniques, and refined by full matrix least-squares techniques on F, minimizing the functions $\Sigma w(||F_o|-|F_c||)^2$, where the weight 'w' is given by $2.8295/[(\sigma(F))^2 + 0.000281F^2]$. Scattering factors for neutral, non-hydrogen atoms and the real parts of the anamolous dispersion correction were taken from ref 17, while H atom scattering factors were taken from Stewart *et al*[19]. Once all the non-hydrogen atoms were located, the structure was transferred to SHELX-76 program[20] to complete the refinement. The 12 phenyl rings were constrained[25] to D_{6h} symmetry (C-C = 1.392 Å) and refined with individual thermal parameters for the ring carbon atoms. At a later stage of refinement, a difference Fourier map showed disorder in the $P(OMe)_3$ ligand. The disorder observed in the $P(OMe)_3$ group is shown in scheme 6.1. The ratio of site occupancy factor for $P(O^aMe)_3$ to $P(O^bMe)_3$ is 75 : 25. The geometry of the disordered $P(OMe)_3$ units were constrained at P-O = 1.60 Å, O-C = 1.43 Å and P...C = 2.625 Å. Refinement continued with a single overall temperature

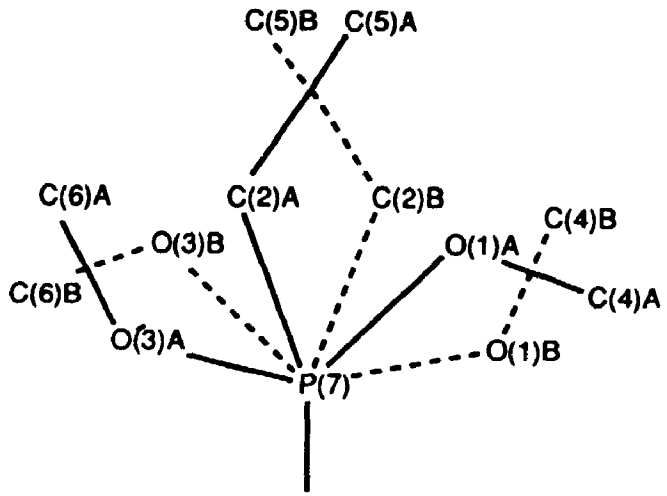

Scheme 6.1: The disorder model for the $P(OMe)_3$ group

factor for the oxygen and carbon atoms of the $P(OMe)_3$ group. A difference Fourier syntheses run at this stage showed the presence of ½ $CH_2C\ell_2$ in the asymmetric unit of the cell, i.e, $1CH_2C\ell_2$ molecule per unit cell. The presence of the solvent molecule was also supported by the ^1H NMR spectrum of 3a which showed signal due to $C\underline{H}_2C\ell_2$ at δ 5.28, integrating to one proton.

Since the unit cell contains 2 molecules of complex 3a, it contains two PF_6^- anions to maintain the electrical neutrality. One of these PF_6^- anions is present at a special position[17]; at coordinates (0.5, 0.5, 0.5), Wyckoff 'f', site symmetry *i*. The second PF_6^- anion was present in the asymmetric unit of the cell and at the same site where the solvent was occupied. Hence the fluorine atoms associated with this anion were poorly defined in the difference Fourier map. The PF_6^- anions were refined as

regular octahedrons with P-F = 1.58 Å. Only the Pt, P and F atoms were assigned anisotropic thermal parameters. The non-hydrogen atoms of the $P(9)F_6$ anion and $CH_2C\ell_2$ molecule were refined with a single overall temperature factor.

All the hydrogen atoms, except those belonging to $P(OMe)_3$ ligand, solvent and the hydride , were in the structural model in calculated positions (sp^2, C-H = 0.90 Å; sp^3, C-H = 0.95 Å) with thermal parameters set at 110% of that of the atom to which they are bonded. The positions were updated as the refinement progressed, but not refined. The hydrogen atom of the hydride ligand could not be located in the difference Fourier map.

The final cycles of refinement included 326 variables, 7581 unique reflections, and converged at agreement factors of $R_1 = 0.0449$ and $R_2 = 0.0471$. The highest residual electron density was 1.28 $eÅ^{-3}$ situated 0.62Å from C(9) and was of no chemical significance. A statistical analysis on $|F_o|$, $\lambda^{-1}\sin\theta$, and various combinations of Miller indices showed no unusual trends and indicated a satisfactory weighting scheme.

Final positional and thermal parameters for the non-hydrogen atoms are given in Table 6.2. Hydrogen atom parameters, anisotropic thermal parameters, selected torsional angles and weighted least-squares planes are given in Tables 6.3, 6.4, 6.5 and 6.6 respectively.

6.3 RESULTS AND DISCUSSION

6.3.1 Formation of the complexes $[Pt_3(\mu_3\text{-}H)(\mu\text{-}dppm)_3L](PF_6)$, 3

The reaction of $[Pt_3(\mu_3\text{-}H)(\mu\text{-}dppm)_3](PF_6)$, 2, with the phosphite ligands $P(OMe)_3$, $P(OEt)_3$, $P(OPh)_3$ and the phosphine ligand PPh_2Me gave the corresponding

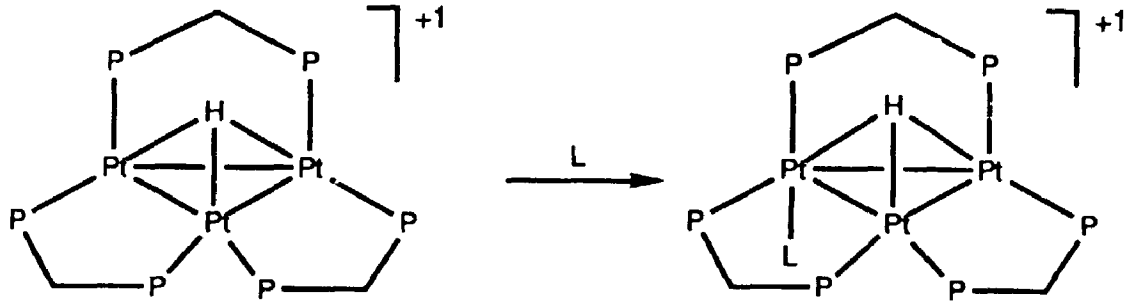

L = $P(OMe)_3$, **3a**
$P(OEt)_3$, **3b**
$P(OPh)_3$, **3c**
PPh_2Me, **3d**
$PPhH_2$, **3e**

Scheme 6.2

complexes 3a-3d respectively in essentially quantitative yield, scheme 6.2. These complexes were thermally stable and could be isolated in analytically pure form as the hexafluorophosphate salts which were red solids. Complex 3a was structurally characterized by a single crystal X-ray diffraction study.

However, reaction of 2 with phenyl phosphine, $PPhH_2$, at -80°C resulted in the formation of a phosphinidene complex, $[Pt_3(\mu_3\text{-}PPh)(\mu\text{-}dppm)_3H](PF_6)$, 6, scheme 6.3. It is possible that the initially formed complex was the adduct 3e, which then reductively

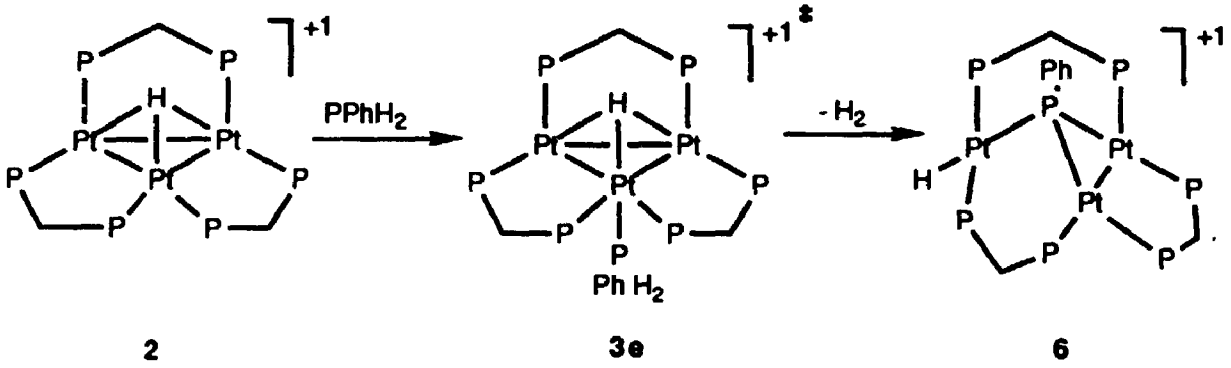

2 3e 6

Scheme 6.3

eliminates a molecule of H_2 to yield complex 6.

6.3.2 Description of crystal and molecular structure of $[Pt_3(\mu_3\text{-}H)(\mu\text{-dppm})_3\{P(OMe)_3\}](PF_6).\frac{1}{2}\ CH_2C\ell_2$, 3a

The structure of 3a deduced spectroscopically (section 6.3.3) was verified by X-ray crystallographic methods. The crystals are built up from discrete cations, anions and loosely entrapped methylene chloride as solvent of crystallization. The shortest non-bonded interactions between the cation and the anion are 2.39(1) Å between HC(76) and F(1), 2.49(1) Å between HC(123) and F(8), 2.43(1) Å between HC(84) and F(1) at (X, Y, Z-1), and 2.23(2) Å between HC(102) and F(6) at (1-X, 1-Y, 1-Z), all less than the sum of Van der Waals radii, 2.8 Å.[27] The structure of the cation is characterized by bond lengths and bond angles shown in Table 6.7. Figures 6.1(a) and 6.1(b) show the structure of the cation with two different orientations of the disordered $P(OMe)_3$ ligand. Figure 6.2

illustrates a stereo view of the cation of the complex 3a.

In the cation the platinum atoms form a triangle with Pt-Pt distances 2.592(1), 2.635(1) and 2.705(1)Å and Pt-Pt-Pt angles 58.06(2), 59.61(2) and 62.33(2)°. The shortest of the three Pt-Pt bonds, 2.592 (1)Å, is associated with Pt(1) and Pt(3) atoms which lack the terminal phosphite ligand. Thus we see that there is a slight increase in the M-M bond overlap between Pt(1) and Pt(3) in order to compensate for the increase in electron density at Pt(2) [due to the presence of a terminal $P(OMe)_3$ ligand bonded to Pt(2) centre]. Hence, the addition of the phosphite ligand to complex 2 increases the electron count from 42e to 44e, with the result that the two Pt-Pt bonds associated with the unique Pt atom, Pt(2), are significantly longer [Pt(2)-Pt(3) = 2.705(1), Pt(2)-Pt(1) = 2.635(1)Å] than the third Pt-Pt bond [Pt(1)-Pt(3)=2.592(1)Å].

The triangle of Pt atoms is held together by three dppm ligands, each of which bridges a Pt-Pt edge. Thus we have three Pt_2P_2C dimetallacycle units fused together to form a $Pt_3(\mu\text{-dppm})_3$ unit. The rotational orientation of the dppm ligands about the Pt-Pt bonds and conformations of the Pt_2P_2C rings are such as to afford a Pt_3P_6 skeleton substantially distorted from an ideal latitudinal M_3L_6 geometry. The distortion is severe at the Pt(2) centre whose coordination number is highest of the three platinum centres [coordination number at Pt(2) is four; Pt(2) is

Table 6.2. Atomic positional ($\times 10^4$) and Thermal ($\times 10^3$) parameters in 3a

Atom	x	y	z	U or U_{eq} ($Å^2$)
Pt(1)	2449.7(3)	3054.7(2)	575.5(4)	39.8(2)
Pt(2)	2020.7(3)	2064.3(2)	690.8(4)	40.1(2)
Pt(3)	3969.6(3)	2416.5(2)	1298.9(4)	43.1(2)
P(1)	842(2)	3379(1)	-117(3)	43(1)
P(2)	438(2)	2242(1)	-802(3)	45(1)
P(3)	2429(2)	1183(1)	825(3)	47(1)
P(4)	4628(2)	1597(1)	1409(3)	48(1)
P(5)	5181(2)	3017(1)	2314(3)	48(1)
P(6)	3526(2)	3701(1)	665(3)	55(1)
P(7)	2168(3)	2169(2)	2697(3)	70(2)
C(1)	-73(8)	2838(4)	-340(10)	45(3)
C(2)	3811(8)	1121(5)	1760(11)	55(3)
C(12)	993(5)	3825(3)	-2203(8)	67(4)
C(13)	618(5)	4059(3)	-3358(8)	81(4)
C(14)	-418(5)	4179(3)	-3914(8)	82(4)
C(15)	-1079(5)	4066(3)	-3314(8)	71(4)
C(16)	-705(5)	3832(3)	-2158(8)	61(4)
C(11)	331(5)	3712(3)	-1603(8)	51(3)
C(22)	741(6)	3592(3)	2165(7)	61(4)
C(23)	623(6)	3900(3)	3100(7)	75(4)
C(24)	329(6)	4415(3)	2875(7)	76(4)
C(25)	153(6)	4622(3)	1715(7)	82(4)
C(26)	271(6)	4314(3)	779(7)	65(4)
C(21)	565(6)	3799(3)	1004(7)	44(3)
C(32)	1177(5)	2409(3)	-2698(7)	54(3)
C(33)	1083(5)	2541(3)	-3893(7)	82(4)
C(34)	123(5)	2653(3)	-4787(7)	90(5)
C(35)	-743(5)	2633(3)	-4486(7)	86(5)
C(36)	-649(5)	2501(3)	-3291(7)	77(4)
C(31)	311(5)	2389(3)	-2397(7)	47(3)
C(42)	-725(6)	1359(3)	-1930(7)	72(4)
C(43)	-1524(6)	999(3)	-2187(7)	93(5)
C(44)	-2254(6)	1066(3)	-1661(7)	100(5)
C(45)	-2186(6)	1494(3)	-878(7)	102(5)
C(46)	-1386(6)	1854(3)	-622(7)	76(4)
C(41)	-656(6)	1787(3)	-1148(7)	46(3)
C(52)	2516(6)	260(3)	-469(7)	71(4)
C(53)	2469(6)	-27(3)	-1519(7)	87(5)
C(54)	2204(6)	214(3)	-2660(7)	104(6)
C(55)	1987(6)	742(3)	-2750(7)	91(5)
C(56)	2034(6)	1029(3)	-1700(7)	68(4)
C(51)	2298(6)	788(3)	-559(7)	55(3)
C(62)	732(7)	676(4)	879(7)	81(4)
C(63)	134(7)	427(4)	1424(7)	106(6)
C(64)	581(7)	261(4)	2646(7)	110(6)
C(65)	1626(7)	345(4)	3322(7)	99(5)
C(66)	2224(7)	594(4)	2778(7)	68(4)
C(61)	1777(7)	760(4)	1556(7)	55(3)
C(72)	6734(7)	1650(4)	2187(8)	83(4)

Table 6.2, continued.

Atom	x	y	z	U or U_{eq}(Å^2)
C(73)	7749(7)	1583(4)	2992(8)	109(6)
C(74)	7967(7)	1296(4)	4063(8)	105(6)
C(75)	7171(7)	1076(4)	4329(8)	115(6)
C(76)	6156(7)	1143(4)	3524(8)	89(5)
C(71)	5938(7)	1430(4)	2453(8)	57(3)
C(82)	4558(6)	1746(3)	-982(8)	70(4)
C(83)	4663(6)	1598(3)	-2087(8)	86(5)
C(84)	4892(6)	1086(3)	-2276(8)	87(5)
C(85)	5017(6)	723(3)	-1360(8)	87(5)
C(86)	4912(6)	871(3)	-255(8)	68(4)
C(81)	4683(6)	1383(3)	-66(8)	48(3)
C(92)	6233(6)	2901(3)	730(7)	71(4)
C(93)	7049(6)	2978(3)	351(7)	94(5)
C(94)	7926(6)	3248(3)	1127(7)	96(5)
C(95)	7988(6)	3441(3)	2283(7)	99(5)
C(96)	7173(6)	3365(3)	2662(7)	74(4)
C(91)	6295(6)	3095(3)	1886(7)	51(3)
C(102)	6070(7)	3395(3)	4816(9)	78(4)
C(103)	6531(7)	3329(3)	6096(9)	96(5)
C(104)	6694(7)	2831(3)	6571(9)	93(5)
C(105)	6396(7)	2399(3)	5765(9)	103(5)
C(106)	5935(7)	2466(3)	4485(9)	86(5)
C(101)	5772(7)	2964(3)	4010(9)	55(3)
C(112)	3605(7)	3279(4)	-1484(9)	76(4)
C(113)	3948(7)	3235(4)	-2458(9)	130(7)
C(114)	4712(7)	3570(4)	-2502(9)	132(7)
C(115)	5133(7)	3950(4)	-1571(9)	117(6)
C(116)	4790(7)	3995(4)	-597(9)	114(6)
C(111)	4026(7)	3659(4)	-553(9)	65(4)
C(122)	2934(7)	4570(4)	1664(8)	95(5)
C(123)	2590(7)	5075(4)	1670(8)	114(6)
C(124)	2413(7)	5385(4)	643(8)	122(6)
C(125)	2580(7)	5190(4)	-390(8)	139(8)
C(126)	2925(7)	4685(4)	-396(8)	114(6)
C(121)	3102(7)	4375(4)	631(8)	68(4)
C(3)	4647(9)	3684(5)	2120(11)	55(3)
O(1)A	2326(9)	2677(4)	3571(11)	108(2)
O(2)A	2995(8)	1776(5)	3563(11)	108(2)
O(3)A	1198(7)	2065(5)	3064(11)	108(2)
C(4)A	3239(13)	2988(6)	3888(23)	108(2)
C(5)A	3030(15)	1672(9)	4784(12)	108(2)
C(6)A	402(9)	1710(8)	2331(19)	108(2)
O(1)B	3099(17)	2533(11)	3572(34)	108(2)
O(2)B	2658(29)	1680(10)	3535(34)	108(2)
O(3)B	1121(18)	2298(12)	2894(42)	108(2)
C(4)B	2937(38)	3072(12)	3734(70)	108(2)
C(5)B	3449(40)	1759(22)	4748(38)	108(2)
C(6)B	270(27)	1869(21)	2462(63)	108(2)
P(8)	5000	0000	5000	99(3)
F(1)	4815	605	4973	127(5)

Table 6.2, continued.

Atom	x	y	z	U or U_{eq}(Å^2)
F(2)	4548	-25	3527	180(7)
F(3)	3888	-100	4990	210(10)
C(9)	3775(47)	4883(22)	6236(90)	350
Cl(1)	3133(47)	4373(22)	5183(90)	350
Cl(2)	2910(47)	5307(22)	6530(90)	350
P(9)	3885(14)	4989(7)	5493(20)	350
F(4)	4262(14)	4473(7)	5050(20)	350
F(5)	4168(14)	5305(7)	4515(20)	350
F(6)	3508(14)	5504(7)	5936(20)	350
F(7)	5003(14)	5093(7)	6500(20)	350
F(8)	2767(14)	4885(7)	4407(20)	350
F(9)	3602(14)	4672(7)	6472(20)	350

$$U_{eq}^{*} = \frac{1}{3} \sum_i \sum_j U_{ij} a_i^{*} a_j^{*} a_i . a_j$$

Table 6.3. Hydrogen atom Positional (×10^3) and Thermal (×10^3) Parameters in 3a

Atom	x	y	z	U(Å^2)
H1C(1)	-17	278	41	34
H2C(1)	-71	292	-98	34
H1C(2)	402	78	162	44
H2C(2)	391	116	262	44
H1C(3)	515	393	210	55
H2C(3)	445	377	280	55
HC(12)	170	374	-182	70
HC(13)	107	414	-377	70
HC(14)	-67	434	-470	70
HC(15)	-179	415	-369	70
HC(16)	-116	375	-175	70
HC(22)	94	324	232	70
HC(23)	74	376	389	70
HC(24)	25	462	351	70
HC(25)	-5	497	156	70
HC(26)	15	446	-1	70
HC(32)	183	233	-209	70
HC(33)	167	255	-410	70
HC(34)	6	274	-560	70
HC(35)	-140	271	-510	70
HC(36)	-124	249	-308	70
HC(42)	-23	131	-229	70
HC(43)	-157	71	-272	70
HC(44)	-280	82	-184	70
HC(45)	-268	154	-52	70
HC(46)	-134	215	-9	70

Table 6.3, continued.

Atom	x	y	z	U(Å²)
HC(52)	270	10	31	70
HC(53)	262	-39	-146	70
HC(54)	217	2	-338	70
HC(55)	181	91	-353	70
HC(56)	189	139	-176	70
HC(62)	43	79	5	70
HC(63)	-58	37	96	70
HC(64)	17	9	302	70
HC(65)	193	23	416	70
HC(66)	294	65	324	70
HC(72)	659	185	146	70
HC(73)	829	173	281	70
HC(74)	866	125	461	70
HC(75)	732	88	506	70
HC(76)	561	99	371	70
HC(82)	440	210	-85	70
HC(83)	458	185	-271	70
HC(84)	496	98	-303	70
HC(85)	517	37	-149	70
HC(86)	500	62	37	70
HC(92)	563	272	20	70
HC(93)	701	285	-44	70
HC(94)	848	330	87	70
HC(95)	859	363	281	70
HC(96)	722	350	345	70
HC(102)	596	374	449	70
HC(103)	673	362	665	70
HC(104)	701	279	745	70
HC(105)	651	206	609	70
HC(106)	573	217	393	70
HC(112)	308	305	-145	70
HC(113)	366	298	-309	70
HC(114)	495	354	-317	70
HC(115)	565	418	-160	70
HC(116)	508	425	4	70
HC(122)	305	436	236	70
HC(123)	248	521	237	70
HC(124)	218	573	65	70
HC(125)	246	540	-109	70
HC(126)	304	455	-110	70

Atom H1C(1) and H2C(1) are bonded to C(1), and so on.

Table 6.4. Anisotropic Thermal Parameters ($\times 10^3$)

Atom	U_{11}	U_{22}	U_{33}	U_{12}	U_{13}	U_{23}
Pt(1)	31.8(3)	40.9(3)	47.6(3)	2.8(2)	16.0(2)	-1.9(2)
Pt(2)	32.8(3)	41.8(3)	42.6(3)	1.8(2)	11.0(2)	-1.5(2)
Pt(3)	30.9(3)	45.3(3)	50.0(3)	4.2(2)	12.2(2)	-3.7(2)
P(1)	35(2)	44(2)	48(2)	4(1)	15(1)	-0(2)
P(2)	37(2)	50(2)	44(2)	5(1)	11(1)	-5(2)
P(3)	44(2)	45(2)	49(2)	2(1)	15(2)	-0(2)
P(4)	37(2)	52(2)	51(2)	10(2)	13(1)	-2(2)
P(5)	33(2)	57(2)	53(2)	-1(1)	15(1)	-8(2)
P(6)	39(2)	51(2)	77(2)	2(2)	25(2)	2(2)
P(7)	89(3)	69(3)	47(2)	19(2)	21(2)	-1(2)
P(8)	166(7)	83(5)	57(4)	64(5)	49(4)	21(3)
F(1)	229(12)	73(7)	88(7)	53(7)	69(7)	7(5)
F(2)	307(17)	145(11)	80(7)	118(11)	62(9)	28(7)
F(3)	186(14)	196(16)	309(20)	85(12)	140(14)	141(14)

The general temperature factor expression is

$$U_{ij} = \left[-2\pi^2\left[U_{11}h^2a^{*2} + U_{22}k^2b^{*2} + U_{33}\ell^2c^{*2} + 2U_{12}hka^*b^* + 2U_{13}h\ell a^*c^* + 2U_{23}k\ell b^*c^* \right]\right]$$

Table 6.5. Selected Torsion Angles (°)

Atom 1	Atom 2	Atom 3	Atom 4	Angle
P(7)	Pt(2)	Pt(3)	Pt(1)	-91.3(1)
Pt(1)	P(1)	C(1)	P(2)	-31.4(6)
Pt(2)	P(2)	C(1)	P(1)	57.3(6)
Pt(2)	P(3)	C(2)	P(4)	-42.5(7)
Pt(3)	P(4)	C(2)	P(3)	46.5(7)
Pt(3)	P(5)	C(3)	P(6)	-26.1(7)
Pt(1)	P(6)	C(3)	P(5)	51.0(7)

Table 6.6. Weighted Least-Squares Plane

Crystallographic Equation of Plane

$$4.1366\,X - 3.1241\,Y - 11.4464\,Z + 0.5997 = 0$$

Atom	X	Y	Z	Distance
Pt(1)	3.1429	7.8505	0.6177	0.000
Pt(2)	2.5041	5.2971	0.7414	0.000
Pt(3)	4.9707	6.1872	1.3942	0.000
		Other Atoms		
P(1)	1.1834	8.7049	-0.1254	0.026(3)
P(2)	0.9358	5.7954	-0.8603	0.998(3)
P(3)	3.0325	3.0230	0.8853	0.291(3)
P(4)	5.8615	4.0744	1.5120	0.403(3)
P(5)	6.2164	7.7058	2.4838	-0.848(3)
P(6)	4.6070	9.5113	0.7140	0.141(4)
P(7)	1.8219	5.5114	2.8944	-2.268(4)
C(1)	0.0050	7.3185	-0.3696	0.077(11)
C(2)	4.5630	2.8389	1.8933	-0.193(12)
C(3)	5.5408	9.4287	2.2760	-1.056(12)

Table 6.7. Selected Bond distances (Å) and angles (°) in 3a

Atom 1	Atom 2	Distance	Atom 1	Atom 2	Distance
Pt(3)	Pt(1)	2.592(1)	Pt(1)	Pt(2)	2.635(1)
Pt(3)	Pt(2)	2.705(1)	Pt(1)	P(1)	2.266(3)
Pt(2)	P(2)	2.298(3)	Pt(2)	P(3)	2.339(3)
Pt(3)	P(4)	2.297(3)	Pt(3)	P(5)	2.248(3)
Pt(1)	P(6)	2.217(3)	Pt(2)	P(7)	2.268(4)
P(1)	C(1)	1.837(11)	P(2)	C(1)	1.852(11)
P(3)	C(2)	1.844(11)	P(4)	C(2)	1.833(12)
P(5)	C(3)	1.863(12)	P(6)	C(3)	1.822(11)
P(1)	C(11)	1.831(9)	P(1)	C(21)	1.832(8)
P(2)	C(31)	1.839(8)	P(2)	C(41)	1.842(9)
P(3)	C(61)	1.835(10)	P(3)	C(51)	1.832(9)
P(4)	C(71)	1.840(10)	P(4)	C(81)	1.818(9)
P(5)	C(91)	1.828(9)	P(5)	C(101)	1.831(10)
P(6)	C(111)	1.805(11)	P(6)	C(121)	1.836(11)

	Angles		Degrees		Angles		Degrees
Pt(3)	Pt(1)	Pt(2)	62.33(2)	P(1)	Pt(1)	Pt(2)	99.82(8)
P(1)	Pt(1)	Pt(3)	162.14(8)	P(6)	Pt(1)	Pt(2)	152.15(9)
P(6)	Pt(1)	Pt(3)	90.04(9)	P(6)	Pt(1)	P(1)	107.73(12)
Pt(3)	Pt(2)	Pt(1)	58.06(2)	P(2)	Pt(2)	Pt(1)	85.60(9)
P(2)	Pt(2)	Pt(3)	136.15(9)	P(3)	Pt(2)	Pt(1)	152.87(8)
P(3)	Pt(2)	Pt(3)	95.65(8)	P(3)	Pt(2)	P(2)	114.08(11)
P(7)	Pt(2)	Pt(1)	91.45(11)	P(7)	Pt(2)	Pt(3)	90.82(11)
P(7)	Pt(2)	P(2)	115.79(13)	P(7)	Pt(2)	P(3)	95.87(13)
Pt(2)	Pt(3)	Pt(1)	59.61(2)	P(4)	Pt(3)	Pt(1)	151.64(8)
P(4)	Pt(3)	Pt(2)	93.68(8)	P(5)	Pt(3)	Pt(1)	95.94(8)
P(5)	Pt(3)	Pt(2)	147.80(8)	P(5)	Pt(3)	P(4)	112.42(11)
C(1)	P(1)	Pt(1)	108.4(4)	C(11)	P(1)	Pt(1)	120.2(3)
C(11)	P(1)	C(1)	103.3(5)	C(21)	P(1)	Pt(1)	115.1(3)
C(21)	P(1)	C(1)	102.0(4)	C(21)	P(1)	C(11)	105.8(4)
C(1)	P(2)	Pt(2)	109.7(4)	C(31)	P(2)	Pt(2)	120.2(2)
C(31)	P(2)	C(1)	101.6(5)	C(41)	P(2)	Pt(2)	121.1(3)
C(41)	P(2)	C(1)	101.3(4)	C(41)	P(2)	C(31)	99.8(4)

Table 6.7, continued.

Angles			Degrees	Angles			Degrees
C(2)	P(3)	Pt(2)	108.6(4)	C(51)	P(3)	Pt(2)	121.6(3)
C(51)	P(3)	C(2)	101.1(5)	C(61)	P(3)	Pt(2)	117.5(3)
C(61)	P(3)	C(2)	105.4(5)	C(61)	P(3)	C(51)	100.6(4)
C(2)	P(4)	Pt(3)	110.8(4)	C(71)	P(4)	Pt(3)	123.6(3)
C(71)	P(4)	C(2)	103.9(5)	C(81)	P(4)	Pt(3)	111.8(3)
C(81)	P(4)	C(2)	106.1(5)	C(81)	P(4)	C(71)	99.0(4)
C(91)	P(5)	Pt(3)	119.3(3)	C(101)	P(5)	Pt(3)	116.1(3)
C(101)	P(5)	C(91)	102.6(4)	C(3)	P(5)	Pt(3)	111.7(4)
C(3)	P(5)	C(91)	102.4(5)	C(3)	P(5)	C(101)	102.7(5)
C(111)	P(6)	Pt(1)	113.2(3)	C(121)	P(6)	Pt(1)	119.6(3)
C(121)	P(6)	C(111)	104.3(4)	C(3)	P(6)	Pt(1)	110.1(4)
C(3)	P(6)	C(111)	105.4(5)	C(3)	P(6)	C(121)	103.0(5)
O(1)A	P(7)	Pt(2)	131.7(6)	O(2)A	P(7)	Pt(2)	110.0(5)
O(2)A	P(7)	O(1)A	103.4(8)	O(3)A	P(7)	Pt(2)	120.3(5)
O(3)A	P(7)	O(1)A	83.8(6)	O(3)A	P(7)	O(2)A	102.4(7)
O(1)B	P(7)	Pt(2)	116.0(16)	O(2)B	P(7)	Pt(2)	113.3(18)
O(2)B	P(7)	O(1)B	90.6(19)	O(3)B	P(7)	Pt(2)	115.8(16)
O(3)B	P(7)	O(1)B	111.4(20)	O(3)B	P(7)	O(2)B	106.8(22)
P(2)	C(1)	P(1)	109.5(6)	P(4)	C(2)	P(3)	114.1(6)
C(12)	C(11)	P(1)	118.6(2)	C(16)	C(11)	P(1)	121.3(2)
C(22)	C(21)	P(1)	116.5(2)	C(26)	C(21)	P(1)	123.3(2)
C(32)	C(31)	P(2)	120.2(2)	C(36)	C(31)	P(2)	119.8(2)
C(42)	C(41)	P(2)	118.3(2)	C(46)	C(41)	P(2)	121.7(2)
C(52)	C(51)	P(3)	120.9(2)	C(56)	C(51)	P(3)	119.0(2)
C(62)	C(61)	P(3)	11 .2)	C(66)	C(61)	P(3)	123.9(2)
C(72)	C(71)	P(4)	116.2(3)	C(76)	C(71)	P(4)	123.5(3)
C(82)	C(81)	P(4)	119.1(3)	C(86)	C(81)	P(4)	120.8(2)
C(92)	C(91)	P(5)	118.7(2)	C(96)	C(91)	P(5)	121.3(2)
C(102)	C(101)	P(5)	122.8(3)	C(106)	C(101)	P(5)	117.2(3)
C(112)	C(111)	P(6)	117.4(3)	C(116)	C(111)	P(6)	122.6(3)
C(122)	C(121)	P(6)	117.9(3)	C(126)	C(121)	P(6)	122.1(3)
P(6)	C(3)	P(5)	108.9(6)				

Numbers in parantheses are estimated standard deviations.

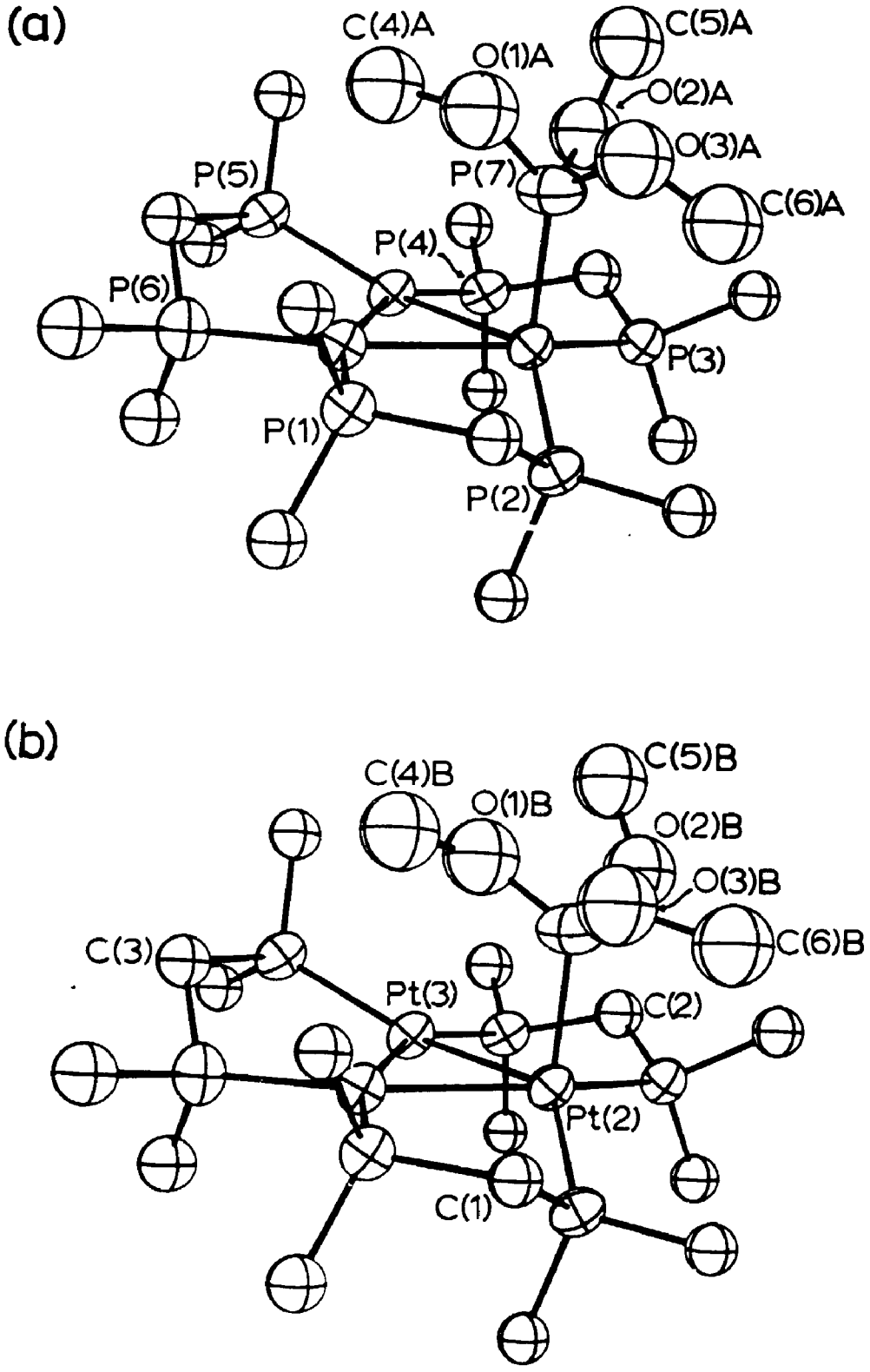

Figure 6.1: Perspective views of the cation 3a showing the disordered $P(OMe)_3$ ligand. Only the *ipso*-carbon atoms of the phenyl rings are shown.

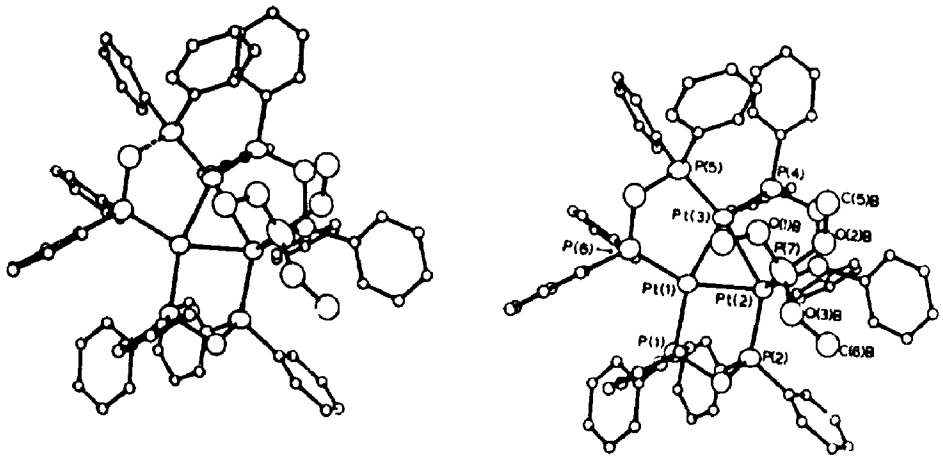

Figure 6.2: A stereo view of the cation in 3a

bonded to the dppm phosphorus atoms P(2), P(3), the phosphite ligand, P(7), and the hydride ligand (which was not located in the X-ray study, but unambiguously established by multinuclear NMR spectroscopy, see section 6.3.3). The coordination number at the other two platinum atoms, Pt(1) and Pt(3) are the same and is equal to three; Pt(1) is bonded to the two dppm phosphorus atoms, P(1), P(6), and the hydride ligand. Similarly, Pt(3) is bonded to P(4), P(6) and the hydride ligand]. Thus the phosphorus atoms P(2) and P(3) lie 0.998(3) and 0.291(3)Å away from the Pt_3 plane, on the side opposite to that of $P(OMe)_3$ ligand. The Pt-P (dppm) bond lengths involving Pt(2) atom [2.339(3)Å, 2.298(3)Å] are longer than those involving Pt(1) and Pt(3) [2.215(3) - 2.297(3)Å]. Such differences in the Pt-P (dppm) distances were also observed in the isoelectronic complex 4, and they were attributed to the rehybridization of Pt orbitals, higher coordination number at Pt(2) and possible steric congestion at Pt(2) centre[10]. The $P(OMe)_3$ ligand is bound terminally to Pt(2) atom and is perpendicular to the Pt_3 plane [P(7)-Pt(2)-Pt(1) = 91.45(11)°, P(7)-Pt(2)-Pt(3) = 90.82(11)°]. The Pt(2)-P(7) distance (2.268(4) Å) is within the range of Pt-P bond lengths in other phosphite complexes[21].

The Pt_2P_2C rings adopt envelope conformations with the methylene carbon at the flap; all of the methylene carbon atoms C(1), C(2) and C(3) are directed towards the $P(OMe)_3$ ligand, and are displaced from the Pt_3 plane by

0.077(11), 0.193(12) and 1.056(12)Å, respectively. In this conformation of the $Pt_3(\mu\text{-dppm})_3$ skeleton, the phenyl rings are directed away from the $P(OMe)_3$ ligand and the steric hindrance is thus minimized.

An analogous complex $[Pt_3(\mu_3\text{-}AuPPh_3)(\mu_2\text{-}CO)_3(PPh_3)_4]^+$, **8**, synthesized and structurally characterized by Bour *et al*[22] is an excellent precedent for the hydride complex **3a**. Complex **8** contains

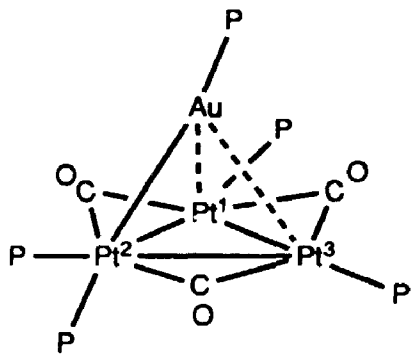

Structure of **8**

$Pt_3(\mu_2\text{-}CO)_3(PPh_3)_4$ unit which is isoelectronic with $[Pt_3(\mu\text{-dppm})_3\{P(OMe)_3\}]$ unit in **3a**. Then, the $AuPR_3^+$ unit which is isolobal to H^+, caps the $Pt_3(\mu\text{-}CO)_3(PPh_3)_4$ unit to yield complex **8**. In complex **3a**, H^+ ion caps the $[Pt_3(\mu\text{-dppm})_3\{P(OMe)_3\}]$ unit to form the cationic complex. In **8**, the $AuPR_3^+$ unit is strongly bound to the most nucleophilic Pt site, which evidently is Pt(2), in spite of the local steric crowding. The strong Au-Pt(2) overlap is reflected in the linearity of P-Au-Pt(2) angle (173.5(1)°), and the Au-Pt distances [Au-Pt(2) = 2.700(1)Å,

Table 6.8: A comparison of selected structural and spectroscopic data for some Pt_3 complexes

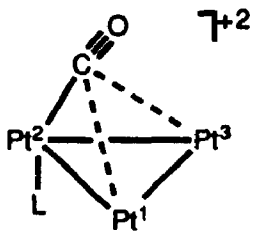

L = $P(OPh)_3$

4

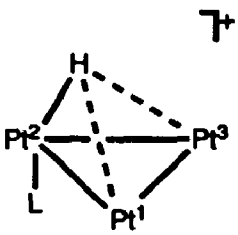

L = $P(OMe)_3$

3a

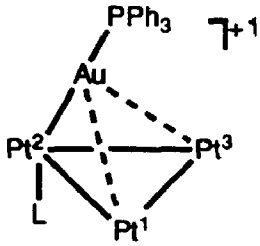

L = PPh_3

8

Complex	4		3a		8
Pt^1-Pt^2	2.656(2)		2.706(1)		2.702(1)
Pt^2-Pt^3	2.626(2)		2.635(1)		2.708(1)
Pt^1-Pt^3	2.636(2)		2.593(1)		2.666(1)
Pt^2-C	1.93(3)		–	Pt^2-Au	2.700(1)
Pt^1-C	2.16(3)		–	Pt^1-Au	2.902(1)
Pt^3-C	2.27((3)		–	Pt^3-Au	2.910(1)
Pt^2-C-O	154.6(21)		–	Pt^2-Au-P	173.5(1)
Pt^1-C-O	121.4(14)		–	Pt^1-Au-P	128.0(1)
Pt^3-C-O	119.0(20)		–	Pt^3-Au-P	127.6(1)
$^1J_{(Pt^2C)}$	960	$^1J_{(Pt^2H)}$	1200		–
$^1J_{(Pt^1C)}$	493	$^1J_{(Pt^1H)}$	268		–
$^1J_{(Pt^3C)}$	493	$^1J_{(Pt^3H)}$	268		–

Bond distances are in Å; bond angles in degrees; and coupling constants in Hz.

Au-Pt(1) = 2.902(1)Å and Au-Pt(3) = 2.910(1)Å].

It is interesting to compare the geometry of the $Pt_3(\mu_3\text{-}H)$ unit in 3a with the $Pt_3(\mu_3\text{-}CO)$ unit in 4 and $Pt_3(\mu_3\text{-}AuPPh_3)$ in 8. A brief summary is provided in table 6.8, where the dppm ligands in 3a and 4, and the ligands in the equatorial Pt_3 plane in 8, are omitted for clarity. The Pt-Pt distances are very similar for the 44e cluster 4, but varies slightly in the 44e cluster 3a and the analogous 56e cluster 8. However, the distortion of the triply bridging ligand (CO in 4, H in 3a and $AuPR_3$ in 8) from the symmetrical μ_3-bonding mode is significant in all these clusters. This distortion will be considered further in the following sections.

6.3.3 Spectroscopic characterization of complexes 3a-3d

The complexes 3a-3d were fluxional in solution at room temperature and hence NMR spectra were recorded at

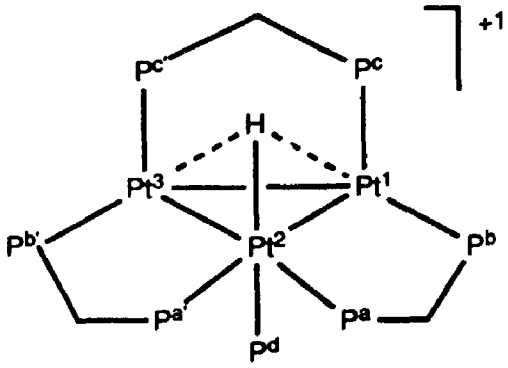

Scheme 6.4: NMR labelling scheme for 3a-3d

low temperature typically at -90°c in $CD_2C\ell_2$ solution. At this temperature the fluxionality in these complexes is

frozen and the static structure 3 is observed. The NMR labelling scheme is seen in scheme 6.4. The ^{31}P and ^{1}H NMR spectral data are given in Tables 6.9 and 6.10 respectively. The ^{195}Pt NMR data for complexes 3a and 3b are given in Table 6.11.

Both the ^{1}H and ^{31}P NMR spectra are characteristic of the static structure 3, which has an apparent plane of symmetry passing through the atoms Pt^{2}, P^{d}, H and bisecting the Pt^{1}-Pt^{3} vector. The ^{31}P NMR spectra are informative and the spectrum of 3a, figure 6.3, will be discussed as a typical example. The ^{31}P NMR spectrum of 3a contains four signals in a 2:2:2:1 intensity ratio. In these trinuclear complexes, the largest J(PP) couplings are the <u>trans</u>-like couplings through the Pt-Pt bonds[10-13], which in 3 are $^{3}J(P^{a}P^{c})$ and $^{3}J(P^{b}P^{b'})$. The spectrum contains two doublet resonances and a singlet resonance in the high-field region. These are due to the phosphorus atoms of the bridging dppm ligands. The singlet at δ-12.3 ($^{1}J(PtP)$ = 2540 Hz) is then readily assigned to P^{b}. The magnitude of $^{3}J(P^{b}P^{b'})$ = 230 Hz, is obtained from the ^{195}Pt satellite spectra. The resonance due to P^{a} (δ -35.5, $^{3}J(P^{a}P^{c})$ = 190 Hz, $^{1}J(PtP)$ = 2280 Hz) and P^{c} (δ -20.6, $^{1}J(PtP)$ = 3720 Hz) are assigned by correlation of $^{1}J(PtP)$ values with the Pt-P bond lengths (PtP^{a} longer than PtP^{c}, Table 6.7) and from a general trend that the ^{31}P chemical shifts move to high-field region when bound to platinum atoms with higher coordination number.

Table 6.9: $^{31}P\{^{1}H\}$ NMR data for complexes **3a-3d** in CD_2Cl_2§

(a) At room temperature

Complex	3a	3b	3c	3d
δP^{a-c}	-21.6	-21.4	-20.1‡	-19.1
$^{1}J(PtP)$	2980	2970	3140	–
δP^{d}	123.6	117.3	95.1	-7.2
$^{1}J(PtP^{d})$	1733	1650	2125	1200¶
$^{2}J(PtP^{d})$	13	13.5	42	21

(b) At low temperature (-90 °C)

Complex	3a	3b	3c	3d
δP^{a}	-35.5	-35.1	-20.0	-25.4
$^{1}J(PtP^{a})$	2280	2240	2400	–
$^{2}J(PtP^{a})$	470	500	–	–
δP^{b}	-12.3	-13.7	-6.9	-16.2
$^{1}J(PtP^{b})$	2540	2540	2700	–
$^{2}J(PtP^{b})$	250	260	–	–
$^{3}J(P^{b}P^{b})$	230	240	–	–
δP^{c}	-20.6	-20.8	-11.0	-7.9
$^{1}J(PtP^{c})$	3720	3640	3700	3520
$^{2}J(PtP^{c})$	169	180	–	–
$^{3}J(P^{a}P^{c})$	190	200	–	150
δP^{d}	125.0	118.2	99.5	-4.0
$^{1}J(PtP^{d})$	4990	4960	6230	3800
$^{2}J(P^{a}P^{d})$	27	–	135	–

‡ The signal was sharp and well resolved. $^{2}J(PtP)$ = 200 Hz, $^{3}J(PtPa)$ = 18 Hz

¶ The error in measurement is ± 100 Hz, as the satellites were broad

§ The data indicated by the symbol " - " in the above table show that the resonances were too broad to measure the coupling constants

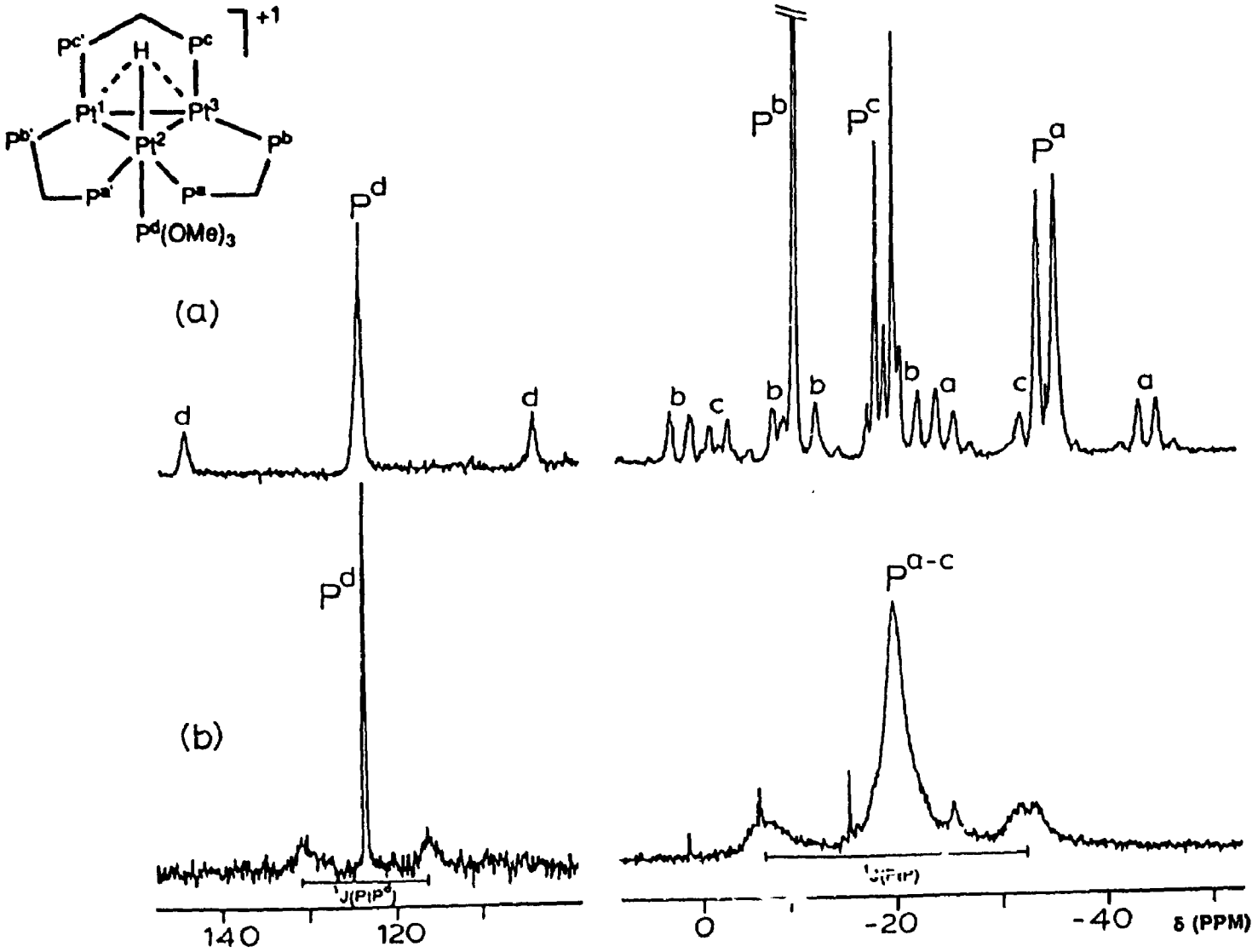

Figure 6.3: $^{31}P(^{1}H)$ NMR spectra of 3a; (a) at -90°C, (b) at 20° C.

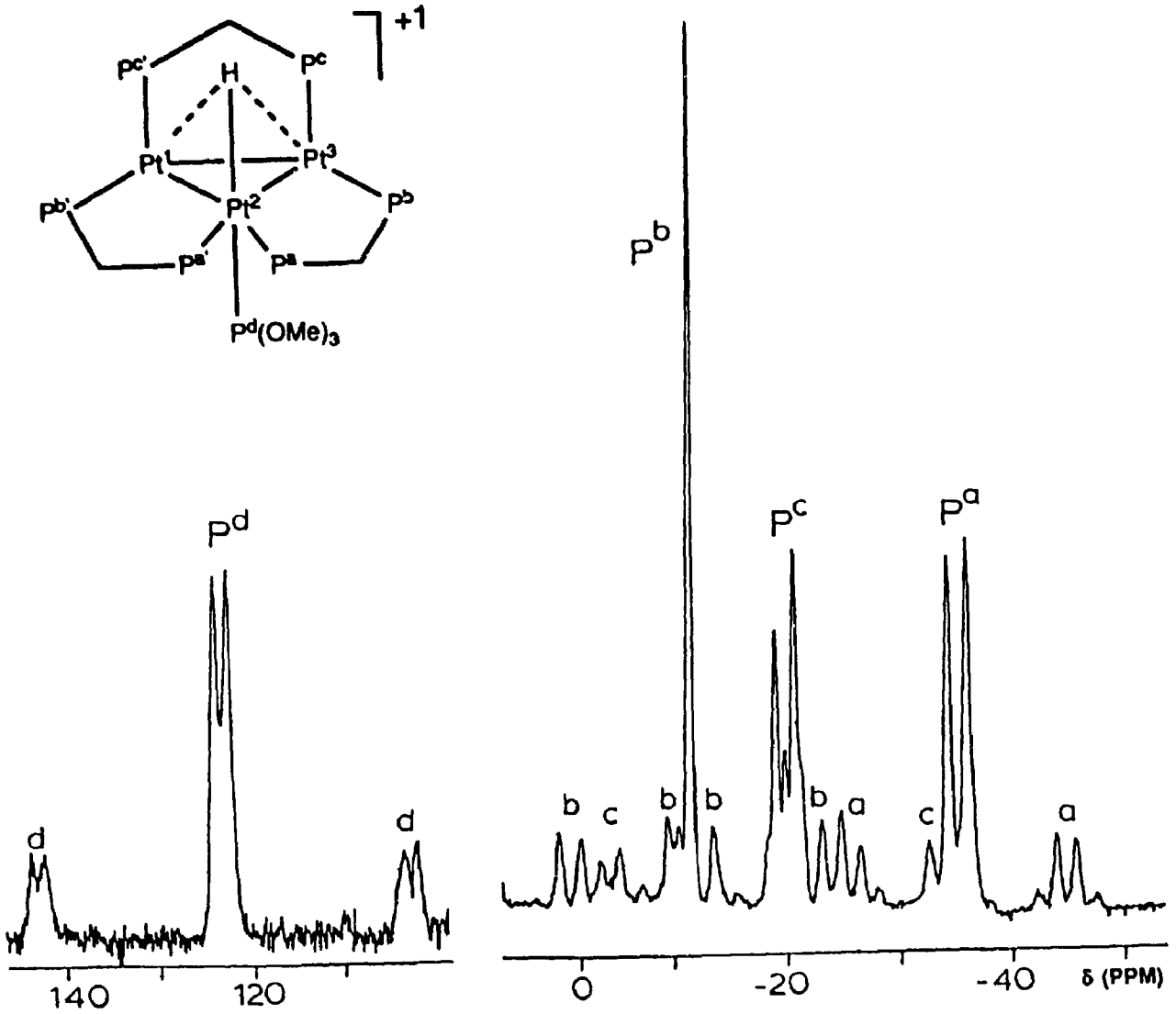

Figure 6.4: ^{1}H-coupled ^{31}P NMR spectrum of 3a.

The resonance due to $P(OMe)_3$ ligand, P^d, was at low-field (δ 125.0) and appeared as a 1:4:1 triplet (due to coupling to Pt^2, $^1J(Pt^2P^d)$ = 4990 Hz). The presence of a single hydride ligand trans to P^d was confirmed by recording a ^1H-coupled ^{31}P NMR spectrum. An extra doublet splitting due to $^1J(P^dH)$~170 Hz was observed in the spectrum (figure 6.4). The $^1J(Pt^1P^d)$ = 6230 Hz in complex 3c [$P^d = P(OPh)_3$], is significantly larger than those found in 3a and 3b suggesting that Pt-$P(OR)_3$ bond in 3c is stronger than those in 3a and 3b. $^1J(PtP^d)$ value for the phosphine complex 3d [$^1J(PtP^d)$ = 3800 Hz] is lower than that of the phosphite complexes 3a-3c. A similar trend was observed in the series of isoelectronic complexes[10], $[Pt_3(\mu_3\text{-}CO)(\mu\text{-}dppm)_3L](PF_6)$, $L = P(OR)_3$, PR_3.

The ^1H NMR spectrum of 3a at -90°c contains two "AB" quartets in the CH_2P_2 region with relative intensities 2:1 as expected for the static structure 3, which has no plane of symmetry containing $Pt_3(PCP)_3$ unit. The hydride signal was observed at δ -0.04 as a doublet due to coupling to the phosphorus atom of the phosphite ligand (P^d), $^2J(PH)$ = 170 Hz, and with satellites due to coupling to ^{195}Pt [$^1J(Pt^1H) = {}^1J(Pt^3H)$ = 268 Hz] having the intensities 1:8:18:8:1, indicating that the hydride is bridged between Pt^1 and Pt^3 in a $Pt_2(\mu_2\text{-}H)$ bonding mode (appendix 7). The sateilites due to coupling to Pt^2 were not observed in the spectrum as the signals were weak and broad, and indistinguishable from the noise. However, the ^{195}Pt and

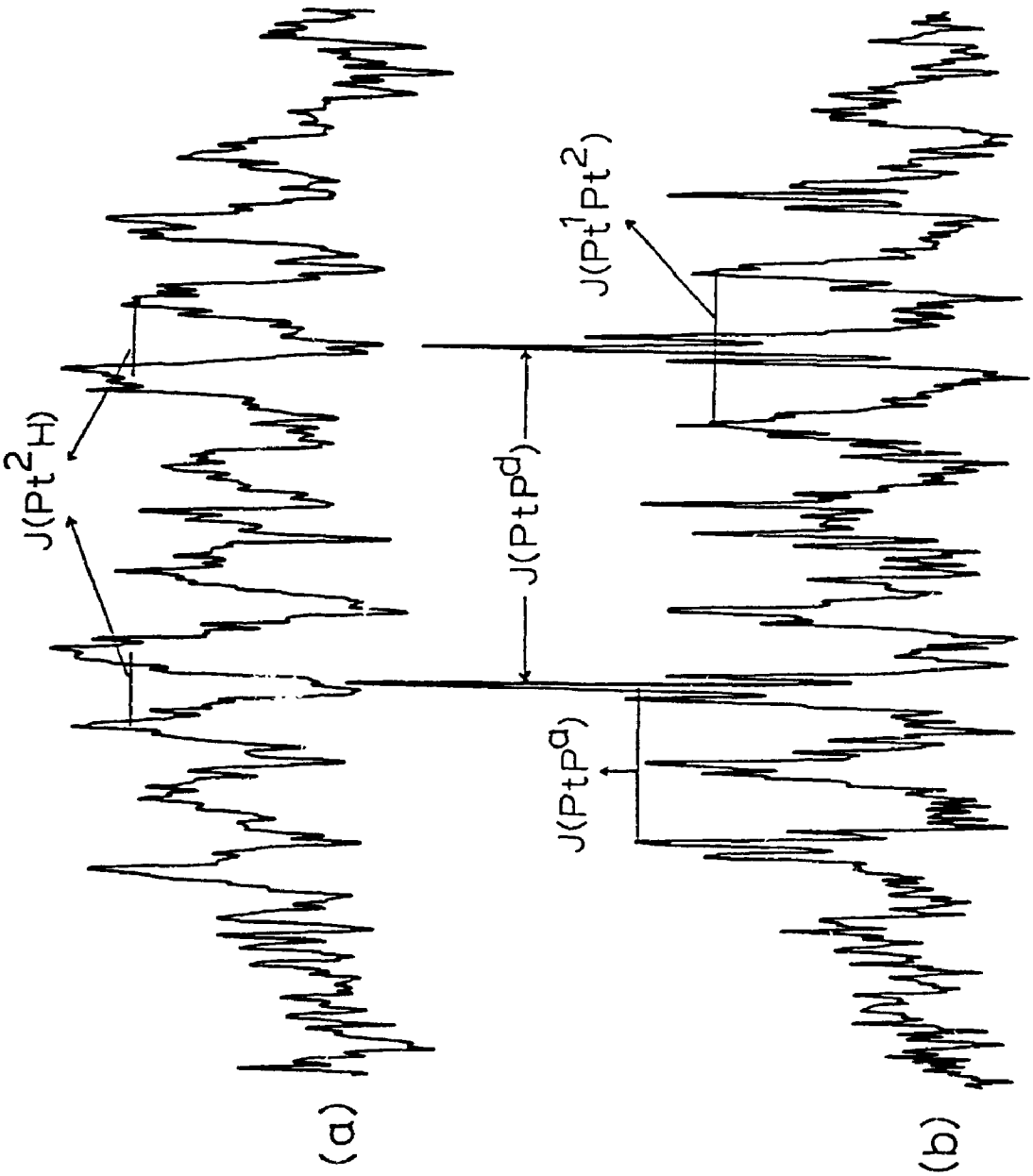

Figure 6.5: (a) ^{195}Pt, and (b) $^{195}Pt\{^{1}H\}$ NMR spectrum of 3a.

$^{195}Pt\{^{1}H\}$ NMR spectra at -90°C (figure 6.5) clearly indicated that $^{1}J(Pt^{2}H)$ = 1200 Hz.

The resonance due to the unique platinum atom, Pt^{2}, in the $^{195}Pt\{^{1}H\}$ NMR of 3a at -90°c was observed at δ -3242 and appeared as doublet of triplets due to coupling to P^{d} and the chemically equivalent P^{a} phosphorus atoms. The presence of a hydride ligand bound to Pt^{2} was confirmed by recording the ^{1}H-coupled ^{195}Pt NMR spectrum of 3a. An extra doublet splitting due to $^{1}J(Pt^{2}H)$~1200 Hz was observed in this spectrum (figure 6.5).

The above spectroscopic data clearly show the structures in solution are of the type found in the solid state for 3a. In particular, the phosphine or phosphite ligands adopt a terminal bonding position and the hydride ligand is asymmetrically triply bridged with a much stronger interaction to Pt^{2} than with Pt^{1} or Pt^{3}.

The structurally characterized complex 8,[22] is a good precedent for complex 3. In complex 8, the $AuPR_3^+$ unit is bound more strongly to the most nucleophilic platinum centre, Pt(2), than to Pt(1) or Pt(3), Table 6.8. Thus, complex 8 serves as a supporting evidence for us to believe that in 3a, the hydride ligand binds to the Pt_3 centre in the same way as the bridging $AuPR_3^+$ unit is bound to the Pt_3 unit in complex 8.

6.3.4 Ligand fluxionality in complexes 3a-3d:

As said earlier, the complexes 3a-3d were

Table 6.10 : ^{1}H NMR data for complexes **3a-3d** in CD_2Cl_2 at room temperature.

Complex	3a	3b	3c	3d
δPtH	-0.49	-0.59	-0.03	-0.96
$^{1}J(PtH)$	590	570	551	–
$^{2}J(P^{d}H)$	160	153	106	126
$^{2}J(PH)$	7.5	7.5	9.5	–
$\delta C\underline{H}^{a}H^{b}$	5.93	6.16	5.88	5.80
$^{3}J(PtH^{a})$	65	78	78	78
$^{2}J(H^{a}H^{b})$	10	–	12	–
$\delta CH^{a}\underline{H}^{b}$	4.60	4.48	4.38	3.95
$\delta P(OCH_3)$	3.45	1.0 ($OCH_2C\underline{H}_3$) 3.87 ($OC\underline{H}_2CH_3$))	–	2.28
J(HH)	–	7.0	–	–
$^{3}J(PH)$	12	7.0	–	–

Table 6.11: ^{195}Pt NMR data for complexes **3a** and **3b** in CD_2Cl_2 at -90°C.

Complex	3a‡	3b‡
δPt^{2}	-3242	-3150
$^{1}J(Pt^{1}Pt^{2})$	2280	2200
$^{1}J(Pt^{2}H)$	1200§	1190§
$^{1}J(Pt^{2}P^{d})$	4990	4960
$^{1}J(Pt^{2}P^{a})$	2300	2250
$^{2}J(Pt^{2}P^{c})$	175	-

‡ The resonance due to Pt^{1} was too broad to be observed

§ $^{1}J(Pt^{1}H)$ coupling obtained from ^{1}H-coupled ^{195}Pt NMR spectrum

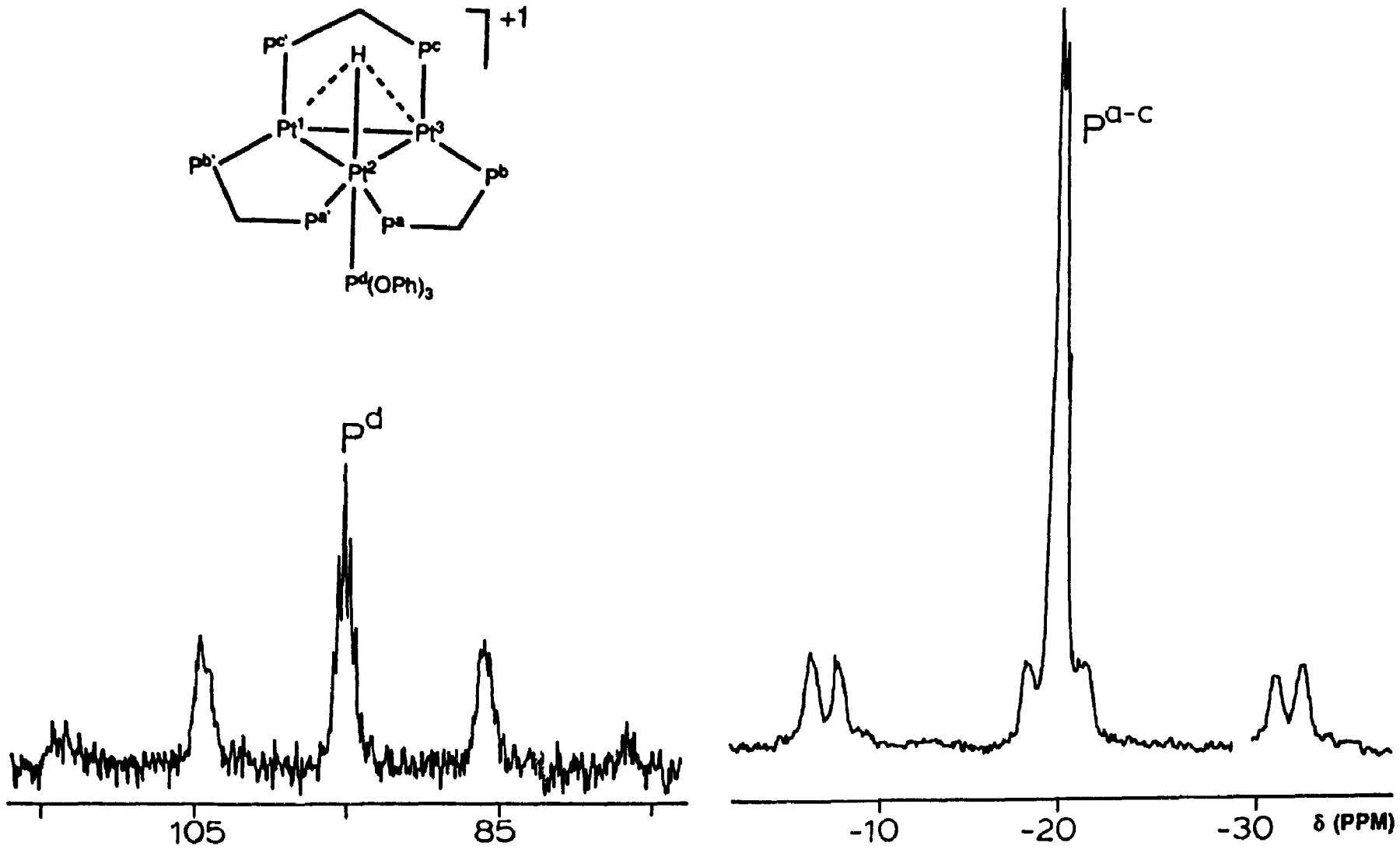

Figure 6.6: $^{31}P\{^{1}H\}$ NMR spectrum of 3c.

undergoing a rapid fluxional process at room temperature. The fluxionality involves migration of the ligand L around the triangular face of the cluster 3, as shown in equation 6.1.

For 3c, the $^{31}P\{^{1}H\}$ NMR spectrum at room

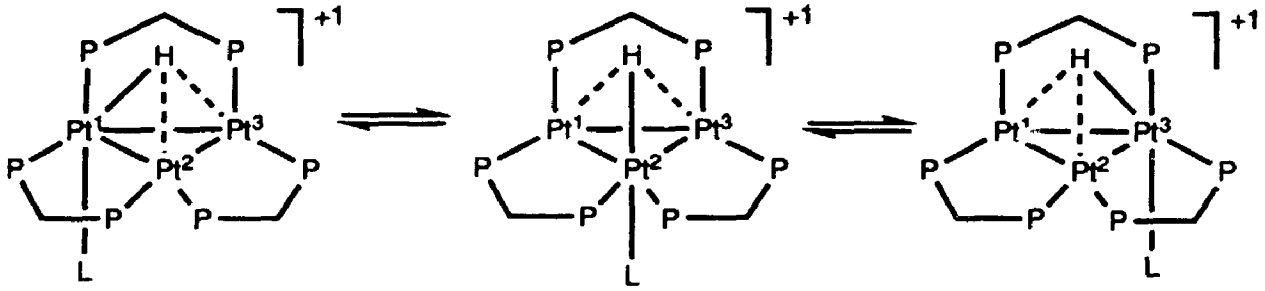

3' 3 3''

Equation 6.1

temperature (figure 6.6) showed a single resonance due to the dppm phosphorus atoms. This was split into a doublet ($^{2}J(PP)$ = 40 Hz) due to coupling the phosphorus atom, P^{d}, of the phosphite ligand. The resonance due to the $P(OPh)_3$ ligand occured as a septet due to coupling to six "equivalent" dppm phosphorus atoms and with satellites due to coupling to ^{195}Pt [$^{1}J(PtP)$ = 2125 Hz] having the intensities 1:4:7:4:1 (a 1:12:49:84:49:12:1 septet is expected, but the weak outer lines are not observed, appendix 7). The ^{195}Pt satellite intensity distribution suggests that the $P(OPh)_3$ ligand is bound as a $Pt_3\{\mu_3\text{-}P(OPh)_3\}$ adduct. Thus, the data indicate that there is an apparent 3-fold symmetry for the complex.

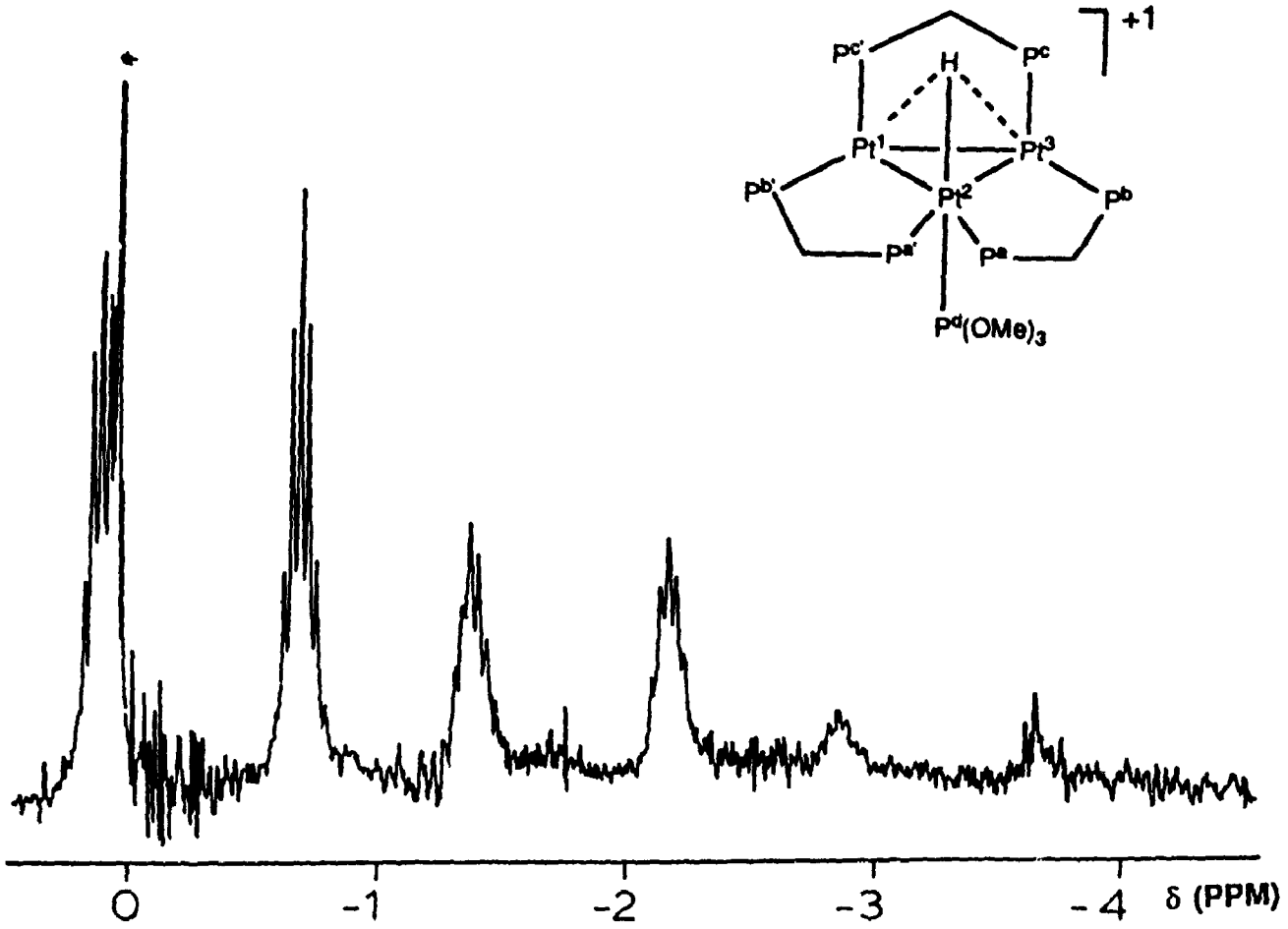

Figure 6.7: ^{1}H NMR spectrum of 3a showing hydride resonances.

Similarly, for complex 3a, the NMR spectrum at room temperature showed a single broad resonance due to the dppm phosphorus atoms [δ -21.6, $^1J(PtP)$ = 2980 Hz]. The resonance due to $P(OMe)_3$ ligand occured as a sharp septet and had broad satellites due to $^1J(PtP)$ = 1733 Hz. The calculated value of $^1J(PtP)$ for rapid intramolecular fluxionality in 3a (equation 6.1) would be $^1J(PtP^d) \sim 1/3 \times 4990 = 1633$ Hz. Similarly for 3c, the calculated value for $^1J(PtP^d) \sim 1/3 \times 6230 = 2077$ Hz. These values are in reasonable agreement with the observed values. When free phosphite ligand was present in solution, no exchange between free and complexed $P(OR)_3$ occurred. This, and the observation of J(PP) and J(PtP) coupling for coordinated $P(OR)_3$ in the fast exchange regime, proves that the fluxionality is an intramolecular process.

Further evidence on the nature of fluxionality was obtained by a combination of ^1H and ^{195}Pt NMR spectroscopy of 3a and 3b. At room temperature the hydride resonance in each case still occurred as a doublet with $^2J(P^dH) \sim 170$ Hz, due to coupling to the phosphite phosphorus, but an average ^{195}Pt coupling of $^1J(PtH)$ = 592 Hz (for 3a) was observed (figure 6.7). The calculated average value of $^1J(PtH) = 1/3 \times 1200 + 2/3 \times 268 = 579$ Hz. Thus, the hydride appears to be symmetrically triply bridging in the fast fluxionality region but the coupling $^2J(PH)$ to the phosphite ligand is still maintained. This confirms that

the fluxionality does not involve reversible dissociation of either the phosphite or the hydride ligand and so supports the mechanism of equation 6.1.

Bour *et al*, report that the Pt_3Au complex, 8, also exhibits a fluxional process involving phosphines.[22] They have not mentioned the details of the fluxionality. We believe that a fluxional process as described in equation 6.1 may be operating in complex 8.

6.3.5 Spectroscopic characterization of $[Pt_3(\mu_3\text{-PPh})(\mu\text{-dppm})_3H](PF_6)$, 6

Complex 6 was characterized unambiguously in solution by IR and multinuclear NMR spectroscopy. It has a structure similar to that of the isoelectronic complex, $[Pt_3(\mu_3\text{-PPh})(\mu\text{-dppm})_3(OH)]^+$, 7, whose structure has been characterized by X-ray crystallography.[16] The ^{31}P, ^{1}H, and ^{195}Pt NMR data of 6 can be found in Table 6.6. The NMR labelling scheme is seen in scheme 6.5.

The $^{31}P\{^{1}H\}$ NMR spectrum (figure 6.8) of 6 appears as four signals in a 2:2:2:1 intensity ratio. The absence of three-bond $^{3}J(P^aP^c)$ coupling mediated through a Pt-Pt bond indicates that this trinuclear platinum system has only a single metal-metal bond and bridging dppm ligands. The signal due to P^c splits into a doublet due to coupling to P^d [$^{2}J(P^cP^d)$ = 197 Hz]. The signal due to the phosphinidene phosphorus atom, P^d, appears at low-field (δ 262) as a triplet (due to coupling to P^c) with ^{195}Pt

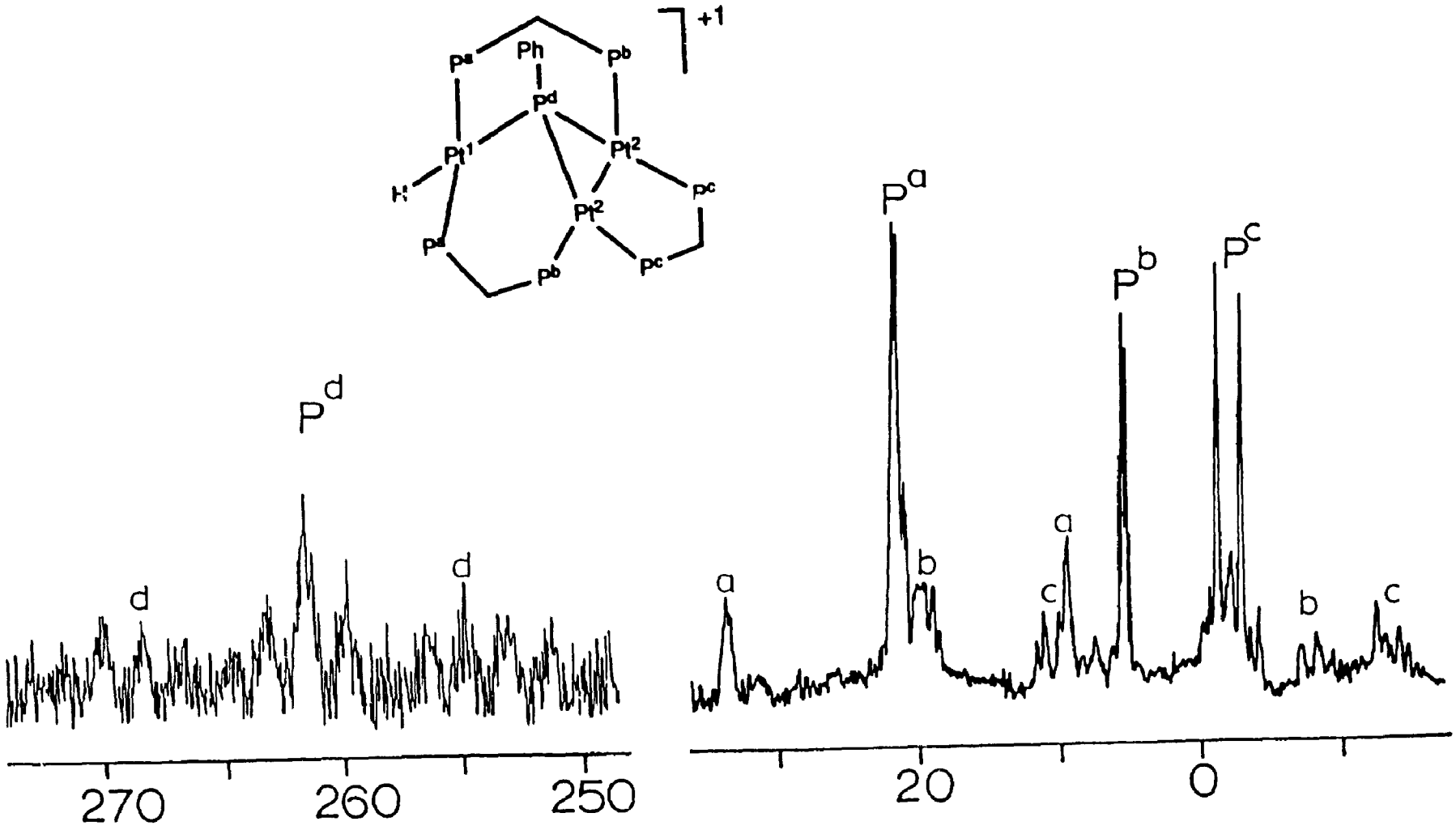

Figure 6.8: $^{31}P\{^{1}H\}$ NMR spectrum of 6.

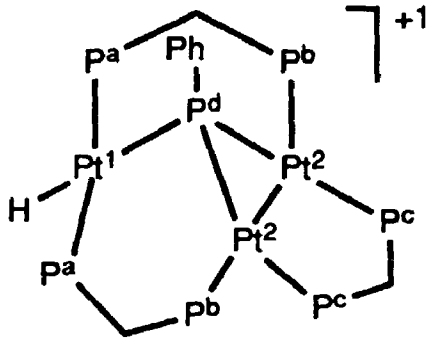

Scheme 6.5: NMR labelling Scheme for complex **6**

satellites. The two sets of platinum satellites yield Pt-P couplings of 1200 and 1920 Hz to Pt^1 and Pt^2, respectively. The $^{195}Pt\{^1H\}$ NMR spectrum aided in the

Table 6.12 : NMR Data for complex **6** in CD_2Cl_2

$^{31}P\{^1H\}$	
δP^a	21.6
$^1J_{(Pt^1P^a)}$	2920
δP^b	5.6
$^1J_{(P^bPt)}$	3360
$^2J_{(P^bPt)}$	340
$^2J_{(P^bP^d)}$	31
$^3J_{(P^bP^b)}$	160
δP^c	-1.7
$^1J_{(P^cPt)}$	3040
$^2J_{(P^cP^c)}$	68
$^2J_{(P^cP^d)}$	197
δP^d	262
$^1J_{(P^dPt^1)}$	1200
$^1J_{(P^dPt^2)}$	1920

^1H	
δPtH	-2.0
$^1J_{(PtH)}$	1002
$^2J_{(P^dH)}$	123
$^2J_{(P^aH)}$	16.5
$^4J_{(P^bH)}$	8.0
$\delta C^1H^aH^b$	3.0, 4.1
$\delta C^2H^cH^d$	5.3
$^2J_{(H^cH^d)}$	12

$^{195}Pt\{^1H\}$	
δPt^1	-3492
δPt^2	-3391
$^1J_{(Pt^1Pt^2)}$	240

assignment of couplings. The resonance due to Pt^1 appeared as a doublet of triplets due to coupling to P^d (1200 Hz) and P^a (2920 Hz), while that of Pt^2 appeared as a doublet of doublets of doublets from coupling to three distinct atoms P^b, P^c and P^d.

The hydride resonance in the ^1H NMR of 6 was observed at δ -2.0 as a doublet of multiplets due to coupling to P^d, P^a and Pt^2 and with satellites due to coupling to Pt^1 [$^1J(Pt^1H)$ = 1002 Hz].

The platinum-hydride stretch was observed in the IR spectrum at 1962 cm^{-1}. This is indicative of a terminal Pt-H bond. Complex 6 can also be obtained by the reaction of 7 with $NaBH_4$.[16] All the spectroscopic data that are reported here are in agreement with the earlier work.[16]

6.3.6 Bonding in complexes 3a-3d

Bonding in the isoelectronic complexes 4, which

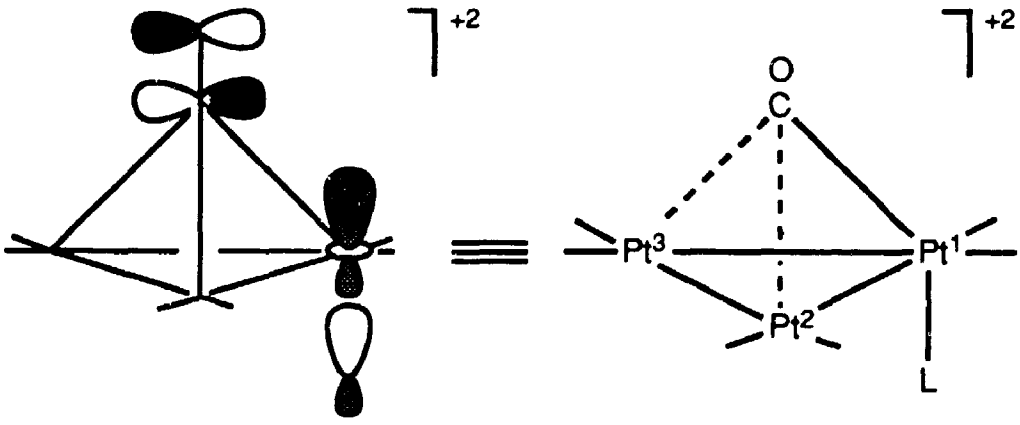

Scheme 6.6

contain an asymmetrically bridged μ_3-CO ligand, has been rationalised in terms of CO ligand acting to a large extent as a Π-acceptor ligand.[11,14] According to EHMO calculations,[12] the platinum acceptor orbital is a $5d_{z^2}$ $6P_z$ hybrid orbital and the enhanced backbonding can then be understood in terms of the bonding interactions shown in scheme 6.6.

This interpretation suggests that in the absence of a Π* orbital on the capping ligand, the capping ligand would slip towards platinum atoms Pt^1 and Pt^3. Thus a capping hydride ligand is expected to form a complex as shown in scheme 6.7, ie, the hydride ligand is strongly bound to the two platinum atoms (Pt^1 and Pt^3) which do not have the extra phosphine ligand. However, this is

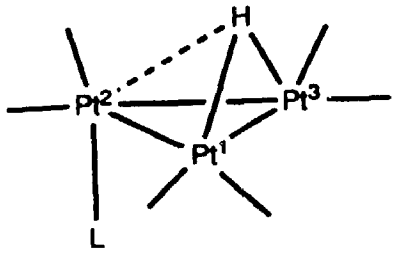

Scheme 6.7

contradictory to what has been observed in complex 3, which clearly shows that the hydride is bonded strongly to the same platinum atom (Pt^2) which has a terminal ligand, L.

Dr. D.-S. Yang of this laboratory has carried out EHMO calculations for complex 3, which has a capping hydride ligand. The results of this study are reproduced

here. The computed overlap populations(ρ) for complex 3 are illustrated in scheme 6.8. It can be clearly seen that

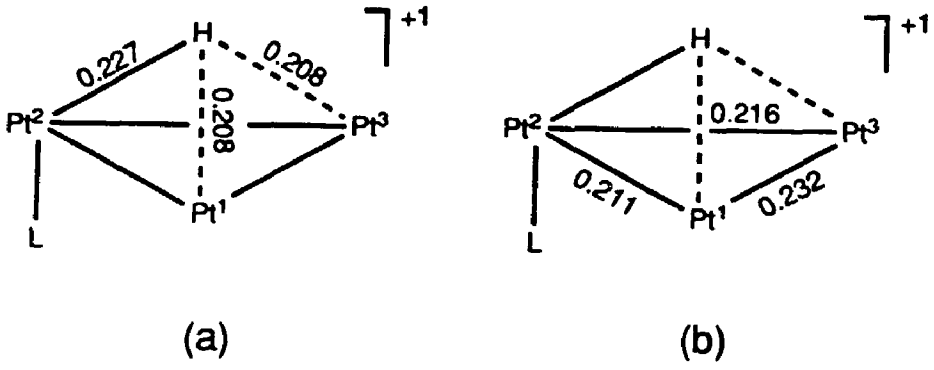

Scheme 6.8: (a) Computed overlap population for Pt-H bond
(b) Computed overlap population for Pt-Pt bond

Pt^2-H bond [$\rho(Pt^2H)$ = 0.227] is stronger than Pt^1-H or Pt^3-H bonds [$\rho(Pt^1H) = \rho(Pt^3H)$ = 0.208]. Similarly, Pt^1-Pt^3 bond (ρ = 0.232) has a greater M-M overlap than either Pt^1-Pt^2 (ρ = 0.216) or Pt^2-Pt^3 (ρ = 0.211) bonds. These data are in good agreement with the crystallographic and NMR spectroscopic data for complex 3a.

A possible bonding scheme to rationalise the asymmetric bridging of the μ_3-H unit in complex 3 is discussed below.

Figure 6.9 illustrates a qualitative picture of this molecular orbital interaction. Initially, a three-centred interaction involving a PtL_3 and two PtL_2 units takes place. The resulting molecular orbital (directed at the centre of the Pt_3 triangle) will be partially polarized, ie, there will be a higher

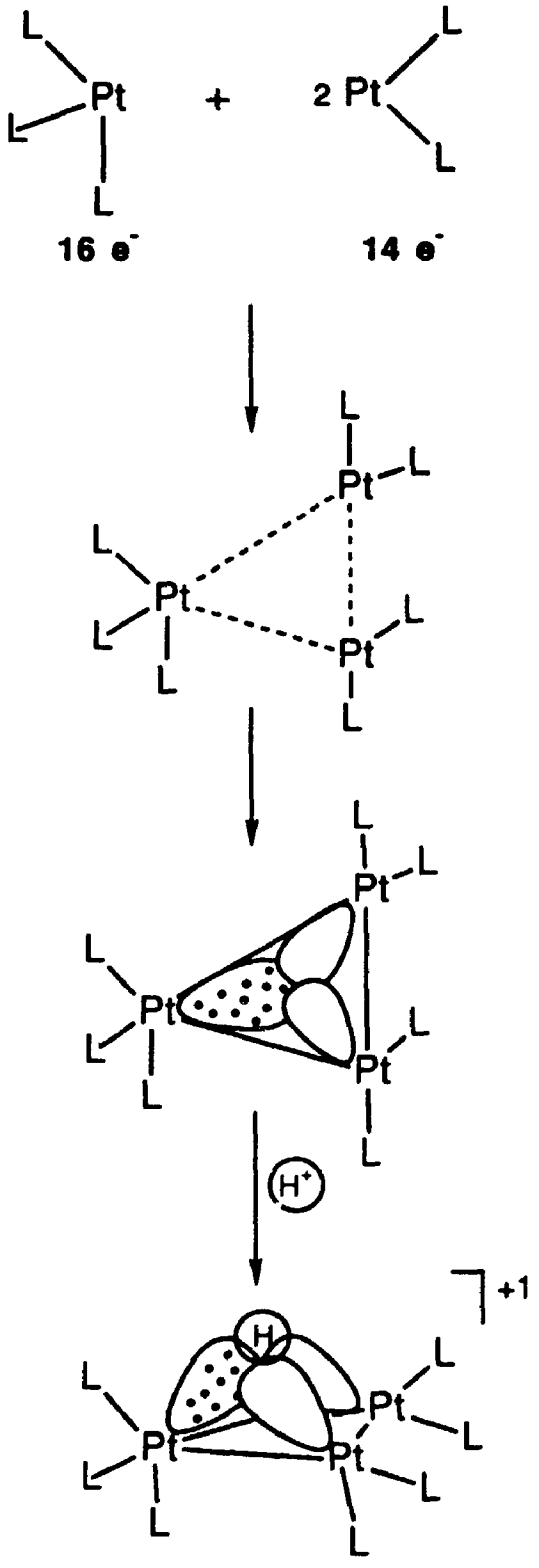

Figure 6.9: A qualitative picture of the molecular orbital interaction in 3

electron-density localization on PtL_3 unit than the PtL_2 units. Now, if an electrophile such as H^+ attacks the (Pt_3L_7) neutral fragment, it would localize on the metal center with greater electron density, namely, the PtL_3 unit. Thus, the resulting product would have the hydride ligand bound more strongly to the PtL_3 unit than the PtL_2 units, with the result that a complex containing an asymmetrically bridged hydride ligand is formed.

6.3.7 Notation for complexes with an asymmetric bridging ligand

Cluster complexes such as 3, 4, 5 and 8 have a capping ligand which bridges the Pt_3 unit in an asymmetric fashion. But, the currently used form of writing molecular formula for clusters does not indicate the asymmetric nature of these ligands. Here we have proposed a notation that could be used as a possible means of representing these types of cluster complexes and this will be discussed below.

Consider a platinum metal complex, $[Pt_n(\mu_n\text{-}X)L_y]$, where X is a capping ligand bridging asymmetrically between n number of platinum atoms. Let 'M_a' represent 'a' number of metal centres having a stronger Pt-X bonds in the complex. Let 'm_b' represent 'b' number of metal centres having weak Pt-X bonds in the same complex. Using these notations, the formula for this complex can be written as $[Pt_n(M_am_b\text{-}X)L_y]$, which clearly indicates the asymmetric

nature of the capping ligand.

Using the above discusssed notations, complex 3 can be written as $[Pt_3(Mm_2\text{-}H)(\mu\text{-}dppm)_3L](PF_6)$. Similarly, complex 4 and 5 can be written as $[Pt_3(Mm_2\text{-}CO)(\mu\text{-}dppm)_3L]^{+2}$ and $[Pt_3(M_2m\text{-}CO)(\mu\text{-}dmpm)_4]^{+2}$ respectively. Thus, by just looking at the formula for complex 5, we know that the bridging CO bonds more strongly to two platinum atoms than to the third platinum atom. Complex 8 can be written as $[Pt_3(Mm_2\text{-}AuPPh_3)(\mu\text{-}CO)_3(PPh_3)_3]^{+}$. It is easy to differentiate between strong and weak Pt-X bonds, since the coupling constant J(Pt-X) would be different for each of these platinum centres. However, it should be noted that this notation holds good only in cases, where there is a clear experimental evidence for the asymmetry of the bridging ligand (such as complexes 3, 4, 5 and 8).

6.4 SUMMARY AND CONCLUSIONS

The chemistry of these trinuclear hydrido clusters of platinum with tertiary phosphine and phosphite ligand has revealed some unique insights into the formation and nature of the asymmetrically bridged μ_3-H ligand. This work has shown (i) that the phosphine and phosphite ligands add to complex 3 as terminal ligands, (ii) that these ligands exhibit a novel fluxional process involving rapid migration about the triangular face of the cluster. The ease with which the fluxional process occurs is attributed

to the coordinative unsaturation of complex 3 and provides a good example of the high reactivity of such clusters. (iii) The ligand addition leads to a slippage of the symmetrically triply bridged μ_3-H to an asymmetrically bridged μ_3-H. This distortion leads to the formation of a stronger bond between the hydride ligand and the electron-rich platinum centre. (iv) Most importantly, this work has demonstrated that the slippage of the capping ligand is not only common for the Π-acid ligands such as CO (as suggested by Evans[12]) but also for the non Π-acid ligands such as hydride. (v) In order to explain the asymmetric bridging of the hydridic ligand in complex 3, a possible bonding scheme is proposed. (vi) Finally, a notation for representing complexes with asymmetrically bridged ligands is proposed which used the symbol 'M' for representing the strongly bonded M-X bonds and 'm' for denoting the weakly bonded M-X bonds. Thus, in this chapter we discussed the synthesis and characterization of a class of cluster complexes containing a $Pt_3(Mm_2-H)$ units.

6.5 REFERENCES:

1. A. Albinati, *Inorg. Chim. Acta,* 22 (1977) L3; A. Albinati, G. Cartman, A. Musco, *Inorg. Chim. Acta,* 16 (1976) L3

2. J. Chatt, P. Chini, J. Chem. Soc. A, (1970) 1538

3. R.G. Vranka, L.F. Dahl, P. Chini, J. Chatt, J. Amer. Chem. Soc., 91 (1969) 1574

4. A. Moor, P.S. Pregosin, L.M. Venanzi, A.J. Welch, *Inorg. Chim. Acta,* 85 (1984) 103

5. J. P. Barbier, R. Bender, P. Braunstein, J. Fischer, L. Ricard, *J. Chem. Res.,* (1978), (S) 230; (M) 2913; R. Bender, P. Braunstein, J. Fischer, L. Ricard, A. Mitscher, *New J. Chem.,* 5 (1981) 81

6. D.G. Evans, M.F. Hallam, D.M.P. Mingos, W.M. Wardle, *J. Chem. Soc., Dalton Trans.,* (1987) 1889

7. D.M.P. Mingos, W.M. Wardle, *Transition Met. Chem.,* 10 (1985) 441; N.K. Ermenko, E.G. Mednikov, S.S. Kurasov, *Russ. Chem. Rev.,* 54 (1985) 394

8. C.S. Browning, D.H. Farrar, R.R. Gukathasan, S.A. Morris, *Organometallics,* 4 (1985) 1750; D.M.P. Mingos, I.D. Williams, M.J. Watson, *J. Chem. Soc. Dalton Trans.,* (1988) 1509

9. G. Ferguson, B.R. Lloyd, R. J. Puddephatt, *Organometallics,* 5 (1986) 344

10. A.M. Bradford, M.C. Jennings, R.J. Puddephatt, *Organometallics,* 7 (1988) 792; A.M. Bradford, G. Douglas, Lj-Manojlovic Muir, K.W. Muir, R.J. Puddephatt, *Organometallics,* in press

11. S.S.M. Ling, N. Hadj-Bagheri, Lj-Manojlovic-Muir, K.W. Muir, R.J. Puddephatt, *Inorg. Chem.,* 26 (1987) 231

12. D.G. Evans, *J. Organomet. Chem.,* 352 (1988) 397

13. B.R. Lloyd, R.J. Pudephatt, *J. Amer. Chem. Soc.,* 1107 (1987) 7785

14. G. Ferguson, B.R. Lloyd, Lj-Manojlovic-Muir, K.W. Muir, R.J. Puddephatt, *Inorg. Chem.,* 25 (1986) 4190; M.C. Jennings, R.J. Puddephatt, *Inorg. Chem.,* 27 (1988) 4280; M.C. Jennings, Lj-Manojlovic Muir, K.W. Muir, R.J. Puddephatt, *J. Chem. Soc. Chem. Commun.,* (1989) 159

15. C. Mealli, *J. Amer. Chem. Soc.,* 107 (1985) 2245

16 M.C. Jennings, Ph.D thesis, University of Western Ontario, (1989), p: 131-162

17. International Tables for X-ray crystallography; Kynoch; Birmingham, England (1969), Vol I; (1974), Vol IV

18. J. de Meulenaer, H. Tompa, *Acta. Crystallogr.*, 19 (1965) 1014

19. R.F. Stewart, E.R. Davidson, W.T. Simpson, *J. Chem. Phys.*, 42 (1965) 3175

20. G.M. Sheldrick, "SHELX-76: A program for crystal structure determination", Cambridge University Press; Cambridge, England (1976)

21. Q.-B. Bao, S.J. Geib, A.L. Rheingold, T.B. Bill, *Inorg. Chem.*, 26 (1987) 3453

22. J.J. Bour, R.P.E. Kanters, P.P.J. Schlebos, W. Bos, W.P. Bosman, H. Behm, P.T. Beurskens, J.J. Steggerda, *J. Organomet. Chem.*, 329 (1987) 405

23. Enraf-Nonius CAD4F users Manual; Enraf-Nonius Delft; Delft, The Netherlands, (1984)

24. "Enraf-Nonius Structure Determination Package,SDP-PLUS", Version 3.0; Enraf-Nonius Delft; Delft, The Netherlands, (1984)

25. R. Eisenberg, J.A. Ibers, *Inorg. Chem,* 4 (1965) 773

26. Md.M. Rahman, H.Y. Liu, A. Prock, W.P. Giering, *Organometallics,* 6 (1987) 650

27. A. Bondi, *J. Phys. Chem.*, 68 (1964) 441

CHAPTER 7

SYNTHESIS, CHARACTERIZATION AND REACTIVITY OF SOME NOVEL TRIPLATINUM HYDRIDE CLUSTER COMPLEXES.

7.1 INTRODUCTION

The ability of transition metal surfaces to chemisorb and thus activate gaseous hydrogen has been intensively studied over many years and this property has led to important applications in heterogeneous catalysis[1]. Current interest in molecular hydrogen as a fuel has led to recent work on the use of the d-block and f-block metal alloys as agents for its storage and transport in high concentrations[2].

Dissociative chemisorption of hydrogen on a Pt(111) surface leads to PtH, $Pt_2(\mu_2\text{-}H)$ and $Pt_3(\mu_3\text{-}H)$ linkages[3-6], but until recently the $Pt_3(\mu_3\text{-}H)$ group had not been reported in platinum hydride clusters[8,10]. Recently, our group described the synthesis and characterization of the first complex containing the $Pt_3(\mu_3\text{-}H)$ group[7]. In fact, a wide range of monophosphine stabilized polynuclear platinum hydride clusters, $[Pt_4H_2(P^tBu_3)_4](BF_4)(HBF_4)_2$, $[Pt_4H_7(P^tBu_3)_4](BPh_4)$, $[Pt_3H_6(P^tBu_3)_3]$, $[Pt_4H_2(P^tBu_3)_4]$ and $[Pt_5H_8(P^tBu_2Ph)_5]$ have contained only terminally bound and doubly bridging hydride ligands.[9,11-14]

The rationale behind studying the structures of metal hydride cluster complexes is that the configuration

of hydrogen atoms in these clusters may serve as a good model for the arrangement of hydrogen atoms adsorbed on a metal surface. Further interest in this class of unusual hydrido-bridged compounds has developed because of their use as precursors for the synthesis of mixed metal clusters[15,16].

In this chapter we will discuss the synthesis and characterization of a number of novel hydrido triplatinum cluster complexes. For example, the cation, $[Pt_3(\mu_3\text{-}H)(\mu\text{-}dppm)_3]^+$, 2, rapidly and reversibly protonates to yield $[Pt_3(\mu_3\text{-}H)_2(\mu\text{-}dppm)_3]^{2+}$, 3, and $[Pt_3(\mu\text{-}H)_3(\mu\text{-}dppm)_3]^{3+}$, 4.[16] The dihydride complex, 3, reacts with CO to reductively eliminate dihydrogen and forms the parent carbonyl complex, $[Pt_3(\mu_3\text{-}CO)(\mu\text{-}dppm)_3]^{2+}$, 1.[17] Reaction of 3 with phosphine and phosphite ligands results in the formation of the 44 electron adducts, $[Pt_3(\mu\text{-}H)H(\mu\text{-}dppm)_3L]^{2+}$, 5. The adduct 5d (L = PPh_3) reacts further to form the diplatinum (I) complex[18], $[Pt_2(\mu\text{-}dppm)_2HL]^+$, 6d.

7.2 EXPERIMENTAL

In all the experiments listed below, the operations were carried out under a dry nitrogen atmosphere.

7.2.1 $[Pt_3(\mu_3\text{-}H)_2(\mu\text{-}dppm)_3](PF_6)_2$, 3a

To a solution of $[Pt_3(\mu_3\text{-}H)(\mu\text{-}dppm)_3](PF_6)$.

2(PF_6), (40 mg, 0.0212 mmol) in $CD_2C\ell_2$ (0.5 mL) in an NMR tube (5 mm), was added aq. HPF_6 (4 μL, 0.0452 mmol). After thoroughly mixing the solutions, a series of variable temperature ^1H, $^{31}P\{^1H\}$ and ^{31}P NMR spectra were recorded. Solvent was then removed under reduced pressure, and a red solid was obtained which was washed with n-pentane and dried under vacuum. Yield : 73%. Mp: 160°C dec. Anal. calcd. for $C_{75}H_{68}P_8F_{12}Pt_3$: C, 44.4; H, 3.4%. Found: C, 47.5; H, 4.1%. Poor analysis due to decomposition of 3a in part to yield 2(PF_6). ^1H NMR data in $CD_2C\ell_2$ at -40°C: -3.68 [sept., $^1J(PtH)$ = 420, $^2J(PH)$ = 20, 2H, Pt<u>H</u>], 4.0 [s, 6H, $P_2C\underline{H}_2$].

7.2.2 [$Pt_3(\mu_3\text{-}H)H(\mu\text{-dppm})_3(CF_3COO)$]($CF_3COO$), 3b

To a solution of 2(CF_3COO) (40 mg, 0.0216 mmol) in $CD_2C\ell_2$ (0.5 mL) in a NMR tube (5 mm), was added CF_3COOH (4 μL, 0.0538 mmol) by syringe. The contents were mixed thoroughly. The $^{31}P\{^1H\}$ NMR spectrum indicated quantitative conversion to 3b. Attempts to isolate the complex in analytically pure form were unsuccessful. ^1H NMR data at 20°C in $CD_2C\ell_2$: δ -3.53 [sept., $^1J(PtH)$ = 415, $^2J(PH)$ = 20, 2H, Pt<u>H</u>], 5.23 [s, 6H, $P_2C\underline{H}_2$]. at -90°C : δ -3.49 [br. mult., satellites too broad to measure J(PtH), 2H, Pt<u>H</u>], 4.71 [s, 2H, $P_2C\underline{H}^aH^b$], 5.47 [s, 2H, $P_2CH^a\underline{H}^b$], 5.92 [s, 1H, $P_2C\underline{H}^cH^d$], 6.25 [s, 1H, $P_2CH^c\underline{H}^d$]; $^{195}Pt\{^1H\}$ NMR data at 20°C: δ -2612 [t, $^1J(PtP)$ = 3100]

7.2.3 $[Pt_3(\mu_3\text{-}H)(H)(\mu\text{-}dppm)_3(CF_3COO)](PF_6)$, 3c

In a similar way, 3c was prepared by the reaction of $2(PF_6)$ (30 mg, 0.0159 mmol) with CF_3COOH (3 μL, 0.0403 mmol). ^1H NMR data at 20°C in $CD_2C\ell_2$: δ -3.60 [sept., $^1J(PtH)$ = 420, $^2J(PH)$ = 20, 2H, Pt<u>H</u>], 5.18 [s, $^3J(PtH)$ = 50, 6H, $P_2C\underline{H}_2$]. at -80°C: -3.53 [br.mult., $^1J(PtH) \simeq 460$, Pt<u>H</u>], 5.48, 4.70 [s, 6H, $P_2C\underline{H}_2$]. $^{195}Pt\{^1H\}$ NMR data at 20°C: -2617 [t, $^1J(PtP)$ = 3150]

7.2.4 $[Pt_3(D)(H)(\mu\text{-}dppm)_3(CF_3COO)](PF_6)$, 3b*

$[Pt_3(\mu_3\text{-}D)(\mu\text{-}dppm)_3](PF_6)$, $2^*(PF_6)$, was prepared as described in chapter 5, using $1(PF_6)$ (40 mg, 0.0212 mmol) and $NaBD_4$. To a solution of $2^*(PF_6)$ (40 mg) in $CD_2C\ell_2$ (0.5 mL) in an NMR tube (5 mm), was added CF_3COOH (2 μL) by syringe. The ^{31}P NMR spectrum indicated a quantitative conversion of $2^*(PF_6)$ to 3b.

7.2.5 $[Pt_3(\mu_3\text{-}D)D(\mu\text{-}dppm)_3(CF_3COO)](PF_6)$, 3b**

Complex 3b** was prepared by the reaction of $2^*(PF_6)$ with an equimolar quantity of CF_3COOD [CF_3COOD was prepared by the reaction of trifluoroacetic anhydride, $(CF_3CO)_2O$, with D_2O].

7.2.6 $[Pt_3(\mu\text{-}H)_3(\mu\text{-}dppm)_3](CF_3COO)_3$, 4

To a solution of $2(PF_6)$ (40 mg, 0.0212 mmol) in $CD_2C\ell_2$ (0.5 mL) at -70°C in an NMR tube (5 mm), was added an excess of CF_3COOH (20 μL, 0.2693 mmol). The contents

were mixed and a series of low temperature (-70°C) multinuclear NMR spectra were recorded. ^{1}H and ^{31}P NMR spectra indicated complex 4 as the only product in solution at this temperature.

$^{31}P\{^{1}H\}$ NMR data at -70°C in $CD_2C\ell_2$: δ -3.28 [s, $^{1}J(PtP)$ = 3160, $^{2}J(PtP)$ = 151 and $^{3}J(PP)$ = 46, PtP]. ^{1}H NMR data at -70°C: δ -6.8 [t, $^{1}J(PtH)$ = 604, $^{2}J(P^{a}H^{a})$ = 70, 3H, Pt<u>H</u>], 4.83 [s, 6H, $P_2C\underline{H}_2$]

7.2.7 Interconversion of 2, 3, and 4:

Following the recording of NMR spectra of the trihydride complex, 4, at -70°C, the solution was allowed to warm to room temperature and a series of ^{1}H and $^{31}P\{^{1}H\}$ NMR spectra were recorded. At this temperature (20°C) the resonances observed were due to the dihydride complex, 3, and free CF_3COOH. The solution was then evaporated to dryness and the residue was washed with diethyl ether (5 mL) and redissolved in $CD_2C\ell_2$ (0.5 mL). The ^{1}H and $^{31}P\{^{1}H\}$ NMR spectra of the resulting product indicated the monohydride complex, 2, as the only product in solution.

7.2.8 Reaction of CO with complex 3a:

A sample of 3a (30 mg, 0.0150 mmol) in $CD_2C\ell_2$ (0.5 mL) was placed in a NMR tube (5 mm) fitted with a teflon tap. The tube was evacuated and excess CO was condensed into the liquid-nitrogen-cooled tube via a vacuum line, and the tap was closed. The colour of the solution rapidly

changed from red to orange. The NMR spectra of the resulting products were recorded. The residual gas inside the NMR tube was analysed by FAB mass spectrometry.

Similar experiments were conducted with complexes 3b, 3c, 3b*, 3b** and an equimolar quantities of 3b and 3b**. In all the cases the FAB mass spectra showed the peak due to H_2, m/e = 2, as the major peak (>90 mole percent). The above experiment was repeated replacing ^{12}CO gas by ^{13}CO in order to obtain ^{13}CO enriched products. $^{13}C\{^1H\}$ NMR data of the resulting products in $CD_2C\ell_2$ at -40°C: δ 210.2 [sept., $^1J(PtC)$ = 777, $^2J(PC)$ = 26, $Pt_3(\mu_3\text{-}CO)$ in 1], 186.3 [m, $^1J(PtC)$ = 586, $Pt_3(\mu_3\text{-}CO)$ in 7]. $^{31}P\{^1H\}$ NMR data at -40°C: δ -6.7 [d, $^1J(PtP)$ = 3710, $^3J(PP)$ = 140, $^2J(PC)$ = 26, ^{31}P in 1], -14.2 [br.s, $^1J(PtP)$ = 3400, ^{31}P in 7].

7.2.9 $[Pt_3(\mu\text{-}H)H(\mu\text{-}dppm)_3\{P(OPh)_3\}](PF_6)(CF_3COO)$, 5c

To a soltution of 3c (30 mg, 0.0150 mmol) in $CH_2C\ell_2$ (5 mL) was added $P(OPh)_3$ (4.3 μL, 0.0164 mmol). The contents were stirred for 10 minutes. During this period the solution turned deep red in colour. The solvent was removed under reduced pressure and the resulting residue was washed with diethyl ether (10 mL) followed by n-pentane (5 mL) and dried under vacuum Yield: 70%. Anal. calcd. for $C_{95}H_{83}F_9O_5P_8Pt_3$: C, 49.4; H, 3.6%. Found: C, 49.1; H, 3.4%.

7.2.10 $[Pt_3(\mu\text{-}H)H(\mu\text{-}dppm)_3\{P(OPh)_3\}](PF_6)_2$, 5c'

Complex 5c (25 mg, 0.0108 mmol) was dissolved in a minimum of acetone (3 mL) and added dropwise into a stirred solution of NH_4PF_6 (100 mg, 0.6098 mmol) in methanol (5 mL). After stirring for 15 minutes, solvent was removed under reduced pressure. The residue was dissolved in $CH_2C\ell_2$ (5 mL), filtered free from the excess NH_4PF_6 and upon removal of solvent, a red crystalline solid was obtained. Yield: 85%. Anal. calcd. for $C_{93}H_{83}F_{12}O_3P_9Pt_3$: C, 47.7; H, 3.6%. Found: C, 47.5; H, 3.5%.

Complexes 5a and 5b were also prepared by similar methods.

7.2.11 $[Pt_3(\mu\text{-}H)H(\mu\text{-}dppm)_3\{P(OMe)_3\}](PF_6)(CF_3COO)$, 5a: Anal. calcd. for $C_{80}H_{77}F_9O_5P_8Pt_3$: C, 45.3; H, 3.7%. Found: C, 45.1; H, 3.6%.

7.2.12 $[Pt_3(\mu\text{-}H)H(\mu\text{-}dppm)_3\{P(OEt)_3\}](PF_6)(CF_3COO)$, 5b: Anal. calcd. for $C_{83}H_{83}F_9O_5P_8Pt_3$: C, 46.1; H, 3.9%. Found: C, 45.9; H, 3.7%.

7.2.13 Reaction of complex 3c with PPh_3 :

To a solution of 3c (30 mg, 0.0150 mmol) in $CD_2C\ell_2$ (0.5 mL) in an NMR tube was added PPh_3 (4 mg, 0.0152 mmol). The contents were mixed thoroughly and transferred to the NMR probe which was precooled to -40°C. $^{31}P\{^1H\}$ NMR spectra of the sample were recorded. The solution was then transferred to a round bottom flask, a small volume of

$CH_2C\ell_2$ (5 mL) was added, and the contents stirred at room temperature for 0.5h. The solvent was then removed under reduced pressure. The reddish-brown solid was washed with ether (10 mL) and dried under vacuum. The resulting product was characterised by multinuclear NMR spectral data to be $[Pt_2(\mu\text{-dppm})_2H(PPh_3)]^+$, 8d. $^{31}P\{^1H\}$ NMR data of 8d at 20°C in $CD_2C\ell_2$: δ 6.94 [m, $^1J(PtP^a)$ = 3532, P^a], 7.95 [m, $^1J(PtP^b)$ = 2894, P^b], 27.1 [m, $^1J(PtP^x)$ = 2181, $^2J(PtP^x)$ = 596, N' = 2777, P^x]. N' = $^1J(PtP)$ + $^2J(PtP)$, N = $^2J(P^aP^b)$ + $^3J(P^aP^{b'})$. ^1H NMR data in $CD_2C\ell_2$ at 20°C: δ -8.97 [m, $^1J(PtH)$ = 1005, $^2J(PH)$ = 9.5, $^3J(H\text{-}Pt\text{-}Pt\text{-}P)$ = 45, Pt<u>H</u>], 4.98 [s, $^3J(Pt^1H)$ = 42, $^3J(Pt^2H)$ = 72, $P_2C\underline{H}_2$]

7.3 RESULTS AND DISCUSSION

7.3.1 Synthesis of the hydrido triplatinum complexes 3a-3c and 4:

The dihydride complex, $[Pt_3(\mu_3\text{-}H)_2(\mu\text{-dppm})_3](PF_6)_2$, 3a, was synthesized by the reaction of 2a with an equimolar quantity of HPF_6, equation 7.1. Similarly, complexes 3b and 3c were formed by the reaction of the trifluoroacetate salt of 2, 2b, with CF_3COOH and HPF_6, respectively, equation 7.2.

The trihydrido complex, 4, was prepared by the reaction of 2 with an excess of CF_3COOH or aqueous HPF_6 at -70°C, equation 7.3. Complex 4 was not thermally stable above -60°C and was characterized in solution by multinuclear NMR spectroscopy.

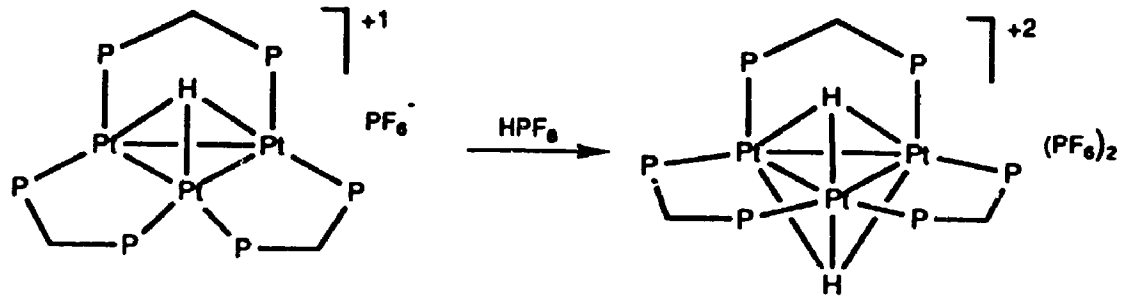

2a 3a

Equation 7.1

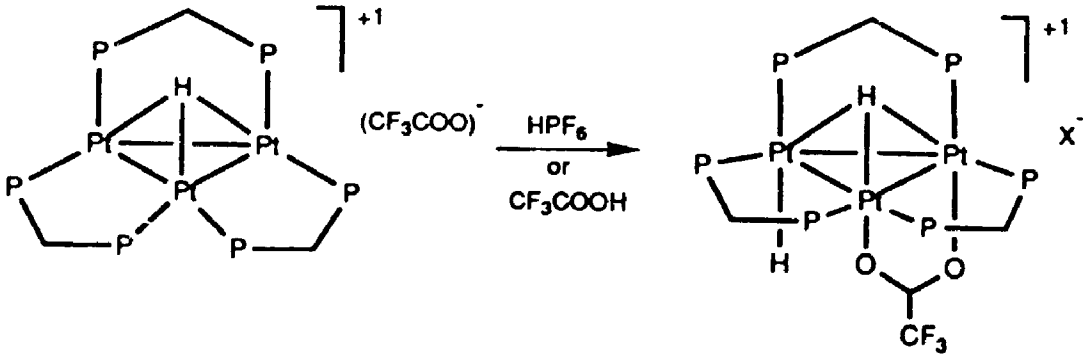

2b

X = CF_3COO, 3b

= PF_6, 3c

Equation 7.2

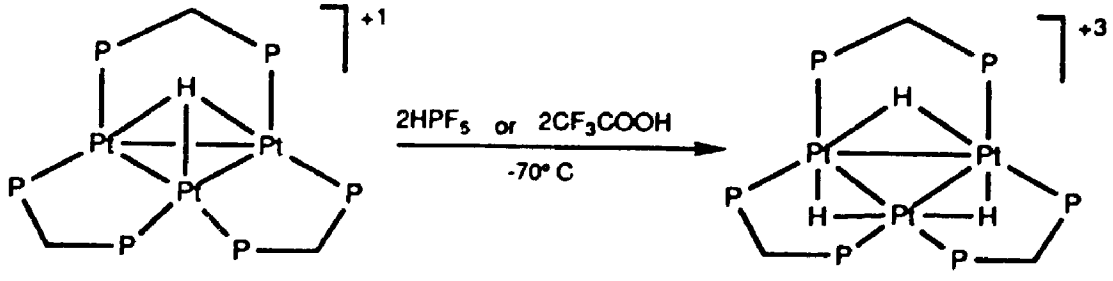

2 4

Equation 7.3

In the above reactions, the three bridging μ-dppm ligands serve to maintain the integrity of the cluster, and avoid the common problem of cluster fragmentation[19], which is prevalent in other triplatinum cluster reactions. For example, reaction of the isoelectronic complex $[Pt_3(\mu\text{-}CO)_3(P^tBu_2Ph)_3]$, with HCl at -50°C results in the fragmentation of the trinuclear cluster, to produce the mononuclear platinum (II) hydride complex, $[PtHCl(CO)(P^tBu_2Ph)]$[20], equation 7.4.

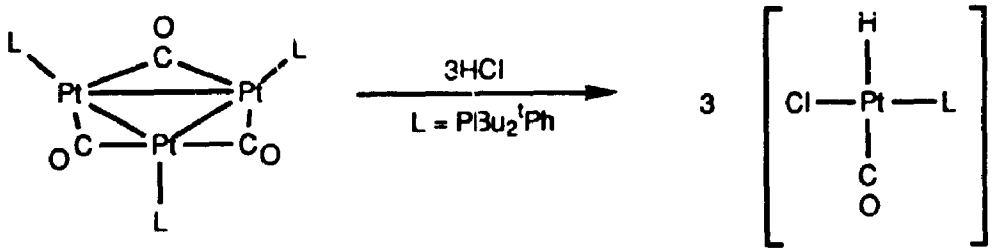

Equation 7.4

7.3.2 Spectroscopic characterization and fluxionality of complexes 3a-3c

Complexes 3a-3c were readily characterized by multinuclear NMR spectroscopy. Complexes 3b and 3c, which have CF_3COO^- as one of the anions, are fluxional in solution at room temperature.

In the $^{31}P\{^1H\}$ NMR spectrum of 3a at room temperature, figure 7.1, the resonance due to the dppm phosphorus atoms appeared as a singlet at δ -5.7,

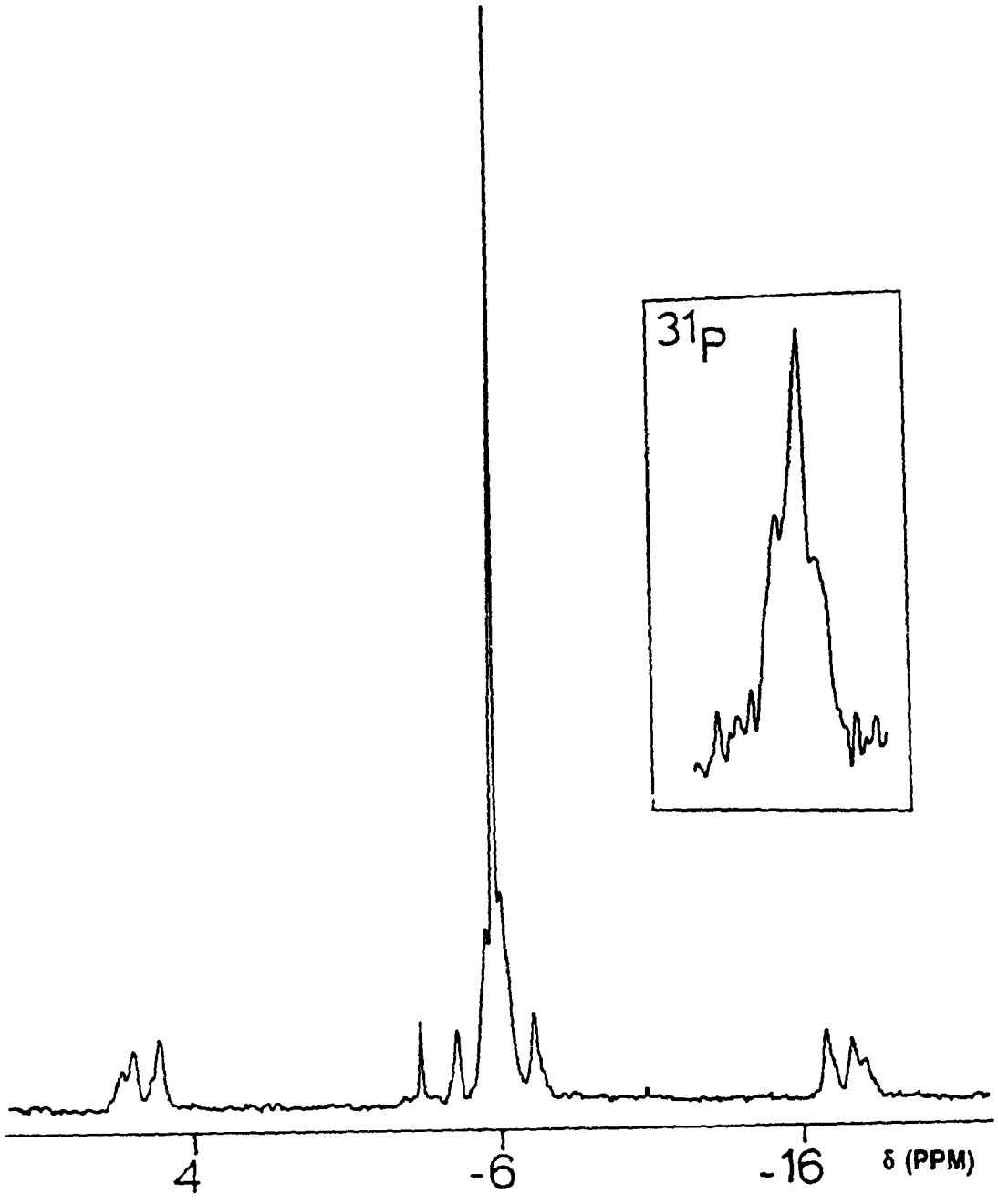

Figure 7.1: $^{31}P(^{1}H)$ NMR spectrum of 3a. Inset shows the ^{1}H-coupled ^{31}P resonance.

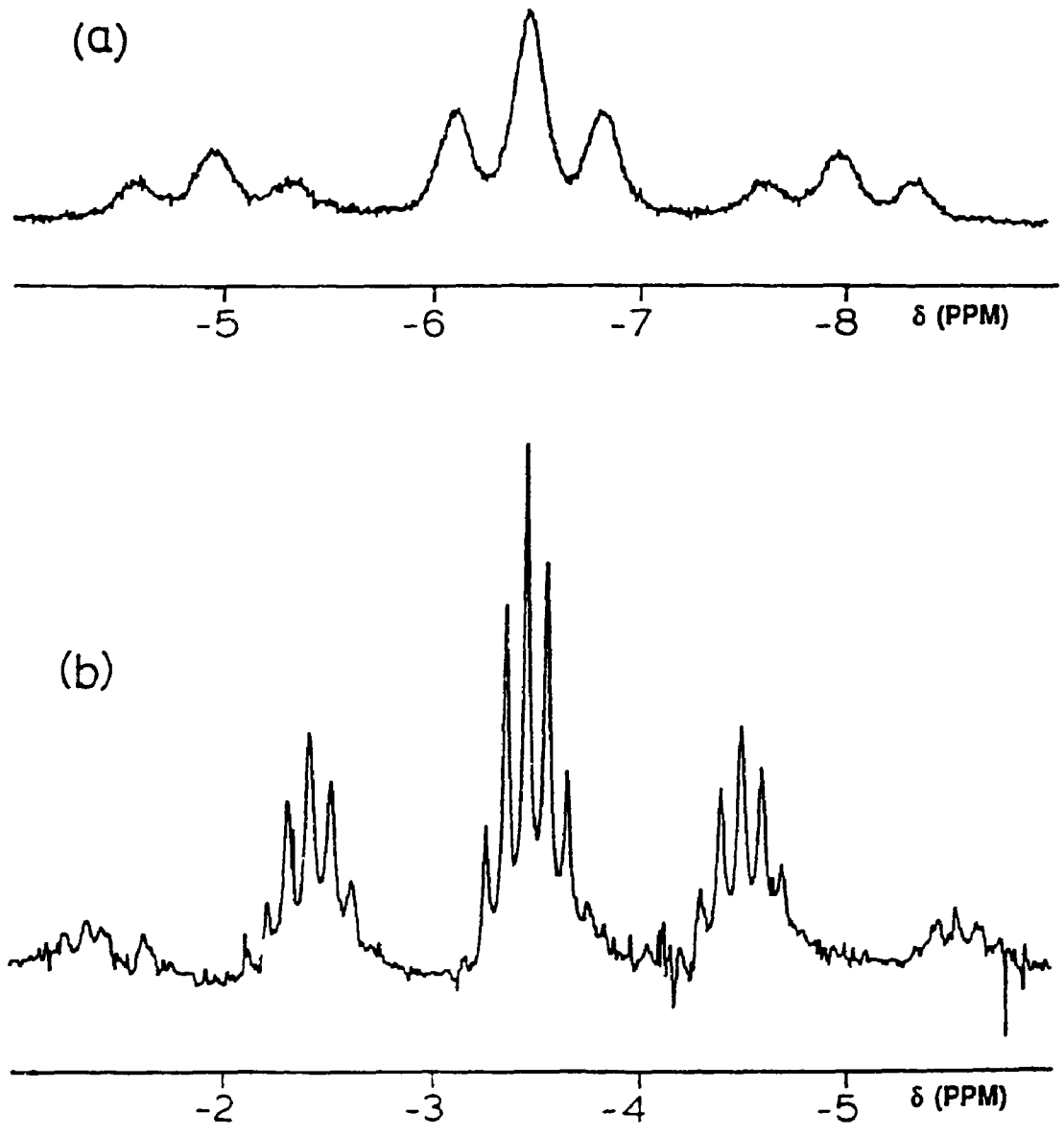

Figure 7.2: Hydride resonances in
(a) ^{1}H NMR spectrum of 4 at -70°C.
(b) ^{1}H NMR spectrum of 3a.

accompanied by satellites due to coupling to ^{195}Pt [$^{1}J(PtP)$ = 3178 Hz, $^{2}J(PtP)$ = 149 Hz], indicating that the six dppm phosphorus atoms are equivalent. The presence of dihydride ligands was confirmed by recording a proton-coupled ^{31}P NMR spectrum of 3a. An extra triplet splitting due to $^{2}J(PH)$ = 20 Hz was observed in this spectrum, figure 7.1.

The hydride signal in the ^{1}H NMR spectrum of 3a, figure 7.2(b), was observed at δ -3.68 as a septet due to coupling to six equivalent phosphorus atoms, $^{2}J(PH)$ = 20 Hz, and with satellites due to coupling to ^{195}Pt [$^{1}J(PtH)$ = 420 Hz] having intensities expected for a $Pt_3(\mu_3\text{-}H)$ group[7] [The inner five lines of the 1:12:52:84:52:12:1 septet was observed, appendix 7]. The resonance due to the methylene protons, CH_2P_2, appeared as a broad singlet at δ 4.0, as expected for the proposed structure 3a, which has a plane of symmetry containing $Pt_3(\mu\text{-}PCP)_3$ unit. We note that the NMR data do not preclude less symmetrical but fluxional structures for 3a, such as a structure with a $Pt_3(\mu_3\text{-}H)H$ unit. However, the NMR data are unchanged at -80°C, and no terminal Pt-H stretch was observed in the IR spectrum, so such structures are improbable for complex 3a.

The NMR data obtained for complexes 3b and 3c at room temperature were similar to that of 3a (see table 7.1 and experimental section). However, at low temperature, -90°C, three different ^{31}P resonances were observed in the

Table 7.1 : $^{31}P\{^{1}H\}$ NMR data of complexes **3a** - **3c** in CD_2Cl_2

(a) At room temperature:

Complex	3a	3b	3c
δP^{a-c}	-5.7	-12.3	-12.1
$^{1}J(PtP)$	3178	3100	3150
$^{2}J(PtP)$	149	235	201
$^{3}J(PP)$	58	120	150

(b) At low temperature:

Complex§	3b	3c
temperature	-90° C	-80° C
δP^{b}	-3.8	-4.8
$^{1}J(PtP^{b})$	2600	2780
$^{2}J(PtP^{b})$	120	¶
$^{3}J(P^{b}P^{b})$	60	¶
δP^{a}	-7.5	-7.9
$^{1}J(PtP^{a})$	4200	4000
$^{3}J(P^{a}P^{c})$		¶
δP^{c}	-24.2	-23.7
$^{1}J(PtP^{c})$	3085	3040
δP_{avg}	-11.9	-12.1

§ The $^{31}P\{^{1}H\}$ Spectral data of **3a** is unchanged even at -90° C

¶ Indicates that the resonances were too broad to obtain coupling constants

$^{31}P\{^{1}H\}$ NMR spectrum, figure 7.3, table 7.1. Scheme 7.1 shows the proposed structure of 3b and 3c along with an NMR labelling scheme. In complex 3b, the resonance due to P^b appeared as a singlet at δ -3.8 with $^{1}J(PtP^b)$ = 2600 Hz. The magnitude of $^{3}J(P^bP^{b'})$ = 60 Hz is obtained from the ^{195}Pt satellite spectra. The resonances due to P^a and P^c appeared as doublets due to coupling with each other,

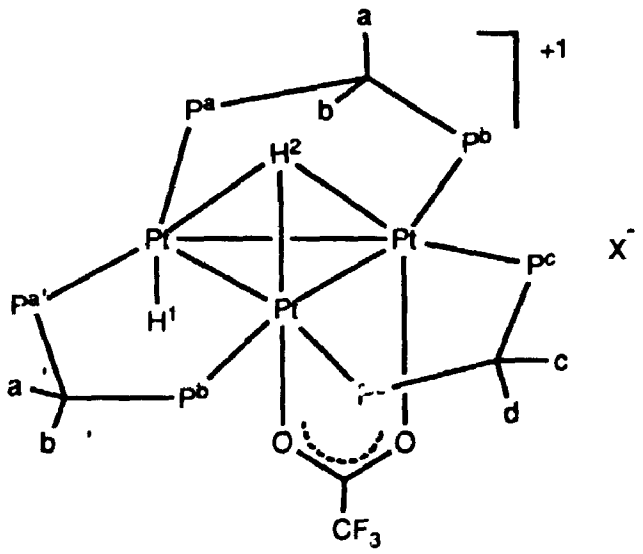

X⁻

CF_3CCO^-, 3b

PF_6^-, 3c

Scheme 7.1: NMR labelling scheme

$^{3}J(P^aP^c)$ = 45 Hz, table 7.1.

In the ^{1}H NMR spectrum of 3c at -90°C, the resonance due to hydride is observed at δ -3.5 as a broad multiplet with broad ^{195}Pt satellites. The hydride resonances, H^1 and H^2, were not resolved as individual peaks at this temperature. However, the signal due to the CH_2P_2 protons, which appeared as a singlet at room temperature (δ5.23), splits into four different resonances at -90°C, in the intensity ratio 2:2:1:1, as expected for

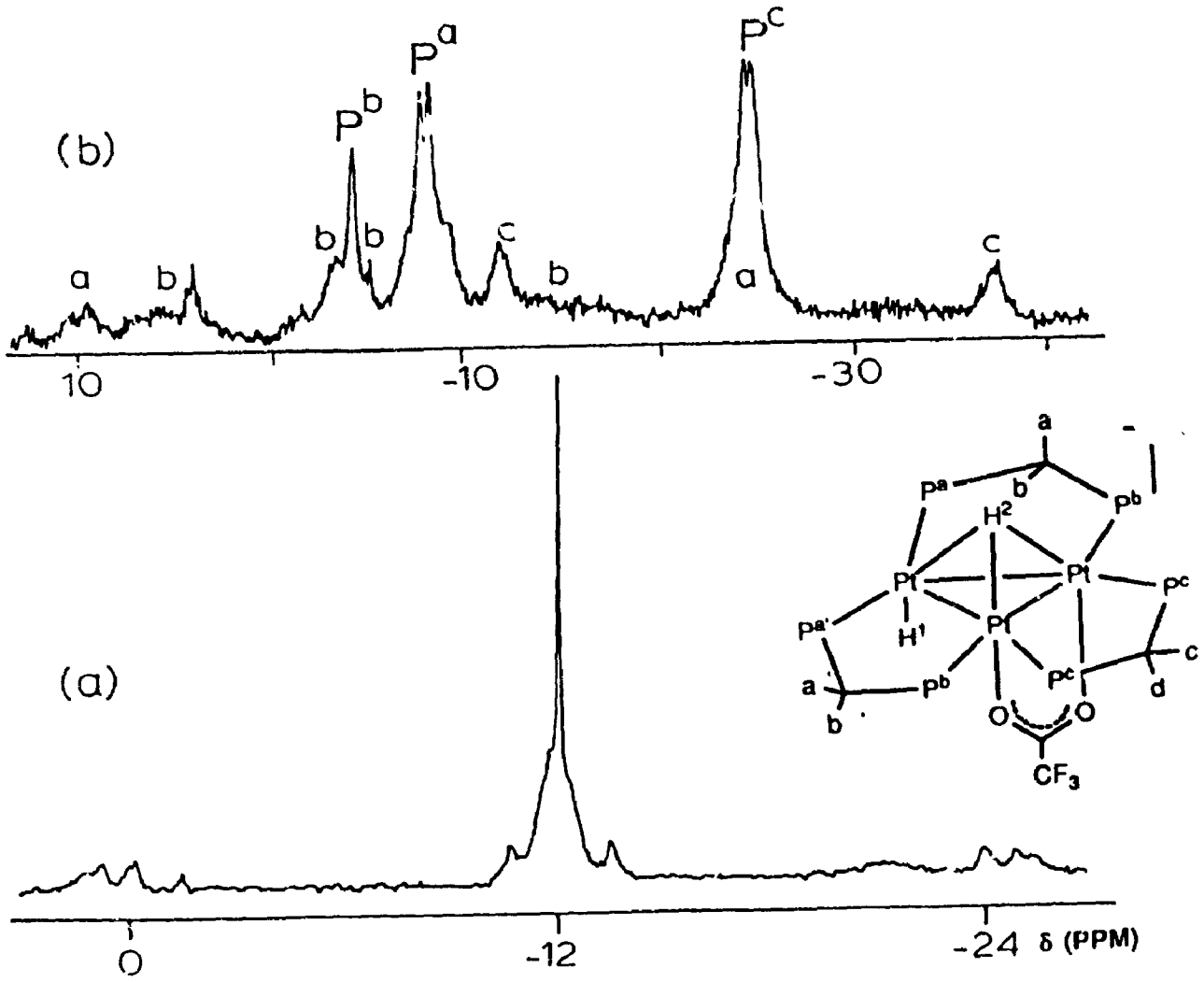

Figure 7.3: $^{31}P\{^1H\}$ NMR spectrum of 3b; (a) at 20°C and (b) at -90° C.

the static structure 3c, see experimental section.

The above NMR data of 3b and 3c are consistent with a fluxional process, as shown in equation 7.5, involving rapid and reversible dissociation of the CF_3COO^- ligand. Thus, the intermediate is a complex containing a symmetrically triply bridged, bicapped, $Pt_3(\mu_3\text{-}H)_2$ group. Equation 7.5 shows that the CF_3COO^- ligand reversibly coordinates to either the top or bottom face of the $Pt_3(\mu\text{-dppm})_3$ triangle, so that the time-averaged structure appears to contain a $Pt_3(\mu_3\text{-}H)_2$ unit.

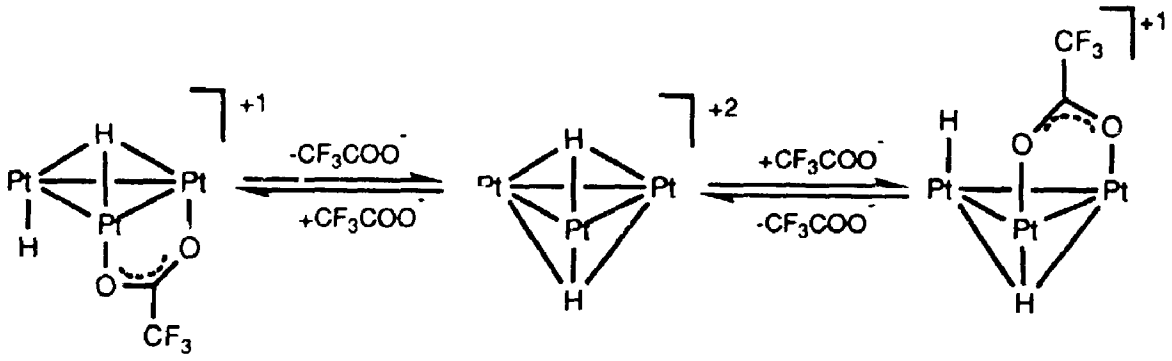

Equation 7.5: μ-dppm ligands omitted for clarity

Thus, we observe that in the hexafluorophosphate salt, 3a, both the hydride ligands cap the Pt_3 triangular face as triply bridging ligands to form a complex which has a $Pt_3(\mu_3\text{-}H)_2$ unit in its ground state structure. The trifluoroacetate salts, 3b and 3c, have a less symmetrical structure, containing a $Pt_3(\mu_3\text{-}H)H$ unit, and the CF_3COO^- is probably coordinated to the triplatinum centre. The role of this anion acting as a bridging ligand is not uncommon,

and has been observed in several binuclear and trinuclear complexes.[29] For example the tripalladium complex[21], $[Pd_3(\mu_3\text{-}CO)(\mu\text{-}dppm)_3](CF_3COO)_2$, contains one CF_3COO^- ion lying close to the capping site of the Pd_3 unit, on the other side of the μ_3-CO ligand. Although the Pd-O distances are very long (2.8 - 3.1 Å), on the basis of additional evidence reported elsewhere[22], this compound has been formulated as $[Pd_3(\mu_3\text{-}CO)(\mu\text{-}dppm)_3(\mu_3\text{-}CF_3COO)](CF_3COO)$.

7.3.3 Spectroscopic characterization of $[Pt_3(\mu\text{-}H)_3(\mu\text{-}dppm)_3]^{+3}$, 4

Complex 4 was characterized in solution by low temperature ^1H, $^{31}P\{^1H\}$ and ^{31}P NMR spectroscopy. Scheme 7.2 shows the NMR labelling scheme for 4.

The $^{31}P\{^1H\}$ NMR spectrum of 4 at -70°C, figure 7.4, shows a single ^{31}P resonance appearing as a singlet at

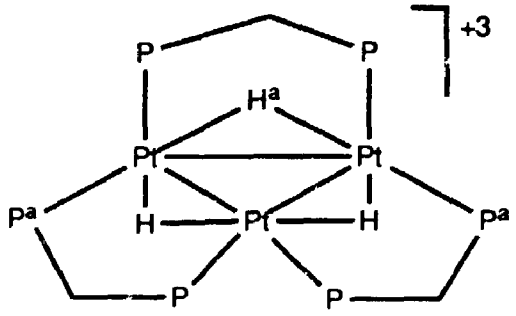

Scheme 7.2: NMR labelling scheme for **4**

δ -3.28 with satellites due to coupling to ^{195}Pt [$^1J(PtP)$ = 3160 Hz, $^2J(PtP)$ = 151 Hz]. The proposed structure 4 has a single hydride, H^a, for each pair of

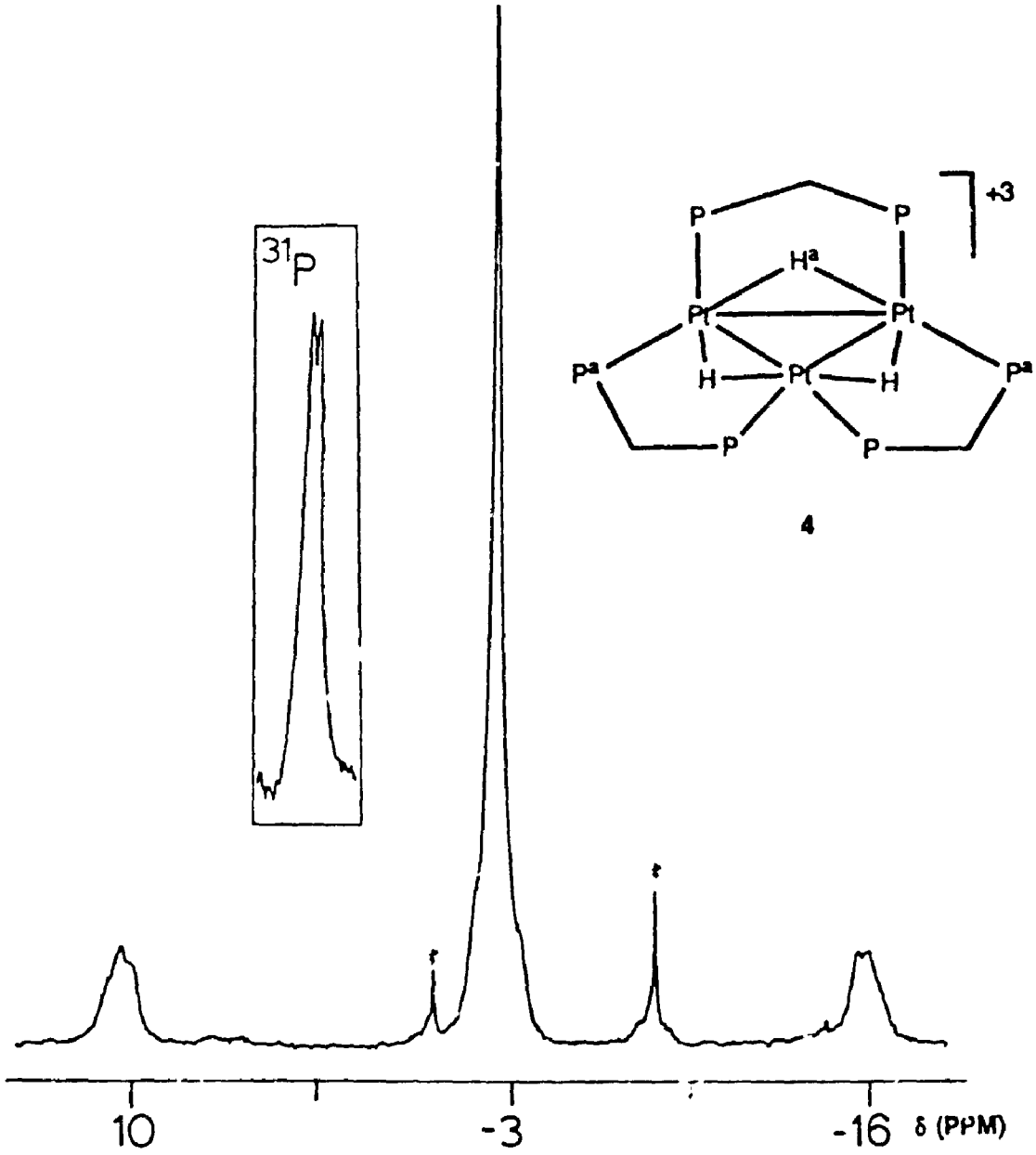

Figure 7.4: $^{31}P\{^{1}H\}$ NMR spectrum of 4 at -70°C. Inset shows the ^{1}H-coupled ^{31}P resonance.

phosphorus atoms, P^a, of the bridging dppm ligands. This was confirmed by recording a proton-coupled ^{31}P NMR spectrum. An extra doublet splitting due to $^2J(P^aH^a)$ = 70 Hz in the ^1H-coupled spectrum was observed, figure 7.4.

In the ^1H NMR spectrum of 4 at -70°C, the signal due to hydrides was observed at δ -6.8, as a triplet due to trans-like coupling to two equivalent phosphorus atoms, P^a, $^2J(P^aH^a)$ = 70 Hz, figure 7.2(a), and with satellites due to coupling to ^{195}Pt [$^1J(PtH)$ = 604 Hz] having the intensities expected for a $Pt_2(\mu\text{-}H)$ group (only the inner three lines of the 1:8:18:8:1 quintet are observed, appendix 7)

The resonance due to the CH_2P_2 protons appeared as a singlet at δ 4.83, as expected for a planar $[Pt_3(\mu\text{-}PCP)_3(\mu\text{-}H)_3]$ unit. The intensity ratio of CH_2P_2 protons to the hydridic protons is 2:1 indicating that there are three hydride ligands in complex 4.

All these observations support the proposed structure of 4, which contains three hydride ligands located in the $Pt_3(\mu\text{-}dppm)_3$ plane, each bridging between

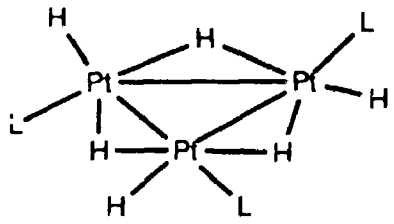

L = PBu^t_3

9

platinum atoms along an edge of the Pt_3 triangle. Thus,

protonation of 3 evidently converts the μ_3-hydrides to μ_2-hydrides. Complex 4 is analogous to the known complex[9], $[Pt_3(\mu\text{-}H)_3(P^tBu_2)_3]$, 9, which has terminal hydrides in place of three of the phosphorus atoms in 4.

7.3.4 Interconversion of 2, 3 and 4:

The trihydride complex, 4, was stable in solution only at temperatures below -60°C. On warming to room temperature, the NMR spectra of the resulting solution shows a quantitive conversion of 4 to the dihydride complex, 3. Upon evaporating the solution of 3 to dryness and washing with diethyl ether, 3 is deprotonated to yield the monohydride complex 2. This sequence of reversible protonation and deprotonation[16] reactions is shown in equation 7.6.

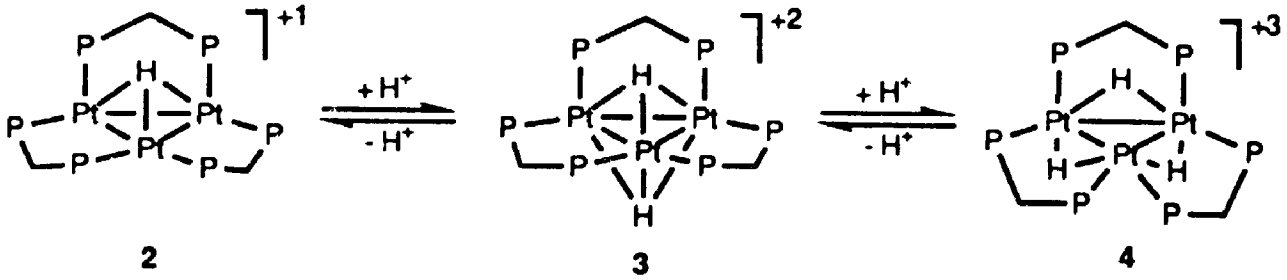

Equation 7.6

7.3.5 Reaction of 3 with CO:

Earlier work[23] has shown that the reaction of CO with the trihydrido diplatinum "A" frame complex[24], $[Pt_2(\mu\text{-}H)H_2(\mu\text{-}dppm)_2]$, 6, results in the quantitative

elimination of hydrogen and the formation of a hydrido-carbonyl complex, $[Pt_2(\mu\text{-dppm})_2H(CO)]^{+1}$, 8, equation 7.7.

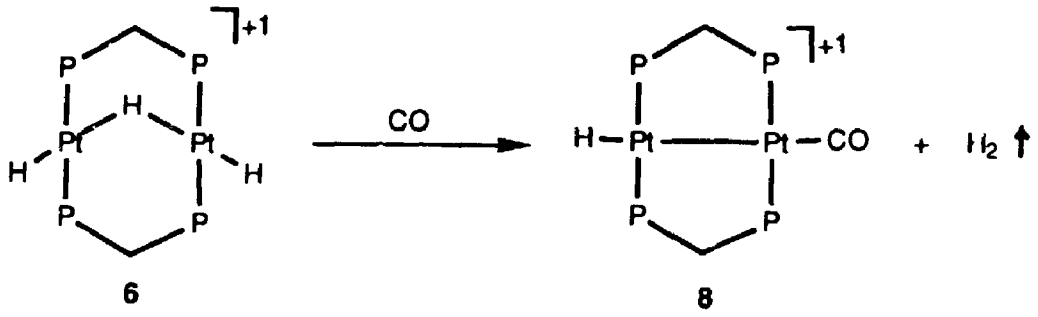

6 8

Equation 7.7

When the dihydride complex, 3, is put under a positive pressure of CO, quantitative elimination of hydrogen is observed along with the formation of the parent carbonyl cluster, $[Pt_3(\mu_3\text{-CO})(\mu\text{-dppm})_3]^{+2}$, 1 and $[Pt_3(\mu_3\text{-CO})(\mu\text{-dppm})_3(CO)]^{+2}$, 7, equation 7.8. Complexes 1 and 7 were characterized by $^{31}P\{^1H\}$ and $^{13}C\{^1H\}$ NMR spectroscopy and the NMR data obtained are in agreement with the reported work[25].

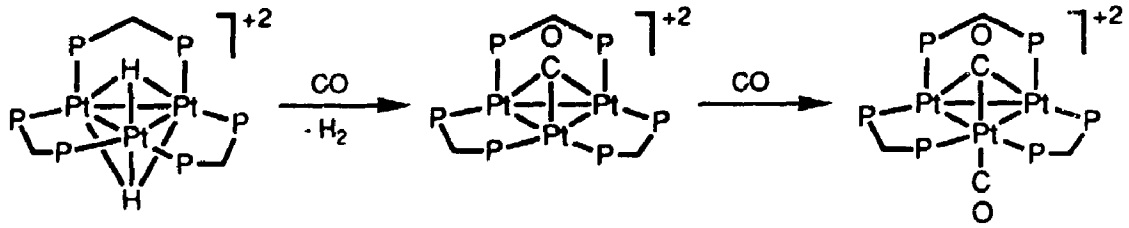

3 1 7

Equation 7.8

Attempts were made to study whether the process of elimination of hydrogen from 3 was an intra- or inter-molecular process. An equimolar quantity of 3b (H_2) and 3b** (** = D_2) were reacted with CO in a sealed tube. After the reaction was over, the residual gas in the tube was analysed by FAB mass spectrometry. The peak due to hydrogen (m/e = 2) appeared as the major peak. A similar experiment with 3b* (* = HD) and CO also yielded hydrogen as the major product. The peak due to HD (m/e = 3) was observed at less than 10 mole percent. These results indicate that the hydrides of 3 scramble rapidly with other protons in the solvent or within the molecule (possibly with the methylenic protons, CH_2P_2, of the dppm ligands which are mildly acidic in nature). Thus, further studies on the mechanistic aspects of the process of elimination of hydrogen from 3 could not be pursued.

7.3.6 Reaction of 3 with phosphines and phosphites:

7.3.6.1 Synthesis of $[Pt_3(\mu\text{-}H)H(\mu\text{-}dppm)_3L]^{+2}$, 5a-5d:

The ligand-induced reductive elimination of hydrogen from the trihydrido 'A' frame complex, 6, is well documented in the literature[18]. Thus, reaction of phosphines (L = PPh_3, $PMePh_2$, PMe_2Ph or η-dppm) with 6 follows one of the reaction pathways shown in scheme 7.3.

The reaction has been shown to proceed through an intermediate, $[Pt_2(\mu\text{-}H)H_2(\mu\text{-}dppm)_2L]^+$, from which intramolecular hydrogen loss occurs.

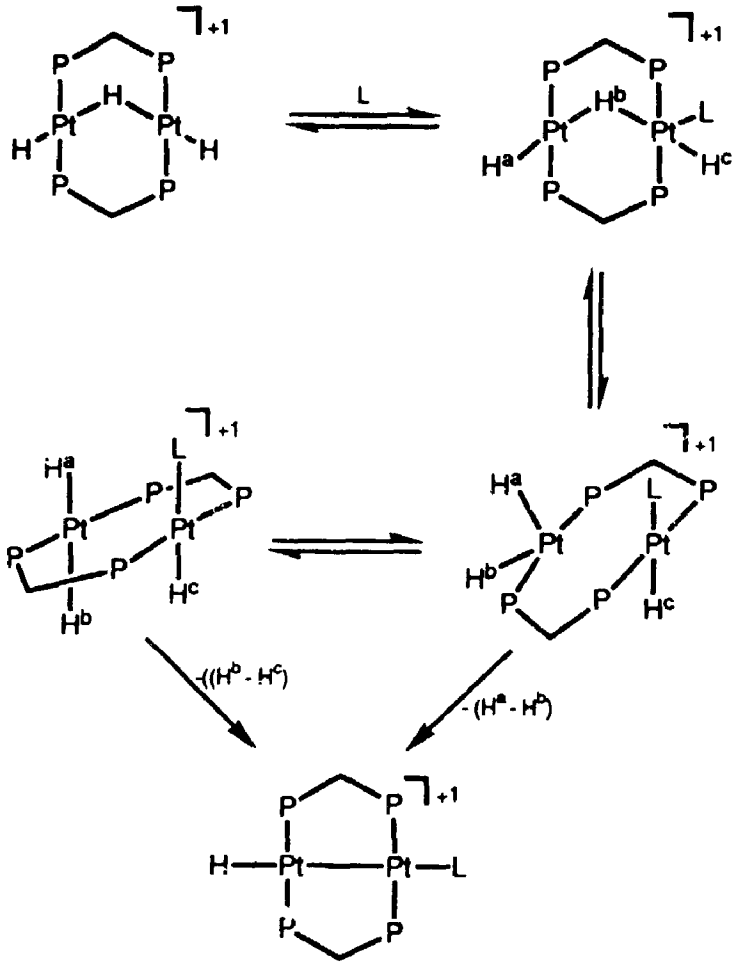

8

Scheme 7.3

Reaction of the triplatinum complex, 3c, with PPh_3 at room temperature resulted in the formation of the diplatinum complex, $[Pt_2(\mu\text{-dppm})_2H(PPh_3)]^+$, 8d, in quantitative yield. The NMR data of the product, 8d, were in full agreement with earlier work. Thus, a cluster fragmentation reaction was observed.

An intermediate complex, $[Pt_3(\mu\text{-H})H(\mu\text{-dppm})_3(PPh_3)]^{+2}$, 5d, was observed when the reaction of 3c with PPh_3 was carried out at low

temperature, -20°C, scheme 7.4. On allowing the solution to warm to room temperature, 5d disintegrates to yield the diplatinum (I) complex, 8d.

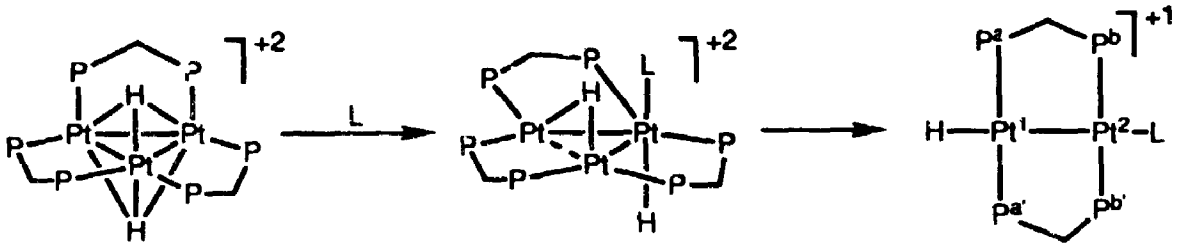

3c

L

L = PPh_3, 8d

$P(OMe)_3$, **5a**
$P((OEt)_3$, **5b**
$P(OPh)_3$, **5c**
PPh_3, **5d**

Scheme 7.4

Reaction of 3c with the less bulky phosphite ligands $P(OMe)_3$, $P(OEt)_3$ and $P(OPh)_3$, resulted in the formation of $[Pt_3(\mu\text{-}H)H(\mu\text{-}dppm)_3\{P(OR)_3\}]^{+2}$, 5a-5c, (scheme 7.4) which were thermally stable and could be isolated in analytically pure form. Even after four weeks, complexes 5a-5c did not rearrange in solution to yield the diplatinum complexes 8a-8c.

7.3.6.2 Spectroscopic characterization of 5a-5d

Complexes 5a-5d were characterized unambiguously in solution by multinuclear NMR spectroscopy. The NMR labelling scheme is shown in scheme 7.5. The $^{31}P\{^1H\}$ and ^1H NMR data are given in tables 7.2 and 7.3 respectively.

Both the ^1H and ^{31}P NMR spectra are characteristic

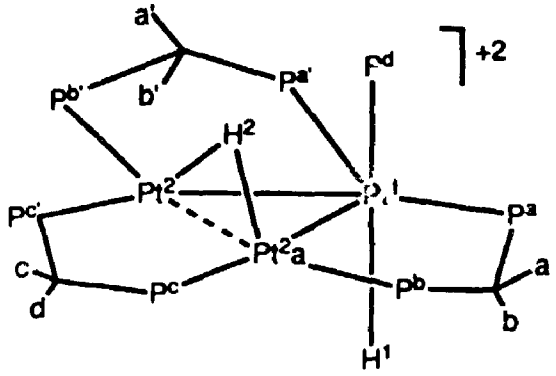

Scheme 7.5: NMR labelling for complexes **5a - 5d**

of the proposed structure 5, which has an apparent plane of symmetry passing through the atoms H^2, P^d, Pt^1 and H^1.

The $^{31}P\{^1H\}$ NMR spectrum of 5b, figure 7.5, will be discussed as a typical example. The spectrum consists of four ^{31}P resonances in a 1:2:2:2 intensity ratio. The resonance due to P^b appears as a singlet at δ -2.0, $^1J(PtP)$ = 3750 Hz. However, it should be noted that the doublet splitting due to $^3J(P^bP^{b'})$ and the long-range $^2J(Pt^2P^b)$ coupling in the ^{195}Pt satellites are absent. This suggests that there is no Pt-Pt bond or only weak Pt-Pt bonding between these two platinum atoms, Pt_a^2 and Pt_b^2. The phosphorus atoms, P^a and P^c, couple to each other and appear as an AB multiplet (δ P^a = -20.5, $^1J(Pt^1P^a)$ = 1670 Hz; δ P^c = -10.0, $^1J(Pt^2P^c)$ = 2490 Hz).

The resonance due to the $P(OEt)_3$ ligand, P^d, was at low-field (δ 101.2) and appeared as a 1:4:1 triplet (due to coupling to Pt^1, $^1J(Pt^1P^d)$ = 3550 Hz). The value of $^1J(Pt^1P^d)$ is lower than that observed in other triplatinum

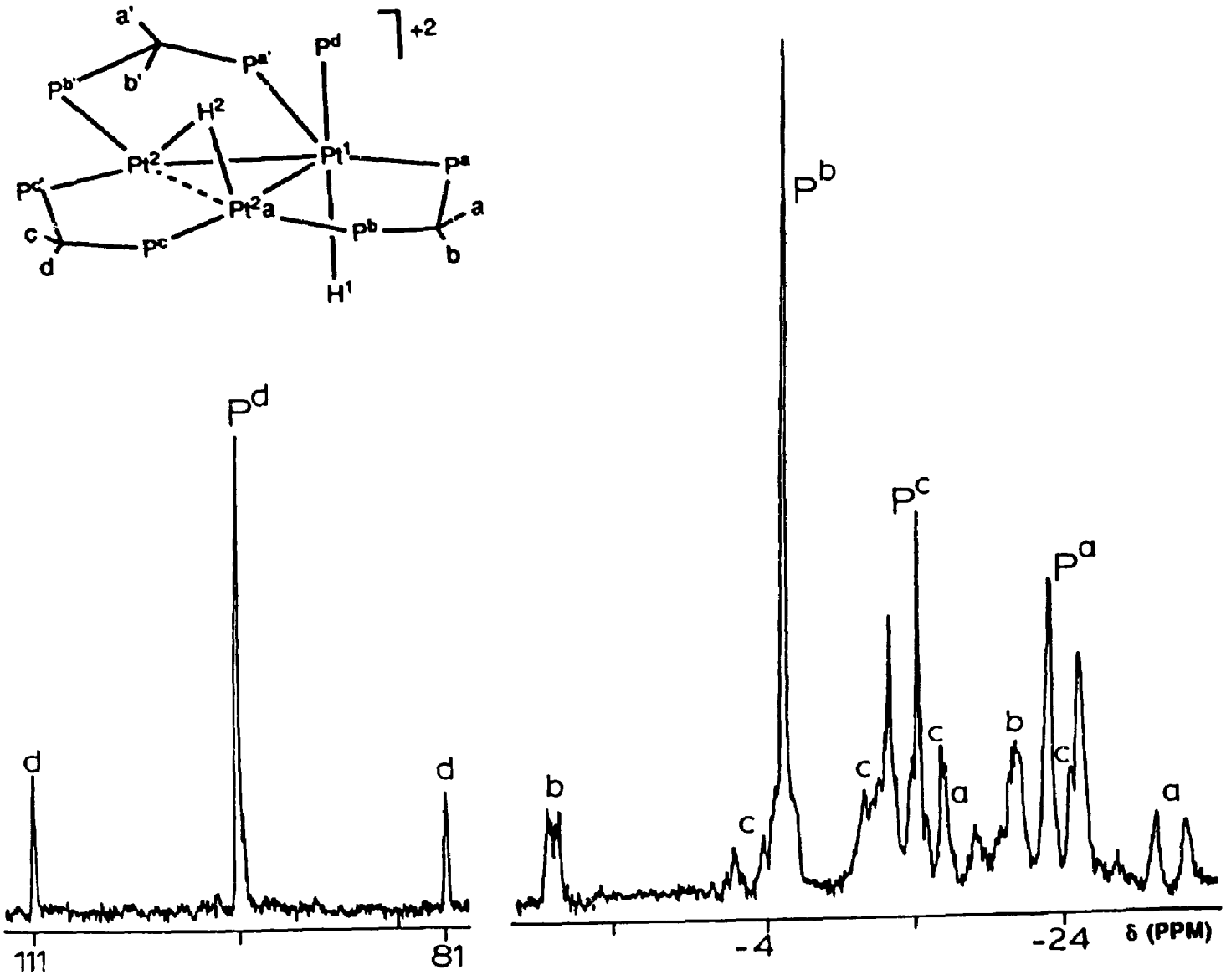

Figure 7.5: $^{31}P\{^{1}H\}$ NMR spectrum of 5b.

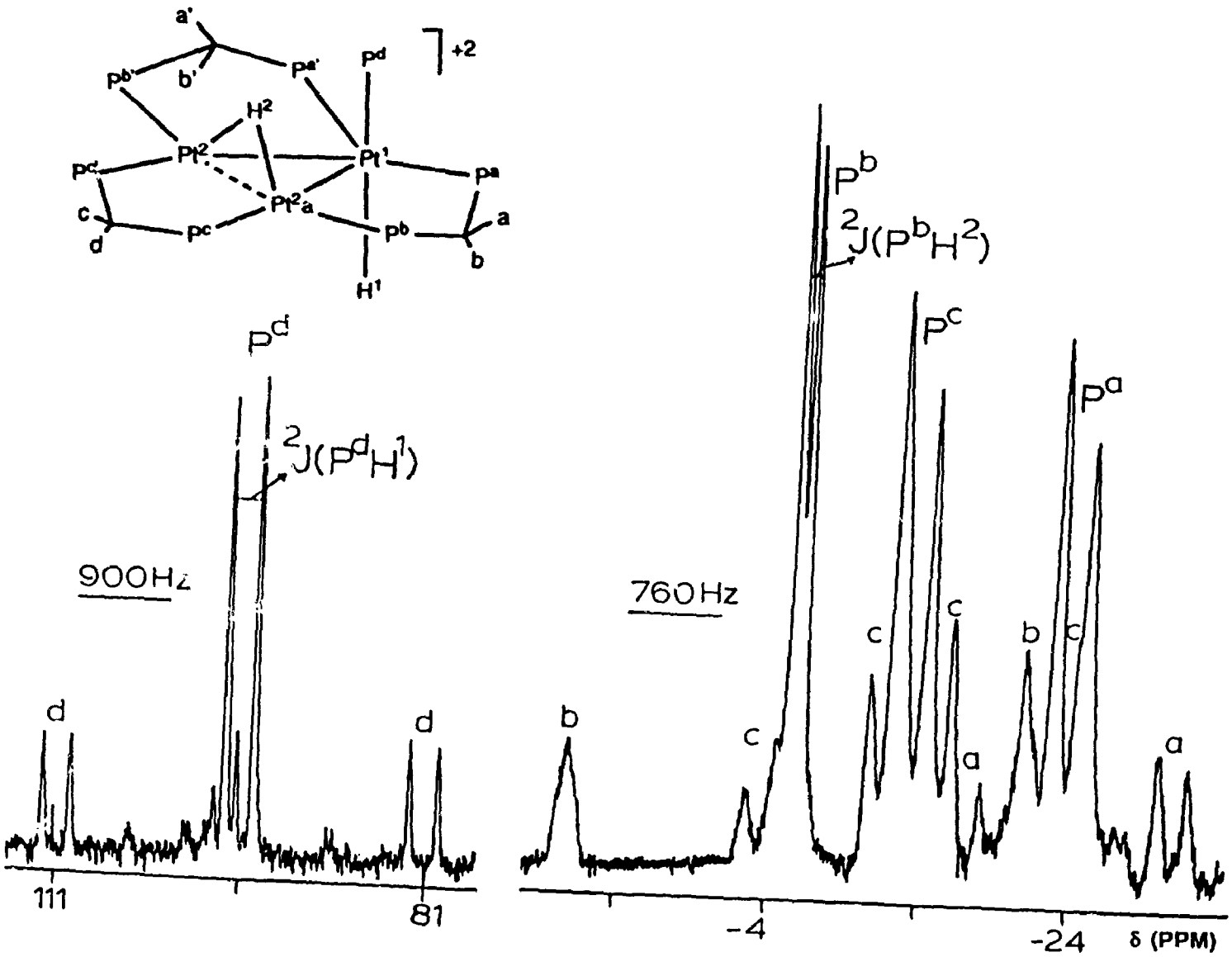

Figure 7.6: ^1H-coupled ^{31}P NMR spectrum of 5b.

Table 7.2 : $^{31}P\{^{1}H\}$ NMR data of complexes **5a - 5d** in CD_2Cl_2

Complex	5a	5b	5c	5c£	5d§
δP^a	-27.1	-25.3	-24.6	-25.5	-39.6
$^1J(Pt^1P^a)$	1715	1670	1750	1700	¶
$^2J(Pt^1P^a)$	490	610	475	500	¶
$^3J(P^aP^c)$	230	223	213	220	380
δP^b	-7.4	-6.8	-6.5	-7.0	-25.2
$^1J(Pt^2P^b)$	3745	3750	3750	3660	¶
$^2J(P^bH^2)$‡	265	267	290	280	¶
δP^c	-15.1	-14.8	-12.9	-13.2	-17.6
$^1J(Pt^2P^c)$	2485	2490	2550	2480	2600
δP^d	102.2	96.4	81.6	102.2	1.8
$^1J(Pt^1P^d)$	3550	3550	3875	3530	¶
$^2J(P^dH^1)$‡	80	70	80	80	¶

£ at -40° C § at -20° C ‡ Data obtained from ^1H-coupled ^{31}P NMR spectrum\
¶ Indicates that the resonances were too broad to obtain coupling constants

Table 7.3: ^1H NMR data of complexes **5a - 5c** in CD_2Cl_2

Complex	5a£	5b	5c£
δH^1§	-4.52	-4.83	-3.74
$^1J(Pt^1H^1)$	730	720	732
$^2J(Pt^2H^1)$	90	90	101
$^2J(P^dH^1)$	268	267	292
$^2J(P^aH^1)$	10.5	10.0	14.0
δH^2‡	-2.91	-2.92	-2.65
$^1J(Pt^2H^2)$	662	650	660
$^2J(Pt^2H^2)$	80	76	80
$\delta P(OCH_3)$	3.68	1.25 (OCH_2CH_3) 3.99 (OCH_2CH_3)	- -
J(PH)	11.5	7.0	-
J(HH)	-	7.0	-
δCH^aH^b	4.42, 4.56	4.76, 4.65	4.30, 4.77
$^2J(H^aH^b)$	16	14	10
δCH^cH^d	3.39, 3.78	3.02, 4.41	6.09, 6.22
$^2J(H^cH^d)$	7	9	9

£ at -40° C § doublet of triplets ‡ triplet

complexes.[27] This is probably due to the strong trans-influence of the hydride ligand, H^1. The presence of a single hydride ligand trans to P^d was confirmed by recording a ^1H-coupled ^{31}P NMR spectrum. An extra doublet splitting due to $^2J(P^dH^1) \simeq 267$ Hz was observed in the spectrum, figure 7.6. $^2J(PH)$ values of this magnitude are also observed in other platinum complexes which contain a hydride ligand trans to a phosphorus donor.[28] The ^1H-coupled ^{31}P NMR spectrum also showed an extra doublet splitting in the resonance due to P^b. This PH coupling is expected to be the trans-like coupling between atoms P^b and H^2, $^2J(P^bH^2) \simeq 76$ Hz. The J(PH) coupling of a similar magnitude is also observed in 9.[9]

The ^1H NMR spectrum of 5b at room temperature contains four different resonances in the CH_2P_2 region with relative intensities 2:2:1:1 as expected for the proposed structure 5, table 7.3. The resonance due to the hydridic proton, H^1, appears at δ -4.8 as a doublet of triplets, figure 7.7, due to coupling to the phosphorus atoms P^d and P^a [$^2J(P^dH^1) = 267$ Hz, $^2J(P^dH^1) = 10$ Hz] and with quarter intensity satellites due to coupling to ^{195}Pt [$^1J(Pt^1H^1) = 720$ Hz, $^2J(Pt^2H^1) = 90$ Hz]. The magnitude of $^1J(PtH)$ is comparable to hydrido-platinum (II) phosphine complexes in which hydride is *trans* to phosphorus.[28] The second hydride resonance due to H^2 was observed at δ -2.9 as a triplet due to coupling to the two phosphorus atoms, P^b and $P^{b'}$, $^2J(P^bH^2) = 76$ Hz, and with satellites due to

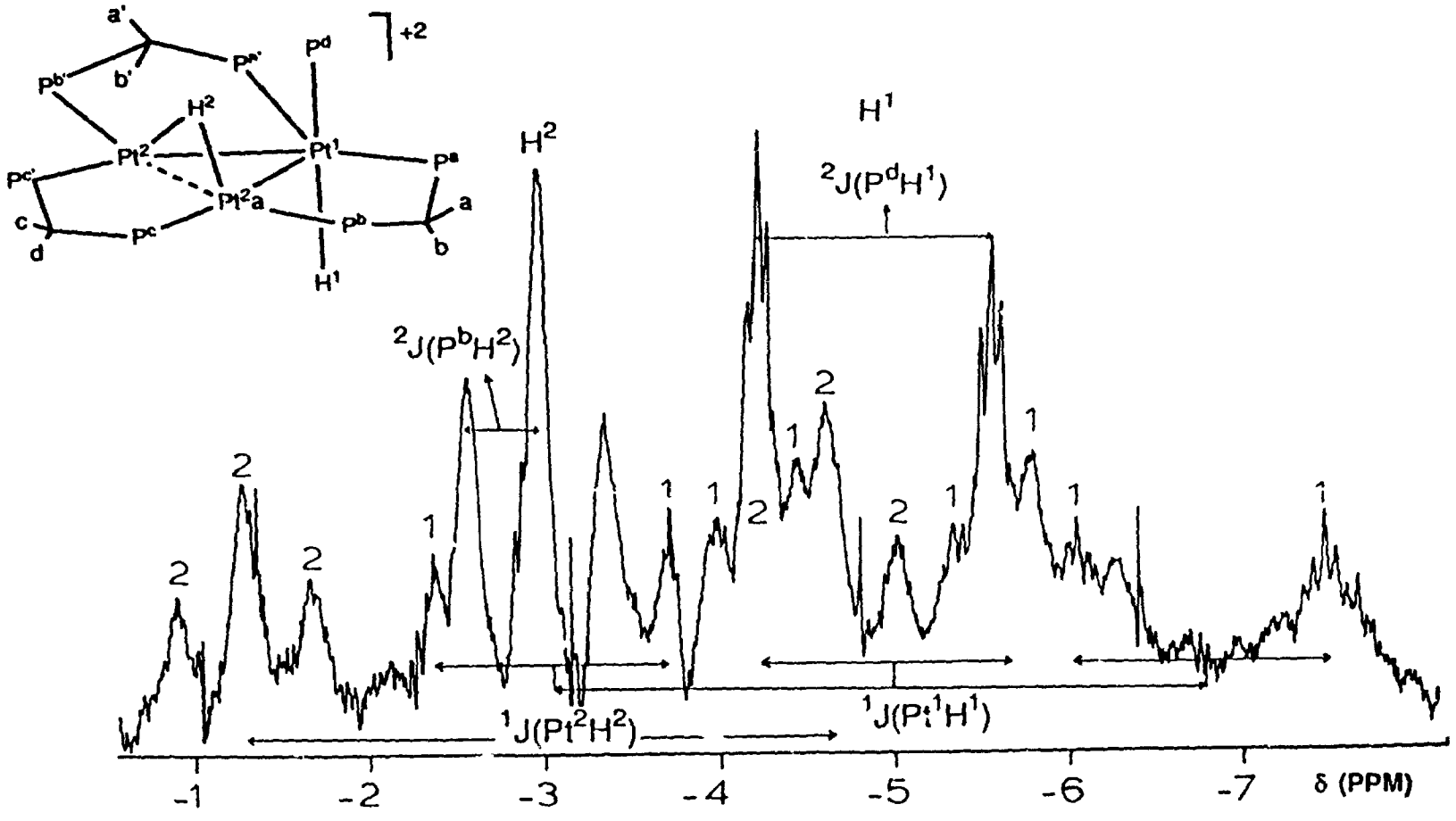

Figure 7.7: ^{1}H NMR spectrum of 5b showing hydride resonances.

coupling to ^{195}Pt [$^{1}J(Pt^{2}H^{2}) = 650$ Hz] having the intensities 1.0 : 2.2 : 1.0, indicating that the hydride H^{2} is bridged between Pt_a^{2} and Pt_b^{2} in a $Pt_2(\mu\text{-}H)$ bonding mode (i.e, only the inner three lines of the 1:8:18:8:1 quintet are observed, appendix 7).

The above mentioned NMR spectral data support the proposed structure of the 44 electron complexes, 5a-5d, and this work illustrates the value of analysis of the multiplicities due to ^{195}Pt couplings in elucidating the molecular structure of platinum clusters.

7.4 SUMMARY AND CONCLUSIONS

The cluster complex $[Pt_3(\mu_3\text{-}H)(\mu\text{-}dppm)_3]^{+}$, 2, can be protonated rapidly and reversibly to give $[Pt_3(\mu_3\text{-}H)_2(\mu\text{-}dppm)_3]^{+2}$, 3a and $[Pt_3(\mu\text{-}H)_3(\mu\text{-}dppm)_3]^{+3}$, 4, thus providing a route to novel platinum cluster hydrides. The interconversion reaction $2 \rightleftharpoons 3$ clearly shows how electrophilic ligand substitution at the cluster can occur by a bimolecular stepwise mechanism[16]. Similar reactions were also observed in Pt_3Au clusters (chapter 5). Such clusters are important as models for intermediates in heterogeneous platinum-catalysed reactions but are still rare compounds[7,10].

The dihydride complexes 3b and 3c have presumably a CF_3COO^{-} anion coordinated to the platinum centres and thus yield triplatinum clusters containing a triply bridged

hydride and a terminal hydride ligand. 3b and 3c are fluxional in solution at ambient temperature. The fluxional process is thought to involve rapid and reversible coordination of the CF_3COO^- anion to the Pt_3 triangle and simultaneously, the hydrides switch their bonding from a terminal mode to triply bridging mode.

This work has demonstrated that "$Pt_3(dppm)_3$" can be protonated either at the centre (as in 2 and 3a) or at the edge (as in 4). This is consistent with the isolobal relationship with cyclopropane[26] which is protonated at an edge (or a corner).

If the capped compounds 2 and 3 are considered to be formed by consecutive additions to the a_1 HOMO of $Pt_3(dppm)_3$ (for a detailed discussion see chapter 5 and elsewhere[26]), then the individual Pt-H bonds are expected to be weaker for the dicapped compounds. This is reflected in the much reduced coupling constants $^1J(PtH)$ in 3 (420 Hz) compared to 2 (710 Hz).

Reaction of 3a-3c with CO resulted in quantitative elimination of hydrogen and the subsequent formation of the parent carbonyl cluster, 1. Attempts to study the reaction pathway were futile due to scrambling of the hydridic protons in 3 with those in solvent and/or the methylenic groups of the dppm ligands.

Reaction of the dihydride complex 3 with the phosphine and phosphite ligands resulted in the formation of adducts 5a-5d. The $(\mu_3\text{-}H)_2$ ligands in 3 convert to a

doubly bridging, (μ_2-H), and a terminal ligand in 5 in order to accommodate the incoming phosphorus donor. This arrangement presumably reduces the steric congestion in the resulting complex, 5. The adduct 5 is thermally stable when the phosphorus donor is a phosphite ligand. However, when the ligand is a bulky phosphine ligand, PPh_3, the adduct 5d is observed only as a kinetic product. 5d reacts further to yield the diplatinum (I) complex, 8d. Thus, by modifying the added ligand, we have successfully isolated a reactive intermediate in the cluster fragmentation process.

7.5 REFERENCES

1 G.G. Libowitz, *'The solid state chemistry of binary metal hydrides'*, Benjamin, New york, 1965; G.C. Bond, *'Catalysis by metals'*, Academic press, New York, (1962).

2. J.J. Reily, G.D. Sandrock, *Scientific American.*, 242 (1980) 98

3. A.M. Baro, H. Ibach, H.D. Brachman, *Surf.Sci.*, 88 (1979) 384

4. A.M. Baro, H. Ibach, *Surf. Sci.*, 92 (1980) 237

5. J. Lee, J.P. Calvin, L. Wharton, *Surf. Sci.*,130 (1983) 1

6. C.M. Sayers, *Surf. Sci.*, 143 (1984) 411

7. B.R. Lloyd, R.J. Puddephatt, *J. Amer. Chem. Soc.*, 107 (1985) 7785

8 L.M. Venanzi, *Coord. Chem. Rev.*, 43 (1982) 251; D.S. Moore, S.D. Robinson, *Chem. Soc. Rev.*, 12 (1983) 415; R. Bau, T.F. Koetzle, *Pure & Appl. Chem.*, 50 (1978) 55

9. P.W. Frost, J.A.K. Howard, J.L. Spencer, D.G. Turner, D. Gregson, *J. Chem. Soc., Chem. Commun.*, (1981) 1104

10. D. Carmichael, P.B. Hitchcock, J.F. Nixon, A. Pidcock, *J. Chem. Soc., Chem. Commun.*, (1988) 1554

11. J.A.K. Howard, J.L. Spencer, D.G. Turner, *J. Chem. Soc., Dalton Trans.*, (1987) 259

12 D. Gregson, J.A.K. Howard, M. Murray, J.L. Spencer, *J. Chem. Soc., Chem. Commun.*, (1981) 716

13 R.J. Goodfellow, E.M. Hamon, J.A.K. Howard, D.G. Turner, *J. Chem. Soc., Chem. Commun.*, (1984) 1604

14 J.F. Almeida, K.R. Dixon, C. Eaborn, P.B. Hitchcock, A. Pidcock, J. Vinaixa, *J. Chem. Soc., Chem. Commun.*, (1982) 1315

15 A.L. Casalnuovo, L.H. Pignolet, J.W.A. Vander Velden, J.J. Bour, J.J. Steggerda, *J. Amer. Chem. Soc.*, 105 (1983) 5957

16 R. Ramachandran, N.C. Payne, R.J. Puddephatt, *J. Chem. Soc., Chem. Commun.*, (1989) 128

17 G. Ferguson, B.R. Lloyd, R.J. Puddephatt, *Organometallics*, 5 (1986) 344

18 M.P. Brown. J.R. Fisher, Lj. Manojlovic-Muir, K.W. Muir, R.J. Puddephatt, *J. Chem. Soc., Chem. Commun.*, (1979) 931; M.P. Brown, J.R. Fisher, R.H. Hill, R.J. Puddephatt, K.R. Seddon, *Inorg. Chem.*, 20 (1981) 3516

19 E.L. Muetterties, *Catal. Rev. - Sci. Engg.*, 23 (1981) 6; H. Vahrenkamp, *Adv. Organomet. Chem.*, 22 (1983) 169; R.D. Adams, I.T. Horvath, *Prof. Inorg. Chem.*, 33 (1985) 127

20 C. Couture, D.H. Farrar, D.S. Fisher, R.R. Gukathasan, *Organometallics*, 6 (1987) 532

21 Lj. Manojlovic-Muir, K.W. Muir, B.R. Lloyd, R.J. Puddephatt,*J. Chem. Soc., Chem. Commun.*, (1983) 1336

22 Lj.Manojlovic-Muir, K.W. Muir, B.R. Lloyd, R.J. Puddephatt, *J. Chem. Soc., Chem. Commun.*, (1985) 536.

23 J.R. Fisher, A.J. Mills, S. Sumner, M.P. Brown, M.A. Thomson, R.J. Puddephatt, A.A. Frew, Lj.Manojlovic-Muir, K.W. Muir, *Organometallics*, 1 (1982) 1421

24 M.P. Brown, R.J. Puddephatt, M. Rashidi, K.R. Seddon *J. Chem. Soc., Dalton Trans.*, (1978) 516

25 B.R. Lloyd, A.M. Bradford, R.J. Puddephatt, *Organometallics*, 6 (1987) 424

26 C. Mealli, *J. Amer. Chem. Soc.*, 107 (1985) 2245

27 A.M. Bradford, M.C. Jennings, R.J. Puddephatt *Organometallics*, 7 (1988) 792; A.M. Bradford, G. Douglas, Lj. Manojlovic-Muir, K.W. Muir, R.J. Puddephatt, *Organometallics*, in press.

28 T.W. Tingle, K.R. Dixon, *Inorg. Chem.*, 13 (1974) 846; Lj. Manojlovic-Muir, I.R. Jobe, S.S.M. Ling, A.J. McLennan, R.J. Puddephatt, *J. Chem. Soc., Chem. Commun.*, (1985) 1725; T.A. Appleton, H.C. Clark, L.E. Manzer, *Coord. Chem. Rev.*, 10 (1979) 2996

29 P. Piraino, G. Bruno, G. Tresoldi, S. Lo Schiavo, P. Zanello, *Inorg. Chem.*, 26 (1987) 91; A.B. Deacon, R.J. Philips, *Coord. Chem. Rev.*, 33 (1980) 227; L. Gelmini, W.H. Armstrong, *J. Chem. Soc. Chem. Commun.*, (1989) 1904

CHAPTER 8

SYNTHESIS, CHARACTERIZATION AND FLUXIONALITY OF TETRAPLATINUM CLUSTERS

8.1 INTRODUCTION

In chapters 5, 6 and 7, we discussed the reactivity of the hydridotriplatinum cluster, $[Pt_3(\mu_3\text{-}H)(\mu\text{-}dppm)_3]^+$, 2, towards various electrophilic and nucleophilic reagents. In this chapter, we will discuss the synthesis and reactivity of the tetraplatinum complexes which are obtained by reaction of the triplatinum complexes 2 and $[Pt_3(\mu_3\text{-}CO)(\mu\text{-}dppm)_3]^{2+}$, 1, with some Pt(0) reagents.

A number of tetraplatinum clusters are known whose electron count ranges from 48 to 60 [1,2]. In general, lower numbers ($\leq$ 56) of bonding electrons lead to tetrahedral geometries, whereas addition of more electron pairs lead to localised bond breaking and formation of a butterfly geometry[3-9]. This behaviour is similar to that of the triplatinum clusters where an increase of each 2 electron unit (from 42 to 44 to 46) is expected to result in the breaking of one or two Pt-Pt bonds.

Tetraplatinum clusters having electron counts of 58 are common and their general formula is $[Pt_4(\mu\text{-}CO)_5(L)_4]$, 7, L = phosphine[3-7]. They are synthesized by various routes; equations 8.1 to 8.3 show a few of these pathways[1-7].

$$K_2PtCl_4 + 2\ PMe_2Ph \longrightarrow [Pt_4(\mu\text{-}CO)_5(PMe_2Ph)_4]$$

Equation 8.1: reagents: MeOH, NH_2NH_2, KOH, CO

$$2\ [Pt_3(\mu\text{-}CO)_3L_4] + 3\ CO \longrightarrow [Pt_4(\mu\text{-}CO)_5L_4] + 2\ [Pt(CO)_2L_2]$$

Equation 8.2: 1 atm, 25°C, L = PPh_3,

$$[Pt(CO)L_3] + [Pt_3(CO)_3L_4] + [Pt_3(CO)_3L_3] \xrightarrow{\text{Alumina column}} [Pt_4(\mu\text{-}CO)_5L_4]$$

Equation 8.3 : L = $PPh_2(CH_2Ph)$

The solid state structure of complexes 7 reveals a 'butterfly' arrangement of Pt atoms. Hence, there are two different chemical environments for both the phosphine ligands and platinum atoms (i.e, the atoms at the 'hinge' of the butterfly are different from those at the 'wing tips'). Hence, one would predict two distinct ^{31}P and

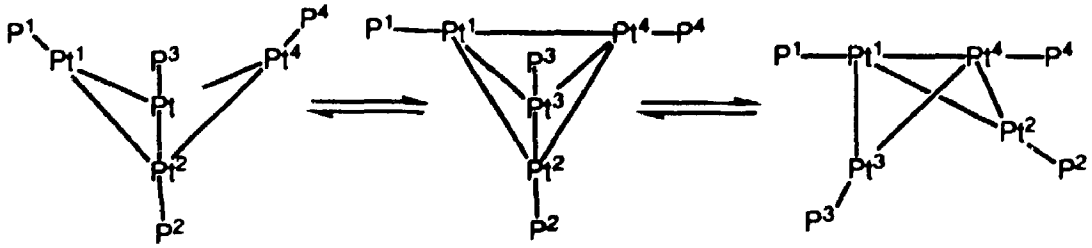

Equation 8.4 : Carbonyls omitted for clarity

^{195}Pt resonances. However, these clusters are fluxional in

solution. The $^{31}P\{^{1}H\}$ and $^{195}Pt\{^{1}H\}$ NMR spectra reveal equivalent ^{31}P and ^{195}Pt spins even at low temperature[6]. This is rationalized in terms of a fluxional process involving Pt-Pt bond breaking and making, and suggests that the 'butterfly' is 'flapping its wings' as shown in equation 8.4.

Our group has also been involved in the chemistry of tetraplatinum clusters. The 58 electron cationic complex, $[Pt_4(\mu\text{-}H)(\mu\text{-}CO)_2(\eta'\text{-dppm-}P)(\mu\text{-dppm})_3](PF_6)$, 5, and the neutral complex, $[Pt_4(\mu\text{-}CO)_2(\mu\text{-dppm})_3\{Ph_2PCH_2P(:O)Ph_2\}]$, 6, have been synthesized and structurally characterized[10,11].

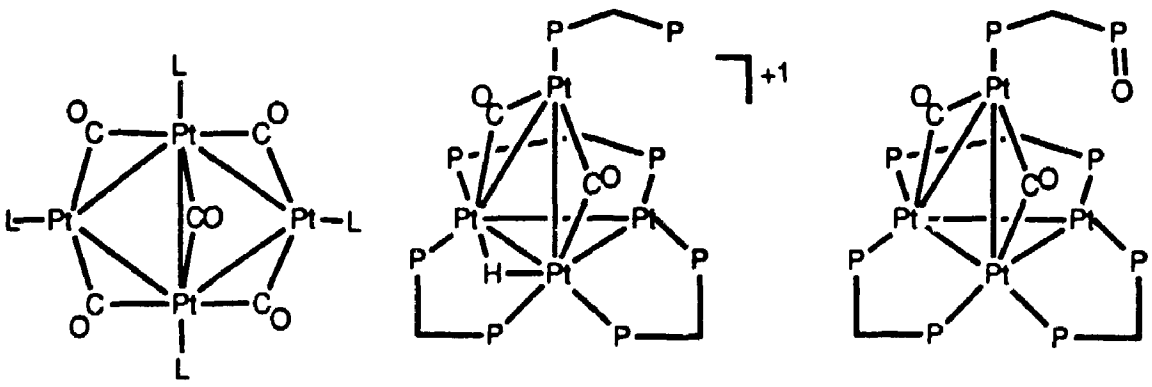

7 5 6

Scheme 8.1

Complexes 5 and 6, like other 58 electron Pt_4 clusters, thus contain a butterfly arrangement of the metal atoms, scheme 8.1. These clusters are synthesized under water gas shift conditions as shown in equations 8.5 and 8.6.

$$[Pt_2(\mu\text{-}H)(H)_2(\mu\text{-dppm})_2](PF_6) \longrightarrow \text{Complex 6}$$

Equation 8.5: conditions: $MeOH/H_2O$, 100°C, 100 psi CO

$[Pt(CF_3COO)_2(dppm)] \longrightarrow$ Complex 5

Equation 8.6: conditions: $MeOH/H_2O$, 100°C, 100 psi CO, 3 days

Complex 5 displays a novel fluxionality involving edge to edge migration of the (μ-H) and [μ-$Pt(CO)_2$(dppm-P] groups with respect to the $Pt_3(\mu\text{-dppm})_3$ triangle (Equation 8.7, complete equivalence requires six such 60° steps) so that the time averaged structure appears to contain a μ_3-H group below, and a rapidly-spinning μ_3-$Pt(CO)_2$(dppm-P) group above, the $Pt_3(\mu\text{-dppm})_3$ unit.

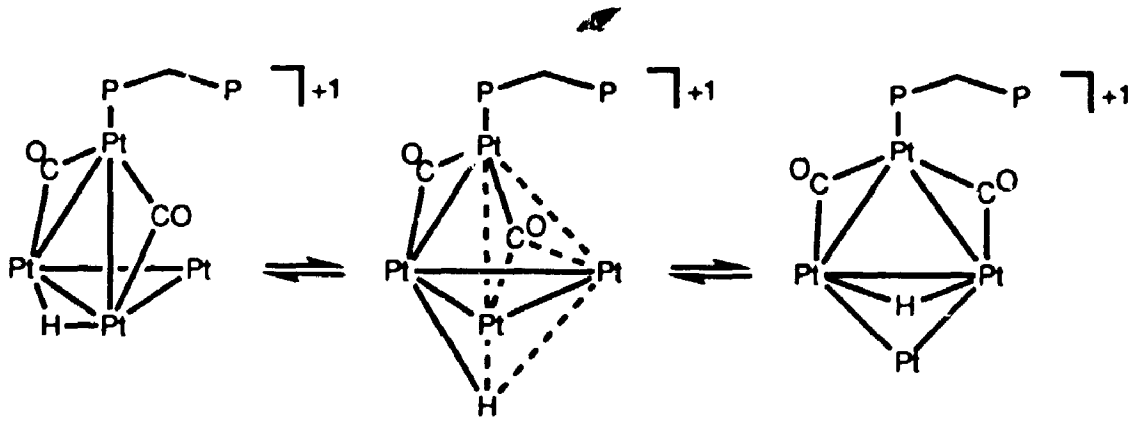

Equation 8.7. μ-dppm ligands omitted for clarity

Formation of complex 5 can also be rationalized in terms of reaction of the Pt(0) complex, $Pt(CO)_2$(dppm-P), with the triplatinum cluster 2. This rationale was put to test and was successfully used to synthesize the 58 electron complex, $[Pt_4(\mu\text{-H})(\mu\text{-CO})_2(\mu\text{-dppm})_3(PPh_3)](PF_6)$ 3, and the 56 electron complex,

$[Pt_4(\mu\text{-}CO)_2(\mu\text{-}dppm)_3(PPh_3)](PF_6)_2$, 4. Complex 3 displays a fluxionality similar to that observed in 5, while 4 displays a slightly different kind of fluxional process by virtue of its postulated tetrahedral Pt_4 skeleton. The details of the synthesis, reactivity and fluxionality of these clusters will be described in this chapter.

8.2 EXPERIMENTAL:

The Pt(0) complexes, $Pt(CO)_2(PPh_3)_2$ and $[Pt_3(\mu\text{-}CO)_3(PPh_3)_3]$, 8, were synthesized by literature methods[7].

8.2.1 Synthesis of $[Pt_4(\mu\text{-}H)(\mu\text{-}CO)_2(\mu\text{-}dppm)_3(PPh_3)](PF_6)$, 3

Complex 3 can be synthesized by two different procedures.

8.2.1.1 From reaction of 2 with $Pt(CO)_2(PPh_3)_2$

To a stirred solution of 2 (40 mg, 0.0212 mmol) in $CH_2C\ell_2$ (10 mL) was added $Pt(CO)_2(PPh_3)_2$ (18 mg, 0.0232 mmol). The contents were stirred under nitrogen atmosphere for 2h. The solution was then concentrated and layered with pentane. The red crystalline solid which precipitates was filtered and dried. Yield: 80%. Anal. calcd. for $C_{95}H_{82}F_6O_2P_8Pt_4$: C, 47.6; H, 3.5%. Found: C, 47.3; H, 3.4%. Mp: 170°C dec. IR. (halocarbon): ν(CO) = 1810, 1773 cm^{-1}; FAB MS: Calcd. for $[Pt_4(H)(CO)_2(dppm)_3(PPh_3)]^+$, m/e

2252; Found, m/e 2252. $\delta(^1H)$ in $CD_2C\ell_2$ at 20°C: -7.4 [m, $^1J(PtH)$ = 518, $^2J(Pt^4H)$ = 31.5, 1H, Pt$\underline{H}$], 4.1 [s, 3H, C$\underline{H}^aH^b$], 6.5 [d, $^2J(H^a\underline{H}^b)$ = 14, $^3J(PtH)$ = 80, 3H, $CH^a\underline{H}^b$]; at -80°C: -7.46 [m, $^1J(Pt^3H) = {}^1J(Pt^2H)$ = 675, $^2J(Pt^1H)$ = 169, 1H, PtH], 3.4, 5.0 [s, 2H, $CH^a\underline{H}^b$], 6.2, 6.7 [s, 4H, C$\underline{H}^aH^b$]. $\delta(^{195}Pt)$ in $CD_2C\ell_2$ at 20°C: -3397 [d. of m., $^1J(Pt^4P^d)$ = 5400, $^2J(PtP)$ = 130, $^1J(PtPt)$ = 140 Hz, $\underline{Pt}^4$].

8.2.1.2 From reaction of 2 with 8 in presence of CO

Complex 2 (50 mg, 0.0265 mmol) was dissolved in acetone (15 mL) saturated with CO gas. To this was added complex 8 (38 mg, 0.0256 mmol) and the solution was stirred for 2.5 h. under an atmosphere of CO. Solvent was then removed under vacuum and the residue was redissolved in $CH_2C\ell_2$ (5 mL) and layered with pentane (10 mL). Complex 3 was obtained as a red crystalline solid. Yield: 75%

8.2.2 Synthesis of $[Pt_4(\mu\text{-}CO)_2(\mu\text{-dppm})_3(PPh_3)](PF_6)_2$, 4

Complex 4 can be prepared by two different procedures.

8.2.2.1 From reaction of 1 with $Pt(CO)_2(PPh_3)_2$

To a solution of 1 (40 mg, 0.0195 mmol) in acetone (10 mL) was added $Pt(CO)_2(PPh_3)_2$ (15 mg, 0.0194 mmol). The contents were stirred under nitrogen for 2.5 h. The orange solution changed colour to red at the end of this period.

The solution was then concentrated to a minimum volume (5 mL) and on layering the solution with pentane, red crystals of 4 separated out. Yield: 85%. Anal. calcd. for $C_{95}H_{81}F_{12}O_2P_9Pt_4$: C, 44.9; H, 3.2%. Found: C, 44.8; H, 3.5%. Mp: 210°C dec. IR (halocarbon): ν(CO) = 1844, 1802 cm^{-1}. FAB MS: Calcd. for $[Pt_4(CO)_2(\mu\text{-dppm})_3(PPh_3)](PF_6)^+$, m/e 2397; Found: m/e 2397. $\delta(^1H)$ in $CD_2C\ell_2$ at 20°C: 4.3 [s, 3H, $C\underline{H}^aH^b$], 6.76 [d, $^2J(H^aH^b)$ = 15, $^3J(PtH)$ = 80, 3H, $CH^a\underline{H}^b$]. at -120°C in $CD_2C\ell_2$/Freon-12 mixture: 3.5, 4.63 [s, 2H, $C\underline{H}^aH^b$], 6.0, 7.4 [s, 4H, $CH^a\underline{H}^b$]. $\delta(^{13}C)$ in $CD_2C\ell_2$ at 20°C: 221.6 [m, $^1J(Pt^4C)$ = 1006, $^1J(Pt^{1-3}C)$ = 112]. at -120°C: 221.2 [m, $^1J(Pt^4C)$ = 1000, $^1J(Pt^2C)$ = $^1J(Pt^3C)$ = 333]. $\delta(^{195}Pt)$ in $CD_2C\ell_2$ at 20°C: -3571 [d. t. of mult., $^1J(Pt^4Pd)$ = 5040, $^1J(Pt^4C)$ = 1000, 1Pt, $\underline{Pt}^4$], -3182 [t. of mult., $^1J(PtP)$ = 3200, 3Pt, $\underline{Pt}^{1-3}$].

8.2.2.2. From reaction of 1 with 8

Complex 1 (50 mg, 0.0243 mmol) was dissolved in acetone (15 mL) saturated with CO gas. To this was added complex 8 (39 mg, 0.0263 mmol) and the contents were stirred for 5h. The colour of the solution changed from orange to red during this period. The solution was then concentrated to 5 mL and layered with hexane (10 mL)). Red crystals of complex 4 were obtained in good yield (80%).

8.2.3 Reaction of 3 with CF_3COOH:

A solution of 3 (40 mg, 0.0187 mmol) in $CD_2C\ell_2$ (5

mL) was taken in an NMR tube (5 mm). To this was added CF_3COOH (8 μL, 0.1077 mmol) by syringe and the contents were shaken thoroughly for 10 minutes. The reaction was then followed by ^{31}P NMR spectroscopy. ^{31}P NMR spectrum showed peaks due to 1 (30%)), 4 (15%) and an unknown species (50%). $\delta(^{31}P)$ in $CD_2C\ell_2$ at 20°C for the unknown species: -18.0 [d, $^1J(PtP)$ = 3480, $^3J(PP)$ = 135, $^3J(PP^d)$ = 19, 6P, $\underline{P}^{a-c}$], 18.6 [m, $^1J(Pt^4P^d)$ = 3660, $^2J(PtP^d)$ = 350, $^3J(P^dP)$ = 19, 1P, $\underline{P}^d$].

8.2.4 Preparation of ^{13}CO-labelled complex 4*

A sample of $[Pt_4(\mu\text{-}^{13}CO)_2(\mu\text{-dppm})_3(PPh_3)](PF_6)_2$, 4*, was prepared by reaction of the ^{12}CO derivative (50 mg) with excess ^{13}CO in $CH_2C\ell_2$ solution, followed by evaporation of the solvent.

8.2.5 Reaction of 4* with excess ^{13}CO:

A sample of 4 (30 mg, 0.0132 mmol) in $CD_2C\ell_2$ (0.5 mL) was placed in an NMR tube (5 mm) fitted with a teflon tap. To this was added Freon-12 (0.3 mL) and the tap was closed. Excess ^{13}CO was condensed into the liquid-nitrogen-cooled tube via a vaccuum line. $^{13}C\{^1H\}$ and $^{31}P\{^1H\}$ NMR spectra were recorded at room temperature and at -120°C, the lowest temperature possible using the $CD_2C\ell_2$/Freon-12 solvent mixture. The $^{13}C\{^1H\}$ NMR spectra showed peaks due to 4* and free ^{13}CO only.

8.3 RESULTS AND DISCUSSION:

8.3.1: Formation of complexes, $[Pt_4(\mu\text{-}H)(\mu\text{-}CO)_2(\mu\text{-}dppm)_3(PPh_3)](PF_6)$, 3, and $[Pt_4(\mu\text{-}CO)_2(\mu\text{-}dppm)_3(PPh_3)](PF_6)_2$, 4

The hydrido tetraplatinum complex 3 was synthesized by the reaction of 2 with the Pt(0) reagent,[7] $Pt(CO)_2(PPh_3)_2$, scheme 8.2.

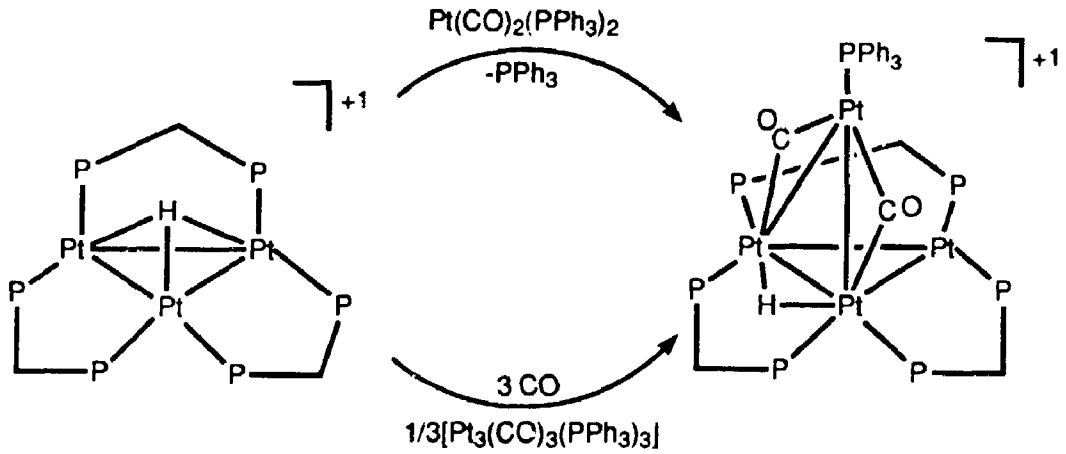

Scheme 8.2

Complex 3 can also be prepared by the reaction of 2 with the triplatinum (0) complex, 8, in the presence of CO, scheme 8.2. In the presence of CO, the trinuclear complex 8 is converted to mononuclear $Pt(CO)_2(PPh_3)_2$,[7] which in turn reacts with 2 to yield 3. This reaction also demonstrates that the μ-dppm ligands of 2 are clearly more effective than μ-CO ligands for maintaining cluster nuclearity[14].

The 56 electron complex 4 can be prepared by the reaction of $[Pt_3(\mu_3\text{-}CO)(\mu\text{-}dppm)_3](PF_6)_2$, 1, with an

equimolar quantity of $[Pt(CO)_2(PPh_3)_2]$, scheme 8.3. It can also be prepared by the reaction of 1 with triplatinum (0) complex, 8, scheme 8.3.

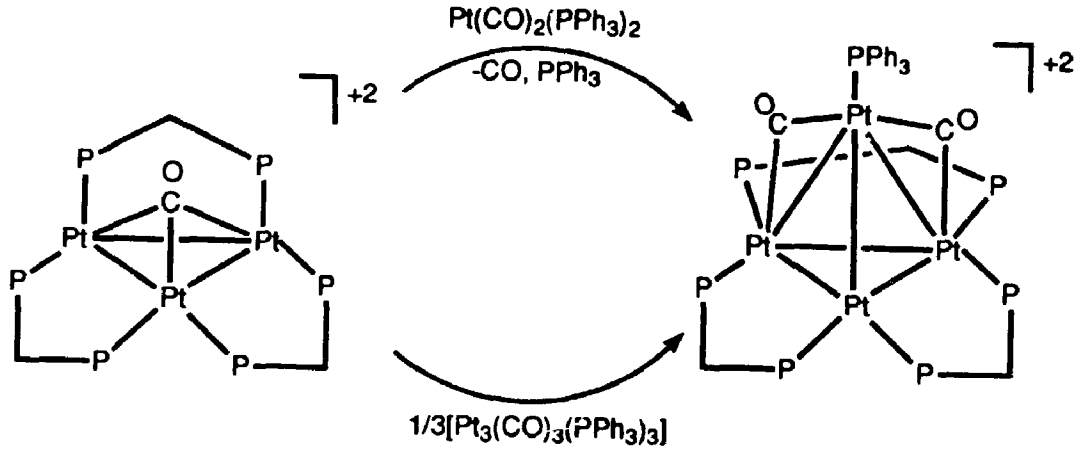

Scheme 8.3

Complexes 3 and 4 were thermally stable, and could be isolated in good yields, in analytically pure form, as the hexafluorophosphate salts which were orange-red solids.

8.3.2 Spectroscopic characterization and fluxionality of complex 3:

Complex 3 was readily characterized by its IR spectrum, mass spectra and by multinuclear NMR spectroscopy. For example, the FAB mass spectra gave peaks such as $[Pt_4(H)(CO)_2(dppm)_3(PPh_3)]^+$ for 3, the parent ion less the $[PF_6^-]$ anion. The assignment could also be confirmed by the shape of the envelope, which can be calculated from the known percentage of the various isotopomers in the predicted ion. Figure 8.1 shows a

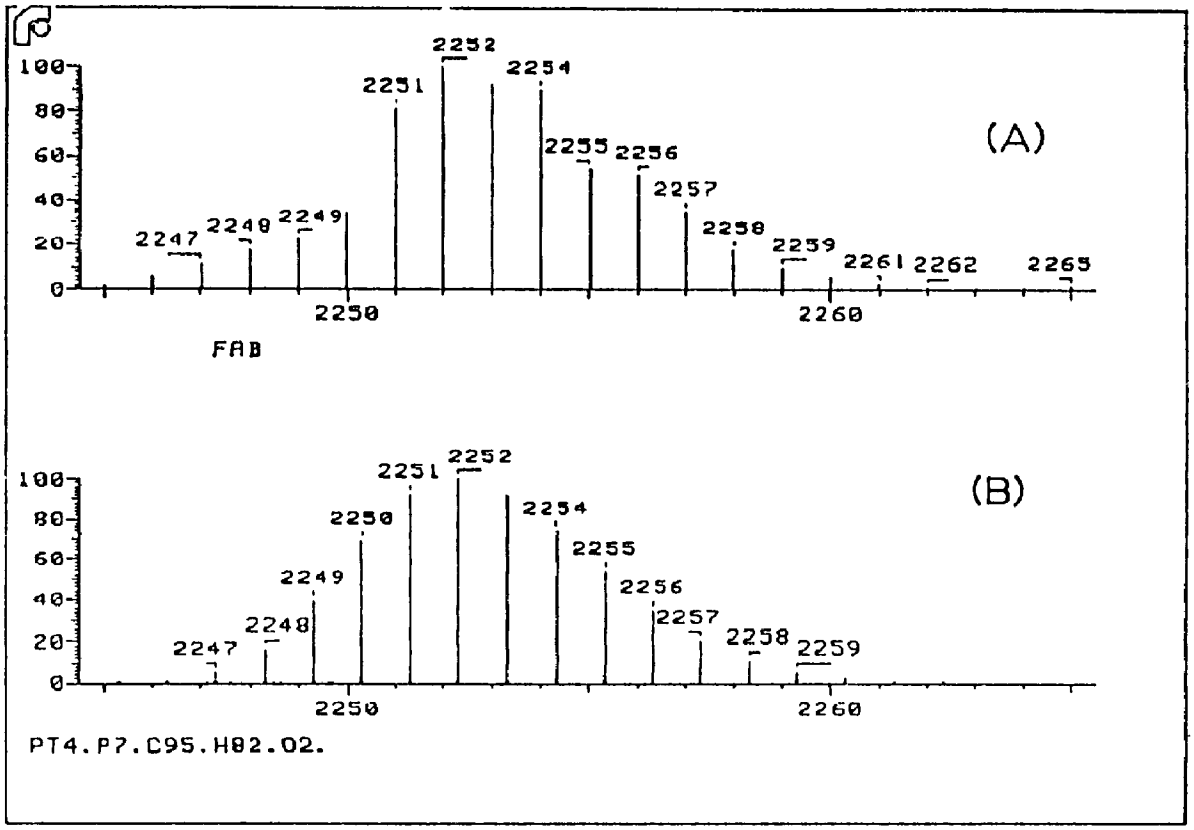

Figure 8.1: (A) Portion of FAB MS of 3 showing the parent ion peak.
(B) Predicted envelope for $Pt_4P_7C_{95}H_{82}O_2$.

typical FAB mass spectrum with predicted and observed envelopes for the fragment $[Pt_4(H)(CO)_2(dppm)_3(PPh_3)]^+$, derived from 3.

Complex 3 was fluxional at room temperature and so NMR spectra were obtained at low temperature, -80°C. A 'butterfly' arrangement of platinum atoms is suggested for 3 by analogy with the isoelectronic complex 5, which has been structurally characterized by X-ray diffraction methods[11]. Unambigous proof of the structure was obtained from the variable temperature ^1H and $^{31}P\{^1H\}$ NMR spectra. The temperature dependence of the ^{195}Pt satellite spectra was a particularly useful tool in determining the bridging network between the Pt_4 core and the ligand atoms.

The symmetry of 3 was readily determined from the variable temperature $^{31}P\{^1H\}$ NMR spectra, Figure 8.2. The NMR labelling scheme is depicted in scheme 8.4. At

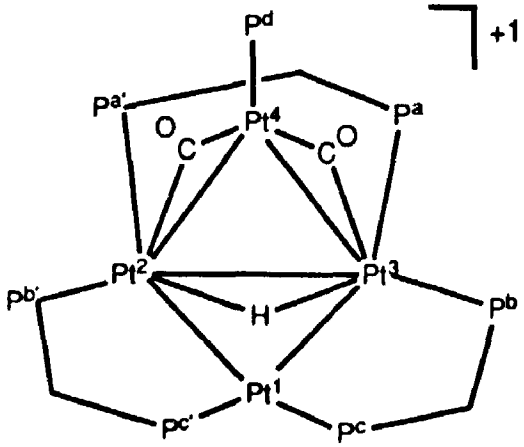

Scheme 8.4: NMR labelling scheme for **3**

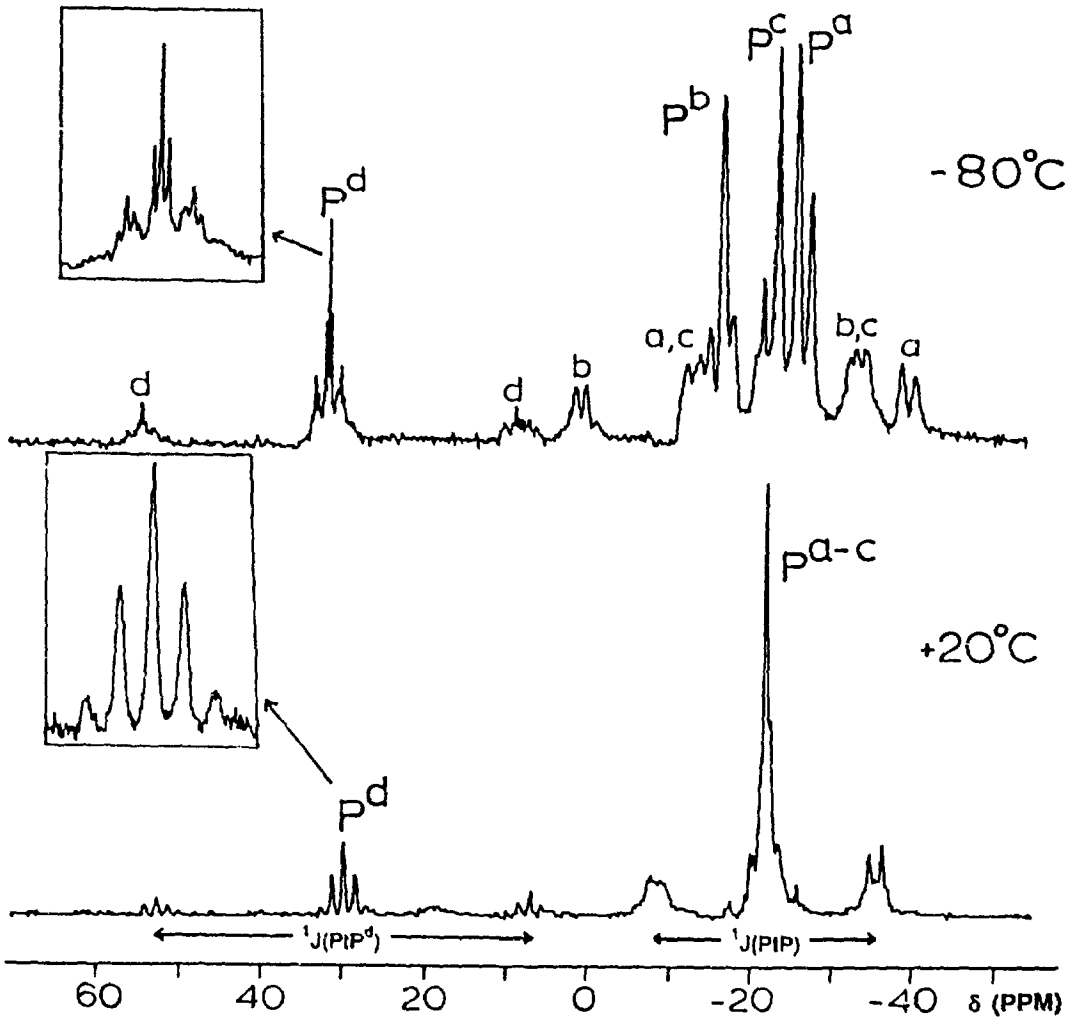

Figure 8.2: Variable temperature $^{31}P\{^{1}H\}$ NMR spectra of 3.

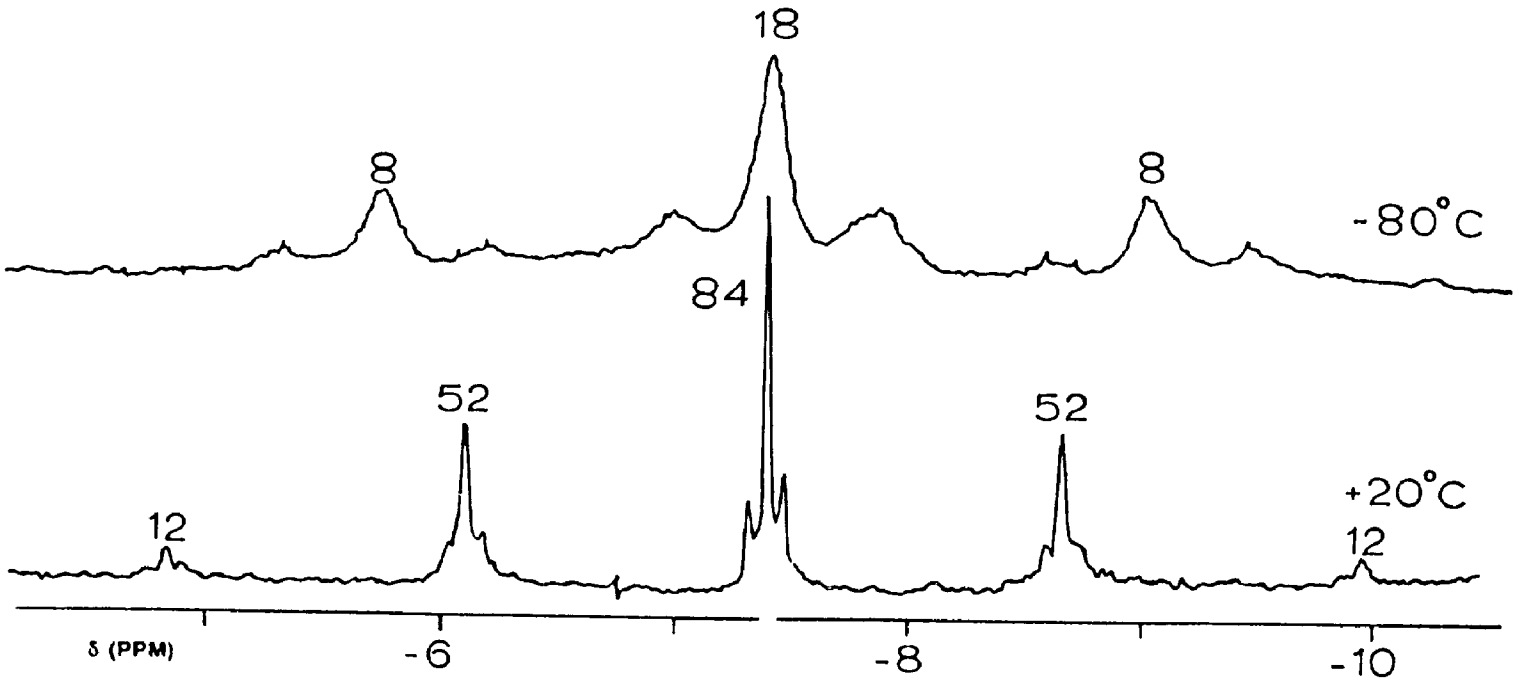

Figure 8.3: Variable temperature ^1H NMR spectra of 3.

room temperature, two resonances are observed, table 8.1, in a 6:1 intensity ratio due to P^{a}-P^{c} and P^{d}, respectively, indicating a three-fold symmetry of the $Pt_3(\mu\text{-dppm})_3$ unit. The signal due to phosphorus atoms P^{a}-P^{c}, appears as a doublet at δ-17.0 with $^{1}J(PtP)$ = 3270 Hz. The resonance due to P^{d} appears as a 1:12:52:84:52:12:1 septet[18] due to equal coupling to Pt^{1}, Pt^{2} and Pt^{3}, with $^{2}J(Pt^{1-3}P^{d})$ = 336 Hz and $^{3}J(P^{d}P)$ = 15 Hz. At -80°C, the μ-dppm ^{31}P resonances split into three signals, table 8.1, as expected for the static structure 3. An AB pattern is observed between P^{a} and P^{c} with $^{3}J(P^{a}P^{c})$ = 210 Hz, and these two resonances occur at higher field (δP^{a} = -17.7 and δP^{c} = -21.2). The resonance due to P^{b} appears as a singlet at δ = -11.5 with $^{3}J(P^{b}P^{b'})$ = 150 Hz (measured from ^{195}Pt satellites). The P^{d} resonance gave a different pattern at low temperature as compared to the room temperature spectrum (figure 8.2). The coupling constant $^{2}J(Pt^{1-3}P^{d})$ = 336 Hz observed at room temperature, splits into two different couplings at -80°C [$^{2}J(Pt^{2}P^{d})$ = $^{2}J(Pt^{3}P^{d})$ =372 Hz; $^{3}J(Pt^{1}P^{d})$ = 248 Hz]. The average of the low temperature coupling constants [$^{2}J(PtP^{d})$ = (372 × 2 + 248)/3 = 331 Hz] is in good agreement with the value measured at room temperature. In addition, the three bond coupling between P^{d} and P^{a-c}, $^{3}J(P^{a-c}P^{d})$ = 15 Hz observed at room temperature, is manifested as $^{3}J(P^{b}P^{d})$ = 45 Hz at -80°C. Again if one averages the 45 Hz coupling over six instead of two

phosphorus atoms, a coupling of 15 Hz is obtained.

In the ^{1}H NMR spectrum at room temperature, figure 8.3, the PtH resonance appeared as a 1:12:52:84:52:12:1 septet[18] due to equal coupling to Pt^{1}, Pt^{2} and Pt^{3}, $^{1}J(PtH)$ = 518 Hz. Thus, the hydride appears to be symmetrically triply bridging the triplatinum face containing Pt^{1}, Pt^{2} and Pt^{3}. At -80°C, a more complex resonance is observed with $^{1}J(Pt^{2}H) = {}^{1}J(Pt^{3}H)$ = 675 Hz [1:8:18:8:1 quintet[18]] and $^{2}J(Pt^{1}H)$ = 169 Hz [1:4:1 triplet[18]] as expected for the static structure 3.

The room and low temperature hydride resonances are compared in figure 8.3. The 'average' J(PtH) is expected to be 1/3 (2 × 675 + 169) = 506 Hz, in reasonable agreement with the observed value, if the hydride is fluxional with respect to $Pt^{1}Pt^{2}Pt^{3}$ triangle.

The ^{195}Pt NMR spectrum of 3 was not very informative. The resonace due to Pt^{4} appeared as a broad doublet due to coupling to P^{d}, $^{1}J(Pt^{4}P^{d})$ = 5460 Hz. This value is typical for a terminal phosphorus atom on a $Pt(\mu\text{-}CO)_{2}Pt_{2}$ unit[2]. The resonances due to Pt^{1}-Pt^{3} were too broad to be observed even at -80°C.

The $^{13}C(^{1}H)$ NMR spectra of 3 could not be obtained as the CO groups in 3 could not be exchanged with ^{13}CO gas. However, it is expected that the carbonyl ligands in 3 would display a fluxional process involving migration about the $Pt^{1}Pt^{2}Pt^{3}$ triangle while remaining bonded to Pt^{4}, as observed in the analogous complex 5.[11]

Together these NMR data describe a fluxional process involving edge to edge migration of the μ-H and μ-$Pt^4(CO)(PPh_3)$ groups with respect to the $Pt_3(\mu\text{-dppm})_3$ unit (scheme 8.5) so the time-averaged structure appears to contain a μ_3-H group below, and a rapidly-spinning μ_3-$Pt^4(CO)_2(PPh_3)$ group above, the $Pt_3(\mu\text{-dppm})_3$ triangle. This is different from the usual "flying butterfly" mechanism proposed for fluxionality of $[Pt_4(\mu\text{-CO})_5L_4]$ complexes.

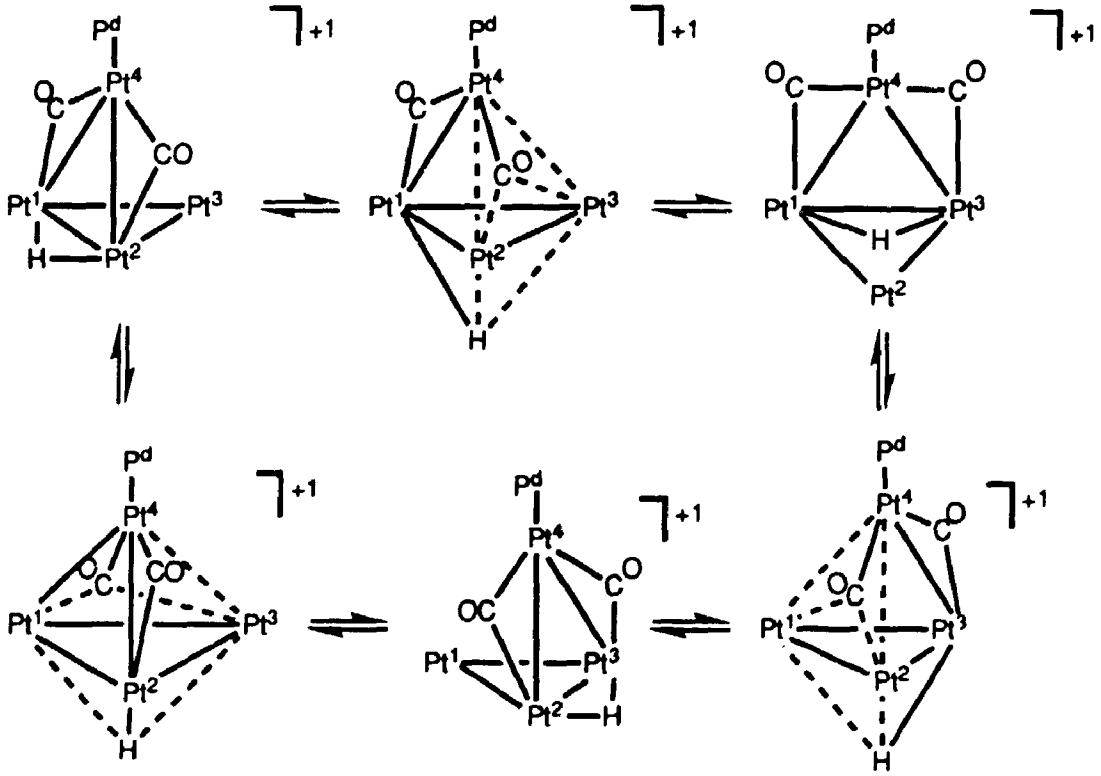

Scheme 8.5: μ-dppm ligands omitted for clatity

The methylene protons, P_2CH_2, of the bridging dppm groups appear to give two resonances at room temperature

Table 8.1: $^{31}P\{^{1}H\}$ NMR Data for complexes 3-5 in CD_2Cl_2

(a) At low temperature

Complex	5	3	4
Temperature (° C)	-40	-80	-120
δP^a	-21.8	-22.5	-25.9
$^1J_{(PtP^a)}$	2484	2400	1770
$^3J_{(P^aP^c)}$	199	210	174
δP^b	-15.2	-16.3	-14.3
$^1J_{(PtP^b)}$	4102	4140	3720
$^2J_{(PtP^b)}$	160	195	134
$^3J_{(P^bP^{b'})}$	144	150	132
δP^c	-26.0	-26.0	-26.9
$^1J_{(PtP^c)}$	3136	3090	3360
δP^d	18.1	28.9	37.3
$^1J_{(Pt^4P^b)}$	5400	5460	5040
$^2J_{(Pt^2P^d)}$¥	378	372	390
$^3J_{(Pt^1P^d)}$	252	248	220
$^3J_{(P^dP^b)}$	41	43	36

¥ - $^2J_{(Pt^2P^d)} = {}^2J_{(Pt^3P^d)}$

(b) At room temperature (20 °C)

Complex	5	3	4
$\delta(P^a,P^c)$	-21.5	-21.8	-19.8
$^1J_{(Pt^4P)}$	3200	3270	3195
$^2J_{(PtP^d)}$	-	200	58
$^3J_{(PP)}$	-	180	180
$^3J_{(PP^d)}$	15	15	14
$^2J_{(Pt^4P)}$	-	152	125
δP^d	18.2	29.2	39.0
$^1J_{(Pt\ P^d)}$	5400	5520	5040
$^2J_{(PtP^d)}$	336	335	336

(see experimental section). At low temperature the "up" protons are split into an unequal doublet, as are the "down" protons. From the coalescence temperature and the difference between the low temperature signals one can calculate the free energy of activation[15]. The calculation given in appendix 8 gives a free energy of activation of 45.5 ± 1 kJ mol^{-1} for the rotation process and is comparable to the value obtained for a similar process in complex 5 (50 ± 1 kJ mol^{-1}).[11]

8.3.3 Spectroscopic characterization and fluxionality of complex 4:

Complex 4 was characterized unambiguously in solution by its IR spectrum, FAB mass spectrum and variable temperature multinuclear NMR spectra (^1H, $^{13}C\{^1H\}$, $^{31}P\{^1H\}$ and $^{195}Pt\{^1H\}$).

The C≡O stretches were observed at 1802 and 1844 cm^{-1} in the IR spectrum of complex 4. This is in the range of stretching frequencies for μ_2-CO groups observed in other Pt_4 cluster complexes[2,11].

All the known tetraplatinum clusters with electron counts <56 have a tetrahedral Pt_4 core. $[Pt_4H_2(P^tBu_3)_4]^{+2}$ and $[Pt_4H_2(P^tBu_3)_4]$ are two very electron deficient clusters which contain tetrahedral cores of platinum atoms. $[Pt_4H_8(P^iPr_2Ph)_4]$ is a 56 electron cluster with an approximately tetrahedral core containing four short and two long Pt-Pt bonds. The loss of electrons from 58

electron Pt_4 clusters results in the formation of a sixth M-M bond and a tetrahedral core of metal atoms.

Complex 4 is a 56 electron cluster and is thus

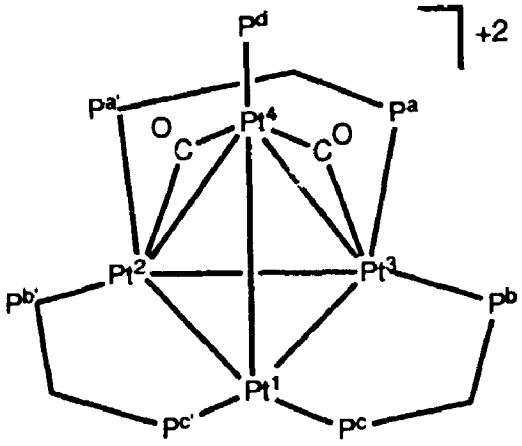

Scheme 8.6: NMR labelling scheme for 4

expected to contain a tetrahedral Pt_4 skeleton, scheme 8.6, unlike the 58 electron 'butterfly' Pt_4 core observed in complexes 3 and 5.[11] Complex 4 was also fluxional at room temperature and hence NMR spectra were recorded at low temperature. At -120°C, the fluxionality in 4 is frozen and the static structure 4 is seen. The NMR labelling scheme is depicted in scheme 8.6.

The ^{31}P NMR data at room temperature and at -120°C is given in Table 8.1. The $^{31}P\{^1H\}$ NMR spectrum at room temperature revealed two resonances in a 6:1 intensity ration due to phosphorus atoms P^{a-c} and P^d, respectively, indicating apparent 3-fold symmetry for the complex. The resonance due to the dppm phosphorus atoms, P^{a-c}, appeared

as a doublet at δ -15.0 due to coupling to P^d, $^3J(PP^d)$ = 13.5 Hz. The resonance due to P^d occured as a septet due to coupling to six "equivalent" dppm phosphorus atoms and had ^{195}Pt satellites due to coupling to Pt^4, $^1J(Pt^4P^d)$ = 5040 Hz (1:4:1 triplet[18]) and Pt^{1-3}, $^2J(Pt^{1-3}P^d)$ = 336 Hz (1:12:52:84:52:12:1 septet[18]).

At -120°C, the resonance due to the ^{31}P atoms of the μ-dppm ligands splits into three signals, as expected for the static structure 4. The resonance due to P^b appears as a singlet at δ -9.5 with $^1J(PtP)$ = 3720 Hz. Phosphorus atoms P^a and P^c couple with each other and an AB multiplet is observed with $^3J(P^aP^c)$ = 174 Hz (δP^a = -21.1, δP^c = -22.1). The P^d resonance gave a different pattern at low temperature as compared to the room temperature spectrum. A single coupling was observed for P^d, due to platinum atoms Pt^{1-3}, at room temperature, $^2J(Pt^{1-3}P^d)$ = 336 Hz, but this became two different couplings at -120°C [$^2J(Pt^2P^d) = {}^2J(Pt^3P^d)$ = 390 Hz, $^3J(Pt^1P^d)$ = 220 Hz]. The mean value of the low temperature couplings, $^2J(Pt^{1-3}P^d)$ = (2×390 + 220)/3 = 333.3 Hz, is in agreement with that observed at room temperature. In addition, the three bond coupling betweeen P^d and P^{a-c} was 13.5 Hz at room temperature. The low temperature spectrum however showed 40 Hz coupling between P^d and P^b only. An 'average' coupling $^3J(P^dP^{a-c})$ = 40/3 = 13.3 Hz is expected at room temperature, in agreement with the observed value.

The $^{195}Pt(^1H)$ NMR spectrum of 4 was also useful in

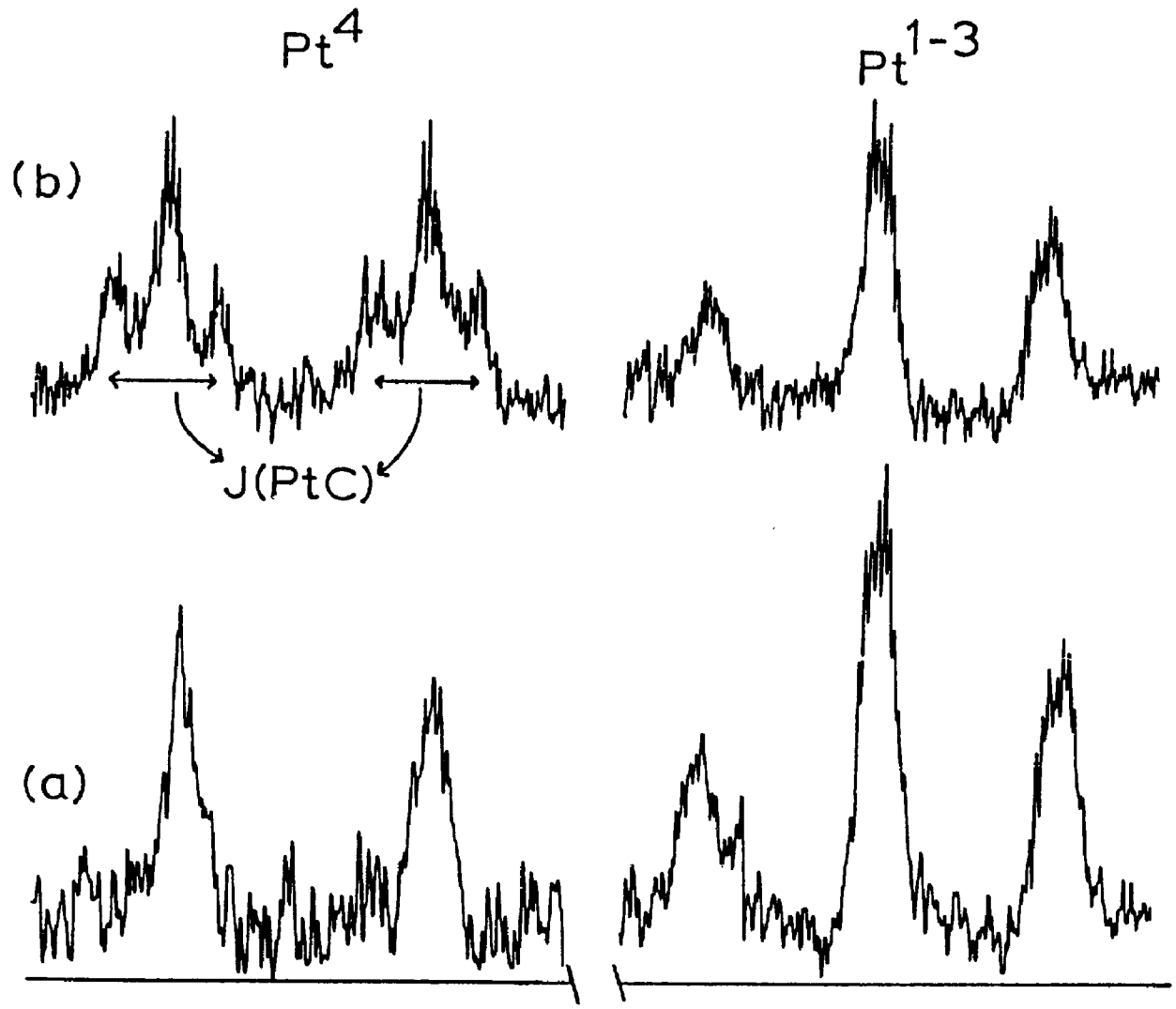

Figure 8.4: $^{195}Pt(^{1}H)$ NMR spectra of (a) 4 and (b) ^{13}CO enriched sample, 4*.

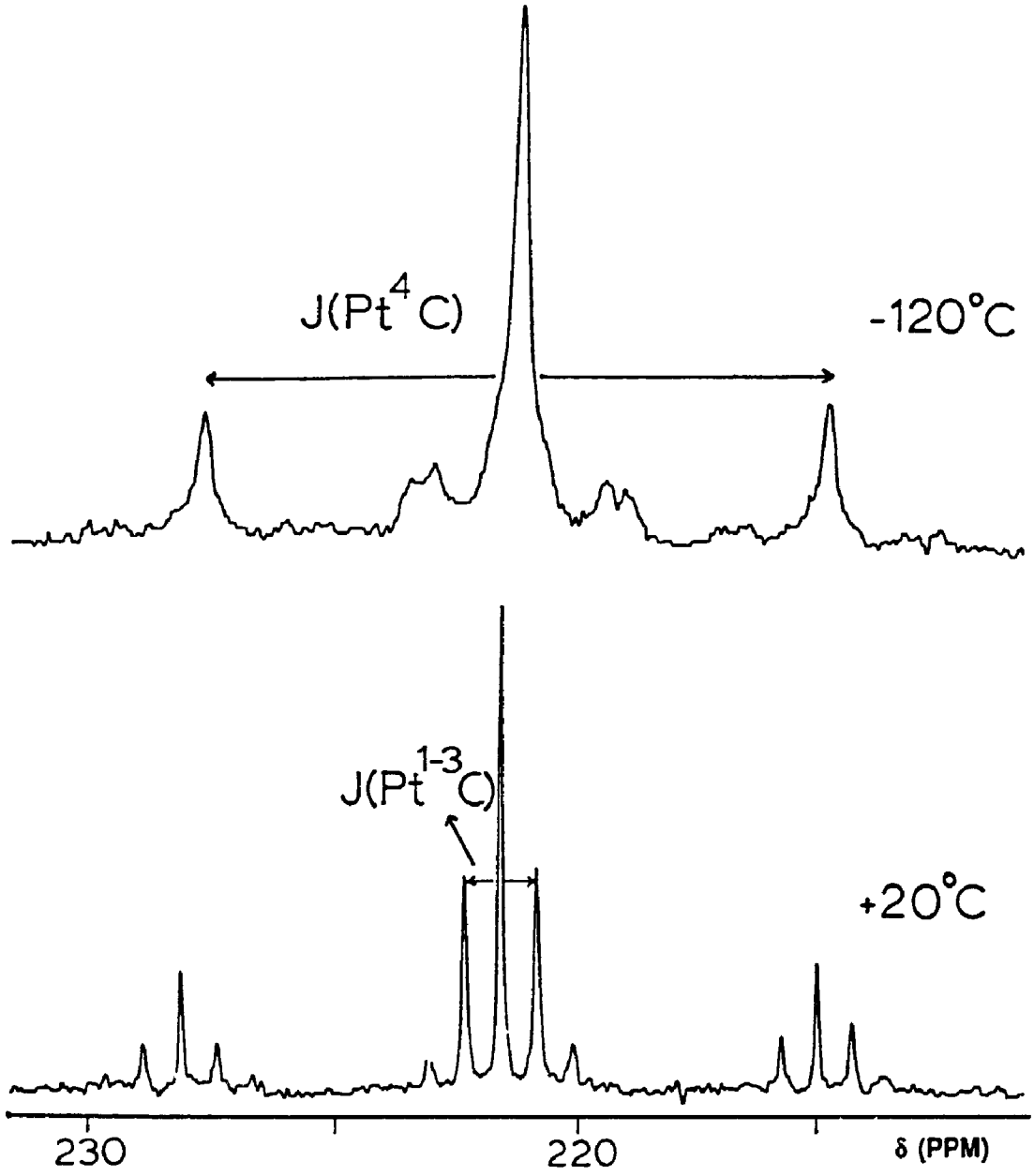

Figure 8.5: Variable temperature $^{13}C\{^{1}H\}$ NMR spectrum of 4.

determining its structure. Figure 8.4 shows the $^{195}Pt\{^{1}H\}$ NMR spectrum of 4 due to both ^{13}CO enriched and unenriched cluster. In the unenriched cluster, the resonance due to Pt^4 appears as a doublet of multiplets due to coupling to P^d, $^1J(Pt^4P^d)$ = 5040 Hz and P^a-P^c, $^2J(Pt^4P^d)$ = 125 Hz. The resonance due to Pt^1-Pt^3 appears as a triplet due to coupling to P^a-P^c, $^1J(PtP)$ = 3200 Hz. In the ^{13}CO enriched complex, we see an extra triplet splitting in the resonance of Pt^4, due to coupling to $(\mu\text{-}^{13}CO)_2$ units, $^1J(Pt^4C) \simeq 1006$ Hz.

The ^{13}CO resonance ι -120°C contained quarter intensity satellites due to $^1J(Pt^4C)$ = 1006 Hz and $^1J(Pt^2C) = {}^1J(Pt^3C)$ = 333 Hz. At room temperature $^1J(Pt^4C)$ was essentially unchanged but an "average" coupling $J(Pt^1C) = J(Pt^2C) = J(Pt^3C)$ = 111 Hz (= 333/3) was observed (figure 8.5) as a 1:12:52:84:52:12:1 septet[18]. This indicates that the carbonyl is fluxional with respect to the $Pt^1Pt^2Pt^3$ triangle while remaining bonded to the apical platinum atom, Pt^4, of the postulated tetrahedron.

The free energy of activation for the fluxional process in 4 was determined as described earlier (section 8.3.2), and was found to be 36 ± 1 kJ mol^{-1} which is significantly different from 45 ± 1 and 50 ±1 kJ mol^{-1} observed in complexes 3 and 5. Together these and the remaining NMR data (Table 8.1 and experimental section) describe a fluxionality as shown in scheme 8.7. The proposed fluxional process is different from both the

"flapping butterfly" mechanism[6] seen in complexes 7 and from that observed in complexes 3 and 5.[11] Since the Pt_4 tetrahedral core structure is retained in the ground and transition states, we do not expect migration involving the μ_3-$Pt^4(P^dPh_3)$ unit. The fluxional process involves an edge

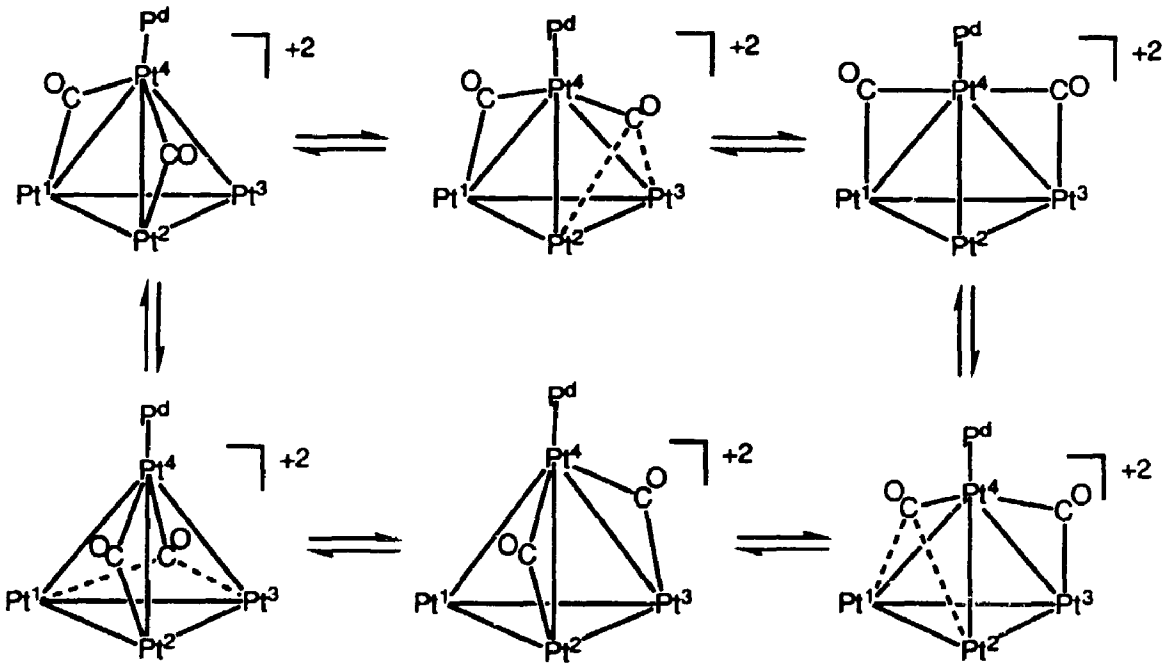

Scheme 8.7 : μ-dppm ligands omitted for clarity

to face to edge migration of <u>only</u> $(\mu\text{-CO})_2$ groups with respect to the $Pt_3(\mu\text{-dppm})_3$ triangular face. The possible tetrahedral Pt_4 skeleton both in the ground state and in the transition state, probably results in the lowering of the activation barrier to fluxionality of carbonyl groups.

However it should be noted that the variable temperature NMR data of 4 is also consistent with the fluxionality as seen in complexes 3 and 5, involving edge

to edge migration of $Pt^4(CO)_2(PPh_3)$ unit above the $Pt_3(dppm)_3$ triangular face. But in the absence of a crystal structure analysis, nothing more can be said.

8.3.4 Reaction of 3 with CF_3COOH:

The reaction of 3 with CF_3COOH was followed by ^{31}P NMR spectroscopy. The $^{31}P\{^1H\}$ NMR spectrum of the resulting solution at room temperature contained signals due to the tetraplatinum complex 4, triplatinum complex 1 and uncharacterized species. Thus we find that the 58

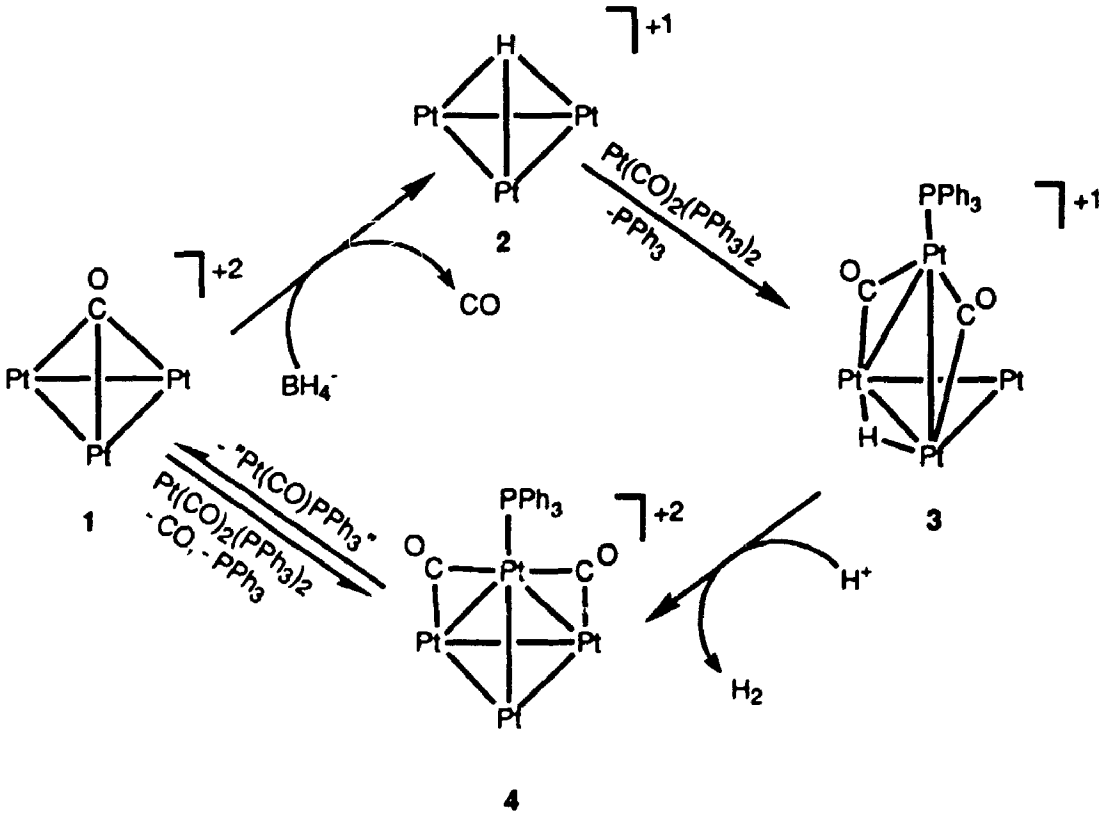

Scheme 8.8: μ-dppm ligands omitted for clarity

electron complex 3 is deprotonated to yield the 56 electron

complex 4, which further disproportionates in the presence of excess of acid to yield the triplatinum complex 1 and an unknown complex. This sequence of reactions is shown in scheme 8.8. Interconversion of metal carbonyl clusters in the acidic medium is also observed in some palladium carbonyl clusters[16].

The unknown complex displayed two ^{31}P resonances (see experimental section). The resonance due to phosphorus atoms of the μ-dppm was observed at δ -18.0 as a broad doublet due to coupling to P^d, $^3J(P^{a-c}P^d)$ = 19 Hz and with ^{195}Pt satellites due to $^1J(PtP)$ = 3480 Hz. The resonance due to P^d was seen at δ 18.6 as a septet due to coupling to six "equivalent" dppm phosphorus atoms and had satellites due to coupling to Pt^4, $^1J(Pt^4P^d)$ = 3660 Hz (1:4:1 triplet[18]) and Pt^{1-3}, $^2J(Pt^{1-3}P^d)$ = 350 Hz (1:12:52:84:52:12:1 septet[18]). These data suggest that the unknown cluster is also a tetraplatinum cluster. Further variable temperature NMR spectroscopic studies are needed to characterize this complex.

8.3.5 Reaction of 4 with excess CO:

A 60 electron tetrapalladium complex, $[Pd_4(\mu\text{-}CO)_6(PBu_3)_4]$, 9, has been structurally characterized by Mednikov et al[17]. It was synthesized by the reaction of $[Pd_4(\mu\text{-}CO)_5(PBu_3)_4]$ with excess CO. An unsuccessful attempt was made to synthesize an analogous Pt_4 complex, 9', by reacting complex 4* with excess ^{13}CO,

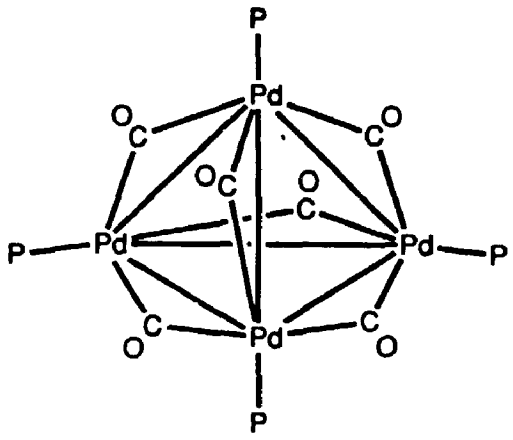

9

equation 8.8. It is possible that the reaction does not occur due to increased steric congestion in the resulting product.

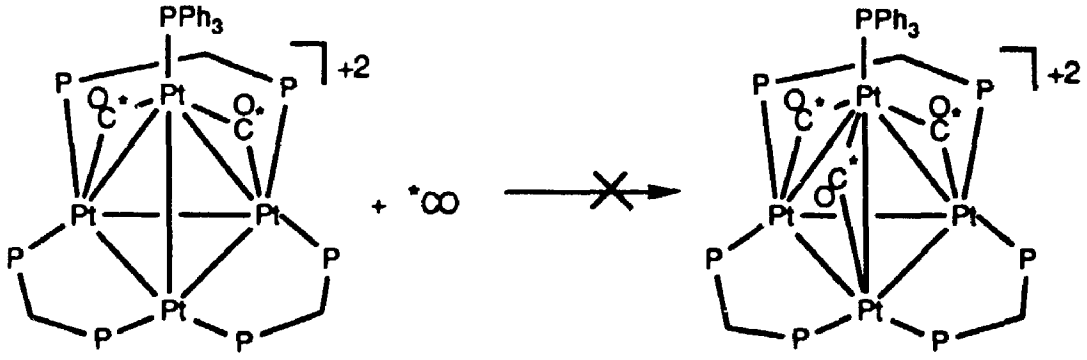

4* 9'

Equation 8.8

8.4 SUMMARY AND CONCLUSIONS:

A systematic synthesis of tetraplatinum clusters

has been achieved. Thus, complexes 3 and 4 have been formed by the reaction of triplatinum complexes 2 and 1 with Pt(0) reagents, respectively. Such a reaction may be the ultimate step in the formation of 5 under water gas shift conditions[11], when the Pt(0) reagent would be $Pt(dppm)(CO)_n$.

A tetrahedral arrangement of platinum atoms is proposed for the 56 electron complex, 4, while the 58 electron complex 3 contains a 'butterfly' arrangement of platinum atoms analogous to the crystallographically characterized, isoelectronic complex 5. Interconversion of complexes 2, 3 and 4 occurs readily in an acidic medium.

Both the complexes, 3 and 4, discussed in this chapter are fluxional. The fluxional process displayed by these complexes is different from the 'flying butterfly' mechanism proposed for the fluxionality of 7.

There are some subtle differences in the fluxional processes observed in 3 and 4. They are, (1) Fluxionality in 3 involves edge to edge migration of μ_3-H and μ_3-$Pt(CO)_2(PPh_3)$ units above and below the $Pt_3(dppm)_3$ unit, whereas in 4, there is an edge to face to edge migration of only the bridging carbonyls, $(\mu$-$CO)_2$, about the tetrahedral faces not constituted by the $Pt_3(dppm)_3$ unit. (2) The butterfly arrangement of platinum atoms in 3 and 5 leads to Pt-Pt bond breaking and formation in the transition state, thus resulting in a higher energy of activation. The probable existence of a tetrahedral Pt_4 arrangement in the

ground state of complex 4 results in lowering of the energy of activation for the migration of carbonyl ligands.

Finally, this study illustrates the value of analysis of the temperature dependence of both coupling constants and multiplicities due to ^{195}Pt coupling in studies of fluxionality of platinum clusters.

8.5 REFERENCES

1. N.K. Ermenko, E.G. Mednikov, S.S. Kurasov, *Russ. chem. Rev.*, 54 (1985) 394.

2. D.M.P. Mingos, R.W.M. Wardle, *Trans. Met. Chem.*, 10 (1985) 441.

3. D.G. Evans, M.F. Hallam, D.M.P. Mingos, R.W.M. Wardle, *J. Chem. Soc. Dalton Trans.*, (1987) 1889.

4. R.G. Vranka, L.F. Dahl, P. Chini, J. Chatt, *J. Amer. Chem. Soc.*, 91 (1969) 1574

5. J. Chatt, P. Chini, *J. Chem. soc. (A)*, (1970) 1538

6. A. Moor, P.S. Pregosin, L.M. Venanzi, A.J. Welch, *Inorg. Chim. Acta.*, 85 (1984) 103

7. P. Chini, G. Longoni, *J. Chem. Soc. (A)*, (1970) 1542

8. N.M. Boag, *J. Chem. Soc. Chem. commun.*, (1988) 617

9. R.J. Goodfellow, E.M. Hamon, J.A.K. Howard, J.L. Spencer, D.G. Turner, *J. Chem. Soc. Chem. Commun.*, (1984) 1604

10. A.A. Frew, R.H. Hill, Lj-Manojlovic-Muir, K.W. Muir, R.J. Puddephatt, *J. Chem. Soc. Chem. Commun.*, (1982) 198

11. G. Douglas, Lj. Manojlovic-Muir, K.W. Muir, M.C. Jennings, B.R. Lloyd, M. Rashidi, R.J. Puddephatt, *J. Chem. Soc. Chem. Commun.*, (1988) 149

12. D.M.P. Mingos, D.G. Evans, *J. Organomet. Chem.*, 251 (1983) C13

13. P.W. Frost, J.A.K. Howard, J.L. Spencer, D.G. Turner, D. Gregson, *J. Chem. Soc. Chem. Commun.*, (1984) 1104

14 .R. Lloyd, A.M. Bradford, R.J. Puddephatt, *Organometallics*, 6 (1987) 424

15. H. Shanan-Atidi, K.H. Bar-Eli, *J. Phys. Chem.*, 74 #4 (1970) 961

16. E.G. Mednikov, N.K. Ermenko, *Izv. Akad. Nauk SSR, Ser. Khim.*, (1982) 2540

17. E.G. Mednikov, N.K. Ermenko, S.P. Gubin, Yu. L. Slovokhotov, Yu.T. Struchkov, *J. Organomet. Chem.*, 239 (1982) 401

18. For an explanation of multiplets refer to appendix 7

CHAPTER 9

SUMMARY

The area of higher nuclearity metal complexes has received much attention in the recent years. However, there are not many reports describing the mechanism of the formation of these large cluster molecules. This thesis documents the chemistry of some of the homo- and heteronuclear cluster complexes of gold and platinum.

The homonuclear complexes of gold presented in this thesis have been prepared by the reaction of the gold(I) complex, [AuCCt-Bu], with various diphosphine ligands. An attempt is also made to rationalize the formation of a novel octanuclear gold cage complex.

The chemistry of heteronuclear and homonuclear clusters of platinum discussed are based on the hydrido triplatinum cluster, $[Pt_3(\mu_3\text{-}H)(\mu\text{-}dppm)_3]^+$, 1. Earlier work carried out in this laboratory focussed on the reactivity of the isoelectronic carbonyl analogue, $[Pt_3(\mu_3\text{-}CO)(\mu\text{-}dppm)_3]^{2+}$, 2. Complexes 1 and 2 are coordinatively unsaturated and possess vacant sites of coordination at the triplatinum core. They should therefore be able to mimic some of the reactions that occur on platinum metal surface.

In chapter 2, the results of the reaction of Au(I)

complex, [AuCC*t*-Bu], with various diphosphine ligands are reported. The resulting complexes, [*t*-BuCC-Au-$R_2PCH_2PR_2$] (R = CH_3 and C_6H_5), undergo a fluxional process involving a 3-coordinate Au(I) center. The dmpm complex dimerizes in chlorinated solvents, with the substitution of acetylide ligand by a chloride ion, to form a cationic gold(I) dimer. The reduced tendency of halide to coordinate in dmpm complexes compared to dppm complexes is attributed to the electronic factors. Thus, the greater basicity of dmpm ligand compared to dppm ligand, overrides the steric effect of the ligands in gold(I) dimers.

In chapter 3, the results of the reaction of [AuCC*t*-Bu] with dmopm ligand are outlined. The unstable initial product upon crystallization from $CH_2C\ell_2$ and then $CHC\ell_3$ gave a novel octanuclear gold cage complex. The cage complex contains four fused nine-membered rings and the first example of a structurally characterized [μ_4-$R_2PCPR_2]^{2-}$ ligand, formed by the deprotonation of the dmopm ligand. The deprotonation of the diphosphines in these complexes has been achieved under mild conditions, contrary to the conventional methods which involve rigorous reaction conditions. It is likely that the very easy deprotonation of the dmopm ligand is aided by the electronegative substituents on phosphorus which may increase the acidity of the CH_2P_2 protons compared to the more common $R_2PCH_2PR_2$ ligands with R = alkyl or aryl. The presence of the basic alkynyl ligand also enhances the possibility of a

nucleophilic attack on the CH_2P_2 protons. In turn, this promises a rich chemistry for the ligands $(RO)_2PCH_2P(OR)_2$ in forming and stabilizing unusual cage and cluster complexes with other elements.

Chapter 4 documents the reaction of [AuCCt-Bu] with the dppm ligand. Under pyrolytic conditions, the initially formed gold(I) dimer is converted to a tetranuclear gold complex containing a singly deprotonated diphosphine ligand. Formation of the octagold complex described in chapter 3 has been rationalised in terms of a sequential metallation of the diphosphine, resulting in the oligomerization of the initial product.

In chapter 5, the chemistry of some Pt-Au hetero bimetallic complexes are reported. Auration of the triplatinum complex 1 results in the stepwise formation of complexes containing $[Pt_3(\mu_3\text{-}H)(\mu_3\text{-}AuPPh_3)]^{2+}$, $[Pt_3(\mu_3\text{-}AuPPh_3)]^{+}$ and $[Pt_3(\mu_3\text{-}AuPPh_3)_2]^{2+}$ units, thus providing a route to novel platinum cluster complexes and showing how electrophilic ligand substitution at the cluster can occur by a bimolecular, stepwise mechanism. The reactivity of these clusters with various main group reagents were also studied. Reaction with CO yields an adduct containing $[Pt_3(\mu_3\text{-}AuPPh_3)(CO)]^{+}$ unit which displays an interesting fluxionality involving migration of CO ligand about the Pt_3 triangular face. The fluxional process observed in this complex is almost certainly a result of the coordinative unsaturation of the triplatinum centre.

Such a fluxional process can be considered to mimic CO ligand migration on a Pt(111) surface.

In chapter 6, the results of the reaction of complex 1 with various tertiary phosphine and phosphite ligands were outlined. These ligands add to complex 1 in a terminal fashion and this leads to a slippage of the μ_3-hydride towards the Pt atom to which the terminal phosphine and phosphite ligands are bound. This work has demonstrated that the slippage of the capping ligand is not only common for Π-acid ligands (as suggested by Evans), but also for the non Π-acid ligands such as hydride. The phosphine and phosphite ligands exhibit a novel fluxional process involving rapid migration about the triangular face of the cluster. A notation has also been proposed for representing the complexes containing an asymmetrically bridged ligand.

Chapter 7 documents the synthesis and reactivity of some novel hydrido triplatinum complexes. Complexes containing $[Pt_3(\mu_3\text{-}H)_2]^{2+}$, $[Pt_3(\mu_3\text{-}H)H]^{2+}$ and $[Pt_3(\mu\text{-}H)_3]^{3+}$ units were prepared and characterized. Such clusters are important as models for intermediates in heterogeneous platinum-catalyzed reactions but are still rare compounds. Reaction of the dihydride complexes with CO results in quantitative elimination of hydrogen and the subsequent formation of the carbonyl capped triplatinum cluster, 2. Reaction with phosphine and phosphite ligands result in the formation of adducts, $[Pt_3(\mu_2\text{-}H)H(L)(\mu\text{-}dppm)_3]^{2+}$

(L = phosphine or phosphite). The rearrangement of the hydrides presumably reduces the steric congestion in the resulting complex. The adducts are thermally stable when the phosphorus donor is a phosphite ligand. However, when the ligand is a bulky phosphine such as PPh_3, the adduct is observed only as a kinetic product, resulting in the degradation of the cluster to yield diplatinum(I) complex, $[Pt_2(\mu\text{-dppm})_2(H)(PPh_3)]^+$. Thus by modifying the added ligand, we have successfully isolated a reactive intermediate in the cluster degradation process.

Finally, chapter 8 outlines a systematic synthesis of some tetraplatinum clusters. Thus, complexes $[Pt_4(\mu\text{-H})(\mu\text{-CO})_2(\mu\text{-dppm})_3]^+$ and $[Pt_4(\mu\text{-CO})_2(\mu\text{-dppm})_3]^{2+}$ have been prepared by the reaction of triplatinum complexes 1 and 2 with Pt(0) reagent, $[Pt(CO)_2(PPh_3)_2]$. The former tetraplatinum cluster has a 58 electron count and contains a butterfly arrangement of platinum atoms, analogous to the crystallographically characterized isoelectronic complex, $[Pt_4(\mu\text{-H})(\mu\text{-CO})_2(\mu\text{-dppm})_3(\eta^1\text{-dppm-P})]^+$; while a tetrahedral arrangement of platinum atoms is proposed for the latter 56 electron cluster. Both of these complexes are fluxional in solution. The fluxional processes displayed by these complexes are different from the usual 'flying butterfly' mechanism observed in other tetraplatinum complexes.

In conclusion, gold forms complexes of varying nuclearity depending on the steric and electronic factors of the bridging diphosphine ligand. In the case of

platinum cluster complexes, the high reactivity of the triplatinum complex 1 is due to its coordinative unsaturation and has allowed modelling of the chemisorption of small molecules on Pt(111) surfaces.

APPENDIX 1

OBSERVED AND CALCULATED STRUCTURE FACTORS

APPENDIX 2

DETAILS OF INSTRUMENTS USED IN EXPERIMENTS AND X-RAY STUDIES

Nuclear Magnetic Resonance Spectroscopy

^{1}H NMR spectra were recorded by using a Varian XL-200 or XL-300 spectrometer. Non-proton spectra ($^{31}P\{^{1}H\}$, $^{13}C\{^{1}H\}$, $^{195}Pt\{^{1}H\}$) were recorded on a Varian XL-300 spectrometer. ^{1}H and $^{13}C\{^{1}H\}$ chemical shifts were measured relative to Me_4Si; $^{31}P\{^{1}H\}$ and $^{195}Pt\{^{1}H\}$ chemical shifts were measured relative to 85% H_3PO_4 and aqueous $K_2PtC\ell_4$, respectively.

Infrared Spectroscopy

Infrared spectra were recorded on a Bruker IR/32 FT-IR spectrometer equipped with a IBM 9000 computer. Solid samples were run as Nujol mulls between $NaC\ell$ plates.

Mass Spectrometry

The FAB mass spectra were recorded using a Finnigan MAT 8230 mass spectrometer on samples prepared as mulls in oxalic acid/ 3-mercapto-1,2-propanediol.

UV-Visible Spectrometery

Ultraviolet and visible spectra were recorded on a Varian Cary 2290 spectrophotometer. Mechanistic and kinetic reaction data were obtained with the aid of either, a Varian Data station or, an Apple II computer which controlled data collection.

Glove Box

A Vacuum atmospheres Company HE-43-2 DRI LAB was used to handle various air sensitive reagents.

Mass Balance

Mass determinations were made using a Fisher Scientific Mettler H80 analytical balance.

Melting point apparatus

The melting points of new compounds were determined using a Fisher Scientific Electrothermal melting point apparatus.

Elemental Analysis

Elemental analyses were performed by Guelph Chemical Laboratories Ltd., Guelph, Ontario.

Preparation of Known compounds

$[Pt_3(\mu_3\text{-}CO)(\mu\text{-}dppm)_3](PF_6)_2$ was prepared as previously described (Ferguson *et al*, *Organometallics*, 5 (1986) 344). It was prepared using a PARR, 300 mL, high pressure, mini reactor equipped with a magnetic drive and an automatic temperature control.

Sources of chemicals

Starting materials $K_2PtC\ell_4$ and bis(diphenylphosphino)methane were obtained from Strem chemicals. Solvents were obtained from Fisher, Aldrich or BDH, and were used without further purification unless the experiment required dry oxygen-free conditions. For these purposes, the solvents were refluxed over anhydrous $CaSO_4$ (acetone), $LiAlH_4$ (diethyl ether), Mg turnings (alcohols), CaH_2 (monoglyme), P_2O_5 (methylene chloride), or Na (Xylene, toluene and tetrahydrofuran) under an atmosphere of nitrogen for several hours. All other chemicals were obtained mainly from Fisher, Aldrich or BDH. All deuterated solvents were obtained from MSD Isotopes. Gases and some low boiling liquids were obtained from the Matheson Gas Company. All reactions were performed at room temperature and atmospheric pressure unless stated

otherwise.

INSTRUMENTS USED IN X-RAY STUDIES

Microscopes

Bausch and Lomb binocular microscope (USA) was used to inspect and identify single crystals.

Ernst Leitz GMBH Wetzlar (W.Germany) polarising microscope fitted with a filar eye-piece was used to measure the crystal dimensions.

Preliminary photography

Preliminary photographs of single crystals were taken using Weissenberg and precession cameras (PHILIPS, Holland).

Optical goniometry

STOE optical goniometer (Darmstadt, Germany) was used to identify and assign indices to various faces of the data collected crystals.

Intensity data collection

Intensity data were collected using an Enraf-Nonius CAD4F diffractometer - DIFFRACTIS 586 (Delft, The Netherlands).

APPENDIX 3
EVALUATION OF BOND LENGTHS AND BOND ANGLES

In order to make comparisons between bond distances and angles within a given structure and with other structures, we have made use of the statistical quantity λ where

$$\lambda = |q_1 - q_2| / \sigma_d$$

q_1 and q_2 are the two values compared,
$\sigma_d = (\sigma_1^2 + \sigma_2^2)^{\frac{1}{2}}$, σ_1 and σ_2 are the errors of the two values compared.

A λ value of 1.96 indicates a probability of 5% that the two structures are the same. $\lambda = 2.58$ corresponds to 1% probability that the two values are the same. In this thesis the 1% probability level has been used to identify significant differences in the values compared.

APPENDIX 4
SUMMARY OF IMPORTANT CRYSTALLOGRAPHIC FORMULAE

1. The general expression for a general structure factor is

$$|F_{hk\ell}| = (A^2_{hk\ell} + B^2_{hk\ell})^{\frac{1}{2}}$$

where

$$A_{hk\ell} = \Sigma f_j \cos 2\pi(hx_j + ky_j + \ell z_j)$$

$$B_{hk\ell} = \Sigma f_j \sin 2\pi(hx_j + ky_j + \ell z_j)$$

and f_j is the scattering factor for the jth atom. The phase angle is defined by

$$\alpha_{hk\ell} = \tan^{-1}(B_{hk\ell}/A_{hk\ell})$$

2. The thermal parameters of the atoms are given by:
   i. isotropic

$$\exp[-B \sin^2\theta_{hk\ell} / \lambda^2] = \exp[-8\pi^2 U \sin^2\theta_{hk\ell} / \lambda^2]$$

   ii. anisotropic

$$\exp[-2\pi^2(U_{11}h^2a^{*2} + U_{22}k^2b^{*2} + U_{33}\ell^2c^{*2} + 2U_{12}hka^*b^* + 2U_{13}h\ell a^*c^* + 2U_{23}k\ell b^*c^*)]$$

   where the U_{ij} are the thermal parameters expressed in terms of mean-square amplitudes of vibrations in Å^2.

3. The error on an observation of unit weight is calculated from:

$$[\Sigma((|F_O| - |F_C|)^2) / (NO - NV)]^{\frac{1}{2}}$$

   where NO is the number of observations and NV is the number of variables.

APPENDIX 5

ORTEP OF DATA COLLECTED CRYSTALS

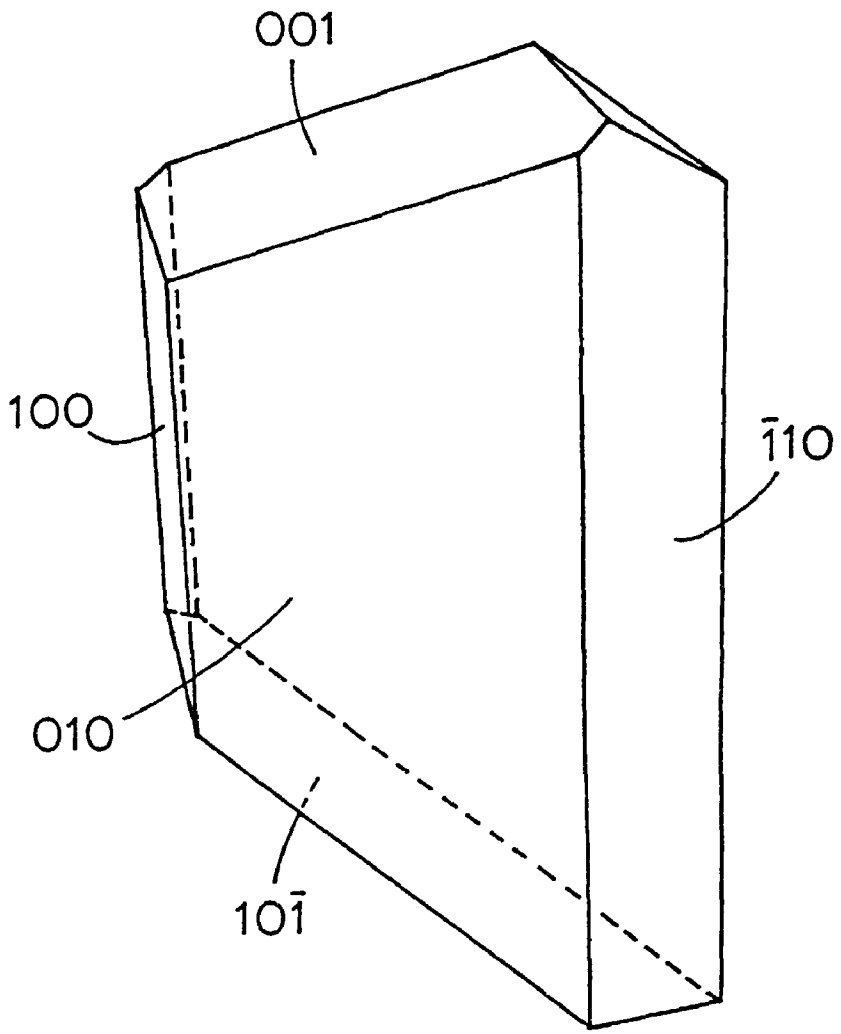

(a) Data crystal of 5a (chapter 2)

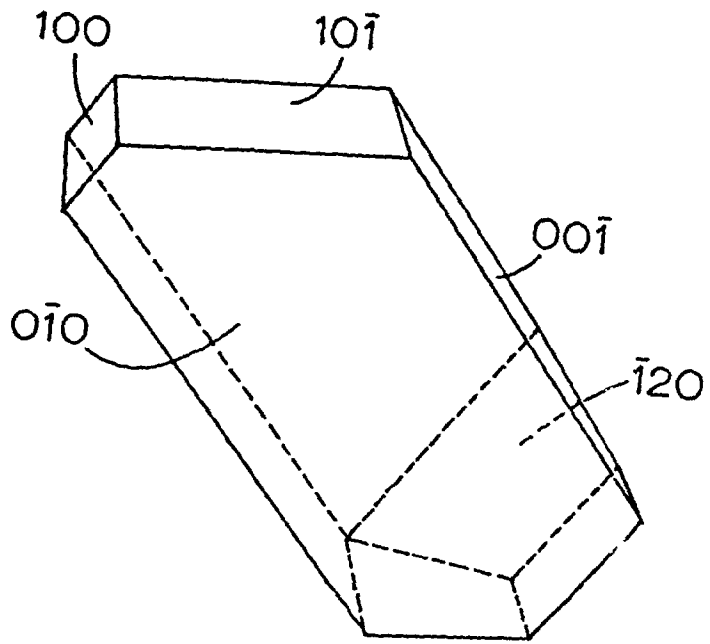

(b) Data crystal of 5b (Chapter 2).

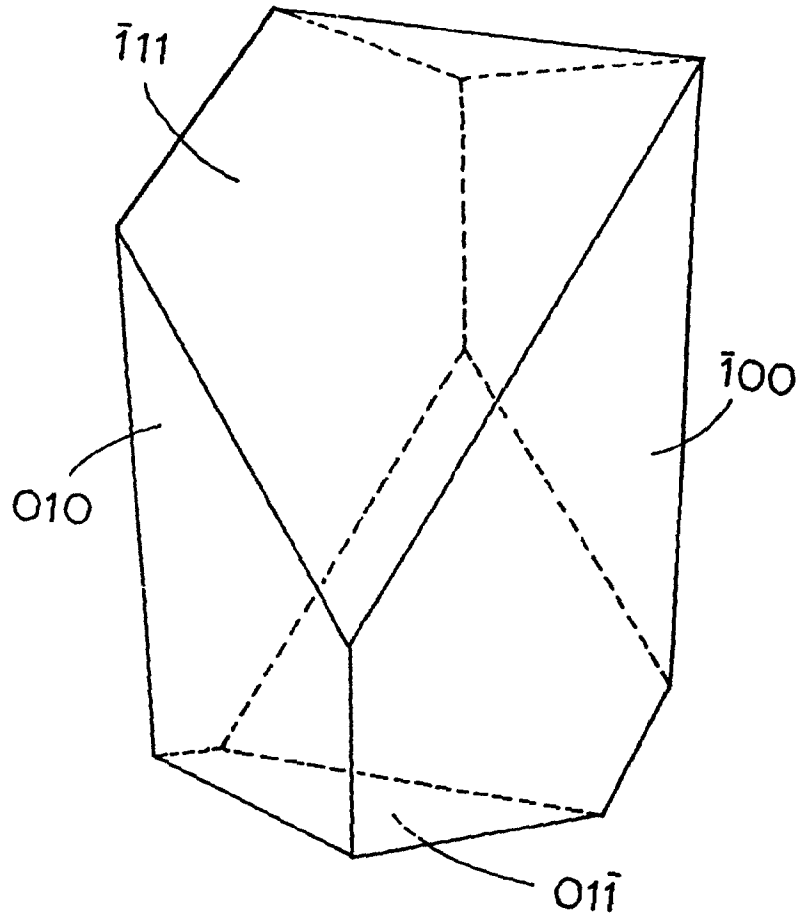

(c) Data crystal of 4 (chapter 3)

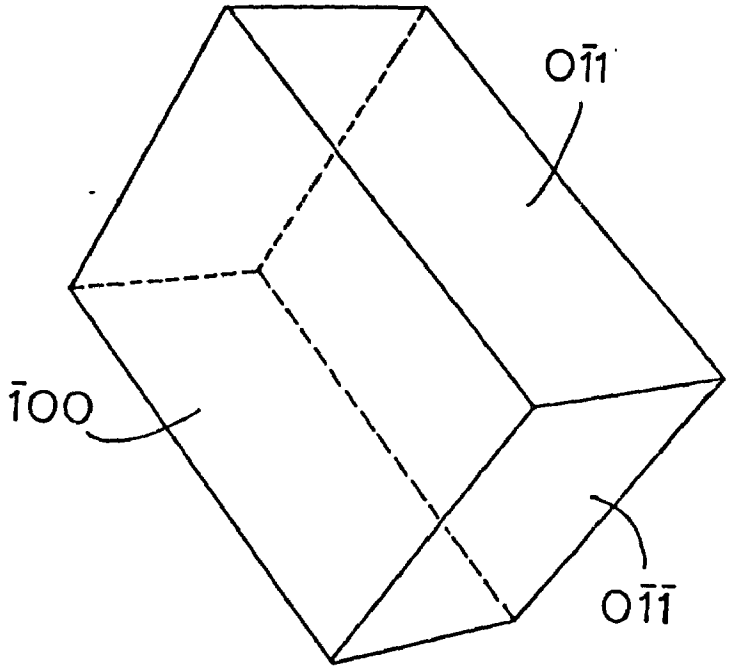

(d) Data crystal of 1b (Chapter 4).

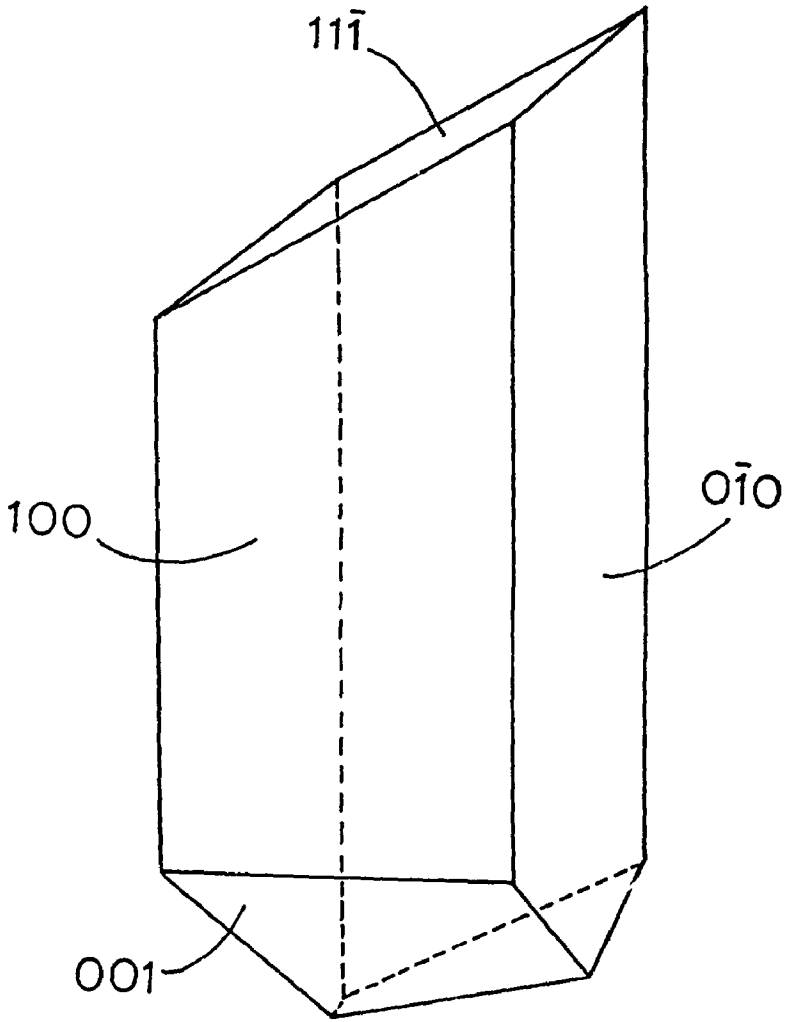

(e) Data crystal of 3a (chapter 6)

Fig. 3

APPENDIX 6

FRACTIONS OF ISOTOPOMERS OF A TRIPLATINUM CLUSTER

i. Platinum-195 is 33.8% abundant and thus the remaining platinum fraction (0.662) is not ^{195}Pt. To determine the fraction present of a given isotopomer of a triplatinum cluster containing three Pt-Pt bonds, one determines the fraction of each platinum atom present, multiplies them together and then multiplies by the number of perturbations possible.

$^{195}Pt \equiv {}^{*}Pt$

Pt^1	Pt^2	Pt^3	$1 \times 0.662 \times 0.662 \times 0.662 = 0.290$	29.0%
$^{*}Pt^1$	Pt^2	Pt^3	$3 \times 0.338 \times 0.662 \times 0.662 = 0.444$	44.4%
$^{*}Pt^1$	$^{*}Pt^2$	Pt^3	$3 \times 0.338 \times 0.338 \times 0.662 = 0.227$	22.7%
$^{*}Pt^1$	$^{*}Pt^2$	$^{*}Pt^3$	$1 \times 0.338 \times 0.338 \times 0.338 = 0.039$	3.9%
				100.0%

ii. In triplatinum clusters containing a mirror plane bisecting Pt^1 and the Pt^2-Pt^2 bond,

Pt^1	Pt^2	Pt^2	$1 \times 0.662 \times 0.662 \times 0.662 = 0.290$	29.0%
$^{*}Pt^1$	Pt^2	Pt^2	$1 \times 0.338 \times 0.662 \times 0.662 = 0.148$	14.8%
Pt^1	$^{*}Pt^2$	Pt^2	$2 \times 0.662 \times 0.338 \times 0.662 = 0.296$	29.6%
$^{*}Pt^1$	$^{*}Pt^2$	Pt^2	$2 \times 0.338 \times 0.338 \times 0.662 = 0.151$	15.1%
Pt^1	$^{*}Pt^2$	$^{*}Pt^2$	$1 \times 0.662 \times 0.338 \times 0.338 = 0.076$	7.6%
$^{*}Pt^1$	$^{*}Pt^2$	$^{*}Pt^2$	$1 \times 0.338 \times 0.338 \times 0.338 = 0.039$	3.9%
				100.0%

APPENDIX 7

CALCULATION OF PLATINUM SATELLITE SPECTRA FOR BRIDGING LIGANDS OR GROUPS EQUALLY BOUND TO PLATINUM ATOMS

A) Biplatinum Centre (*Pt ≡ ^{195}Pt)

active platinum	isotopomer[(i)] fraction	multiplicity	intensity
Pt Pt	0.4382	singlet (1)	0.4382
*Pt Pt	0.4475	doublet (1:1)	O.2238 : 0.2238
*Pt *Pt	0.1142	triplet (1 : 2 : 1)	0.0285 : 0.057 : 0.0285

(i) Isotopomer fraction calculated in Appendix 6

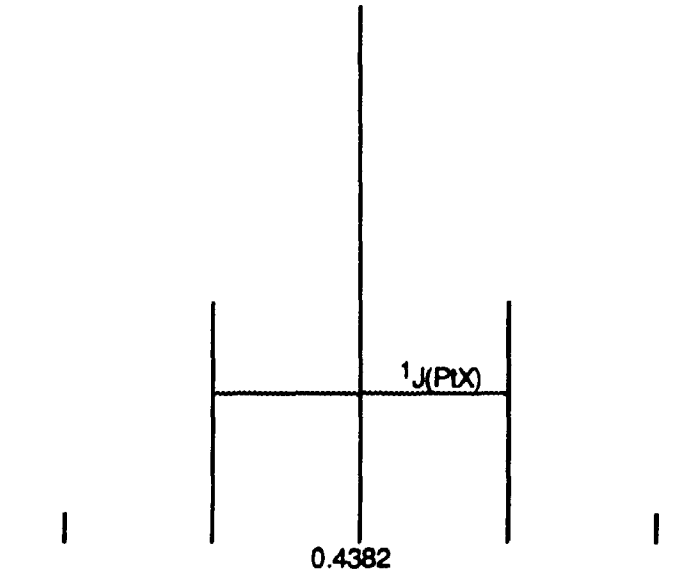

SUM: 0.0285 : 0.2238 : 0.3952 : 0.2238 : 0.0285

1 : 7.8 : 17.3 : 7.8 : 1

1 : 8 : 18 : 8 : 1

B) Triplatinum Centre (*Pt = ^{195}Pt)

active platinum	isotopomer[(i)] fraction	multiplicity	intensity
Pt Pt Pt	0.290	singlet (1)	0.290
*Pt Pt Pt	0.444	doublet (1 :1)	0.222 : 0.222
*Pt *Pt Pt	0.227	triplet (1 : 2 : 1)	0.057 : 0.114 : 0.057
*Pt *Pt *Pt	0.0386	quartet (1 : 3 : 3 :1)	0.005 : 0.0144 : 0.0144 : 0.005

(i) Isotopomer fraction calculated in Appendix 6

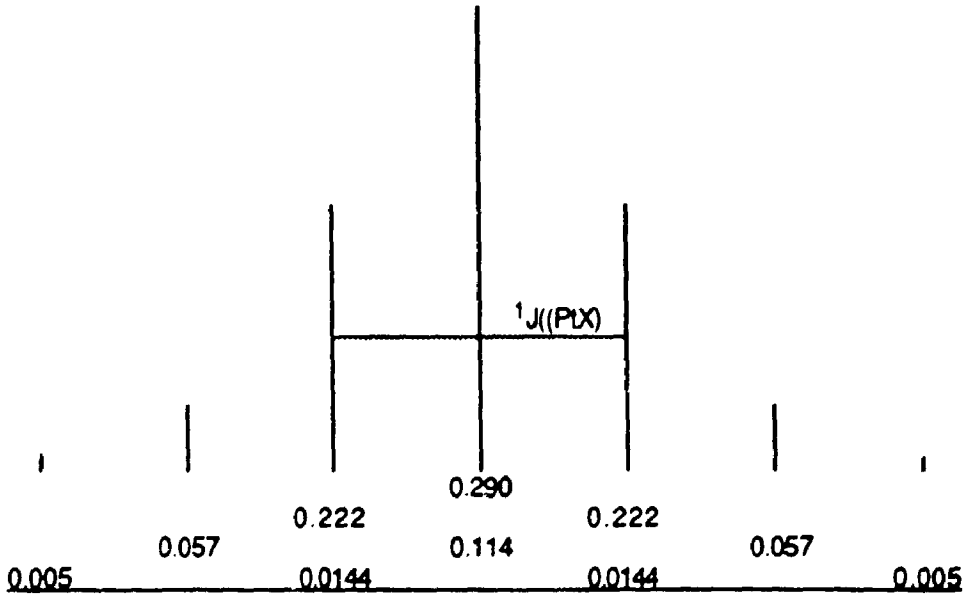

SUM:	0.005	:	0.057	:	0.236	:	0.404	:	0.236	:	0.057	:	0.005
	1	:	11.8	:	49.0	:	83.5	:	49.0	:	11.8	:	1
	1	:	12	:	52	:	84	:	52	:	12	:	1

APPENDIX 8

CALCULATION OF FREE ENERGY OF ACTIVATION FOR AN UNEQUAL DOUBLET

The determination of the free energy of activation using NMR data is a straight forward calculation using the coalescence temperature and the splitting at the low temperature limit. Usually one deals with the coalescence of an equal doublet. The case of an unequal doublet occurs less often and although line shape analysis give a very accurate result, Shanan-Atidi and coworkers [Shanan-Atidi *et al, J. Chem. Phys.*, 74 #4 (1970) 961] developed a more convenient method for obtaining the free energy of activation for the case of an unequal doublet.

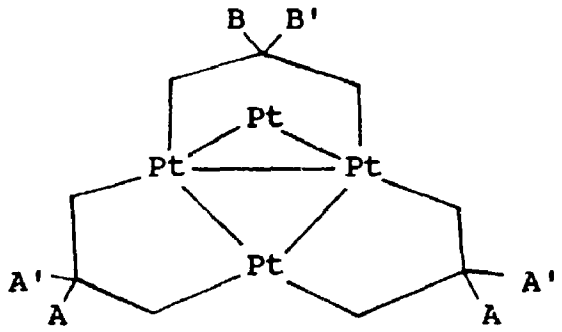

The protons A and B from the scheme are identical at room temperature. The equations to be used from the paper by Shanan-Atidi and Bar-Eli are as follows:

$$\Delta G_a^{\ddagger} = R\ T_C\ ln\left[\ \frac{k}{h\ \pi} \times \frac{T_C}{\Delta\nu} \times \frac{X}{1 - \Delta P}\ \right]$$

$$\Delta G_b^{\ddagger} = R\ T_C\ ln\left[\ \frac{k}{h\ \pi} \times \frac{T_C}{\Delta\nu} \times \frac{X}{1 - \Delta P}\ \right]$$

Where $R = 8.314\ J\ mol^{-1}\ K^{-1}$

$k = 1.381 \times 10^{-23}\ J\ K^{-1}$

$h = 6.63 \times 10^{-34}\ J\ s$

T_c is the coalescence temperature which is equal to -40°C or 233 K for $[Pt_4(\mu\text{-H})(\mu\text{-CO})_2(\mu\text{-dppm})_3(PPh_3)](PF_6)$. But we still need $\Delta\nu$, ΔP and X. The following values are obtained from experiment:

ν_a = 1050 Hz

ν_b = 1210 Hz $\qquad \Delta\nu = \nu_a - \nu_b = 160$ Hz

ν_{avg} = 1133 Hz

$$\nu_{avg.calc.} = P_a\nu_a + P_b\nu_b$$
$$= 0.66 \times 1210 + 0.33 \times 1055 = 1147 \text{ Hz}$$

which is close agreement to the experimental value above.

P_a (0.666) and P_b (0.333) are the probabilities of the proton being in state a or state b.
$\Delta P = P_a - P_b = 0.333$ for all similar species (unequal doublets in a 2:1 ratio).

$X = 2\pi\,\Delta\nu\,\tau$ but we do not know τ without line-shape analysis. However....

$$\Delta P = \left[\frac{X^2 - 2}{3}\right]^{3/2} \frac{1}{X}$$

which we rearrange to give

$$27(\Delta P)^2 = 3 = \frac{(X^2 - 2)^3}{X^2}$$

thus we can determine X = 2.087 by trial and error, and now we have all the values needed to calculate:

$\Delta G_a^{\ddagger}$ = 45.2 kJ mol^{-1} and $\Delta G_b^{\ddagger}$ = 45.7 kJ mol^{-1}